

Forschungszentrum Karlsruhe

Technik und Umwelt

Wissenschaftliche Berichte

FZKA 6100

QUENCH-01 Experimental and Computational Results

P. Hofmann, W. Hering, C. Homann, W. Leiling, A. Miassoedov,
D. Piel, L. Schmidt, L. Sepold, M. Steinbrück

Institut für Materialforschung
Hauptabteilung Ingenieurtechnik
Institut für Reaktorsicherheit
Projekt Nukleare Sicherheitsforschung

Forschungszentrum Karlsruhe GmbH, Karlsruhe
1998

Abstract

This report presents the results of Test QUENCH-01 performed in the QUENCH test facility at the Forschungszentrum Karlsruhe on February 26, 1998.

The QUENCH experiments are to investigate the hydrogen source term that results from the water injection into an uncovered core of a Light-Water Reactor (LWR). The test bundle is made up of 21 fuel rod simulators with a length of approximately 2.5 m. 20 fuel rod simulators are heated over a length of 1024 mm, the one unheated fuel rod simulator is located in the center of the test bundle. The rod cladding is identical to that used in LWRs: Zircaloy-4, 10.75 mm outside diameter, 0.725 mm wall thickness. Heating is carried out electrically using 6-mm-diameter tungsten heating elements, which are installed in the center of the rods and which are surrounded by annular ZrO₂ pellets. The test bundle is instrumented with 63 thermocouples attached to the cladding and the the shroud at 17 different elevations between -250 mm and 1350 mm. Cladding thermocouples are arranged at four different orientations. The superheated steam together with the argon as carrier gas enters the test bundle at the bottom end and leaves the test section at the top together with the hydrogen that is produced in the zirconium-steam reaction. The hydrogen is analyzed by two different instruments: a mass spectrometer and a "Caldos 7 G" hydrogen detection system.

The objective of Test QUENCH-01 was the investigation of the behaviour on reflood of partially oxidized PWR fuel rods, i. e. on test rods pre-oxidized to a maximum oxide layer thickness of 300 micrometres, and quenched from the bottom at a maximum temperature of 1870 K.

Test QUENCH-01 consisted of (a) a heatup phase, (b) a phase at ca. 1000 K in which small amounts of helium were injected into the test section to determine delay times for the hydrogen transport, (c) a second heatup phase, (d) a pre-oxidation phase at ca. 1400 K - 1600 K for 8280 s, (e) a transient phase, and (f) a quench phase. All phases except the quench phase were conducted in an argon/steam atmosphere. Withdrawing of one of the solid Zry corner rods from the hot bundle near the end of the pre-oxidation period showed that a maximum oxide layer thickness of 300 µm at 900 mm elevation was reached. Afterwards the test bundle was ramped at 0.5 K/s to a maximum rod cladding temperature of 1870 K (extrapolated at 950 mm

elevation) and a maximum shroud temperature of 1800 K at the same elevation. At the end of the transient phase the shroud was heated up at a rate of 1.5 K/s at 1150 mm, i. e. above the heated zone. This suggests that the shroud material (Zircaloy-4) had experienced a moderate temperature escalation.

The quench phase was initiated by cutting off the argon and steam flow, filling the lower plenum with quench water at a high rate (80 g/s), injecting argon at the upper bundle head. Thirty seconds later the electrical power was reduced from 20 kW to 4 kW within 15 s, and the test section was reflooded from the bottom at 52 g/s H₂O for 89 s achieving an injection velocity of 1.7 cm/s. During the reflood phase the bundle appeared to quench steadily with no evidence of any temperature excursion. The precursory cooling of the test rods, i. e. the cooldown prior to quenching, occurred simultaneously, namely within one second, for all axial positions and exactly at the time when the quench water level was at -250 mm. The maximum cooldown rates during quenching on the basis of the cladding thermocouple responses were determined to be between 100 and 430 K/s with the higher rates in the upper elevations of 1250/1350 mm. The cladding thermocouples showed sharp temperature decreases at temperatures occurring between 640 K at -250 mm and 1200 K at 1150 mm elevation. The propagation rates of this temperature decreases were between 0.4 cm/s and 7 cm/s. These rates seem to have the tendency to be larger at higher elevations.

The total amount of hydrogen generated during the pre-oxidation phase was 26 -30 g determined by the Caldos device and the mass spectrometer, respectively. In addition, 8 - 9 g are associated with the transient + reflood phase. The contribution from this phase is relatively small because no temperature excursion took place.

The post-test appearance of the test bundle shows no signs of any melt but significant oxidation of the bundle between the 700 and 1100 mm elevations. In this region the oxide layer is of a gray color and some larger cracks in the cladding have formed. The shroud is intact and undeformed. All rod cladding thermocouples in the hot region are destroyed.

Experimentelle und Rechen-Ergebnisse des Versuchs QUENCH-01

Zusammenfassung

In diesem Bericht sind die Ergebnisse des Experiments QUENCH-01, das am 26. Februar 1998 in der QUENCH-Versuchsanlage des Forschungszentrums Karlsruhe durchgeführt wurde, beschrieben. In den QUENCH-Versuchen soll der Wasserstoffquellterm, der sich bei einer Einspeisung von Notkühlwasser in einen trockenen, überhitzten Reaktorkern eines Leichtwasserreaktors (LWR) ergibt, ermittelt werden. Das QUENCH-Testbündel ist mit 21 Brennstabsimulatoren einer Gesamtlänge von ca. 2,50 m bestückt. 20 Brennstabsimulatoren sind auf einer Länge von 1024 mm beheizt, der Zentralstab ist unbeheizt. Die Stabhüllen sind identisch mit LWR-Hüllrohren: Zircaloy-4, 10,75 mm Außendurchmesser und 0,725 mm Wanddicke. Die Brennstabsimulatoren werden elektrisch mit Hilfe von 6 mm-Wolfram-Stäben, die sich in der Mitte der Brennstabsimulatoren befinden und von ZrO_2 -Ringtabletten umgeben sind, direkt beheizt. Testbündel und Shroud sind mit 63 Thermoelementen instrumentiert. Sie sind auf 17 Messebenen von -250 mm bis 1350 mm angeordnet. An den Stabhüllen sind die Thermoelemente in vier Umfangslagen befestigt. Der überhitzte Dampf tritt zusammen mit Argon als Trägergas am unteren Ende in die Teststrecke ein und verläßt diese zusammen mit dem Wasserstoff, der sich durch die Zirkonium-Dampf-Reaktion gebildet hat, am oberen Ende. Der Wasserstoff wird mit Hilfe von zwei Messgeräten analysiert: einem Massenspektrometer und einem Caldos-7G-Analysegerät.

Ziel des Versuchs QUENCH-01 war die Untersuchung des Verhaltens von teilweise oxidierten DWR-Brennstäben während der Flutung eines Reaktorkerns mit Notkühlwasser. Die Versuchsstäbe wurden in der QUENCH-Anlage bis zu einer maximalen Oxidschichtdicke von 300 μm voroxidiert und von einer maximalen Temperatur von 1870 K abgeschreckt. Test QUENCH-01 bestand aus folgenden Versuchsphasen: (a) einer Aufheizphase, (b) einer Phase, in der Laufzeitmessungen mit Helium-Einspeisung bei ca. 1000 K zur Feststellung der Verzögerungszeiten bezügl. des Wasserstoff-Transports durchgeführt wurden, (c) einer zweiten Aufheizphase, (d) einer Voroxidationsphase, (e) einer transienten (Aufheiz-)phase und (f) einer Abschreck- bzw. Quench-Phase. Alle Testphasen außer der Quench-Phase wurden in einer Argon/Dampf-Atmosphäre durchgeführt. Die Voroxidation fand bei ca. 1400 K

bis 1600 K bei einer Zeitdauer von 8280 s statt. Diese Bedingungen ergaben eine maximale Oxidschichtdicke von 300 μm in der 900 mm-Ebene. Kurz vor dem Ende der Voroxidationsphase wurde bei hohen Betriebstemperaturen, d. h. ohne Unterbrechung des Versuchsbetriebs, ein 6 mm-Zircaloy-Eckstab aus dem Bündel gezogen und die Oxidschichtdicke bestimmt. Nach der Voroxidation wurde das Versuchs-bündel mit einer Aufheizrate von 0,5 K/s auf die maximale Stab-Hüllrohrtemperatur von 1870 K (extrapolierter Wert in der 950 mm-Ebene) bzw. auf eine maximale Shroud-(Dampfführungsrohr)-temperatur von 1800 K – auf der gleichen Höhenkote – gebracht. Die höhere Aufheizrate des Shrouds von 1,5 K/s in der 1150 mm-Ebene, d. h. oberhalb der beheizten Zone, gegen Ende der Transiente läßt vermuten, dass das Shroudmaterial (Zircaloy-4) eine moderate Temperaturskalation erlebt hat.

Die Quench-Phase wurde mit dem Abschalten der Argon/Dampf-Zufuhr, dem Auf-füllen des unteren Bündel-Plenums mit einem erhöhten Quench-Wasserstrom (80 g/s) und der Argon-Einspeisung am oberen Bündelkopf vorbereitet. 30 Sekunden nach dieser Aktion wurde die Bündelheizung innerhalb von 15 s von 20 kW auf 4 kW heruntergefahren und die Teststrecke mit einer Wassereinspeiserate von 52 g/s für eine Zeitdauer von 89 s – entsprechend einer Einspeiserate von 1,7 cm/s – von un-ten her geflutet. Während dieser Flutphase war keine Temperaturexkursion im Ver-suchsbündel erkennbar. Die Kühlung der Teststäbe (vor dem Abschrecken) geschah für alle axialen Ebenen gleichzeitig, nämlich innerhalb einer Sekunde, und zwar bereits zu dem Zeitpunkt, an dem sich der Wasserspiegel bei -250 mm befand. Die maximalen Abkühlraten während des Abschreckens wurden auf der Grundlage der gemessenen Temperaturen zu 100 bis 430 K/s bestimmt, wobei die höheren Werte von den Thermoelementen der Ebenen 1250/1350 mm stammen. Die Quench-Temperaturen, die auf der Grundlage der Hüllrohr-Thermoelemente ermittelt wurden, lagen zwischen 641 K bei -250 mm und 1199 K bei 1150 mm Höhe. Die Abschreck-geschwindigkeiten lagen zwischen 1 cm/s und 7 cm/s. Diese Abschreckraten scheinen die Tendenz zu haben, dass sie in den oberen Ebenen größer werden.

Die Gesamtmenge an Wasserstoff, die während der Voroxidationsphase erzeugt wurde, ist am Massenspektrometer und Caldos-Gerät mit 30 bzw. 26 g gemessen worden. Zusätzlich entstanden während der Transiente und der Flutphase 8 – 9 g H_2 . Der Beitrag dieser Phase ist so gering, weil keine Temperaturexkursion stattfand.

Nach dem Experiment läßt das Versuchsbündel keinerlei Schmelze, dafür aber eine deutliche Oxidationszone zwischen 700 und 1100 mm Höhe erkennen. In diesem Bereich weist die Oxidschicht eine graue Farbe und einige größere Risse in den Hüllrohren auf. Das Dampfführungsrohr (Shroud) ist unversehrt. Alle Hüllrohr-Thermoelemente, die in der heißen Zone eingesetzt waren, sind zerstört.

List of Tables

- Table 1: QUENCH Test Matrix
- Table 2: Design characteristics of QUENCH test bundle
- Table 3: List of instrumentation for the QUENCH-01 Test
- Table 4: Test QUENCH-01; Evaluation of cool-down data
- Table 5: Test QUENCH-01; Quench temperatures and quench rates based on shroud temperature data
- Table 6: Hydrogen release measured by mass spectrometer and Caldos system during test QUENCH-01
- Table 7: Test QUENCH-01; Failures of thermocouples mounted to claddings of fuel rod simulators
- Table 8: Synchronisation of the data from the main data acquisition system and from the mass spectrometer
- Table 9: QUENCH 01; Cross sections
- Table 10: Procedure of the preparation of the samples for the metallographic examination

Appendix

- Table A-1: Test program of the gas flow delay measurements and designation of the data files
- Table A-2: Results of the time-lag measurements in the QUENCH facility (Febr. 20, 1998) H₂ injection at ambient temperature
- Table A-3: Results of the time-lag measurements in the QUENCH facility (Febr. 26, 1998) Helium injection at 1000 K
- Table A-4: Reaction times of the CALDOS system in the QUENCH facility

List of Figures

- Fig. 1 QUENCH Test Facility, Flow Diagram
- Fig. 2 QUENCH Test Section, Flow Lines
- Fig. 3 QUENCH Facility, Main components
- Fig. 4 QUENCH Facility, H₂ Measurement with Caldos
- Fig. 5 QUENCH Facility, H₂ Measurement, Mass Spectrometer
- Fig. 6 QUENCH Fuel Rod Simulator Bundle
- Fig. 7 Heated Fuel Rod Simulator
- Fig. 8 Unheated Fuel Rod Simulator
- Fig. 9 QUENCH Test Bundle, TC Instrumentation and Rod Designation
- Fig. 10 QUENCH Test Section, TC Elevations
- Fig. 11 TC Instrumentation of the Test Bundle
- Fig. 12 TC Attachment on the Cladding
- Fig. 13 TC Fastening Concept for the QUENCH Test Rods
- Fig. 14 QUENCH-01 Test Conduct
- Fig. 15 QUENCH-01, Overview, Temperature TCRC 13
- Fig. 16 Test QUENCH-01, Pre-Oxidation Phase
Axial Temperature (at 6000 s) and Axial Oxide Profile
- Fig. 17 QUENCH-01, Transient + Quench Phase, Temperature at 950 mm
- Fig. 18 QUENCH-01, Transient + Quench Phase, Temperature at 1150 mm
- Fig. 19 QUENCH-01, Transient + Quench Phase, Gas temperature
- Fig. 20 QUENCH-01, Quenching Phase, Quench water flow rate
- Fig. 21 QUENCH-01, Quenching Phase, Temperatures
- Fig. 22 QUENCH-01, Quenching Phase, Temperature TFS 2/17, 1350 mm
- Fig. 23 Evaluation of Quench Rate, Example
- Fig. 24 QUENCH-01, Quenching Phase, Temperatures TFS 2/1 at – 250 mm,
TFS 2/6 at 250 mm

- Fig. 25 QUENCH-01, Quenching Phase, Temperatures TFS 2/17 at 1350 mm, TFS 2/2 at -150 mm, TFS 2/7 at 350 mm
- Fig. 26 QUENCH-01, Quenching Phase, Temperatures TFS 5/17 at 1350 mm, TFS 5/9 at 570 mm
- Fig. 27 QUENCH-01, Quenching Phase, Temperatures TFS 5/14 at 1050 mm, TFS 5/6 at 250 mm
- Fig. 28 QUENCH-01, Quenching Phase, Temperatures TFS 5/16 at 1250 mm, TFS 5/4/180 at 50 mm
- Fig. 29 Test QUENCH-01, Cladding thermocouples compared to shroud thermocouples at 50 mm elevation with respect to the onset of quenching
- Fig. 30 Test QUENCH-01, Quench rate evaluated from temperatures (onset of quenching) of thermocouple pairs fixed at different rods at elevations located closest to each other
- Fig. 31 Test QUENCH-01, Temperature at onset of quenching as a function of elevation
- Fig. 32 Test QUENCH-01, Onset of quenching as a function of elevation
- Fig. 33 Test QUENCH-01, Onset of cooling as a function of elevation
- Fig. 34 Test QUENCH-01, Temperature at onset of cooling as a function of elevation
- Fig. 35 QUENCH-01, Pre-oxidation Phase, H₂ concentration
- Fig. 36 QUENCH 01, Quench Phase, H₂ production rate
- Fig. 37 QUENCH-01, Pre-oxidation, transient, and quench phase Hydrogen measurement and data of the facility
- Fig. 38 QUENCH 01, Quench phase, Hydrogen measurement and data of the facility
- Fig. 39 QUENCH 01, Electric and chemical power during the transient and quench phase
- Fig. 40 QUENCH 01, Absorbed hydrogen in the remaining Zry-4 metal of cladding, shroud, and corner rod and oxide layer thickness
- Fig. 41 Cut-out of an Observation Window at the Shroud, Schematic
- Fig. 42 QUENCH-01, Test Bundle, Cut-out of Shroud and Rod Removal (Top View)
- Fig. 43 QUENCH-01, Posttest view of the bundle

- Fig. 44 QUENCH-01, Post-Test, Cladding Breaches in the Region of 900 mm
- Fig. 45 Sectioning of Test Bundle QUENCH-01
- Fig. 46a QUENCH 01 – Cross sections at elevations given
- Fig. 46b QUENCH 01 – Cross sections at elevations given
- Fig. 46c QUENCH 01 – Cross sections at elevations given
- Fig. 46d QUENCH 01 – Cross sections at elevations given
- Fig. 47 Horizontal cross section of the bundle at elevation 913 mm
- Fig. 48 Horizontal cross section of the bundle at axial elevation 913 mm
- Fig. 49 Macroscopic appearance of one fuel rod simulator at different bundle elevations
- Fig. 50 Oxidation of Zircaloy cladding at different axial bundle elevation
- Fig. 51 Oxidation of crack surfaces which formed during flooding
- Fig. 52 Oxidation of crack surfaces which formed during flooding quenching
- Fig. 53 Oxidation of the outer and inner Zircaloy shroud surfaces
- Fig. 54 Localized, increased oxidation of Zircaloy cladding and rod surfaces
- Fig. 55 External and internal Zircaloy cladding tube oxidation of the central rod
- Fig. 56 Trough-wall crack formation in cladding tube of central rod
- Fig. 57 Physico-chemical behavior of the grid spacer an cladding tubes
- Fig. 58 Oxidation of Zircaloy cladding tubes and grid spacer
- Fig. 59 Localized, increased oxidation of the cladding inner surface
- Fig. 60 Oxidation of crack surfaces which formed during flooding
- Fig. 61 Oxidation behavior of the wire thermocouples
- Fig. 62 Oxidation of Zircaloy cladding tubes
- Fig. 63 Oxide layer thicknesses at bundle elevation 573 mm
- Fig. 64 Oxide layer thicknesses at bundle elevation 763 mm
- Fig. 65 Oxide layer thicknesses at bundle elevation 913 mm
- Fig. 66 Oxide layer thicknesses at bundle elevation 1000 mm

- Fig. 67 Oxide layer thicknesses at bundle elevation 1163 mm
- Fig. 68 Oxide layer thicknesses of Zircaloy cladding tubes
- Fig. 69 Oxide layer thicknesses of cladding tubes at different bundle elevations
- Fig. 70 Oxide layer thicknesses distribution at various axial bundle elevations
- Fig. 71 Oxide layer thicknesses of the Zircaloy rods before and after the quench test
- Fig. 72 Oxide layer thicknesses versus bundle elevation of various components after the quench test
- Fig. 73 Axial temperature and oxide layer thickness profiles at various times of an anticipated LOOP in a commercial reactor
- Fig. 74 Nodalization of the QUENCH facility for SCDAP/RELAP5
- Fig. 75 Pre-test calculation of power, clad temperatures, oxide layer thickness, hydrogen production rate, and cumulated hydrogen mass
- Fig. 76 Comparison of measured and calculated temperature developments (original modelling)
- Fig. 77 Power, calculated clad temperatures and oxide layer thickness, comparison of measured and calculated hydrogen production rate and cumulated hydrogen mass (original modelling)
- Fig. 78 Comparison of measured and calculated temperature developments ($T_{in} = 700 \text{ K}$)
- Fig. 79 Comparison of measured and calculated axial temperature profiles ($T_{in} = 700 \text{ K}$)
- Fig. 80 Comparison of measured and calculated temperature developments ($T_{in} = 700 \text{ K}$, $R_0 = 4.2 \text{ m}\Omega$)
- Fig. 81 Comparison of measured and calculated axial temperature profiles ($T_{in} = 700 \text{ K}$, $R_0 = 4.2 \text{ m}\Omega$)
- Fig. 82 Power, calculated clad temperatures and oxide layer thickness, comparison of measured and calculated hydrogen production rate and cumulated hydrogen mass ($T_{in} = 700 \text{ K}$, $R_0 = 4.2 \text{ m}\Omega$)
- Fig. 83 Comparison of measured and calculated axial temperature and oxide layer thickness profiles and calculated hydrogen production rate ($T_{in} = 700 \text{ K}$, $R_0 = 4.2 \text{ m}\Omega$)

Appendix

- Fig. A-1 Explanation of terms used in the tables of the appendix
- Fig. A-2 Gas flow delay measurements under steam/argon atmosphere at 1000 K
- Fig. A-3 MKS flow meter calibration with helium
- Fig. A-4 MKS flow meter calibration for H₂ using N₂

Contents

1	Introduction	1
2	Description of the Test Facility	3
3	Test Bundle Assembly	5
4	Test Bundle Instrumentation	7
5	Hydrogen Measurement Devices	8
6	Data Acquisition and Process Control	10
7	Test Conduct	11
8	Test Results	12
8.1	Temperature Measurements	12
8.2	Hydrogen Measurements	14
8.2.1	Hydrogen Measurements by the Caldos System	14
8.2.2	Mass Spectrometer Measurements	15
9	Posttest Examination	16
9.1	Posttest Appearance	16
9.2	Hydrogen Absorbed by Zircaloy	16
9.3	Sectioning of the Test Bundle	18
9.4	Metallographic Examination	18
10	Calculational Support	21
10.1	Reactor Specific Conditions	22
10.2	Parameters Specific for the QUENCH Facility	23
10.3	Post-test Calculations	26
10.4	Conclusions Depending on the Calculational Support	29
11	References	31
12	Acknowledgements	32
	Appendix	133

1 Introduction

The most important accident management measure to terminate a severe accident transient in a Light-Water Reactor (LWR) is the injection of water to cool the uncovered degraded core. Analysis of the TMI-2 [1] accident and the results of integral out-of-pile (CORA) [2] and in-pile experiments (LOFT [3], PHEBUS, PBF) have shown that before the water succeeds in cooling the fuel pins there will be an enhanced oxidation of the Zircaloy cladding that in turn causes a sharp increase in temperature, hydrogen production and fission product release. In the CORA BWR-type tests, additional energy and hydrogen production was caused by a steam reaction with the remnant B_4C absorber (B_4C oxidation in steam is more exothermic and produces more hydrogen per gram material than Zircaloy does) [4].

Besides, quenching is considered a worst-case accident scenario regarding hydrogen release to the containment. For in- and ex-vessel hydrogen management measures one has to prove that the hydrogen release rates and total amounts do not exceed safety-critical values for the considered power plant. It is important that the hydrogen generation rate is known so that accident mitigation measures can be designed appropriately:

- Passive autocatalytic recombiners require a minimum hydrogen concentration to start. Moreover, they work slowly, and their surface area and their position in the containment have to be quantified carefully.
- The concentration of hydrogen in the containment may be combustible for only a short time before detonation limits are reached. This limits the period during which igniters can be used.

The physical and chemical phenomena of the hydrogen release are, however, not sufficiently well understood. Presently it is assumed new metallic surfaces by cracking and fragmentation of the oxygen-embrittled cladding tubes are formed as a result of the thermal shock during flooding and their influence on enhanced oxidation and hydrogen generation. In most of the code systems describing severe fuel damage, the quench phenomena are either not considered or only modeled in a simplified empirical manner.

No models are yet available to predict correctly the thermal-hydraulic or the clad behaviour of the quenching processes in the CORA and LOFT LP-FP-2 tests. No experiments have been conducted that are suitable for calibrating the existing models. Since the increased hydrogen production during quenching cannot be determined on the basis of the available Zircaloy/steam oxidation correlations, new experiments are therefore necessary. An extensive experimental database is needed as a basis for model development and code improvement.

The Forschungszentrum Karlsruhe has therefore started a QUENCH program on the determination of the hydrogen source term. The main objectives of the QUENCH program are:

- The provision of an extensive experimental database for the development of detailed mechanistic fragmentation models,
- The examination of the physico-chemical behavior of overheated fuel elements (core) under different flooding conditions,
- The provision of an improved understanding of the effects of water injection at different stages of a degraded core,
- The determination of cladding failure criteria, cracking of oxide layers, exposure of new metallic surfaces to steam which are currently supposed to result in renewed temperature escalation and hydrogen production, and
- The determination of the hydrogen source term.

The experimental part of QUENCH program began with small-scale experiments with short Zircaloy fuel rod segments [10]. On the basis of these results well-instrumented large-scale bundle experiments experiments with fuel rod simulators under nearly adiabatic conditions are performed in the newly erected QUENCH facility at FZK because for a number of questions single-rod experiments are not representative. The parameters of the bundle test program are (see [Table 1](#)): Quench medium, i.e. water or steam, fluid injection rate, cladding oxide layer thickness, and the starting temperature for quenching.

This report describes the test facility and the test bundle, and the main results of the QUENCH-01 experiment. In addition, one section is dedicated to the calculational support performed with the SCADAP/RELAP5 computer code.

2 Description of the Test Facility

The QUENCH test facility consists of the following groups:

- the test section with the fuel element simulators
- the electric power supply for the test bundle heating
- the water and steam supply system
- the argon gas supply system
- the hydrogen measurement devices
- the process control system
- the data acquisition system.

A simplified flow diagram of the QUENCH test facility is given in [Fig. 1](#). The main component of the facility is the test section with the test bundle ([Fig. 2](#)). The superheated steam from the steam generator and superheater together with argon as the carrier gas enters the test bundle at the bottom end. The steam that is not consumed, the argon, and the hydrogen produced in the zirconium-steam reaction flow from the upper bundle outlet via a water-cooled off-gas pipe to the condenser ([Figs. 1 and 3](#)). Here the steam is separated from the volatile gases argon and hydrogen. During the quench phase the quench water enters the test bundle at the bottom via a separate line and argon is injected at the upper end of the test bundle to provide a carrier gas for the hydrogen to be transported to the H₂ detection systems.

The design characteristics of the test bundle are given in [Table 2](#). The test bundle is made up of 21 fuel rod simulators, each with a length of approximately 2.5 m, and of four corner rods. The fuel rod simulators are held in their positions by five grid spacers, four of Zircaloy, and one of Inconel in the lower electrode zone. The cladding of the fuel rod simulators is identical to that used in LWRs with respect to material and dimensions (Zircaloy-4, 10.75 mm outside diameter, 0.725 mm wall thickness). The rods are filled with argon to approx. 2.2 bar, i.e. to a pressure slightly above the sys-

tem pressure. The gas filling of all rods is realized by a channel-like connection system inside the lower insulation plate. Twenty fuel rod simulators are heated electrically over a length of 1024 mm, the one unheated fuel rod simulator is located in the center of the test bundle.

The unheated fuel rod simulator ([Fig. 8](#)) is filled with ZrO_2 pellets (bore size 2.5 mm ID). For the heated rods 6 mm diameter tungsten heating elements are installed in the center of the rods and are surrounded by annular ZrO_2 pellets ([Fig. 7](#)). In the axial direction the tungsten heater is located in the central part and connected to electrodes made of molybdenum and copper at each end of the heater. The molybdenum and copper electrodes are joined by high-frequency/high-temperature brazing performed under vacuum. For electrical insulation the surfaces of both types of electrodes are plasma-coated with 0.2 mm ZrO_2 . To protect the copper electrodes and the O-ring-sealed wall penetrations against excessive heat they are water-cooled (lower and upper cooling chamber). Sliding copper contacts at the top and bottom of the copper electrodes are used to make contact to the cables connected to the electric power supply (DC). The total heating power available is 70 kW, distributed among the two groups of heated rods with 35 kW each. The first group consists of the inner eight rods (rod numbers 2 – 9), the second group consists of the outer twelve rods (rod numbers 10 – 21).

The four corner positions of the bundle are occupied by three solid zircaloy rods with a diameter of 6 mm, and one Zry tube (6 \varnothing x 0.9 mm) for gas injection purposes ([Fig. 6](#)). The positioning of the four corner rods avoids an atypical large flow cross section at the outer positions and hence helps to obtain rather a uniform radial temperature profile. One Zry rod can be pulled out to determine the axial oxide thickness profile after pre-oxidation. This profile is then compared to that of another rod which was exposed to oxidation during the whole experiment.

The lower boundary for the lower cooling chamber is an Al_2O_3 plate for thermal insulation, sealed to the system by O-shaped rings. The upper boundary of the cooling chamber is a sealing plate of stainless steel. The bundle design at the top is similar. Also here an insulation plate made of plastic (PEEK) forms the top of the upper cooling chamber, and a sealing plate of Al_2O_3 is the lower boundary of the cooling chamber (see [Fig. 7](#)).

In the region below the upper Al_2O_3 plate the copper electrode is connected firmly to the cladding. This is done by hammering the cladding onto the electrode with a sleeve of boron nitride put between electrode and cladding for electrical insulation. Movement of the cladding tube relative to the electrodes and the tungsten heater, respectively, is possible as a result of temperature changes. The fixed point between cladding and electrode is in the test bundle region below the upper Al_2O_3 plate (hammered zone). The axial position of the fuel rod simulator in the test bundle (fuel element simulator) is provided by a groove and a locking ring in the top Cu electrodes. A split ring supported by the so-called header plate is placed into this groove. Referred to the test bundle the fixing of the fuel rod simulators is located directly above the upper edge of the upper insulation plate. So, during operation the fuel rod simulators are allowed to expand downwards. Clearance for expansion of the test rods is provided in the regions of the lower insulation plate. Relative movement between cladding and internal heater/electrode, however, can only take place in the region of the lower insulation plate.

The test bundle is surrounded by a 2.38 mm thick shroud made of Zircaloy with a 35 mm thick ZrO_2 fiber insulation and an annular cooling jacket whose walls are made of stainless steel (Fig. 6). The 7 mm annulus of the cooling jacket is cooled by a countercurrent argon flow. Above the heated zone, i.e. above the 1024 mm elevation there is no ZrO_2 fiber insulation to allow for higher radial heat losses. This region of the cooling jacket is cooled by a countercurrent water flow (Figs. 2 and 10). Both the lack of ZrO_2 insulation above the heated region and the water cooling force the axial temperature maximum downward.

3 Test Bundle Assembly

The test section consists of three subassemblies pre-assembled separately. One subassembly comprises the cooling jacket with the bundle head casing; the second subassembly includes the instrumented shroud with the bundle foot; and the third subassembly is composed of the instrumented test bundle with the bundle head. The test bundle and the shroud, including the respective thermocouples, must be replaced for each experiment. The instrumentation of the bundle head and the foot as well as the cooling jacket, however, remains unchanged.

Assembling the test bundle is a very complicated and difficult procedure. First of all, the bundle structure consisting of the head and the base plate of the bundle, and the spacers, is built up from the central rod and two edge rods in a horizontal position on a special assembly device. Then, one by one, starting from the inside, the rods are slid through the thermal shield, i.e. ceramic plate in the bundle head, into the bundle structure, and the thermocouples are added. Only after a leak test in the bundle base plate (He leak test) after each rod insertion – the rods and the thermocouples are sealed with O-rings in the base plate – the thermocouples are attached to the rod. The rods and the thermocouples are checked electrically after each assembly step (insulation resistance and contact resistance).

In the bundle head, the rods are sealed by high-temperature O-rings that are located in a ceramic plate (Al_2O_3). Then the insulating plate made of a polymer (PEEK) is installed, again with O-ring seals. Also this assembly step requires extensive leak tests.

Finally, the rods are attached to the upper edge of the insulating plate by means of an arrangement consisting of a groove and a snap ring, and the power supply leads for the heaters are installed.

Assembling the shroud is slightly less problematic than assembling the bundle. First of all, the shroud is bolted to the bundle foot. Once the thermocouples have been attached, the shroud is insulated by ZrO_2 shells, installed in the cooling jacket, and this is followed by a leak test. As in the bundle assembly step, electrical tests of the thermocouples must be conducted after each assembly step.

Now the cooling jacket and the bundle head casing are screwed together, installed in the test vessel, and connected to various supply lines (steam supply, offgas pipe, quench line, gas pipe, and cooling water pipe). Graphite seals have proved to work well in numerous connections, especially at high temperatures.

Prior to installation, the bundle and shroud are turned into the vertical position, lowered into the test vessel from the top by means of the hall crane, and the bundle head is bolted to the bundle head casing. Next, the insulating plate, which is the outside face of the bundle foot cooling chamber, is assembled in a complicated procedure, and the power supply leads are slid onto the heaters by means of sliding con-

tact rings. Finally, cable connections are established between the electrodes and the power supply, and all measurement cables are connected.

4 Test Bundle Instrumentation

The test bundle is instrumented with 35 sheathed thermocouples attached to the cladding at different elevations between -250 mm and 1350 mm and at four different orientations (Figs. 9, 10, and 11). Two thermocouples are inserted in the center of the unheated fuel rod simulator, one thermocouple from the bottom and one from the top. The elevations of the 26 shroud thermocouples are from -250 mm to 1250 mm. In the lower bundle region, i.e. up to the 350 mm elevation NiCr/Ni thermocouples (1 mm outside diameter) are used for temperature measurement of rod cladding and shroud. The thermocouples of the hot zone are high-temperature thermocouples with W-5 Re/W-26 Re wires, HfO₂ insulation, and a duplex sheath of tantalum (internal)/Zircaloy (2.1 mm outside diameter). The leads of the thermocouples from -250 mm to 650 mm leave the test section at the bottom whereas the TCs above 650 mm penetrate the test section at the top. The wall of the inner tube of the cooling jacket is instrumented between -250 mm and 1150 mm with 22 NiCr/Ni thermocouples. Five NiCr/Ni thermocouples are fixed at the outer surface of the outer tube of the cooling jacket. A list of all instruments is given in Table 3.¹

The thermocouple attachment technique is illustrated in Figs. 12 and 13. The TC tip is held in place by two clamps of Zr. As these clamps are prone to oxidation and embrittlement in a steam environment an Ir – Rh wire of 0.25 mm diameter is used for support. This wire was tested together with other materials and was best with respect to melting point and handling performance [5]. As indicated in Fig. 13 the wire is used for the experiments with pre-oxidation only. In a test without pre-oxidation the wire material would react with the cladding because there would be no protection of the cladding by a ZrO₂ layer.

¹ Please notice that for measurement levels 8 - 10 the thermocouples in the bundle and shroud are displaced by 20 mm with respect to the thermocouples in the cooling jackets.

5 Hydrogen Measurement Devices

The hydrogen is analyzed by two different measurement systems: (1) a mass spectrometer located at the off-gas pipe behind the test section, (2) a hydrogen detection system "Caldos 7 G" (Fig. 4) located in a bypass to the off-gas line behind the condenser. The argon and hydrogen pass the Caldos hydrogen detection system in a bypass line (Fig. 1) before they exit to the outside. Due to these different locations the mass spectrometer responds almost immediately whereas the delay time of the Caldos system is about 100 s (see Appendix). The principle of measurement of the Caldos system is based on the different heat conductivities of different gases. The Caldos device used is calibrated for the hydrogen-argon gas mixture. To avoid any moisture in the analyzed gas a gas cooler, which is controlled at 296 K, and a drier (molecular sieve, zeolite) are connected in series before the gas analyzer (Fig. 4). The response of the gas analyzer is documented to be 2 s, i. e. in this time 90 % of the final value is reached. In contrast to the mass spectrometer the Caldos device only measures the hydrogen content. Gases other than H₂ cannot be analyzed by this system.

The mass spectrometer (MS) "BALZERS GAM 300" used is a completely computer-controlled quadrupole MS with an 8 mm rod system which allows quantitative measurement of gas concentrations down to about 10 ppm. The gas specimen for the MS measurement is taken at the end of the off-gas pipe in front of the orifice and the condenser (Figure 5a). The sampling tube which is inserted in the off-gas pipe and which has several holes at different elevations should guarantee a representative sampling gas composition (Figure 5b). To avoid steam condensation in the gas pipes between the sampling position and the MS the temperature of the gas at the MS inlet is controlled by a heat exchanger to be between 110 °C and 150 °C (the upper operating temperature of the MS inlet valves). Therefore, in principle the MS can analyse the steam production rate. But during the test QUENCH-01 the penetration of the sampling tube through the cooling jacket of the off-gas pipe (Figure 5b) caused partial condensation of steam at this position. After the test, the sampling tube has been modified. An additional tube with an internal heater was inserted into the original tube with an insulating gap between the both. This arrangement was tested to work well, i. e. steam condensation is prevented. So, starting with test QUENCH-02, quantitative analysis of the steam production during the quench phase will be also possible.

Additionally, the MS is used to control the atmosphere in the facility, e. g., to monitor the gas composition at the beginning of the test. If the fuel rod simulators are filled with a tracer gas in addition to the argon (e. g. helium or krypton) the tracer gases can be measured and used as an indicator for the first cladding failure. In test QUENCH-01 the fuel rod simulators were filled with pure argon, i. e. without any tracer. Therefore, the concentrations of the following species were continuously measured by the mass spectrometer during all test phases: argon, hydrogen, steam, nitrogen, and oxygen.

The temperature and pressure of the analysed gas are measured near the inlet valve of the MS. The MS is calibrated for hydrogen with well-defined argon/hydrogen mixtures and for steam with mixtures of argon and steam supplied by the steam generator of the QUENCH facility. Contrary to the original plan to feed the MS off-gas back into the facility, it is released to the atmosphere because the amount of hydrogen taken out of the system is negligible.

For the Caldos device as well as for the MS the hydrogen mass flow rate is calculated by referring the measured H₂ concentration to the known argon mass flow rate according to equation (1):

$$\dot{m}_{H_2} = \frac{M_{H_2}}{M_{Ar}} \cdot \frac{C_{H_2}}{C_{Ar}} \cdot \dot{m}_{Ar} \quad (1)$$

with M representing the molecular masses, C the concentrations and \dot{m} the mass flow rates of the corresponding gases.

With an argon-hydrogen (two-component) mixture that in fact exists at the location of the Caldos analyzer equation (1) can be written as follows

$$\dot{m}_{H_2} = \frac{M_{H_2}}{M_{Ar}} \cdot \frac{C_{H_2}}{1 - C_{H_2}} \cdot \dot{m}_{Ar} \quad (2)$$

6 Data Acquisition and Process Control

A PC-based control and data acquisition system is used in the QUENCH experimental facility. Data acquisition, data storage, online visualization as well as process control, control engineering and system protection are accomplished by three computer systems that are linked in a network.

The data acquisition system allows the acquisition of about 200 measurement channels at a maximum frequency of 25 Hz per channel. The experimental data and the date and time of the data acquisition are stored as raw data in the binary format. After the experiment the raw data are converted into SI units and stored as ASCII data.

For process control, a system flow chart with the most important actual measurement values selected is displayed on the computer screen. Furthermore, the operating mode of the active components (pumps, steam generator, superheater, DC power system, valves) is indicated. Blocking systems and limit switches ensure safe plant operation. Pre-defined operating test phases, e.g. heatup or quenching phases, can be pre-programmed and started on demand during the experiment. The parameter settings of the control circuits and devices can be modified online.

Online visualization allows to observe and to document the current values of selected measurement positions in the form of tables or graphics. Eight diagrams with six curves each can be displayed as graphics. This means that altogether 48 measurement channels can be displayed online and selected during the course of the experiment.

The data of the test facility and of the mass spectrometer (MS) are stored on different computers. Both PCs are synchronized by radio-controlled clocks. The data files have different structures: the MS data are stored in one file starting with time zero, whereas the acquisition of the data of the facility is restarted at every new test phase. Table 6 contains the differences between the time scales of the two data acquisition systems for comparison purposes.

7 Test Conduct

Test QUENCH-01 ([Fig. 14 and 15](#)) consisted of (a) a heatup phase, (b) a phase at ca. 1000 K in which well-defined amounts of helium were injected into the test section at 700 mm elevation to determine delay times for the hydrogen transport to the mass spectrometer and the Caldos system, (c) a second heatup period, (d) a pre-oxidation phase, (e) a transient phase, and (f) a quench phase. All phases except the quench phase were conducted with an argon (3 g/s) plus steam flow (3 g/s). The accuracy of the argon flow measurement is discussed in the Appendix. More detailed information on the test conduct of QUENCH-01 is provided in [6].

The pre-oxidation phase started after a ramp rate of 0.5 K/s and lasted for 8280 s at maximum temperatures of about 1400 K - 1600 K to obtain the required maximum oxide layer thickness of 300 μm at the 900 mm elevation. The electrical power was adjusted such that the hydrogen production rate, measured on-line with the mass spectrometer, was fairly constant. This control allowed to minimize the pre-oxidation time for such a large bundle and at the same time to avoid a premature temperature escalation. At about 6000 s into the pre-oxidation phase one of the solid Zircaloy rods was withdrawn from the hot bundle to check the extent of oxidation achieved immediately by means of an eddy current device. [Fig. 16](#) shows the axial temperature profile at that time. At the end of the pre-oxidation phase the test bundle was ramped at 0.5 K/s to a maximum rod cladding temperature of 1870 K (extrapolated at 950 mm) and a maximum shroud temperature of 1800 K at the 950-mm elevation.

For the quench phase the fluid temperatures in the inlet pipe and at the bundle outlet are shown in [Fig. 19](#). Initiation of the quench phase was done in the following way. The steam and argon flow through the test section were turned off, argon was injected at the upper end of the test bundle, and the lower plenum was filled with quench water at a high rate of 80 g/s. Thirty seconds later the electrical power was reduced from 20 kW to 4 kW (representing the decay heat level) within 15 s, and the bundle was flooded with 52 g/s H_2O for 89 s, until water reached the bottom of the upper plenum ([Fig. 20](#)). The oscillations seen in [Fig. 20](#) stem from the quench water pump. They are damped before the inlet pipe. The large oscillations will be reduced in the next experiments. The injection rate corresponds to a velocity of 1.7 cm/s in the bundle, based on the quench water flow F 104 of 187 l/h and the coolant channel

cross section of 30 cm². The experiment was terminated by shutting off the electric power and the quench water and argon flow. Altogether the amount of water injected at a rate of 80 g/s and 52 g/s was 2.4 l and 4.6 l, respectively, so that the total amount of water injected was 7.0 l.

Altogether 19 high-temperature thermocouples had failed as listed in [Table 7](#). Five TCs had been damaged during handling, i.e. prior to the test. 14 TCs had failed during the experiment due to the severe oxidation (5 TCs during pre-oxidation, 4 TCs during the transient, and 5 TCs during the quench phase).

8 Test Results

8.1 Temperature Measurements

[Fig. 17](#) gives the temperature history of the transient phase at 950 mm with a maximum temperature of about 1800 K. The centerline thermocouple TCRC13 shows similar behavior as that of the shroud thermocouples. During quenching, however, the shroud thermocouples exhibit a slightly faster response than TCRC13. As all cladding thermocouples failed at this elevation the maximum cladding temperature is not known and had to be extrapolated at the 950 mm elevation resulting in 1870 K. At the shroud a maximum temperature of 1800 K was reached at 1150 mm, an elevation well above the shroud insulation where radial heat losses are larger than in the insulated region ([Fig. 18](#)). The high heatup rate of 1.5 K/s at 1150 mm suggests that the shroud material had experienced a slight temperature escalation.

As a consequence of the shut-off of the argon/steam flow (initiation of the quenching) the rod temperatures increased at lower elevations up to the middle of the heated zone but dropped at the upper elevations. This is demonstrated with [Fig. 21](#). The temperature drop for the temperature of the thermocouple TFS 2/17 at 1350 mm is shown in detail in [Fig. 22](#).

During the reflood phase the bundle appeared to quench steadily with no evidence of any temperature excursion. Toward the end of the flooding phase when all rod cladding temperatures were already at the lowest level the thermocouple signals of the upper elevations exhibit a renewed temperature peak (see [Fig. 21](#) and [Figs. 25](#)

through 28). The shroud temperatures of the upper regions do not show this behavior (see 1150 mm elevation in Fig. 18).

As can be deduced from the previous figures cooling of the test bundle occurs in two stages, firstly a cooling period (period before the water level is at a given axial location) with a moderate cooldown rate then secondly a very pronounced cooldown. The latter period is caused by a drastic improvement in heat transfer. The beginning of this period is called “quench temperature” and “onset of quenching”, respectively (see Fig. 23). Figure 23 provides the definitions for onset of cooling, onset of quenching, and injection and flooding rate used in this report. It must be noted that the cladding temperatures experience the quenching before wetting of the test rods takes place. This fact that rods with cladding external surface thermocouples quench earlier than bare rods was demonstrated in various flooding experiments, e. g. in the PBF Thermocouple Effects Tests at INEL (Idaho National Engineering Laboratory). Therefore, quench temperature indicates a first local wetting of the rods at the locations of cladding thermocouples. It does not mean that the water level is at the axial location of the test rods at that time. The quench temperature “seen” by the shroud thermocouples occurs later in time as is demonstrated for the 50-mm elevation in Fig. 29.

The precursory cooling (before quenching) is not affected by the rod surface thermocouples. This “onset of cooling” occurs simultaneously, namely within one second, for all axial positions (Fig. 33). This happened exactly at the time when the quench water level (saturation temperature) was at -250 mm which was indicated by the thermocouple TFS 2/1. The pertinent temperatures are given in Table 4 and Fig. 34. The quench temperatures determined by the cladding temperature measurements were between 641 K at the -250 mm and 1199 K at the 1150 mm elevations as shown in Table 4 and Fig. 31. The axial profile of the onset of quenching can be seen in Fig. 32. The function of elevations appears to be more increasing from the bottom of the heated zone (0 mm) to approximately 500 mm (middle of the heated zone) than from there to the top of the heated zone. It seems that quenching occurs almost simultaneously in the upper (hot) region of the test bundle. Taking the quench temperatures from the shroud thermocouple readings somewhat lower quench temperatures are obtained from the bottom of the test section (-250 mm) to 550 mm (middle of the heated zone). In the upper bundle section quench temperatures measured by the shroud thermocouples seen to be even higher than those evaluated from the clad-

dine thermocouples (see [Table 5](#) in comparison to Table 4). Cladding thermocouples at the instrumentation levels 12, 13, and 15, however, failed so that a direct comparison is not possible.

The evaluation of the so-called quench rate is of great interest. The quench rate is a measure of how fast the test rods are flooded with water or clearly wetted by the two-phase flow consisting of water droplets and steam. The determination of the quench rate is illustrated by an example in [Fig. 23](#) (lower schematic) using pairs of thermocouples located on the same test rod in taking the distance between a pair of thermocouples on the same test rod and relating it to the times of the onset of quenching. The quench rates evaluated for thermocouple pairs fixed at one rod, namely at rods 4, 6, 10, 18, and 21 ([Figs. 24 through 28](#)) were between 1 cm/s (rod 6, -150/350 mm) and 2.9 cm/s (rod 10, 570/1350 mm). The quench rates evaluated from temperatures (onset of quenching) of thermocouple pairs fixed at different rods, at elevations closest to each other lie then between ca. 0.4 and 7 cm/s with the majority of the rates between ca. 0.4 and 1 cm/s as is illustrated in [Fig. 30](#). The quench rates determined from the shroud thermocouple signals at elevations closest to one another lie in the same range, i. e. between 0.4 and 4.7 cm/s (Table 5). In any case, the quench rates seem to have the tendency to be larger at the upper elevations. The maximum cool-down rates, i.e. temperature decreases that occur during quenching, on the basis of the cladding thermocouple responses were determined to be between 100 and 430 K/s with the higher rates at the upper elevations of 1250/1350 mm (see Table 4).

8.2 Hydrogen Measurements

8.2.1 Hydrogen Measurements by the Caldos System

As [Fig. 35](#) shows the maximum hydrogen production rate during the pre-oxidation phase was about 3 vol % H₂ which corresponds to 3 - 4 mg/s. The maximum amount of hydrogen was produced during this phase, i. e. 26 g determined by the Caldos device. In addition, 8 – 9 g are associated with the transient + reflood phase ([Fig. 36](#)). The contribution from this phase is relatively small because no temperature excursion took place.

8.2.2 Mass Spectrometer Measurements

Due to partial condensation of the steam near the MS sampling position at the off-gas pipe of the facility, the steam flow rate could not be evaluated quantitatively as was explained in the section describing the hydrogen measurement devices. The concentrations of nitrogen and oxygen were measured to be below 0.02 and 0.002 vol%, respectively, during the whole test.

The integral hydrogen releases at low temperatures (< 1000 K) during the heat-up phase and during the delay time measurements were 0.5 g and 0.4 g, respectively.

During the pre-oxidation phase, the hydrogen measurement was used to control the oxidation process and the electrical power on-line. The rate and the integral value of hydrogen release were calculated continuously and compared with the results of the SCDAP/RELAP5 pre-test calculations. The power was increased stepwise in order to compensate the lower oxidation rate with increasing oxide layer thickness. This procedure worked very well, the maximum oxide layer thickness at the end of the pre-oxidation phase was measured to be 300 μm , which was exactly the target value. The hydrogen production rate was at a constant value of about 3 - 4 mg/s during the whole pre-oxidation phase. At about 4700 s a local temperature escalation which was rapidly suppressed by a decrease of the electrical power (see central diagram in [Fig. 37](#)) caused a slightly enhanced hydrogen release.

[Figure 37](#) shows the hydrogen production (rate and integral value) measured by the mass spectrometer and the CALDOS system together with some relevant data of the facility during the pre-oxidation, transient and quench phases. Altogether, 38 g of hydrogen were produced and released during these three phases. The hydrogen production rate and the integral value measured by the mass spectrometer correspond very well with data from the CALDOS system (34 - 35 g, see [Table 6](#)). The maximum hydrogen rate was 0.08 g/s during the transient/quench phase.

[Figure 38](#) presents the same data as [Figure 37](#), but zoomed in on the end of the transition phase and the quenching. The upper diagram shows two curves for the H_2 rate and integral H_2 release each of them according to two different evaluation algorithms, i.e. one curve is based on constant 3 g/s argon flow rate; and the other one is based on the measured argon flow rate which was slightly increased during the initiation of the quench phase (see lower figure). The hydrogen peak is initiated by an en-

hanced steam production due to the quench water flow into the lower head of the test section. Three sub-peaks can be identified. The first and largest sub-peak is turned around by the start of the power reduction from 20 kW to 4 kW. The third and smallest hydrogen sub-peak is connected with the end of the power reduction. The intermediate one may be caused by a temporary increase of the temperature of the upper part of the bundle at elevation 1250 and 1350 mm.

In general, the hydrogen production during the quench phase of about 3 g was very low compared to the results obtained during the commissioning tests (about 40 g) [9].

Based on the hydrogen production the chemical power was calculated and is compared to the electric power input in [Fig. 39](#). The contribution of the exothermal energy to the total energy is small in this experiment.

9 Posttest Examination

9.1 Posttest Appearance

To view the bundle after the test a window had to be cut into the shroud as illustrated with [Figs. 41 and 42](#). The post-test appearance of the test bundle shows no signs of any melt but significant oxidation of the bundle between 700 and 1100 mm elevation ([Fig. 43](#)). In this region the oxide layer is of gray color and some larger cracks in the cladding have formed ([Fig. 44](#)). The central rod that lacks the support of the central heating element (tungsten rod) is broken and pellets are found outside the rod cladding. The grid spacer (zircaloy) at 1050 mm is destroyed and parts of it relocated downward. The shroud is intact and undeformed. The region of the shroud above the heated zone that is without insulation exhibits a bronze-like color. This is the region where a slight temperature escalation of the shroud might have taken place. All rod cladding thermocouples in the hot region are destroyed (see also [Table 7](#)).

9.2 Hydrogen Absorbed by Zircaloy

Prior to the encapsulation of the test bundle fuel rod simulator #18 was removed from the bundle for further investigations, especially for the determination of the axial oxide layer thickness distribution and for the analysis of the hydrogen absorbed in the remaining Zircaloy-4 metal. For this reason the cladding tube was sectioned and

specimens were taken every 100 mm. Additionally, three specimens each from the shroud and from a 6 mm corner rod were taken at elevations 700, 900 and 1100 mm.

The hydrogen absorbed in the remaining Zircaloy-4 metal was analysed in the so-called LAVA facility which is an inductively heated furnace coupled with a mass spectrometer. Two-centimeter long cladding segments taken from rod #18 were heated for 20 minutes at about 1500 °C under a well-defined argon flow. The hydrogen released was measured by a mass spectrometer. Test measurements with Zr and Ti standard specimens have shown that the experimental error of these analyses is lower than 10 % in any case.

The results of both measurements are shown in [Figure 40](#). The oxide layer thickness distribution is discussed in detail later and is here only used for comparison reasons. Both curves obtained from the cladding tube (hydrogen absorbed and oxide layer thickness vs. axial elevation) show a similar shape, the hydrogen curve is only slightly shifted to higher elevations. The maximum value of the hydrogen absorbed is about 5 at-% which is far away from saturation with respect to SIEBERTS' law but near saturation of the α -phase with respect to the phase diagram Zr-H. It seems that most of the hydrogen is absorbed at that elevation where it is produced by steam oxidation of Zry-4. No indications were found for hydrogen uptake at higher parts of the bundle. Furthermore, it was estimated that no significant relocation of the hydrogen due to axial diffusion in the metal phase should have happened during quenching.

Some hydrogen was absorbed by the shroud and the 6 mm corner rods with a maximum amount of about 2.5 at-% in the hot zone.

An extrapolation of the data obtained at one cladding tube and three specimens each from the shroud and the 6 mm rod gives a value of about 1 g hydrogen absorbed by the whole bundle, which is only 3 % of the hydrogen totally produced during the test QUENCH-01.

9.3 Sectioning of the Test Bundle

To obtain cross sections a mould was set up horizontally and the bundle was filled with epoxy resin. For the encapsulation of the bundle the epoxy system Rütapox 0273 with the hardener designated LC (Epoxy resin and hardener manufactured by Bakelite GmbH, Iserlohn) was chosen based on the experience with the CORA test bundles. The epoxy showed some heating during the curing stage but the shrinkage effect was negligible. After epoxying the bundle the resin was allowed to harden for one week. A saw with a 2.0 mm-thick diamond blade (mean diamond size 138 μm) of 350 mm OD was used to cut the slabs at 1300 rpm. The sectioning map for test bundle QUENCH-01 is given in [Fig. 45](#) as an overview. The exact elevations are listed in [Table 9](#). Cross-section 1 can be taken as the as-received condition because it is located in the lower, i. e. unchanged, cold region. Numbers 2, 3, and 4 represent the hot region of the test section with the maximum temperatures and oxide layer thicknesses. Number 5 is located above the heated and insulated test section where the shroud temperature was at its maximum. No. 6 is above the shroud, and No. 7 was chosen to be taken at the 550 mm elevation. This location represents a thermocouple measurement point.

Five sections were selected for metallographic examination ([Table 9](#)) and had therefore to be polished. So, the samples were infiltrated by "Araldit" resin to close up residual voids, then ground and polished. The entire procedure of the preparation for the metallographic examination is given with [Table 10](#). The steps described in the list were performed using a semi-automatic machine with a closed water circuit for grinding and an automatic lubricant feeder for the polishing steps.

The cross sections (unpolished condition) are shown as bottom and top of the various bundle discs in [Figs. 46a through 46d](#).

9.4 Metallographic Examination

The physico-chemical state of the Zircaloy cladding material was examined and evaluated by light microscope and by scanning electron microscope examinations. Of special interest was the determination of the oxide layer thicknesses on the Zircaloy

cladding tubes and the shroud, the formation of through-wall cracks in the cladding tubes and the oxidation of the crack surfaces.

The original state of the bundle could be recognized at the lowest examined cross-section elevation of 573 mm, where one of Zircaloy grid spacers was located. [Figure 57](#) shows details of the grid spacer and the Inconel springs which keep the fuel rods in place. One of the fuel rods (# 18) was taken out for chemical examinations (oxide layer thickness and absorbed hydrogen in the cladding tube as function of the bundle elevation). The oxidation of the Zircaloy components at the 573 mm bundle elevation is very small as a result of the low bundle temperatures. The Inconel spring shows no evidence of any oxidation ([Figure 58](#)).

[Figures 47 and 48](#) show as an example details of the heated rods and the unheated central rod as well as the 6 mm Zircaloy rods at higher elevation (913 mm) within the hot zone. The Zircaloy cladding tubes are partially oxidized and cracked.

The formation and number of through-wall cracks depends on the thickness of the ZrO_2 oxide layer which determines the thicknesses of the oxygen-stabilized α -Zr(O) and the transformed β' -phase; the latter is the only ductile part of the "sandwich" structure. [Figures 49 and 50](#) show the extent of the cladding oxidation at three different axial bundle elevations of 763, 913, and 1000 mm. As a result of the axial temperature distribution within the bundle, the thicknesses of the various phases are different. No or only a few through-wall cracks form at ZrO_2 layer thicknesses $\leq 200 \mu m$ ([Figures 49 and 50](#)) since the remaining β' -phase is still present and sufficient thick to prevent them.

[Figure 50](#) shows in addition the oxidation of the crack surfaces which must have formed during flooding. [Figures 51 and 52](#) show different appearances of cracked cladding tubes at the cross-section elevation 913 mm. The reason for the formation of the needle-like structures in the α -Zr(O) has still to be clarified. SEM/EDX examinations of the chemical composition of needles indicate that they consist of ZrO_2 .

At some locations a strong internal localized cladding tube oxidation could be observed, independent on the examined bundle elevations ([Figures 54 and 55](#)). [Figure 55](#) (unheated rod) shows a similar external oxide layer cracking together with a rather strong internal cladding oxidation. Also at the elevation of 763 mm the crack surfaces

are oxidized. In addition, a pore-like structure in the cladding tube can be observed ([Figure 56](#)). The reason for the formation of these channels and the subsequent oxidation of their surfaces are not yet clarified. The white metallic phases in some parts of the cladding tube consist of a (Zr, Cr, Fe) alloy of variable chemical composition which contains different amounts of oxygen ([Figure 56](#), right picture).

The physico-chemical behavior of the Zircaloy cladding tubes at the upper bundle elevation of 1000 mm is shown in [Figures 59 and 60](#). One can recognize also localized internal cladding oxidation with through-wall cracks through the external and internal oxide layers. [Figure 60](#) shows details of the crack morphology.

The bundle elevation of 1163 mm is outside the heated region. The cross sections of the fuel rod simulators shows inside the cladding tubes the Mo electrodes ([Figure 62](#)). At this elevation the extent of cladding oxidation is small, therefore, no through-wall cracks have formed. At all elevations the central cladding tube is more oxidized than the other cladding tubes.

Beside the cladding tubes also the Zircaloy shroud was oxidized on its internal ($\approx 380 \mu\text{m}$, at the 913 mm bundle elevation) and external ($\leq 5 \mu\text{m}$) surface ([Figure 53](#)).

[Figure 54](#) (right photo) shows the extent of oxidation of the calibration rod. As a result of the smaller diameter (6 mm compared to 10.75 mm of the cladding tube) the oxide layer cracks at some locations of the circumference where then an increased localized oxidation takes place.

The behavior of the high-temperature thermocouples is depicted in [Figure 61](#). The outer Zircaloy cladding tube of the thermocouples is in hot bundle regions almost completely oxidized (right figure). The other thermocouple (left figure) which almost shows the original state must have relocated from cooler regions of the bundle.

The five examined cross-section elevations of 573, 763, 913, 1000 and 1163 mm were evaluated concerning the oxide layer thicknesses of all cladding tubes except that of fuel rod simulator # 18 which was taken out for detailed chemical examinations (hydrogen uptake). The results are given in [Figures 63 through 67](#) together with those of the two remaining Zircaloy rods. The evaluation of the oxide layer thicknesses versus axial bundle elevation was done for the central rod cladding tube, for the rod # 9 cladding tube, for the remaining 18 cladding tubes of the fuel element

simulator and the two remaining Zircaloy oxidation calibration rods of 6 mm diameter (Figure 68). One can recognize that the central cladding tube and the lower part (≤ 913 mm) of the cladding tube # 9 are more oxidized than the others (compared with the mean value). The bandwidth of the oxide layer thicknesses at the examined cross-section elevations for the 18 fuel rods is given in Figure 69. A three-dimensional plot of the oxide layer thickness distribution at the different examined cross-section elevations is given in Figure 70.

The Zircaloy rod (6 mm \varnothing) which was taken out of the hot bundle after pre-oxidation before quenching was examined with respect to oxide layer thickness over its total length. The result is shown in Figure 71 and compared with the oxide layer thickness of another Zircaloy rod which remained in the bundle over the whole test sequence. One can recognize that the maximum oxidation occurred at the bundle elevation of about 900 mm and that there is a pronounced oxide layer thickness increase during the transient heat-up and quench process.

The cladding tube of rod # 18 and a Zircaloy shroud strip were examined over their total length with respect to external and internal oxidation. The results are plotted versus axial bundle elevation in Figure 72 and compared with that of the Zircaloy rod oxidation. In all the various plots one can recognize the strongest oxidation of the bundle components in the very upper part of the heated zone (900 – 950 mm) at the transition to the unheated part. This observation is in agreement with the temperature measurements.

10 Calculational Support

Within FZK institutional R&D activities calculations have been made to define experimental parameters of the first quench experiment, QUENCH-01, and to interpret the experimental results after the experiment had been performed. For all calculations documented here the code SCDAP/RELAP5 (S/R5) mod 3.1 rel. F, made available for the planning of the QUENCH experiments, has been used. The improved model for heat transfer in the transition boiling region [7] and an adaptation of the CORA heater rod model to the conditions of the QUENCH facility are included in the FZK version of the programme.

10.1 Reactor Specific Conditions

The QUENCH experiments are performed to support the investigation of the consequences of severe accidents which may occur in commercial nuclear power reactors, and hence essential test parameters for the QUENCH experiments should be based on such accident conditions. One of the reactors for which these investigations are performed is the projected European Pressurised Water Reactor EPR. Among others loss of coolant (LOCA), loss of offsite power (LOOP), and station blackout (SB) accidents are considered as relevant scenarios, using S/R5. Especially the results for LOOP have been found useful to define important parameters, relevant for reactor conditions, for the quench phase of the QUENCH experiment.

In the LOOP scenarios it is assumed that the diesel engines become available about four hours after the power failure and reactor scram. In a parameter study flooding of the core is assumed to begin at different maximum core temperatures between 1700 K and 2300 K and with a different number of pumps of the emergency core cooling systems [8]. The results show that this is the temperature range that should be considered for investigations in the QUENCH facility. At the low end of this temperature range the consequences in the reactor are predicted to be rather benign with respect to hydrogen generation and related temperature increase in the rods, whereas at the upper end cooling of the overheated reactor core cannot always be guaranteed. Since the time for temperature increase in the reactor from 1700 K to 2300 K is only about two minutes, the accident sequence is very sensitive to the actual parameters, and some care should be spent on the definition of test parameters for the QUENCH facility. Because of the more severe consequences in a reactor quench experiments with high initial temperatures and low flow rates are expected to give more valuable information than other parameter combinations.

The results of the parameter study show further that before reflood is initiated temperatures and axial temperature increase in the lower part of the core are considerably lower than in the upper part. Representative axial temperature profiles at various times are shown in [Fig. 73](#). A representative value for the axial temperature increase before quenching is about 700 K/m in the upper part of the core, but it can reach much higher values at later times. When reflood is initiated at a given time, flooding velocities (velocity of the collapsed water level) vary between about 10 to 20 cm/s in the lower part of the core and 0.2 cm/s to 1 cm/s in the upper part because of the

very steep axial temperatures increase. Fig 73 also shows that the wide temperature range leads to an equally wide range of oxide layer thickness of about 50 μm to 300 μm . The pressure in the primary system of the reactor is about 1 MPa. During reflood a peak value of 3 to 4 MPa is reached.

Due to experimental limitations only quenching of the upper part of the core can be modelled in the QUENCH facility. To be representative for reactors like EPR and to investigate the parameter range which is more relevant for safety considerations the following data for the first quench experiment are suggested. A maximum oxide layer thickness of about 300 μm should be reached before quenching. The maximum temperature before quenching should be about 2000 K. After the pre-oxidation phase this temperature should be reached with a heat-up rate of about 1.0 K/s at the position of maximum temperature, when 1500 K are reached. The electrical power during the quench phase should be 4 kW to correspond to the decay heat in the reactor. The flooding velocity should be about 0.5 cm/s. Assuming a vaporisation of about 50 %, this corresponds to an injection rate of 30 g/s. The system pressure in the primary system of the reactor and the pressure peak value during reflood are the only relevant parameters which are outside the range that can be modelled in the QUENCH facility. The consequence of this shortcoming on calculations of the quench phase will be discussed later.

10.2 Parameters Specific for the QUENCH Facility

Some experimental parameters like the power history which must be known in advance to run a test successfully depend on the test facility. To determine such parameters pre-test calculations have been done. They are intended to suggest test parameters which depend on the very conditions of the QUENCH facility. As a basis the experience gained from post-test calculations for the commissioning tests IBS_02 and IBS_03 as reported in [9] is used.

The modelling of the QUENCH facility is shown in [Figure 74](#). Axially the heated part is discretized with ten 0.1 m long meshes. In the lower and upper unheated part 0.45 and 0.6 m, respectively, of the test section are considered, each by three meshes, assuming molybdenum as electrode material. In the radial direction the whole facility including the containment is modelled, because the ambient room temperature is the

only reliable boundary condition to calculate adequately the radial heat losses out of the bundle. The unheated rod, the two rows of rods to be heated independently, the inner and outer cooling jacket, and the containment are modelled as SCDAP components. In this way two-dimensional heat conduction within the structures and radiation between adjacent structures are taken into account. The bundle flow is represented by one channel. The off-gas pipe and the tubes for the water cooling are taken into account with their whole length of 3 m, including the orifice at the position where the gas sample for the mass spectrometer is taken and the orifice at the outlet of the off-gas pipe; the respective mass flows are modelled to be one-dimensional, the tubes are modelled as heat structures, thus taking into account radial heat transfer within the structures.

During the heat-up phase of the bundle the steam cannot be introduced from the beginning because of condensation at the cold surfaces, but it should be added to the argon flow as soon as possible for a quicker heat-up. Therefore the following scenario was assumed for the pre-test calculations. The argon mass flow in the bundle is constant at 3 g/s. The argon inlet temperature is assumed to increase from 300 K to 800 K within 100 s. Then 3 g/s steam at an inlet temperature of 800 K are added. The reference pressure at the bundle outlet is 2 bar during the whole calculation. The argon and the water cooling are counter-current flows with mass flow rates of 6 g/s and 100 g/s, respectively, and an inlet temperature of 300 K. The atmosphere in the containment and outside the containment are assumed to be stagnant, thus neglecting natural convection. The temperature at both ends of the heated rods are assumed to be 300 K during the whole calculation. All structure temperatures are set to an initial value of 300 K.

A power pulse and a plateau are assumed for the first 1200 s of the calculation to simulate a heat-up phase ([Fig. 75](#)), where elevated temperatures in the bundles are to be reached. The temperature must, however, be low enough to avoid oxidation. Then a second power pulse is applied to reach high temperatures for the pre-oxidation phase as quickly as possible. In this way one can avoid oxidation at low temperature which may lead to breakaway effects. A power plateau follows to achieve the requested oxidation of the rods. Afterwards a power transient is applied to reach the desired high rod temperatures before quenching. During the first part of the quench phase the power is reduced somewhat to reduce the escalation potential,

later on the bundle power is reduced to 4 kW. The rod powers for the inner and the outer heated rings are assumed to be equal.

Fig. 75 shows typical calculated results from the beginning of the experiment until the end of the pre-oxidation phase. During the first 800 s temperatures are still rather low, and a small amount of steam is predicted to condense in the bundle. In the off-gas pipe condensation occurs during much longer times. For the problems to be solved by pre-test calculations steam condensation in the off-gas pipe is, however, not important. In the experiment the time, when a low power is applied, is much longer, because during that time several tests are made to verify the correct working of the various systems. During this time any condensed water can evaporate.

For the run presented in Fig. 75 the pre-oxidation phase begins at $t = 1200$ s. When the oxide layer grows, further oxidation and hence chemical power release are slowed down, if all other experimental conditions are kept constant, because the oxygen must diffuse through thicker and thicker oxide layers to reach the metallic region. As a consequence rod temperature decrease with time. However, constant clad temperatures are preferable for the pre-oxidation phase. So the electrical power must be increased with time to compensate the decrease of chemical power release. For the case presented in Fig. 75 the increase of electrical power might be somewhat larger because the hydrogen production rate still decreases for a long time. The results suggest, however, that the duration of the pre-oxidation phase is much longer than, say, one hour, because at sensibly higher temperatures, necessary for a shorter pre-oxidation phase, the danger of a temperature escalation would be too large. As a practical solution for the experiment it is suggested to control the hydrogen production rate on-line and to increase the electrical power stepwise when the hydrogen production rate becomes too small, but being very cautious because a longer pre-oxidation phase does less harm than a premature temperature escalation.

For the results given in Figure 75, the power ramp would be applied before $t = 8000$ s, because at that time the oxide layer has already reached a thickness of $300 \mu\text{m}$, and further oxidation occurs during the power increase, adding some tens of μm to the oxide layer thickness.

For the quench phase calculations were not possible because of modelling errors, leading to unacceptably high mass errors. They are a consequence of numerical dif-

fusion, associated with first order upwind differences, and are more severe for the low pressure, applied in the QUENCH facility, than for the high pressure in a reactor. This is a principal problem in S/R5 mod 3.1. It has been notified to code developers at INEL. Efforts have been made to overcome this problem in the new programme version S/R5 mod 3.2.

10.3 Post-test Calculations

After the experiment had been done, calculations had been performed with S/R5 with the same modelling as for the pre-test calculations, only using the correct experimental conditions of mass flows, inlet temperatures, and electrical power. Though the modelling had been validated on the basis of commissioning tests IBS_02 and IBS_03 [9], temperatures in the bundle and the inner cooling jacket are calculated to be too high. As a minimum request for the credibility of a calculation the experimental value should be between the calculated rod surface and fluid temperatures. Consequently the oxidation layer thickness, and hydrogen release are overestimated (Figs. 76 and 77). In particular a temperature excursion is calculated when the power pulse at the begin of the experiment is applied. This temperature excursion is calculated to end due to subsequent decrease of electrical power. The overestimation of rod temperatures cannot be overcome by increasing the values of thermal conductivity of the shroud insulation material and hence modelling a better radial heat removal, because the calculated temperatures in the inner cooling jacket are already overestimated when the original modelling is used.

A comparison of calculated and measured rod temperatures in the lower unheated part of the bundle suggests that the bundle inlet temperature, as measured by thermocouple T 511, overestimates the bulk value of the inlet temperature (Fig. 76). This effect is comprehensible. Firstly the thermocouple measures a local value in the centre of the inlet pipe. Since the inlet pipe is not insulated thermally in that region, there is a radial temperature decrease, and the average value is below the local one in the centre of the cross section. Secondly there are heat losses between the location of thermocouple T 511 and the inlet plane. Therefore another thermocouple should be used in further experiments to derive the bundle inlet temperature.

For further calculations the fluid inlet temperature was set to a constant value of 700 K for the whole experiment. In this way a better agreement between calculated and measured temperatures in the lower unheated part of the bundle was achieved (Fig. 78). However, temperatures are still calculated to be too high. As a consequence the calculated hydrogen production rate is about 5 mg/s for a long time of the pre-oxidation phase in comparison to 3 to 4 mg/s measured. This results in about 56 g of cumulated hydrogen mass calculated at the end of the pre-oxidation phase in comparison to about 30 g measured during the experiment.

At the end of the pre-oxidation phase the bundle tends to steady state conditions. For steady state bundle temperatures are determined by the bundle mass flow and inlet temperature, the electrical power input and the radial heat losses. Additional tests suggest that the experimental values for the mass flows should be correct. The bundle inlet temperature cannot be reduced further without deteriorating the agreement between experimental and calculated results in the lower unheated part of the bundle. As for commissioning tests IBS_02 and IBS_03 the electrical resistance calculated with S/R5 agrees quite well with that derived from measured electrical current and voltage, such suggesting that the electrical power input should be reliable. Inspection of axial temperature profiles (Fig. 79) reveals, however, that the calculated temperature increase in the heated zone is somewhat steeper than the measured one. The same observation holds also for commissioning tests IBS_02 and IBS_03, but since the temperature levels were much lower, the effects were much less pronounced. A comparison of measured and calculated temperatures in the cooling jackets shows that the radial heat loss is correct or somewhat overestimated and hence cannot be modelled to be higher.

The ideas outlined above suggest that the electrical heat input is overestimated and, consequently, that the electrical resistance is not a sufficiently sensible indicator for power input. To calculate the local input of electrical power into the bundle, the electrical resistance outside the computational domain but inside the domain of voltage measurement is taken into account by a constant additional resistance R_0 . In the programme it refers to a single rod. A value of $R_0 = 1.6 \text{ m}\Omega$ per rod is used in the current version, based on calculations of CORA experiments. Since the voltage measured in the QUENCH facility contains not only the voltage drop at the rods, but also the voltage drop at the sliding contacts at both ends of the rods (Fig. 7), at wires

which lead to the power supply, and at screws which fix the wires at their ends, it is possible that the current value of R_0 is underestimated. Therefore it has been increased to $R_0 = 4.2 \text{ m}\Omega$ per rod. This is still a small value which can hardly be measured, but since the electrical resistance of the tungsten and of the molybdenum is 10 to 20 $\text{m}\Omega$, R_0 plays an important role to correctly simulate local power input. The value of 4.2 $\text{m}\Omega$ has been chosen to give a sufficient agreement of cumulated hydrogen mass at the end of the pre-oxidation phase; the time-dependent development of hydrogen production rate and cumulated hydrogen mass have not been used for this purpose.

Besides to this programme change the four corner rods are modelled as SCDAP components for further calculations. In this way the hydrogen production can be calculated somewhat more accurately. The results are shown in Figs. 80 - 82 from the beginning of the experiment to the end of the power transient. The calculated temperatures agree much better with the experimental ones than in previous calculations, and so do the hydrogen production rate and cumulated hydrogen mass as a consequence. In the first 3000 s of the experiment the calculated hydrogen production rate is somewhat too high, according to the somewhat too high calculated temperature, but afterwards the agreement is even better.

At the time when one of the corner rods was drawn out of the bundle ($t = 7200 \text{ s}$) the calculated oxide layer thickness is flatter and has a lower maximum than the measured one (Fig. 83). However, the oxidation rate increases strongly with temperature and local electrical heat input also increases with temperature. Therefore, if at a given location a somewhat too high temperature is calculated, a positive feed-back exists, and a slight error in the calculated axial temperature profile may lead to rather sensible deviations of the oxide layer profile during the long time of pre-oxidation.

Inspection of experimental and calculated temperatures shows that for the slight increase of electrical power at $t \approx 3450 \text{ s}$ and $t \approx 6400 \text{ s}$, which amounted to about 400 W in the bundle, there was only a limited temperature increase in the bundle, whereas the increase of electrical power at $t \approx 4060 \text{ s}$, which amounted to about 1 kW in the bundle, triggered a premature temperature excursion, which was stopped by a subsequent reduction of electrical power. Since the hydrogen production rate at the time of the increase of electrical power is about 3 mg/s, approximately 480 W are released in the bundle due to oxidation. An increase of the electrical power of about

the same size as the chemical power, released at that time, was acceptable, an increase of twice that size was not.

Therefore we propose for further experiments that for a slow change of the bundle status, as to compensate for the decrease of chemical power due to increasing oxide layer thickness, the increase of electrical power in the bundle is not larger than the actual release of chemical power. Since the hydrogen production rate is monitored during the experiment and since the chemical power is proportional to the hydrogen production rate, this is an easy way to determine the amount of additional electrical power. For faster transients the situation would be more complicated. The hydrogen production rate would be larger, more hydrogen would be absorbed in the Zry, leading locally to higher temperatures, because the absorption is exothermic. Since local electrical power input depends on local temperature, the axial temperature profile and hence local oxidation rates would be different from the low transient case. Besides the hydrogen production rate detected downstream of the bundle is underestimated because of the absorption, and chemical power release is also underestimated.

The duration of the premature temperature excursion, mentioned above, is not only a measure for the time available for the operators to judge the situation and to apply counter-measures. Since the calculated hydrogen production rate agrees well with the measured one, it is also a measure of the quality of the actual modelling of the QUENCH facility for S/R5 calculations.

10.4 Conclusions Depending on the Calculational Support

S/R5 calculations were made to suggest the test conduct of the quench experiment QUENCH-01. Important test parameters depend on reactor conditions and must therefore be derived from analyses for commercial reactors. For this purpose analyses of accident scenarios for the projected European Pressurised Water Reactor EPR have been used, especially Loss of Offsite Power scenarios. They give valuable Information for the initial conditions of the quench phase and for test parameters of the quench phase itself.

Further important test parameters, above all for the pre-oxidation phase and the subsequent power transient depend on the very conditions of the QUENCH facility and can therefore only be gained from special calculations for this facility. They are based

on the experience gained from analyses of the commissioning tests. Since the pre-oxidation phase should be performed at constant rod temperature and since oxidation power release decreases with increasing oxide layer thickness, it is suggested to increase electrical power stepwise during this phase. It is further suggested to use the hydrogen production rate, monitored during the experiment, as a sensitive measure for this power increase: electrical power should be increased, when the hydrogen production rate falls below a certain limit. Evaluation of post-test data suggests further to use the hydrogen production rate also to determine the amount of electrical power increase. Test parameters for the quench phase cannot be derived from special calculations for the QUENCH facility, because of general programme shortcomings that can only be overcome in future programme versions.

Post-test analyses of the quench experiment showed that the thermocouple T 511, intended to measure the bundle inlet temperature of the fluid does not give a representative value. Therefore thermocouple TFS 2/1 will be devoted to this aim for future experiments. The electrical resistance outside the calculational domain, but inside the domain of voltage measurement is identified as a possible source of deviations between calculated and measured temperatures. Adjusting the value of this resistance such that the cumulated hydrogen mass at the end of the pre-oxidation phase is calculated correctly was sufficient to improve the agreement calculated and measured temperatures and of hydrogen production rate and cumulated hydrogen mass during the whole pre-oxidation phase, even during a short event as the premature limited temperature excursion.

11 References

- [1] J.M. Broughton, P. Kuan, and D.A. Petti, "A Scenario of the Three Mile Island Unit 2 Accident," Nuclear Technology, 87, 34, 1989.
- [2] P. Hofmann, S. Hagen, V. Noack, G. Schanz, L. Sepold, "Chemical-Physical Behavior of Light Water Reactor Core Components Tested under Severe Reactor Accident Conditions in the CORA Facility", Nuclear Technology, Vol. 118, 1997, pp. 200.
- [3] R.R. Hobbins and G.D. McPherson, "A Summary of Results from the LOFT LP-FP-2 Test and Their Relationship to Other Studies at the Power Burst Facility and of the Three Mile Island Unit 2 Accident", OECD/LOFT Final Event, ISBN 92-64-03339-4, 1991.
- [4] S. Hagen, P. Hofmann, V. Noack, L. Sepold, G. Schanz, G. Schumacher, "Comparison of the Quench Experiments CORA-12, CORA-13, CORA-17", FZKA 5679, Forschungszentrum Karlsruhe, 1996.
- [5] L. Sepold, S. Horn, W. Leiling, FZK Internal Report, 1997
- [6] L. Sepold, S. Horn, W. Leiling, FZK Internal Report, 1998
- [7] V. Sanchez, E. Elias, Ch. Homann, W. Hering, D. Struwe: "Development and Validation of a Transition Boiling Model for the RELAP5/MOD3 Reflood Simulation", FZKA 5954, Forschungszentrum Karlsruhe, 1997.
- [8] W. Hering: "Status of Reflood Analyses for the LOOP Scenario using SCDAP/RELAP5 mod 3.1", in „Projekt Nukleare Sicherheitsforschung, Jahresbericht 1997“, FZKA 6126, Forschungszentrum Karlsruhe, 1998
- [9] P. Hofmann, W. Hering, C. Homann, W. Leiling, A. Miassoedov, D. Piel, L. Schmidt, L. Sepold, M. Steinbrück.: "Results of the Commissioning Tests", FZKA 6099, Forschungszentrum Karlsruhe, 1998.
- [10] P. Hofmann, V. Noack, M.S. Veshchunov, A.V. Berdyshev, A.V. L.V. Matweev, A.V. Palagin, V.E. Shestak: „Physico-Chemical Behavior of Zircaloy Fuel Rod Cladding Tubes During LWR Severe Accident Reflood“, FZKA 5846, Forschungszentrum Karlsruhe, 1997

12 Acknowledgements

This work was executed under the multi-partners research contract FI4S-CT95-0013 (Investigation of Core Degradation) co-financed by the European Commission under the Euratom Fourth Framework Programme on Nuclear Fission Safety 1994 – 1998 (Report No. INV-COBE (98)-D010). It is also part of the cooperation with the German nuclear industry, co-financed by Siemens/KWU and the German utilities under the leadership of EnBW and RWE.

At the Forschungszentrum Karlsruhe a variety of support needed for preparation, conduct and evaluation of the experiment is hereby gratefully acknowledged. In particular, the authors would like to thank E. Mackert for the assembly of the test rods, J. Moch and R. Vouriot for the assembly and instrumentation of the test bundle, and S. Horn for the preparation of the hydrogen measurement with the Caldos system and the support for the test data evaluation. Furthermore, the authors would like to express their gratitude to L. Anselment for sectioning of the epoxied bundle and for the preparation of the metallographic samples, H. Metzger for examination of the metallographic samples by optical microscope.

Table 1: QUENCH Test Matrix

Test	Quench medium	Flooding rate	Heat-up rate	Max. ZrO ₂ layer thickness ¹⁾	Temp. at onset of quenching ¹⁾	Remarks	Date of Test Conduct
QUENCH-00	water	2.8 cm/s from bottom	1.0 K/s	≈ 500 μm	≈ 1500°C	commissioning tests	October 10, 97
QUENCH-01	water	1.0 cm/s; from the bottom	0.5 K/s	≈ 300 μm	≈ 1600°C	partial fragmentation of pre-oxidized cladding	February 26, 98
QUENCH-02	water	1.0 cm/s; from the bottom	0.5 K/s	determined by heat-up rate	1600 - 1700°C	reference test; no additional pre-oxidation	July 7, 98
QUENCH-03	water	0.5 cm/s from the bottom	1.0 K/s	determined by heat-up rate	1600 – 1700°C	fast heat-up and low flooding rate	10/98
QUENCH-04	steam	≈ 10 g/s; from the bottom		determined by heat-up rate	≈ 1600°C	cool-down behavior in steam; refer. test to QUENCH-03	3/99
QUENCH-05	water	0.5 cm/s; from the bottom		determined by heat-up rate	1400 - 2000°C	impact of absorber rod failure on H ₂ generation	
QUENCH-06	water	x g/s; from the top		≈ 300 μm	≤ 1400°C	effectiveness of top flooding on quenching	
QUENCH-07	water	3.0 cm/s; from the bottom		determined by heat-up rate	1400 → 2000°C	fast flooding with pre-heated water	

- All tests should be conducted with reduced electrical power input after quenching of the bundle has been initiated; simulation of the fission product decay heat (4 - 5 kW)
- Flooding rate: rise of the water level at the -250 mm bundle elevation
- ¹⁾ Measured at the bundle elevation of maximum temperature

Revised: July 15, 1998

Table 2: Design characteristics of QUENCH test bundle

Bundle type		PWR
Bundle size		21 rods
Number of heated rods		20
Number of unheated rods		1
Pitch		14.3 mm
Rod outside diameter		10.75 mm
Cladding material		Zircaloy-4
Cladding thickness		0.725 mm
Rod length	heated rods (elevation) unheated rods (elevation)	2480 mm (-690 to 1790 mm) 2842 mm (-827 to 2015 mm, incl. extension)
Heater material		Tungsten (W)
Heater length		1024 mm
Heater diameter		6 mm
Annular pellet	heated rods unheated rods	ZrO ₂ ; Ø 9.15/6.15 mm; L=11 mm ZrO ₂ ; Ø 9.15/2.5 mm; L=11 mm
Pellet stack	heated rods unheated rods	0 to 1020 mm 0 to 1553 mm
Grid spacer	material length location of the lower edge	Zircaloy-4, Inconel 718 Zry 42 mm, Inc 38 mm -200 mm Inconel 50 mm Zircaloy-4 550 mm Zircaloy-4 1050 mm Zircaloy-4 1410 mm Zircaloy-4
Shroud	material wall tickness outside diameter length (elevation)	Zircaloy-4 2.38 mm 84.76 mm 1600 mm (-300 to 1300 mm)
Shroud insulation	material insulation thickness elevation	ZrO ₂ fiber 35 mm -300 to 1000 mm
Molybdenum-copper electrodes:		
length of upper electrodes		766 mm (576 Mo, 190 mm Cu)
length of lower electrodes		690 mm (300 Mo, 390 mm Cu)
diameter of electrodes:	- prior to coating - after coating by ZrO ₂	8.6 mm 9.0 mm
Cooling jacket	material inner tube outer tube	Stainless steel, 1.4541 Ø 158.3 / 168.3 mm Ø 181.7 / 193.7 mm

Table 3: List of instrumentation for the QUENCH-01 Test

Chan- nel	Designation	Instrument, location	Output in
0	TCR 13	TC (W/Re) central rod, cladding, 950 mm	°C
1	TFS 2/11	TC (W/Re) fuel rod simulator 8 (type 2), 750 mm, 135°	°C
2	TFS 2/13	TC (W/Re) fuel rod simulator 2 (type 2), 950 mm, 225°	°C
3	TFS 2/15	TC (W/Re) fuel rod simulator 4 (type 2), 1150 mm, 315°	°C
4	TFS 2/17	TC (W/Re) fuel rod simulator 6 (type 2), 1350 mm, 45°	°C
5	TFS 3/8	TC (W/Re) fuel rod simulator 5 (type 3), 470 mm, 45°	°C
6	TFS 3/10	TC (W/Re) fuel rod simulator 7 (type 3), 670 mm, 135°	°C
7	TFS 3/12	TC (W/Re) fuel rod simulator 9 (type 3), 850 mm, 225°	°C
8	TFS 3/13	TC (W/Re) fuel rod simulator 3 (type 3), 950 mm, 315°	°C
9	TFS 3/14	TC (W/Re) fuel rod simulator 5 (type 3), 1050 mm, 45°	°C
10	TFS 4/11	TC (W/Re) fuel rod simulator 14 (type 4), 750 mm, 45°	°C
11	TFS 4/13	TC (W/Re) fuel rod simulator 20 (type 4), 950 mm, 135°	°C
12	TFS 5/10	TC (W/Re) fuel rod simulator 12 (type 5), 670 mm, 225°	°C
13	TFS 5/11	TC (W/Re) fuel rod simulator 13 (type 5), 750 mm, 45°	°C
14	TFS 5/12	TC (W/Re) fuel rod simulator 15 (type 5), 850 mm, 315°	°C
15	TFS 5/13	TC (W/Re) fuel rod simulator 16 (type 5), 950 mm, 135°	°C
16	TFS 5/14	TC (W/Re) fuel rod simulator 18 (type 5), 1050 mm, 45°	°C
17	TSH 16/180	TC (W/Re) shroud outer surface, 1250 mm, 180°	°C
18	TSH 13/90	TC (W/Re) shroud outer surface, 950 mm, 90°	°C
19	TSH 14/90	TC (W/Re) shroud outer surface, 1050 mm, 90°	°C
20	TSH 11/0	TC (W/Re) shroud outer surface, 750 mm, 0°	°C
21	TSH 12/0	TC (W/Re) shroud outer surface, 850 mm, 0°	°C
22	TFS 2/5	TC (NiCr/Ni) fuel rod simulator 2 (type 2), 150 mm, 225°	°C
23	TFS 2/7	TC (NiCr/Ni) fuel rod simulator 6 (type 2), 350 mm, 45°	°C
32	TCRC 9	TC (W/Re) central rod, center, 570 mm	°C
33	TCRC13	TC (W/Re) central rod, center, 950 mm	°C
34	TCR 9	TC (W/Re) central rod, cladding, 570 mm	°C
37	TFS 3/16	TC (W/Re) fuel rod simulator 7 (type 3), 1250 mm, 135°	°C
40	TFS 5/8	TC (W/Re) fuel rod simulator 21 (type 5), 470 mm, 225°	°C
41	TFS 5/9	TC (W/Re) fuel rod simulator 10 (type 5), 570 mm, 315°	°C
47	TFS 5/15	TC (W/Re) fuel rod simulator 19 (type 5), 1150 mm, 225°	°C
48	TFS 5/16	TC (W/Re) fuel rod simulator 21 (type 5), 1250 mm, 225°	°C
49	TFS 5/17	TC (W/Re) fuel rod simulator 10 (type 5), 1350 mm, 315°	°C

Channel	Designation	Instrument, location	Output in
50	TSH 9/270	TC (W/Re) shroud outer surface, 570 mm, 270°	°C
51	TSH 11/270	TC (W/Re) shroud outer surface, 750 mm, 270°	°C
52	TSH 13/270	TC (W/Re) shroud outer surface, 950 mm, 270°	°C
53	TSH 14/270	TC (W/Re) shroud outer surface, 1050 mm, 270°	°C
54	TSH 11/180	TC (W/Re) shroud outer surface, 750 mm, 180°	°C
55	TSH 12/180	TC (W/Re) shroud outer surface, 850 mm, 180°	°C
56	TSH 13/180	TC (W/Re) shroud outer surface, 950 mm, 180°	°C
57	TSH 15/180	TC (W/Re) shroud outer surface, 1150 mm, 180°	°C
59	TSH 9/90	TC (W/Re) shroud outer surface, 570 mm, 90°	°C
60	TSH 11/90	TC (W/Re) shroud outer surface, 750 mm, 90°	°C
65	TSH 13/0	TC (W/Re) shroud outer surface, 950 mm, 0°	°C
66	TSH 15/0	TC (W/Re) shroud outer surface, 1150 mm, 0°	°C
67	TSH 16/0	TC (W/Re) shroud outer surface, 1250 mm, 0°	°C
68	T 512	Gas temperature bundle outlet	°C
69	-		
70	-		
71	Ref. T 01	Reference temperature 1	°C
72	TFS 2/1	TC (NiCr/Ni) fuel rod simulator 4 (type 2), -250 mm, 315°	°C
73	TFS 2/2	TC (NiCr/Ni) fuel rod simulator 6 (type 2), -150 mm, 45°	°C
74	TFS 2/3	TC (NiCr/Ni) fuel rod simulator 8 (type 2), -50 mm, 135°	°C
76	TFS 2/6	TC (NiCr/Ni) fuel rod simulator 4 (type 2), 250 mm, 315°	°C
78	TFS 5/4/0	TC (NiCr/Ni) fuel rod simulator 15 (type 5), 50 mm, 315°	°C
79	TFS 5/4/180	TC (NiCr/Ni) fuel rod simulator 21 (type 5), 50 mm, 135°	°C
80	TFS 5/5	TC (NiCr/Ni) fuel rod simulator 16 (type 5), 150 mm, 225°	°C
81	TFS 5/6	TC (NiCr/Ni) fuel rod simulator 18 (type 5), 250 mm, 45°	°C
82	TFS 5/7	TC (NiCr/Ni) fuel rod simulator 19 (type 5), 350 mm, 225°	°C
83	TSH 4/270	TC (NiCr/Ni) shroud outer surface, 50 mm, 270°	°C
84	TSH 3/180	TC (NiCr/Ni) shroud outer surface, -50 mm, 180°	°C
85	TSH 4/180	TC (NiCr/Ni) shroud outer surface, 50 mm, 180°	°C
86	TSH 7/180	TC (NiCr/Ni) shroud outer surface, 350 mm, 180°	°C
87	TSH 4/90	TC (NiCr/Ni) shroud outer surface, 50 mm, 90°	°C
88	TSH 1/0	TC (NiCr/Ni) shroud outer surface, -250 mm, 0°	°C
89	TSH 4/0	TC (NiCr/Ni) shroud outer surface, 50 mm, 0°	°C
90	TSH 7/0	TC (NiCr/Ni) shroud outer surface, 350 mm, 0°	°C
91	TCI 9/270	TC (NiCr/Ni) cooling jacket inner tube wall, 550 mm, 270°	°C

Channel	Designation	Instrument, location	Output in
92	TCI 10/270	TC (NiCr/Ni) cooling jacket inner tube wall, 650 mm, 270°	°C
93	TCI 11/270	TC (NiCr/Ni) cooling jacket inner tube wall, 750 mm, 270°	°C
94	TCI 13/270	TC (NiCr/Ni) cooling jacket inner tube wall, 350 mm, 270°	°C
95	-		
95	TCO 16/180	TC (NiCr/Ni) cooling jacket outer tube surface, 1250 mm, 180°	°C
96	TCI 1/180	TC (NiCr/Ni) cooling jacket inner tube wall, -250 mm, 180°	°C
97	TCI 4/180	TC (NiCr/Ni) cooling jacket inner tube wall, 50 mm, 180°	°C
98	TCI 7/180	TC (NiCr/Ni) cooling jacket inner tube wall, 350 mm, 180°	°C
99	TCI 11/180	TC (NiCr/Ni) cooling jacket inner tube wall, 750 mm, 180°	°C
100	TCI 12/180	TC (NiCr/Ni) cooling jacket inner tube wall, 850 mm, 180°	°C
101	TCI 13/180	TC (NiCr/Ni) cooling jacket inner tube wall, 950 mm, 180°	°C
102	TCI 15/180	TC (NiCr/Ni) cooling jacket inner tube wall, 1150 mm, 180°	°C
103	-		
104	TCI 9/90	TC (NiCr/Ni) cooling jacket inner tube wall, 550 mm, 90°	°C
105	TCI 10/90	TC (NiCr/Ni) cooling jacket inner tube wall, 650 mm, 90°	°C
106	TCI 11/90	TC (NiCr/Ni) cooling jacket inner tube wall, 750 mm, 90°	°C
107	TCI 13/90	TC (NiCr/Ni) cooling jacket inner tube wall, 850 mm, 90°	°C
108	-		
109	TCI1/0	TC (NiCr/Ni) cooling jacket inner tube wall, -250 mm, 0°	°C
110	TCI 4/0	TC (NiCr/Ni) cooling jacket inner tube wall, 50 mm, 0°	°C
111	TCI 7/0	TC (NiCr/Ni) cooling jacket inner tube wall, 350 mm, 0°	°C
112	TCI 11/0	TC (NiCr/Ni) cooling jacket inner tube wall, 750 mm, 0°	°C
113	TCI 12/0	TC (NiCr/Ni) cooling jacket inner tube wall, 850 mm, 0°	°C
114	TCI 13/0	TC (NiCr/Ni) cooling jacket inner tube wall, 950 mm, 0°	°C
115	TCI 15/0	TC (NiCr/Ni) cooling jacket inner tube wall, 1150 mm, 0°	°C
116	-		
117	TCO 9/270	TC (NiCr/Ni) cooling jacket outer tube surface, 550 mm, 270°	°C
118	TCO 4/180	TC (NiCr/Ni) cooling jacket outer tube surface, 50 mm, 180°	°C
120	TCO 1/0	TC (NiCr/Ni) cooling jacket outer tube surface, -250 mm, 0°	°C
121	TCO 7/0	TC (NiCr/Ni) cooling jacket outer tube surface, 350 mm, 0°	°C
122	TCO 13/0	TC (NiCr/Ni) cooling jacket outer tube surface, 950 mm, 0°	°C
123	T 601	Temperature before off-gas flow instrument F 601	°C
124	T 513	Temperature bundle head top (wall)	°C

Channel	Designation	Instrument, location	Output in
125	T 514	Temperature bundle head, at outlet (wall)	°C
126	-		
127	-		
128	T 104	Temperature quench water	°C
129	T 201	Temperature steam generator heating pipe	°C
130	T 204	Temperature before steam flow instrument location 50 g/s	°C
131	T 205	Temperature before steam flow instrument location 10 g/s	°C
132	T 301A	Temperature behind superheater	°C
133	T 302	Temperature superheater heating pipe	°C
134	T 303	Temperature before total flow instrument location	°C
135	T 401	Temperature before gas flow instrument location	°C
136	T 403	Temperature at inlet cooling gas	°C
137	T 404	Temperature at outlet cooling gas	°C
138	T 501	Temperature at containment	°C
139	T 502	Temperature at containment	°C
140	T 503	Temperature at containment	°C
141	T 504	Temperature at containment	°C
142	T 505	Temperature at containment	°C
143	T 506	Temperature at containment	°C
144	T 507	Temperature at containment	°C
145	T 508	Temperature at containment	°C
146	T 509	Temperature bundle head outside (wall)	°C
147	T 510	Temperature at containment	°C
148	T 511	Gas temperature at bundle inlet	°C
149	T 901	Temperature before off-gas flow instrument F 901	°C
150	-		
151	Ref. T 02	Reference temperature 2	°C
152	P 201	Pressure steam generator	bar
153	P 204	Pressure at steam flow instrument location 50 g/s	bar
154	P 205	Pressure at steam flow instrument location 10 g/s	bar
155	P 303	Pressure before total flow instrument location	bar
156	P 401	Pressure before gas flow instrument location	bar
157	P 511	Pressure at bundle inlet	bar
158	P 512	Pressure at bundle outlet	bar
159	P 601	Pressure before off-gas flow instrument F 601	bar

Channel	Designation	Instrument, location	Output in
160	P 901	Pressure before off-gas flow instrument F 901	bar
161	L 201	Liquid level steam generator	mm
162	L 501	Liquid level quench water	bar
163	L 701	Liquid level main condenser	mm
164	Q 901	H ₂ concentration, off-gas (Caldos)	% H ₂
165	P 411	Pressure helium supply	bar
166	-		
167	-		
168	F 104	Flow rate quench water	l/h
169	F 204	Flow rate steam 50 g/s	m ³ /h
170	F 205	Flow rate steam 10 g/s	m ³ /h
171	F 303	Flow rate at bundle inlet (steam + argon), orifice	mbar
172	F 401	Argon gas flow rate	Nm ³ /h
173	F 403	Flow rate cooling gas	Nm ³ /h
174	F 601	Flow rate off-gas (orifice)	mbar
175	F 901	Off-gas flow rate before Caldos (H ₂)	m ³ /h
176	E 201	Electric current steam generator	A
177	E 301	Electric current superheater	A
178	E 501	Electric current inner ring of fuel rod simulators	A
179	E 502	Electric current outer ring of fuel rod simulators	A
180	E 503	Electric voltage inner ring of fuel rod simulators	V
181	E 504	Electric voltage outer ring of fuel rod simulators	V

3/98

Table 4: Test QUENCH-01; Evaluation of cool-down data

Cladding Thermo-couple	Elevation Rod number	Onset of cooling		Onset of quenching		Max. cooldown during quenching (K/s)
		Time (s)	Temp. (K)	Time (s)	Temp. (K)	
TFS 2/1	- 250 mm (rod 4)	494	653	495	641	240
TFS 2/2	- 150 mm (rod 6)	494	768	495	757	160
TFS 2/3	- 50 mm (rod 8)	477	839	494	817	100
TFS 5/4/180	50 mm (rod 21)	495	907	497	877	100
TFS 2/5	150 mm (rod 2)	494	1043	520	782	130
TFS 5/5	150 mm (rod 16)	495	1035	513	874	110
TFS 2/6	250 mm (rod 4)	494	1179	531	897	200
TFS 5/6	250 mm (rod 18)	494	1144	531	866	100
TFS 2/7	350 mm (rod 6)	495	1282	543	942	430
TFS 5/7	350 mm (rod 19)	495	1247	547	919	260
TFS 3/8	470 mm (rod 5)	495	1384	558	972	150
TFS 5/9	570 mm (rod 10)	495	1391	532	1013	210
TFS 5/10	670 mm (rod 12)	495	1571	568	984	140
TFS 5/14	1050 mm (rod 18)	495	1600	569	1199	100
TFS 5/16	1250 mm (rod 21)	495	1227	572	1064	410
TFS 2/17	1350 mm (rod 6)	*	*	549	1060	320
TFS 5/17	1350 mm (rod 10)	*	*	569	929	430

3/98

*) Ambiguous data interpretation

Table 5: Test QUENCH-01: Quench temperatures and quench rates based on shroud temperature data

Shroud thermocouple	Elevation (mm)	Onset of quenching		Mean values		Quench rate (cm/s)
		Time (s)	Temp. (K)	Time (s)	Temp. (K)	
TSH 1/0	- 250	495	620			
TSH 4/0	50	521	691	522	680	1.1
TSH 4/90	50	523	694			
TSH 4/180	50	523	688			
TSH 4/270	50	521	674			
TSH 9/90	550	653	618			0.4
TSH 9/270	550	-	-			
TSH 12/180	850	658	1249	659	1198	4.7
TSH 12/0	850	660	1146			
TSH 13/0	950	658	1315	658	1343	-
TSH 13/90	950	658	1337			
TSH 13/180	950	659	1384			
TSH 13/270	950	658	1337			
TSH 15/0	1150	680	949	681	971	0.9
TSH 15/180	1150	681	992			

Table 6: Hydrogen release measured by mass spectrometer and Caldos system during test QUENCH-01

Test phase	Mass spectrometer	Caldos system
1 st heat-up	0.5 g	-
He injection	0.4 g	-
2 nd heat-up & pre-oxidation	30 g	27 g
Transient & quench	8 g	8 g
Σ	39 g	35 g

Table 7: Test QUENCH-01; Failures of thermocouples mounted to claddings of fuel rod simulators

Thermocouple	First failure occurred
TFS 5/8	During handling, prior to test
TFS 5/4/0	During handling, prior to test
TCR 9	During handling, prior to test
TFS 3/10	During handling, prior to test
TCRC 9	During handling, prior to test
TFS 2/13	Pre-oxidation, 4800 s
TCR 13	Pre-oxidation, 5000 s
TFS 4/13	Pre-oxidation, 6800 s
TFS 5/12	Pre-oxidation, 7000 s
TFS 4/11	End of pre-oxidation
TFS 2/11	Transient, 100 s
TFS 3/12	Transient, 100 s
TFS 5/13	Transient, 100 s
TFS 5/11	Transient, 150 s
TFS 3/16	Quenching, 500s
TFS 2/15	Quenching, 500s
TFS 5/15	Quenching, 500s
TFS 3/13	Quenching, 550s
TFS 3/14	Quenching, 550s

3/98

Table 8: Synchronisation of the data from the main data acquisition system and from the mass spectrometer

Test phase	Time difference between MS data and data of the facility, s
Heat-up	0
Pre-oxidation	908
Transient + Quench	9188

Table 9: QUENCH 01 – Cross sections

Sample	Sample length (mm)	Axial position		Remarks
		bottom (mm)	top (mm)	
QUE-01-a	488	- 430	58	Remnant
Cut	2	58	60	
QUE-01-1	13	60	73	Reference, almost unoxidized
Cut	2	73	75	
QUE-01-b1	483	75	558	
Cut	2	558	560	
QUE-01-7	13	560	573	573 mm polished
Cut	2	573	575	
QUE-01-b2	173	575	748	
Cut	2	748	750	
QUE-01-2	13	750	763	763 mm polished
Cut	2	763	765	
QUE-01-c	133	765	898	
Cut	2	898	900	
QUE-01-3	13	900	913	Max. oxidation; 913 mm polished
Cut	2	913	915	
QUE-01-d	83	915	998	
Cut	2	998	1000	
QUE-01-4	13	1000	1013	1000 mm polished
Cut	2	1013	1015	
QUE-01-e	133	1015	1148	
Cut	2	1148	1150	
QUE-01-5	13	1150	1163	Max. shroud temp.; 1163 mm polished
Cut	2	1163	1165	
QUE-01-f1	65	1165	1230	
Cut	2	1230	1232	
QUE-01-f2	86	1232	1318	
Cut	2	1318	1320	
QUE-01-6	13	1320	1333	
Cut	2	1333	1335	
QUE-01-g	455	1335	1790	Remnant

9.6.1998

Table 10: Procedure of the preparation of the samples for the metallographic examination

	Grinding	Lapping	Polishing I	Polishing II	Polishing III	Polishing IV	Polishing V
Abrasive	Diamond disc 120 µm Diamond disc 220 µm (Disc „Piano“ *)	Disc „Allegro“ *)	Cloth MD-Pan	Cloth MD-Dur	Cloth MD-Dac	Cloth MD-Dac	OP-Chem
Particle size		Diamond spray 9 - 15 µm	Diamond spray 15 µm	Diamond spray 6 µm	Diamond spray 3 µm	Diamond spray 1 µm	OP-S***)
Lubricant	Water	White lubricant **)	White lubricant	White lubricant	White lubricant	White lubricant	-
Revolutions of disc	150 rpm	150 rpm	150 rpm	150 rpm	150 rpm	150 rpm	150 rpm
Pressure	100-200 N	150 N	150 N	150 N	150 N	150 N	150 N
Time	to level	max. 60 min	20 min	15 - 30 min	20 min	20 min	5 - 10 min

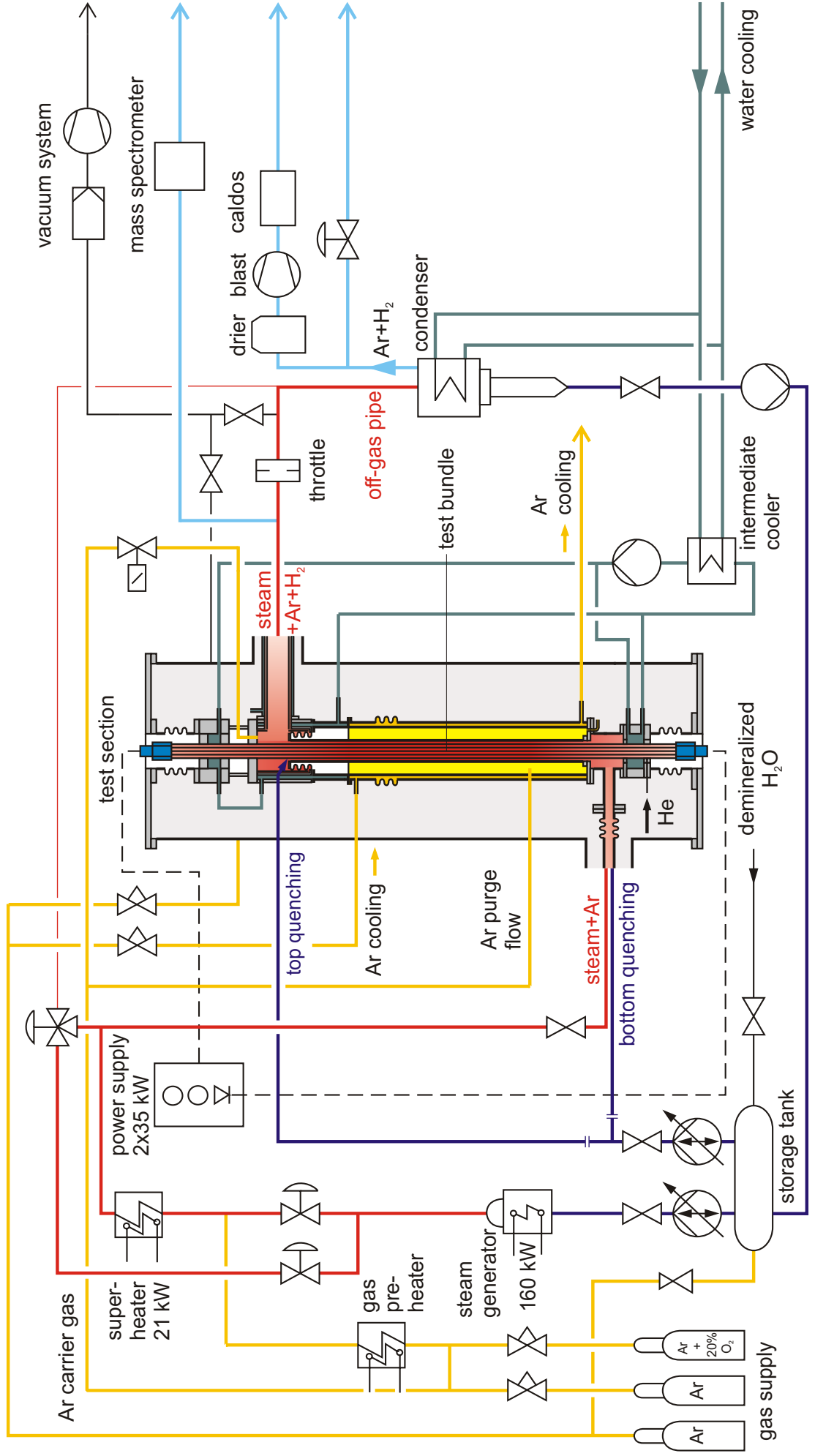
*) Disc and cloth designations are registered trade marks of the Struers company

***) "White lubricant" of Struers; liquid on an oil/alcohol/glycerin basis

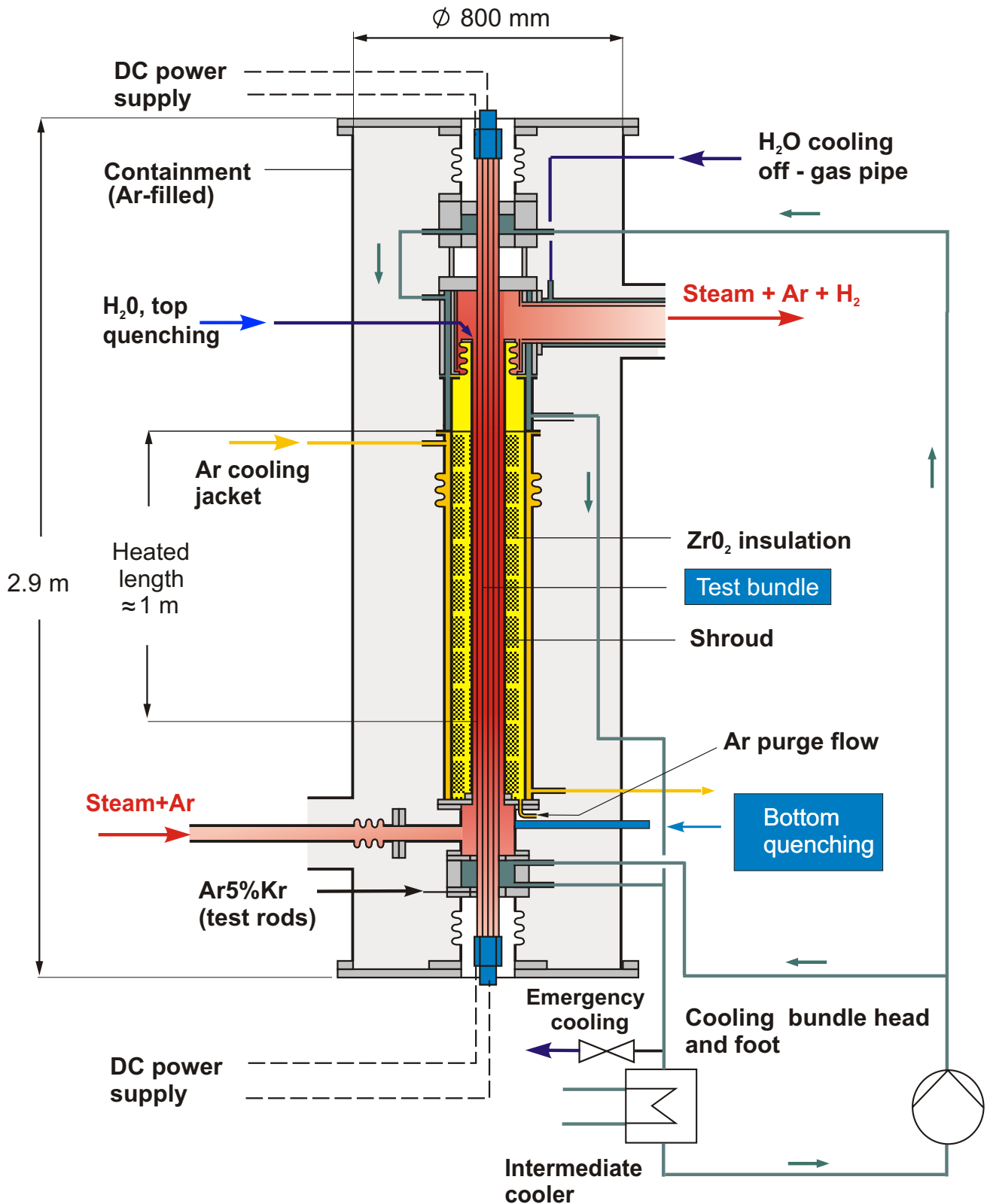
****) Colloidal silica suspension

QUENCH Test Facility

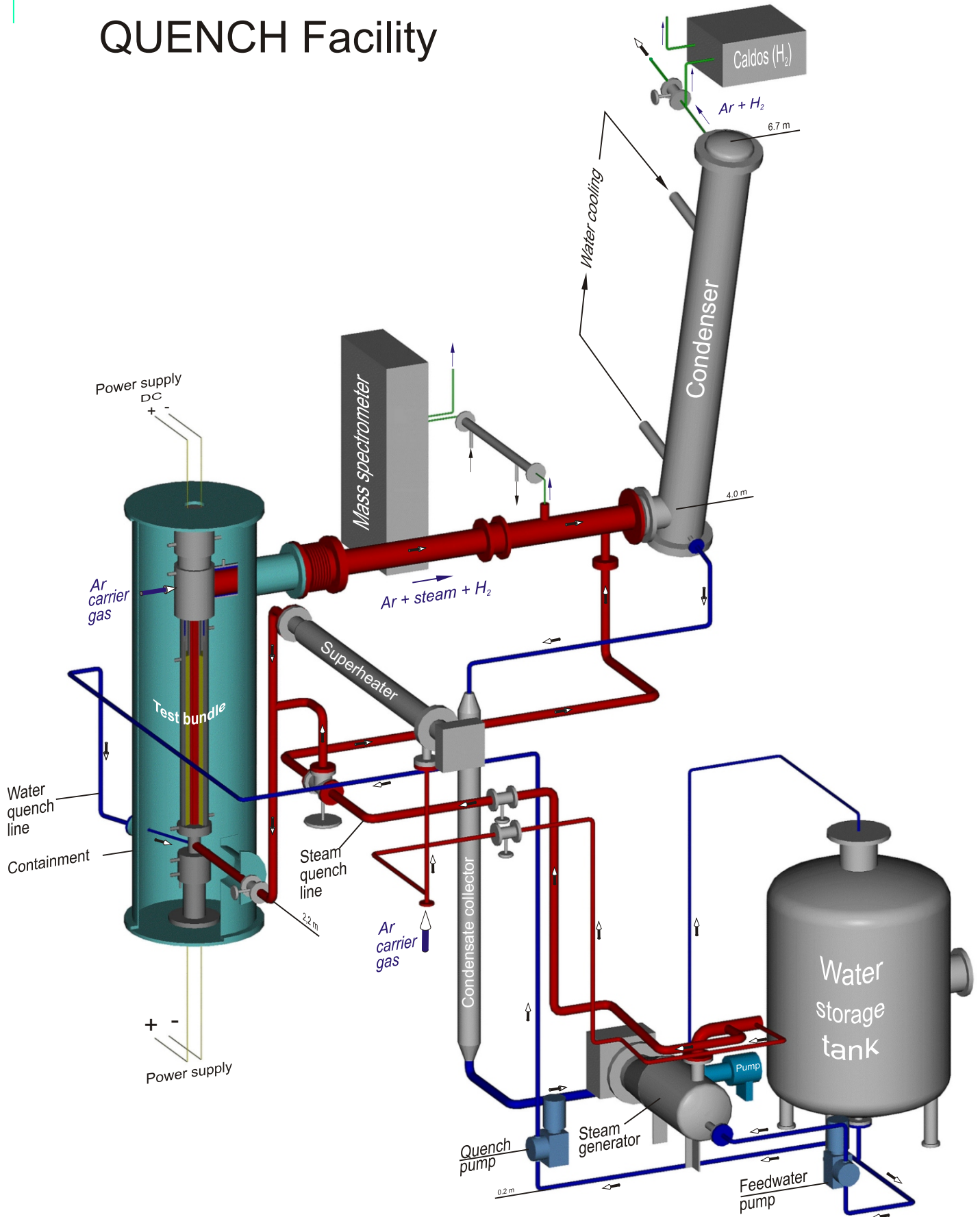
Flow Diagram



QUENCH Test Section - Flow lines



QUENCH Facility



QUENCH Facility

H₂ measurement with CALDOS
(bypass to off-gas line)

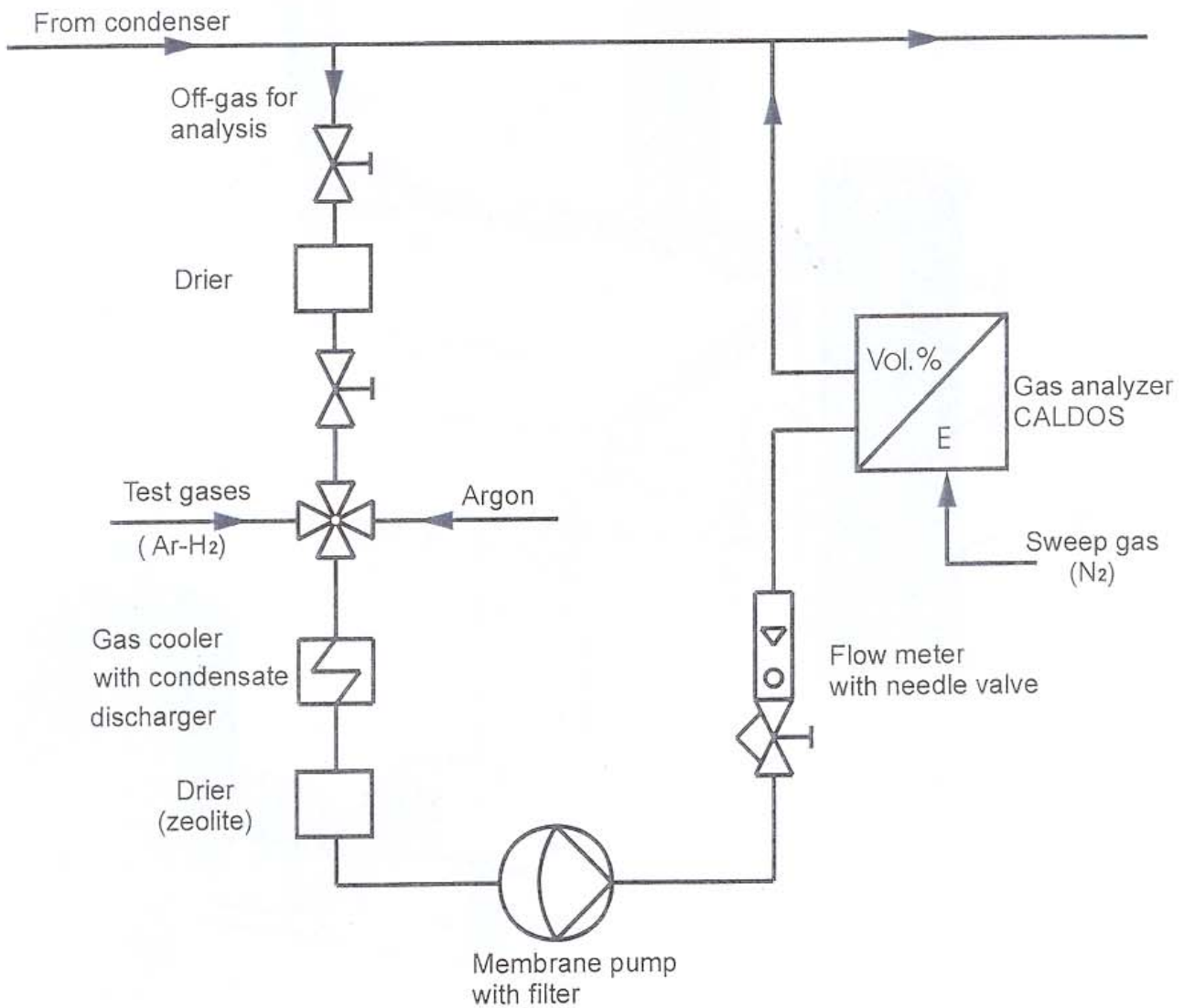


Fig.4

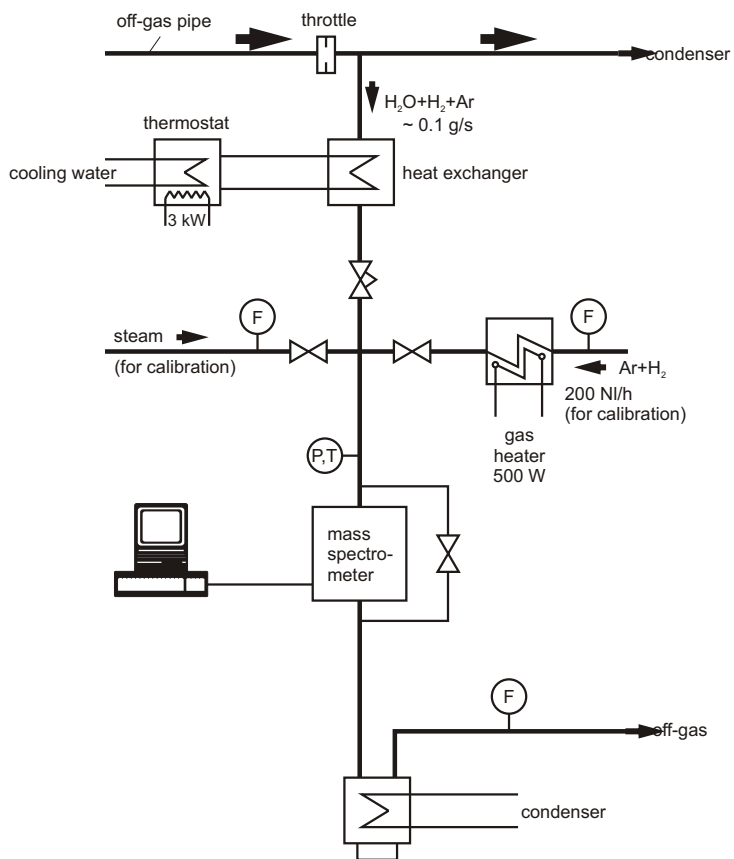


Fig. 5 a: MS connection to the QUENCH Facility

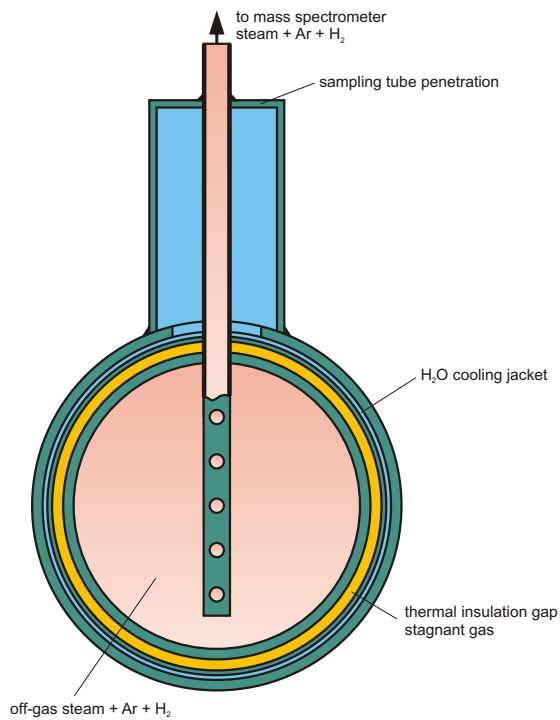


Fig. 5 b: Cross section through the off-gas pipe at the MS sampling position

Fig. 5

Heated Fuel Rod Simulator

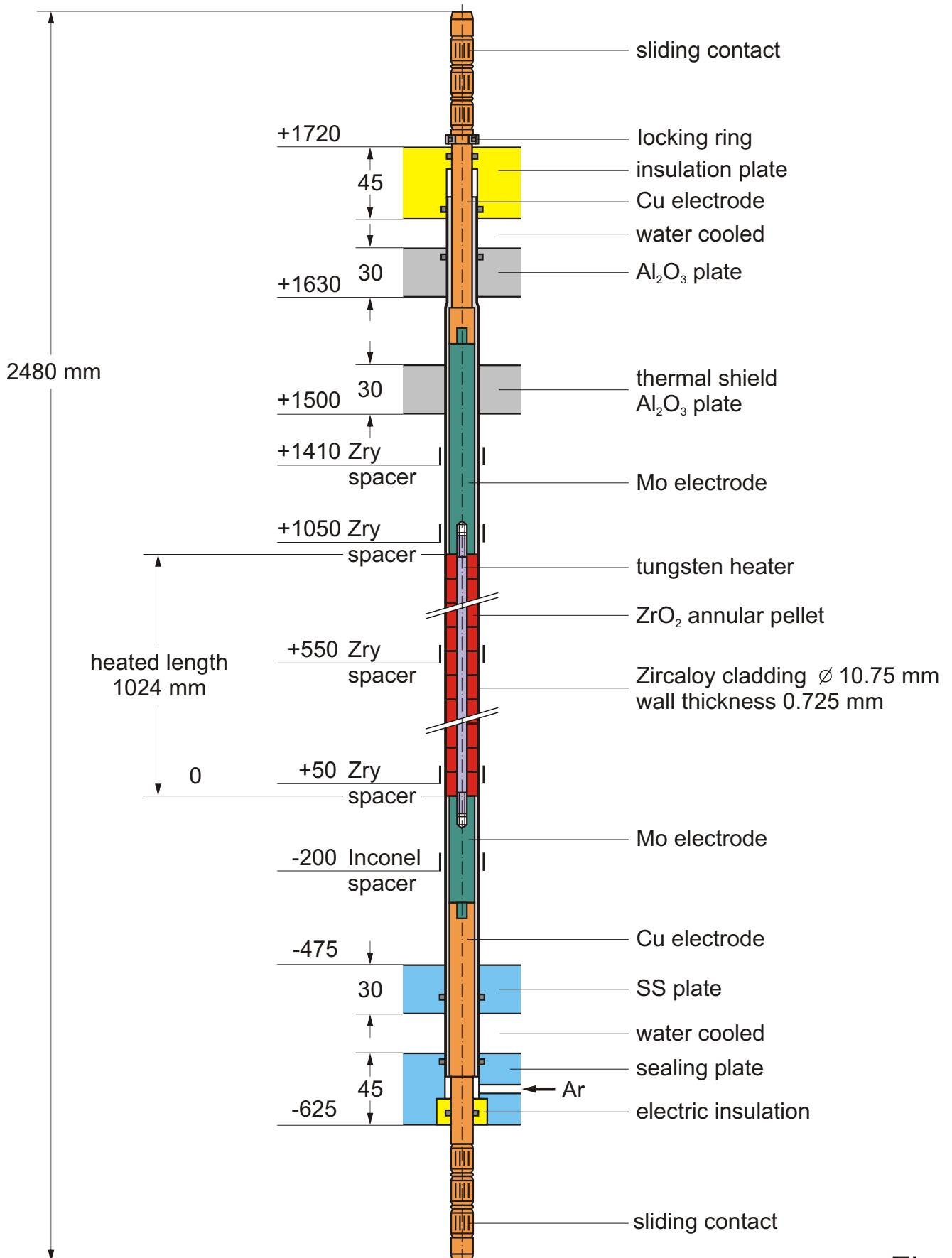


Fig. 7

Unheated Fuel Rod Simulator

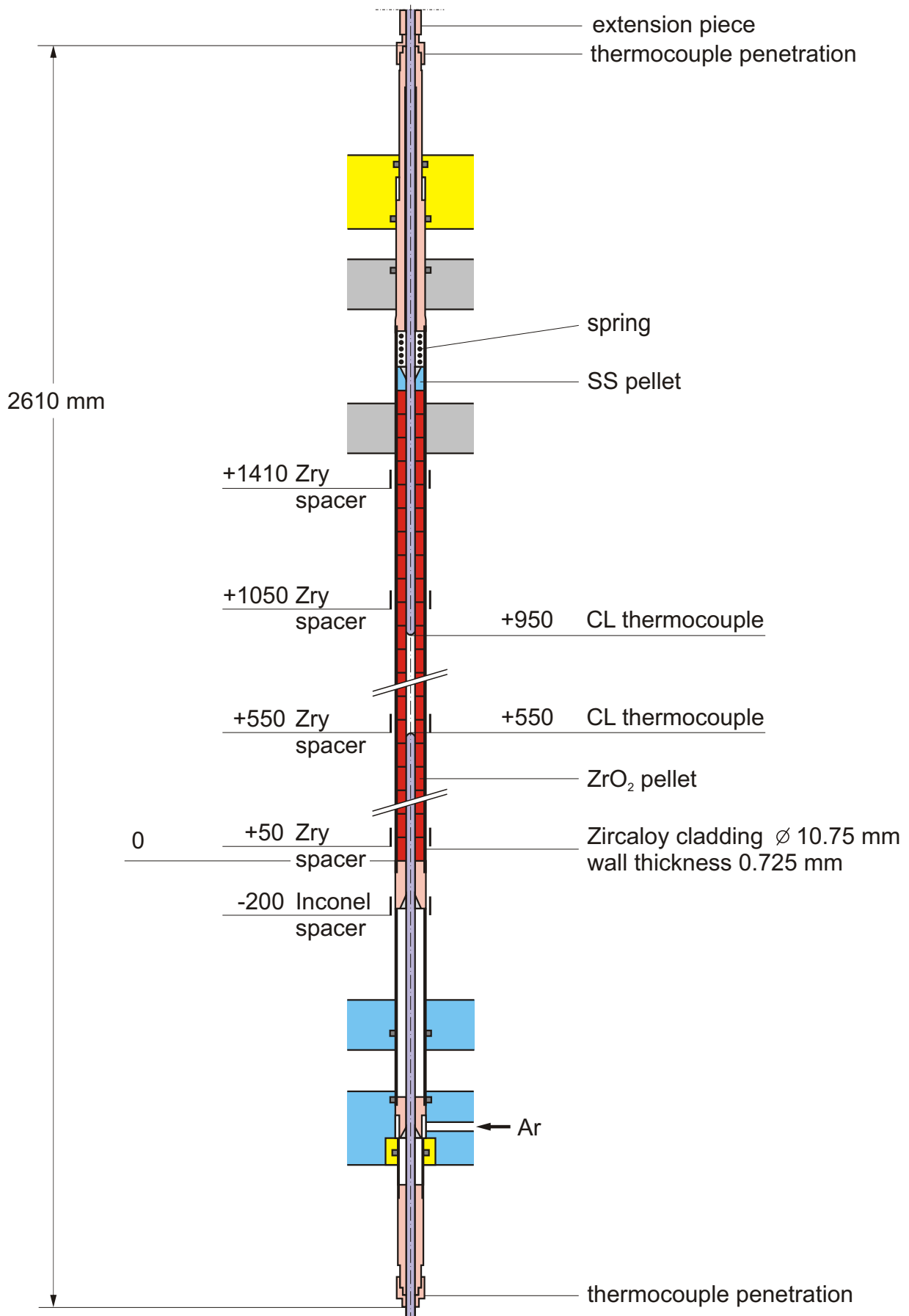
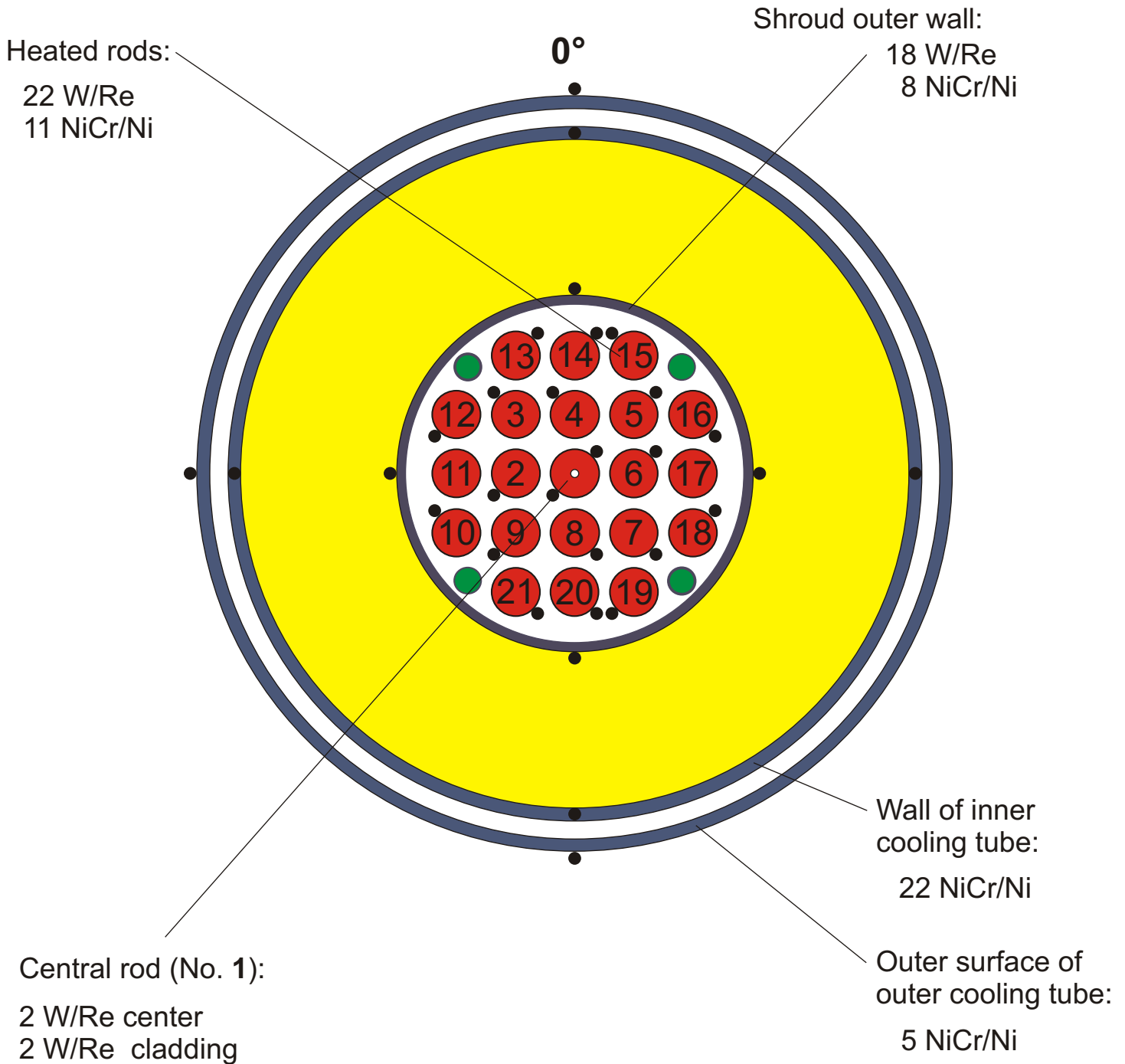


Fig 8

QUENCH Test Bundle

TC Instrumentation and Rod Designation (Top View)



Thermocouples at **17 axial elevations:**
From -250 mm to +1350 mm with distances of 100 mm

Fig 9

QUENCH Test Section Instrumentation

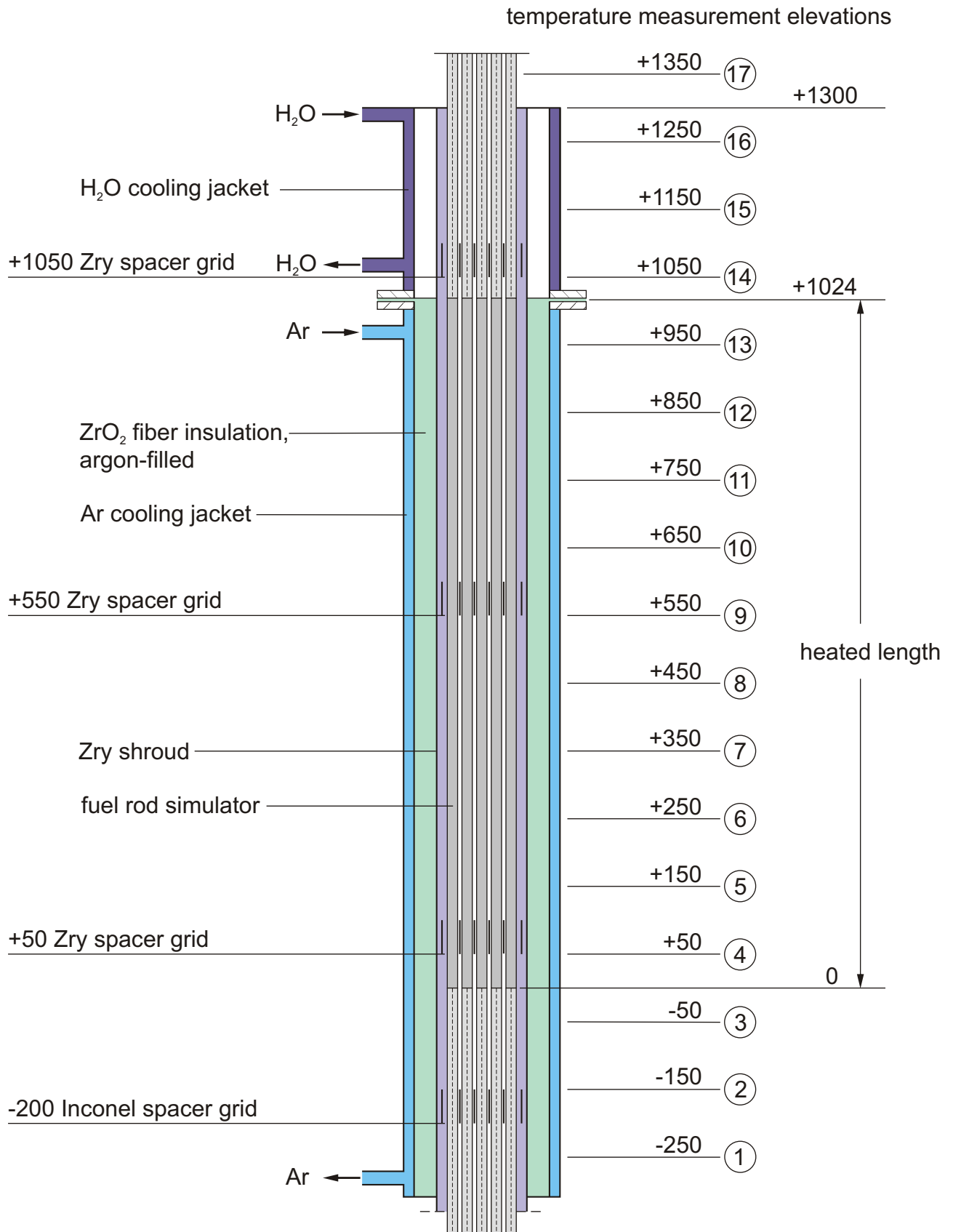
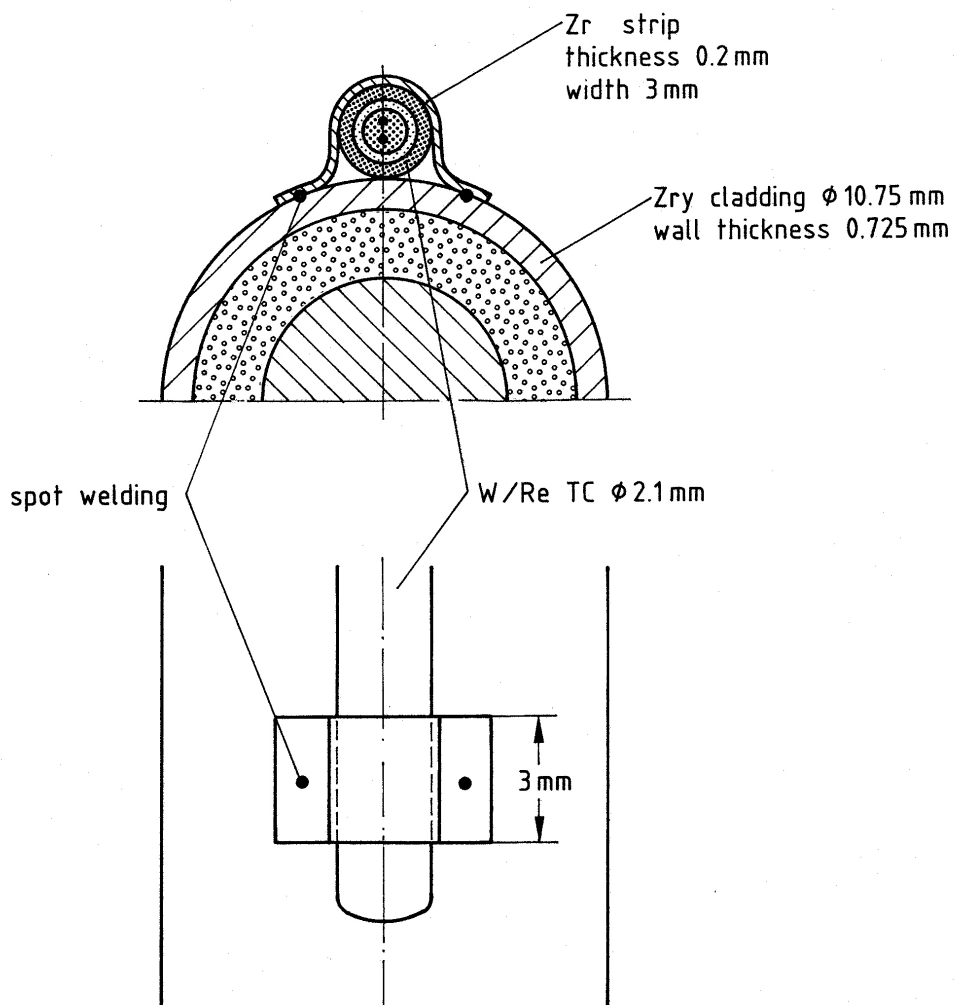


Fig 10

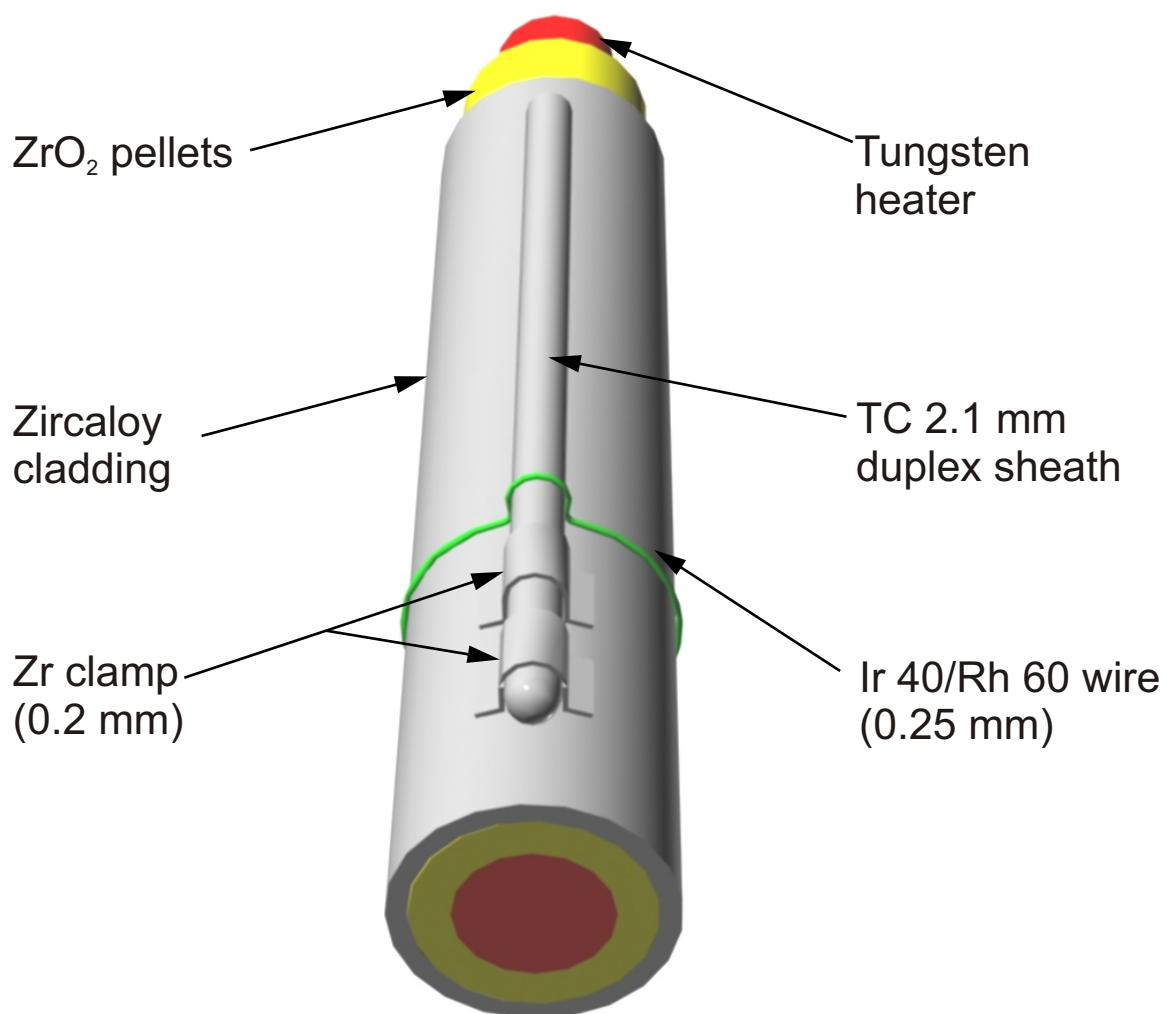
QUENCH Facility TC Attachment on the cladding



IMF III / 02.97

Fig 12

TC Fastening Concept for the QUENCH Test Rods



With pre-oxidation: Zr clamp + wire

Without pre-oxidation: Zr clamp

Fig 13

Quenchch-01 Test Conduct

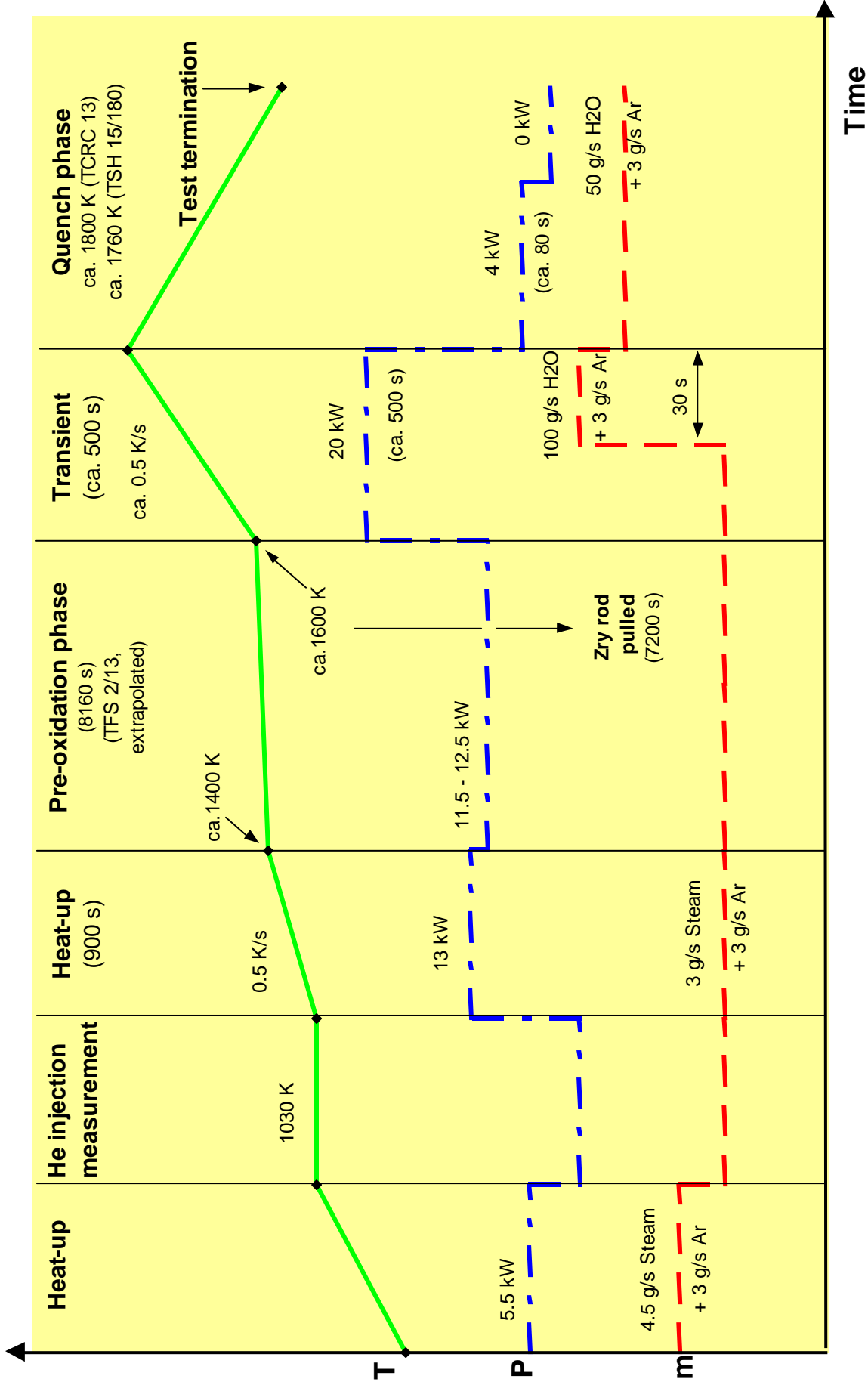
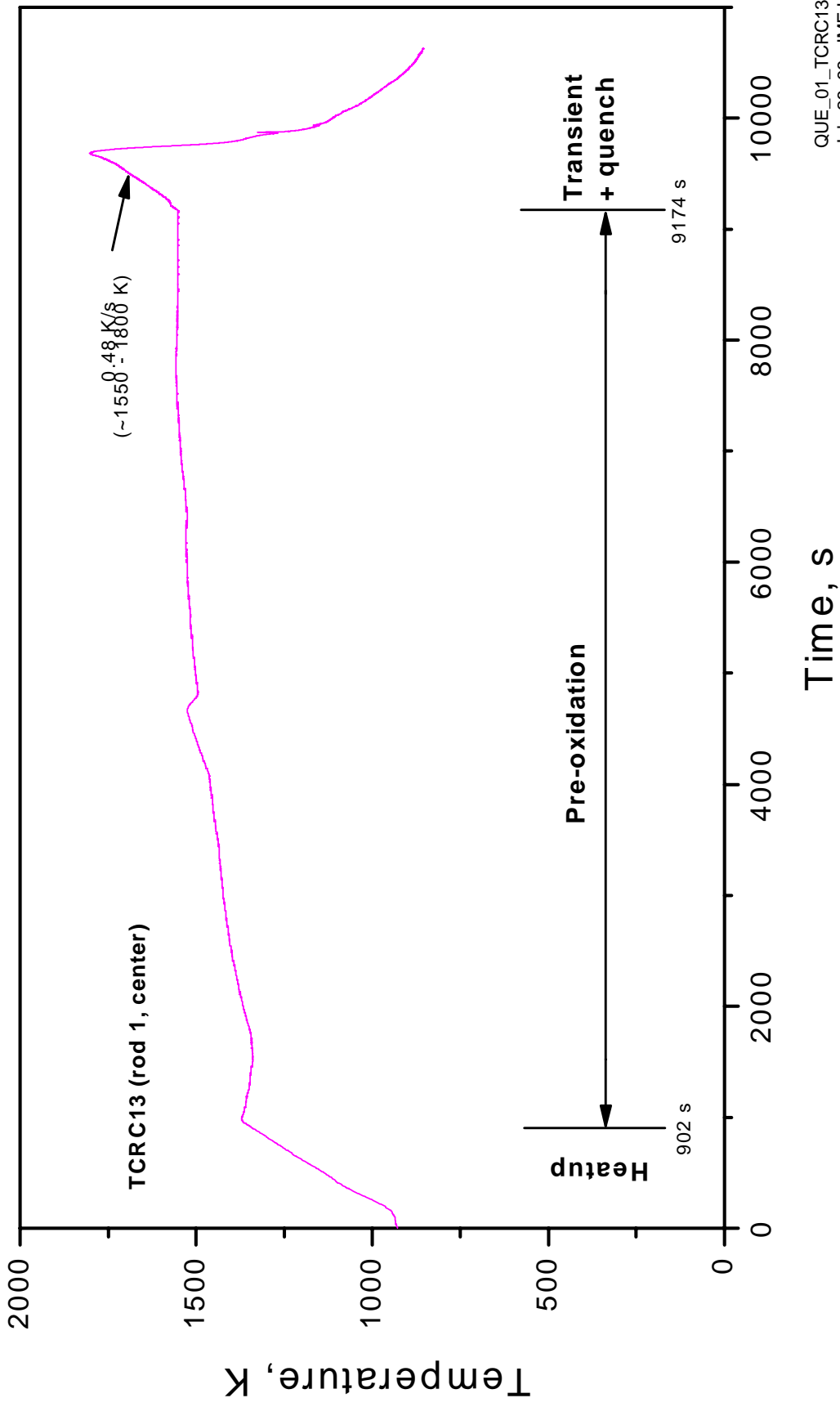


Fig 14

QUENCH-01 Test Phases, Overview



QUE_01_TCRC13
July 26, 99 - IMF III

Fig 15

Test QUENCH-01 - Pre-Oxidation Phase

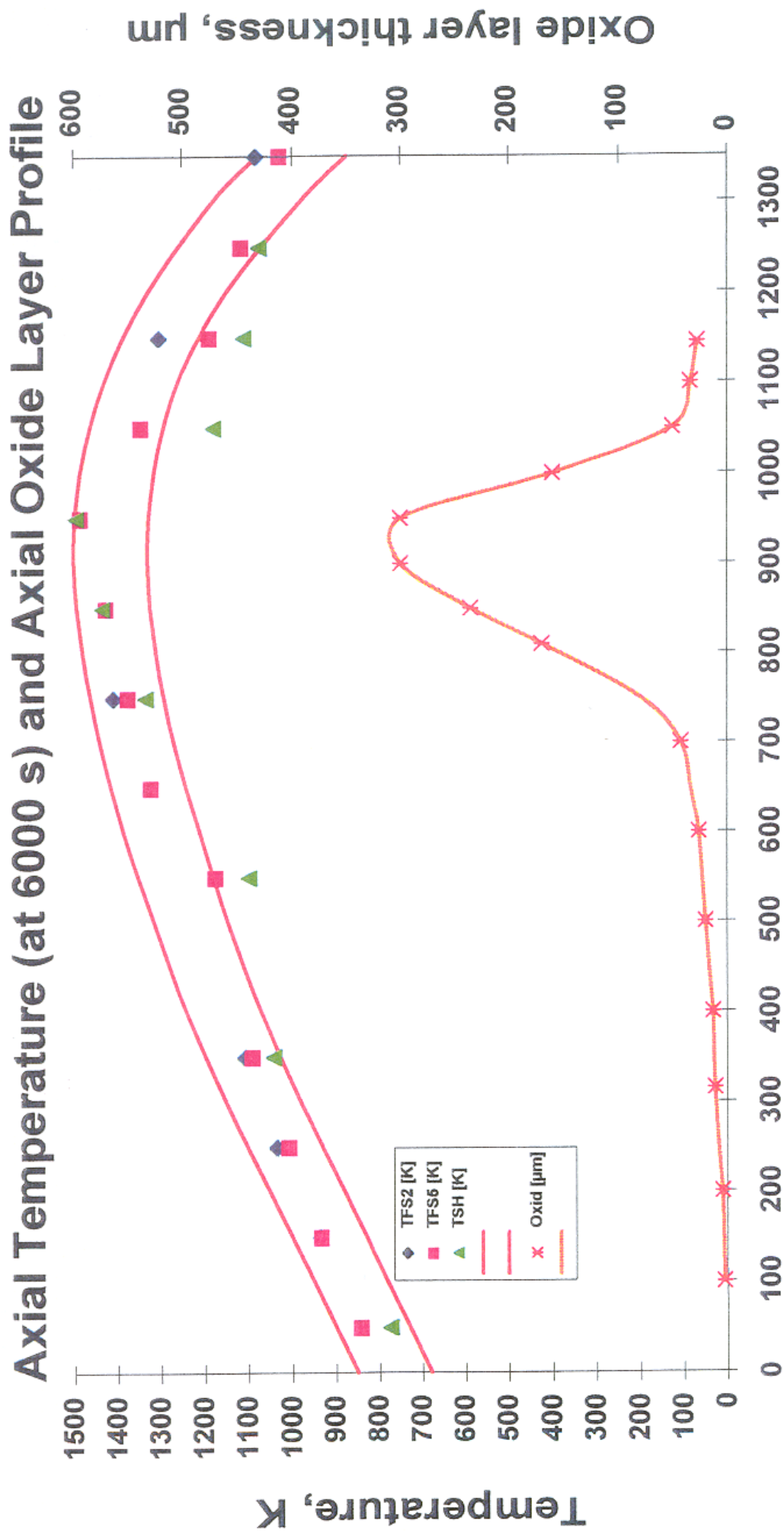
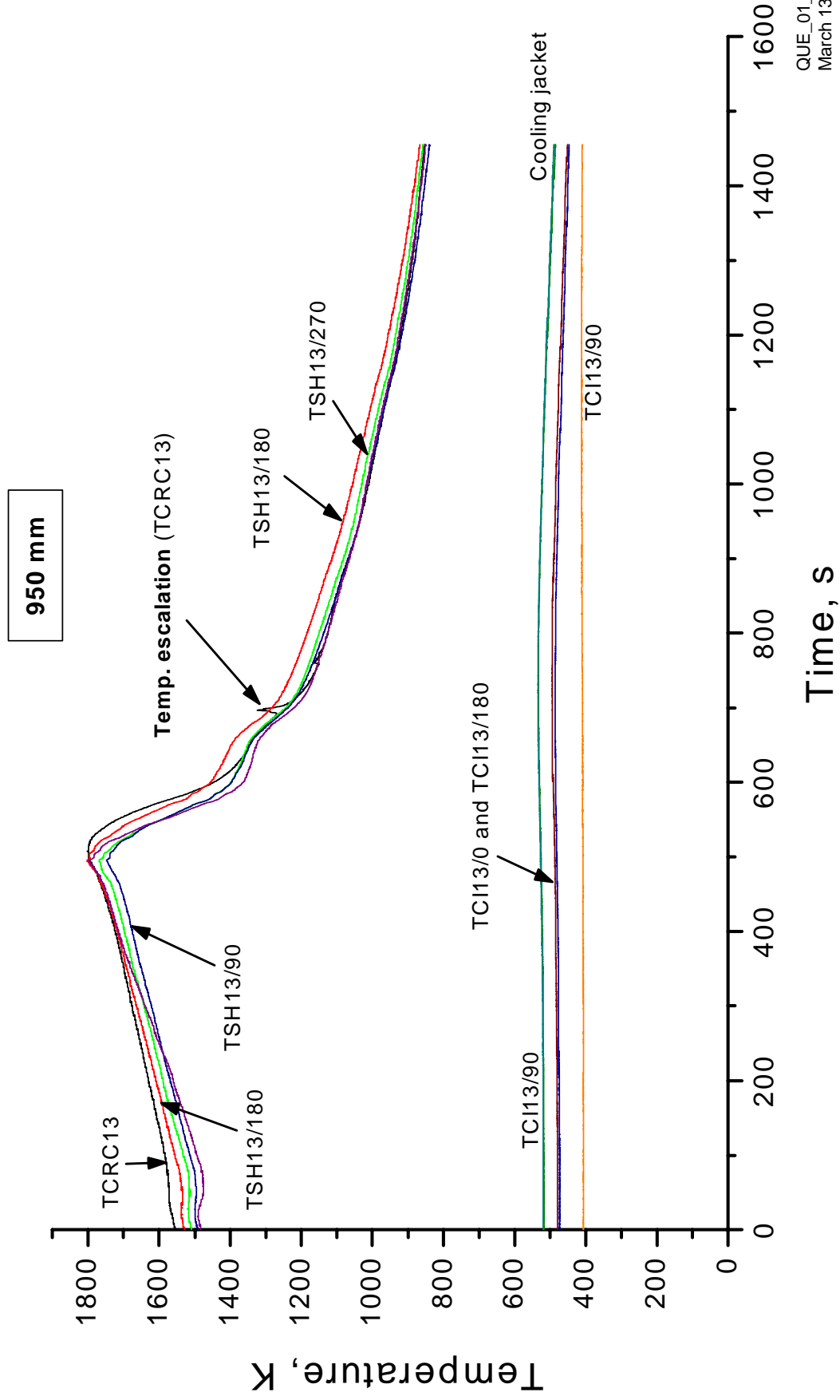


Fig. 16

QUE_01_axial_zeit_b_ox1
April 23, 98_HIT

QUENCH-01 (Febr. 26, 1998)

Transient + Quenching Phase

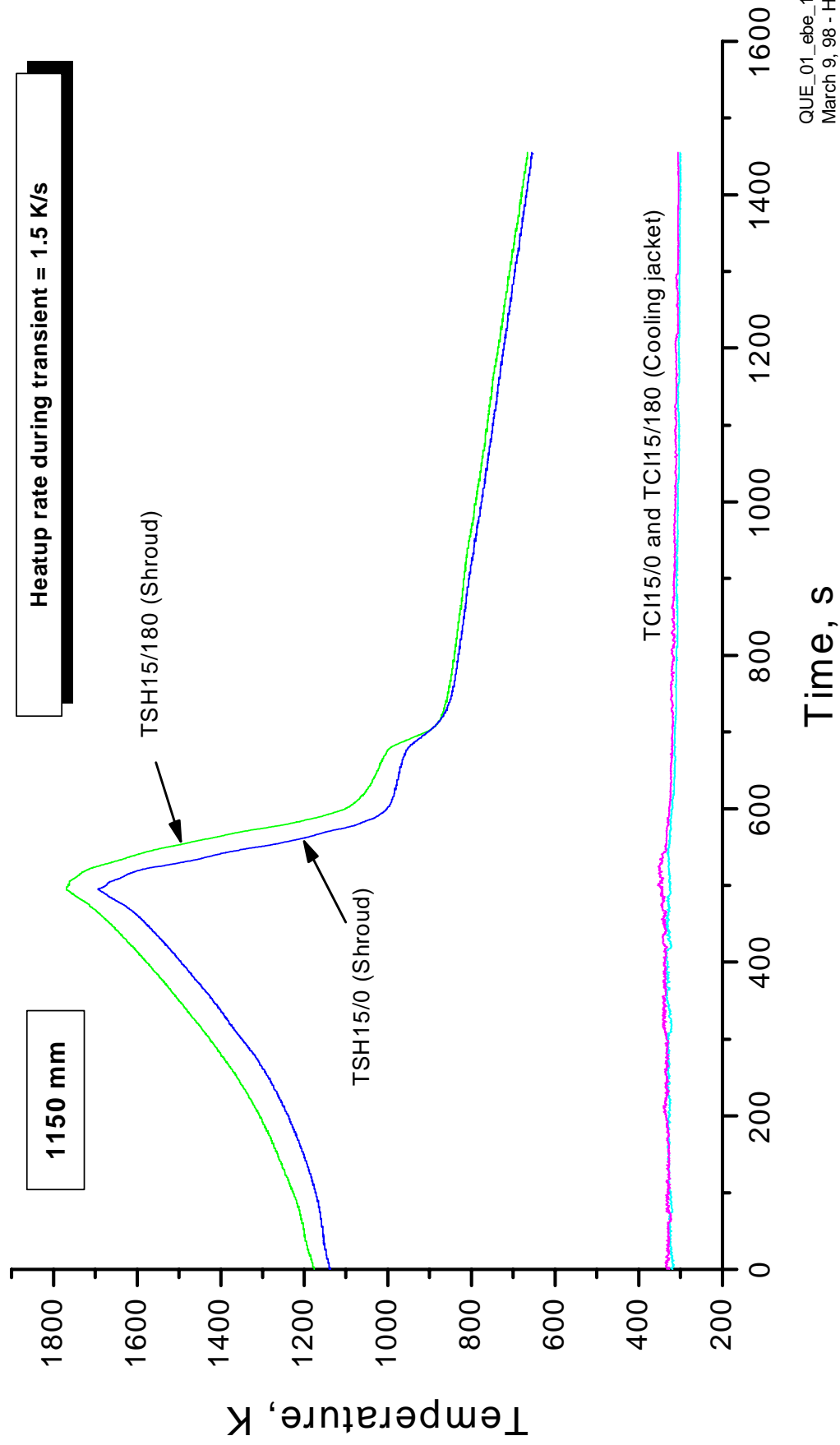


QUE_01_ebe_13
March 13, 98 - HIT

Fig 17

QUENCH-01 (Febr. 26, 1998)

Transient + Quenching Phase

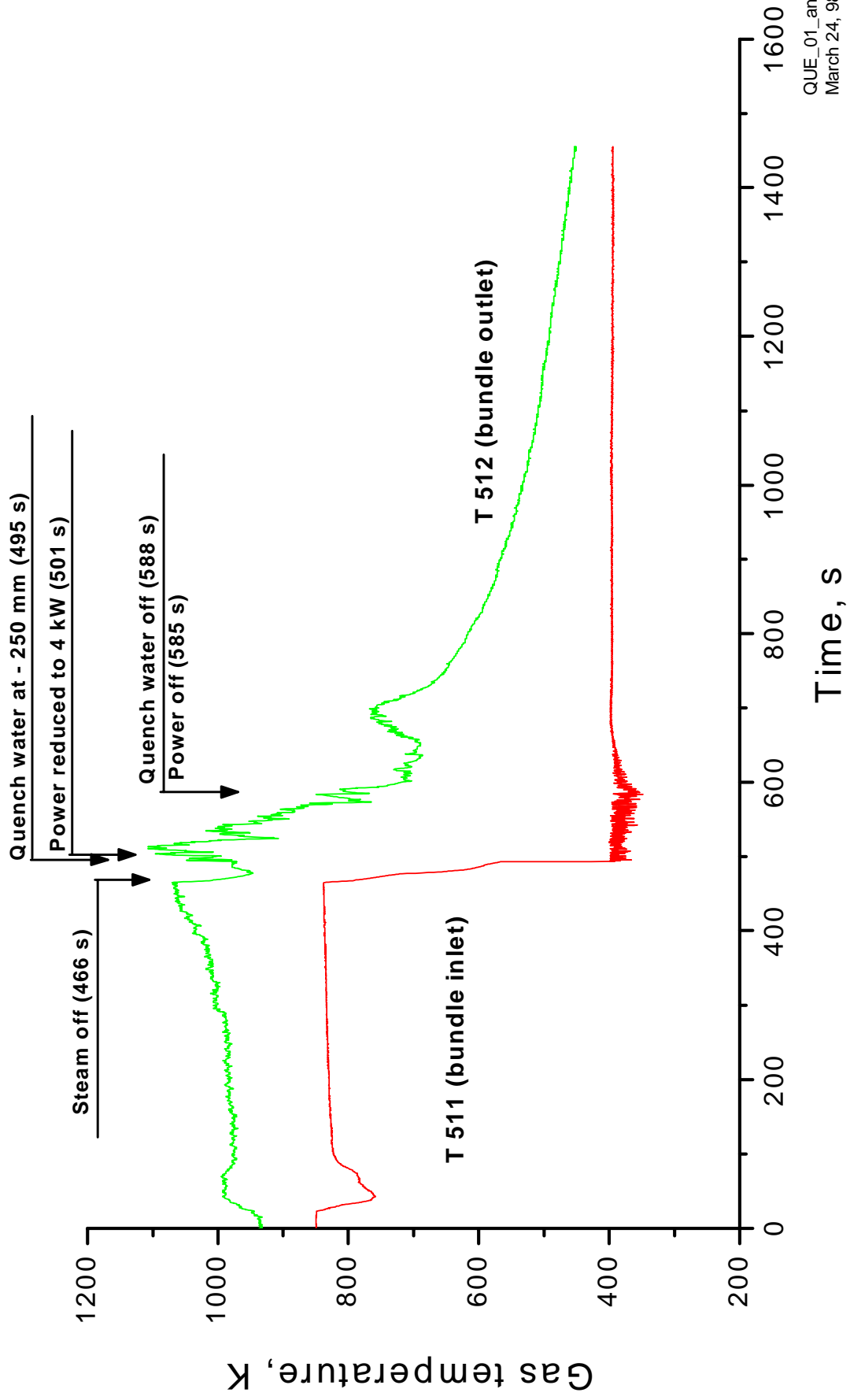


QUE_01_ebe_15
March 9, 98 - HIT

Fig 18

QUENCH-01 (Febr. 26, 1998)

Transient + Quench Phase



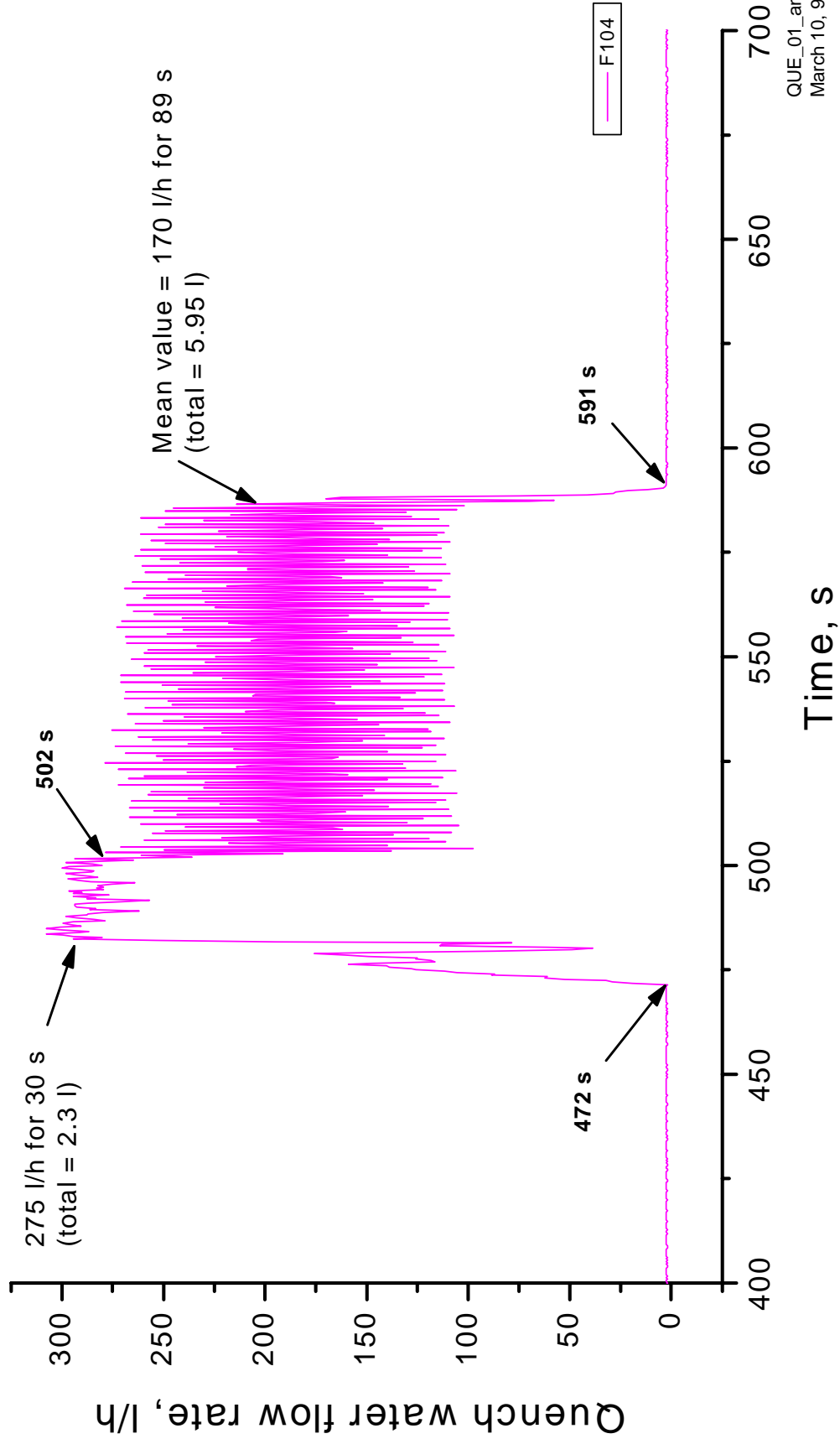
QUE_01_anlage.c
March 24, 98 - HIT

Fig 19

QUENCH-01 (Febr. 26, 1998)

Quenching Phase

Injection rate: 1.6 cm/s (coolant channel cross section = 30 cm²)

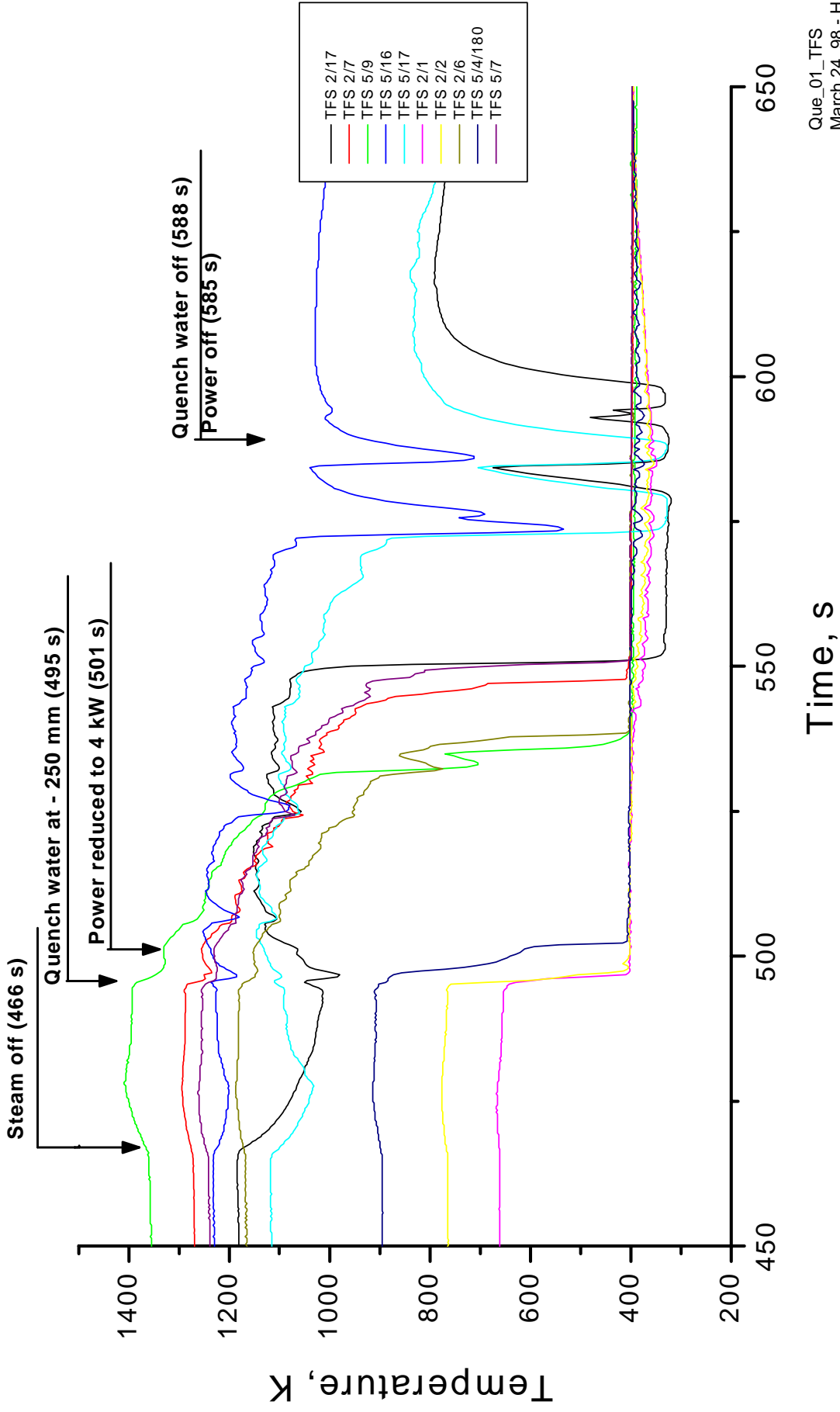


QUE_01_anlage.c
March 10, 98 - HIT

Fig 20

QUENCH-01 (Febr. 26, 1998)

Quenching Phase

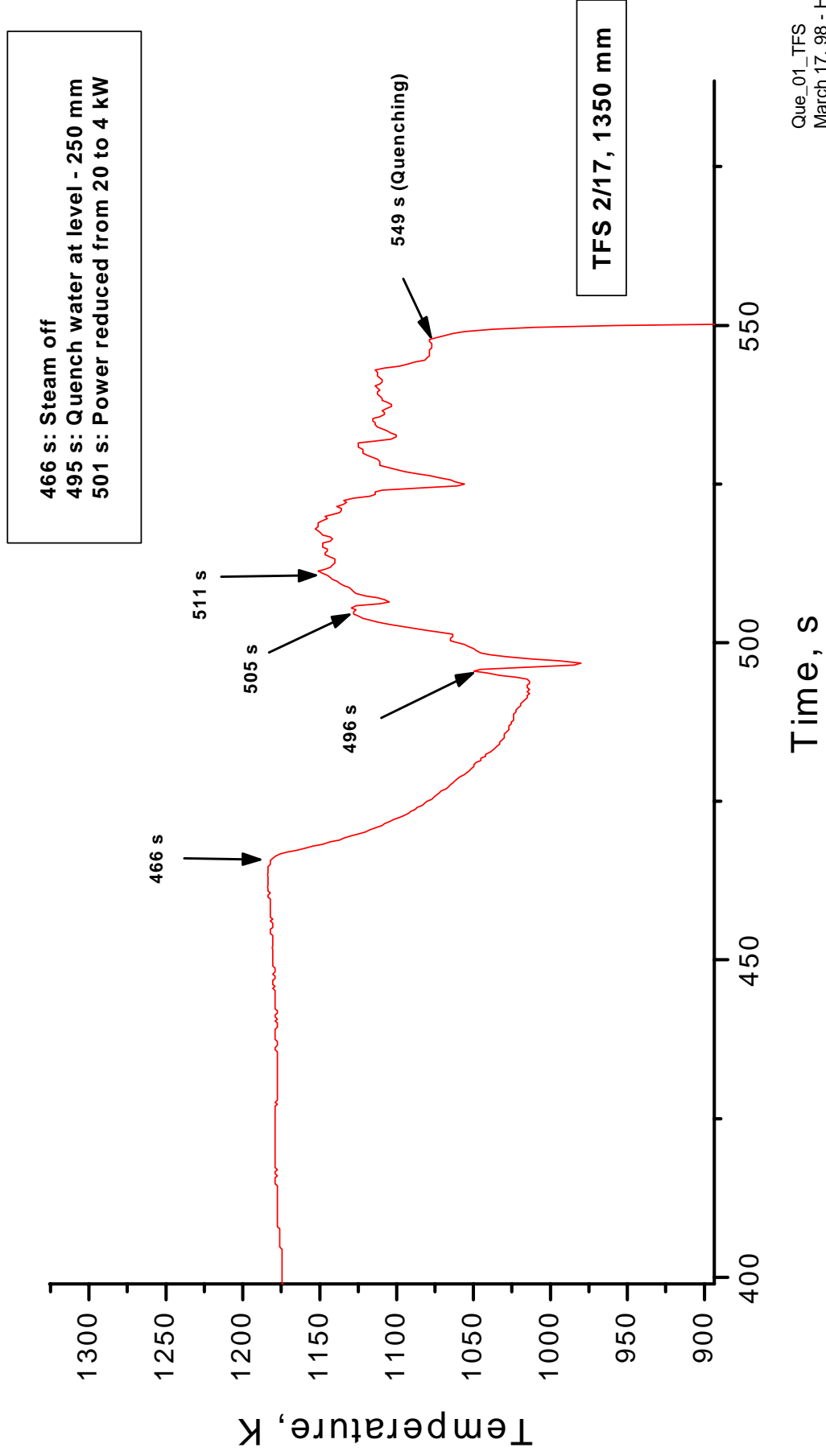


Que_01_TFS
March 24, 98 - HIT

Fig 21

QUENCH-01 (Febr. 26, 1998)

Quenching Phase

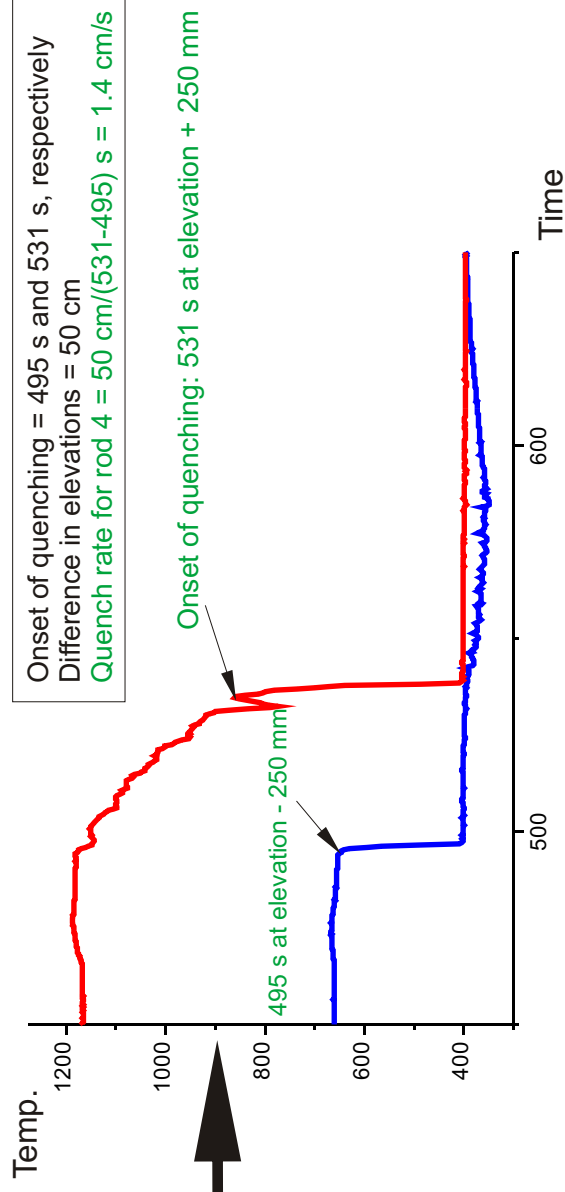
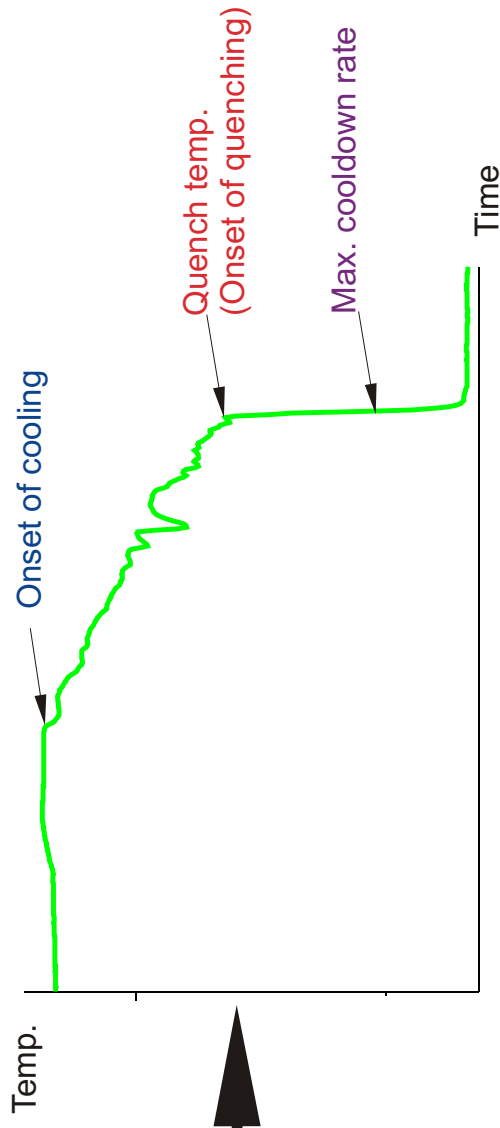


Que_01_TFS
March 17, 98 - HIT

Fig 22

Definitions

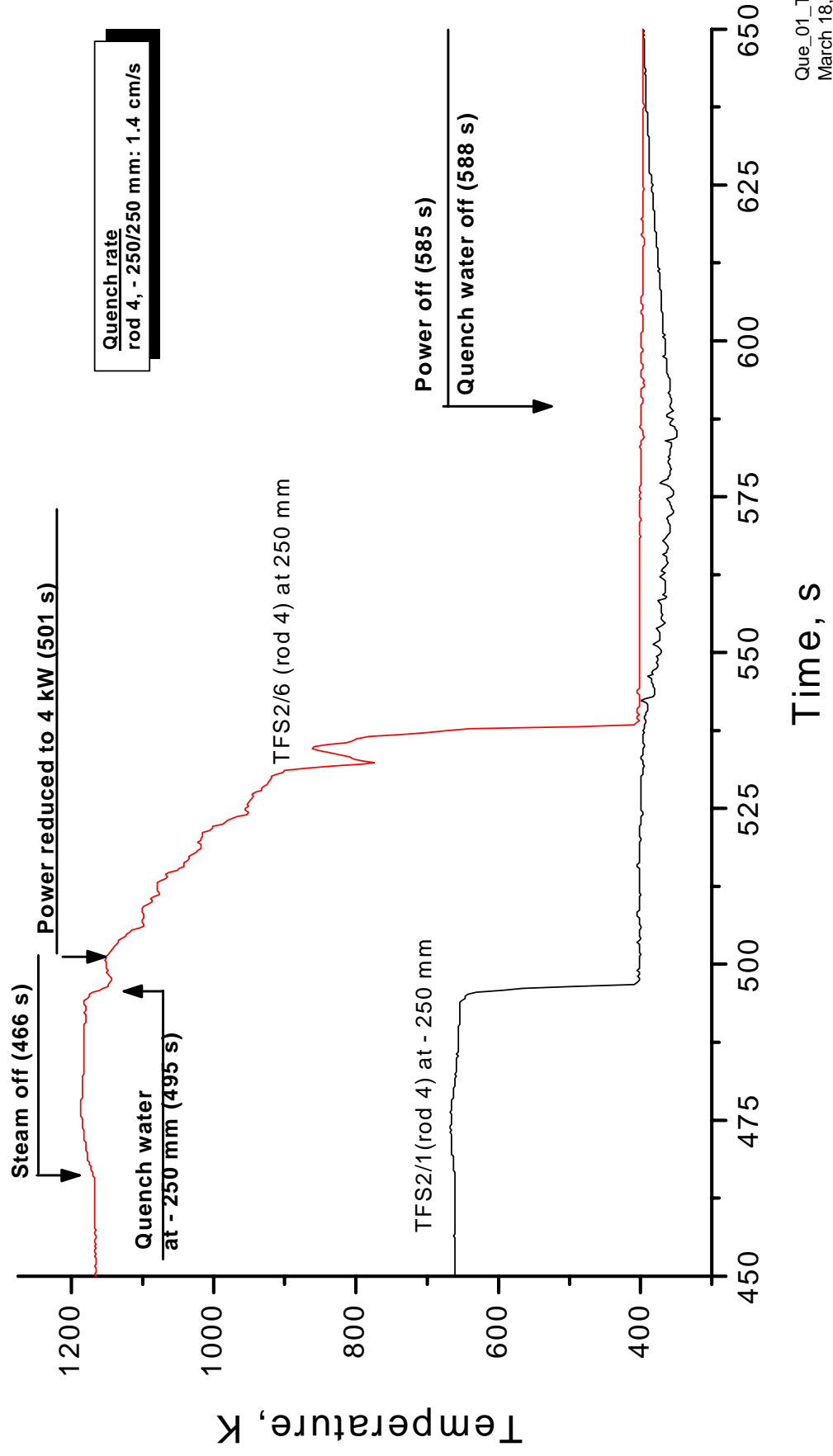
- Onset of cooling
- Onset of quenching
- Max. cooldown rate



- Injection rate = Quench water flow entering the bottom of the test section determined by quench pump rate
- Flooding rate = Injection rate minus water evaporation in the test section; function of elevation

QUENCH-01 (Febr. 26, 1998)

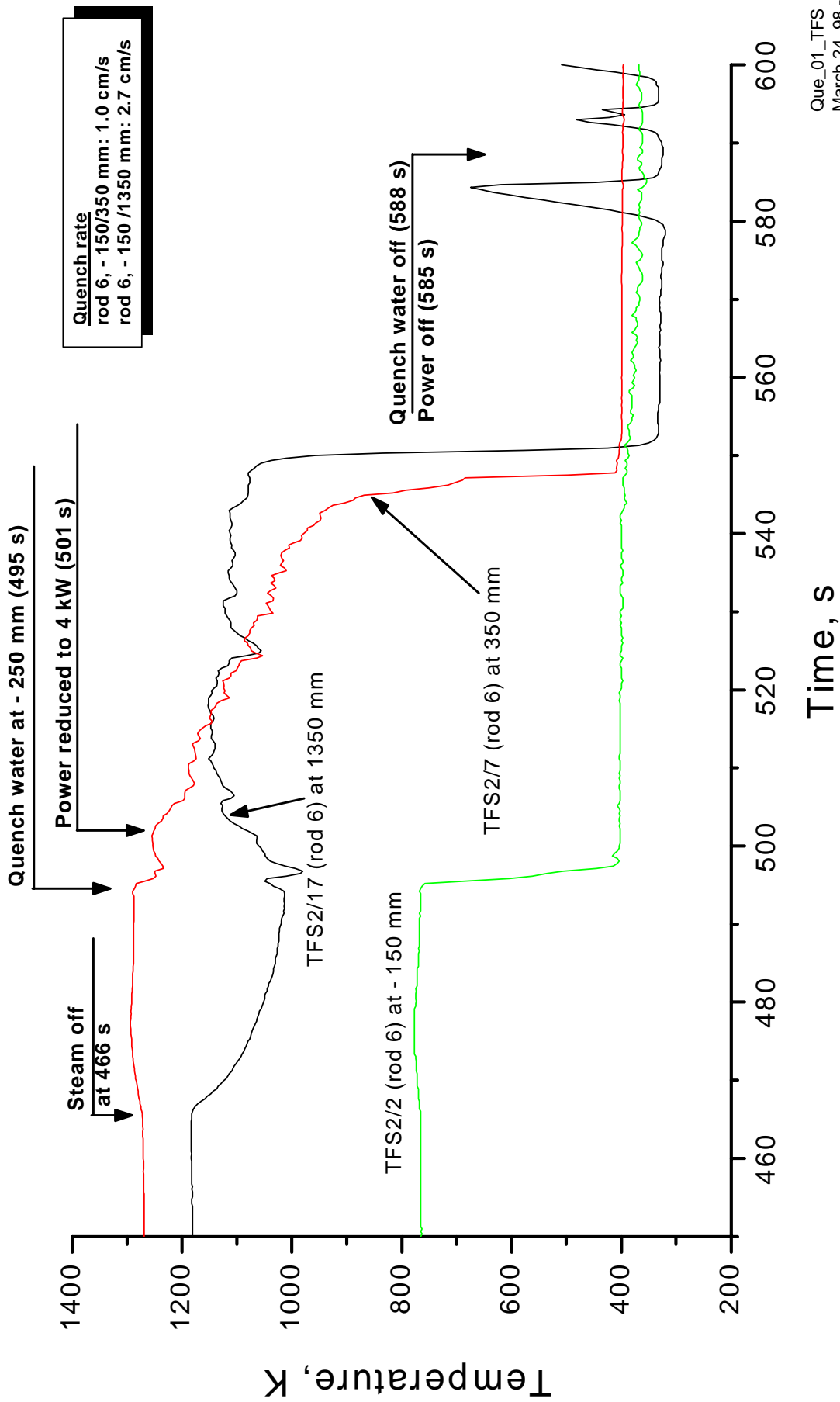
Quenching Phase



Que_01_TFS
March 18, 98 - HIT

Fig 24

QUENCH-01 (Febr. 26, 1998) Quenching Phase

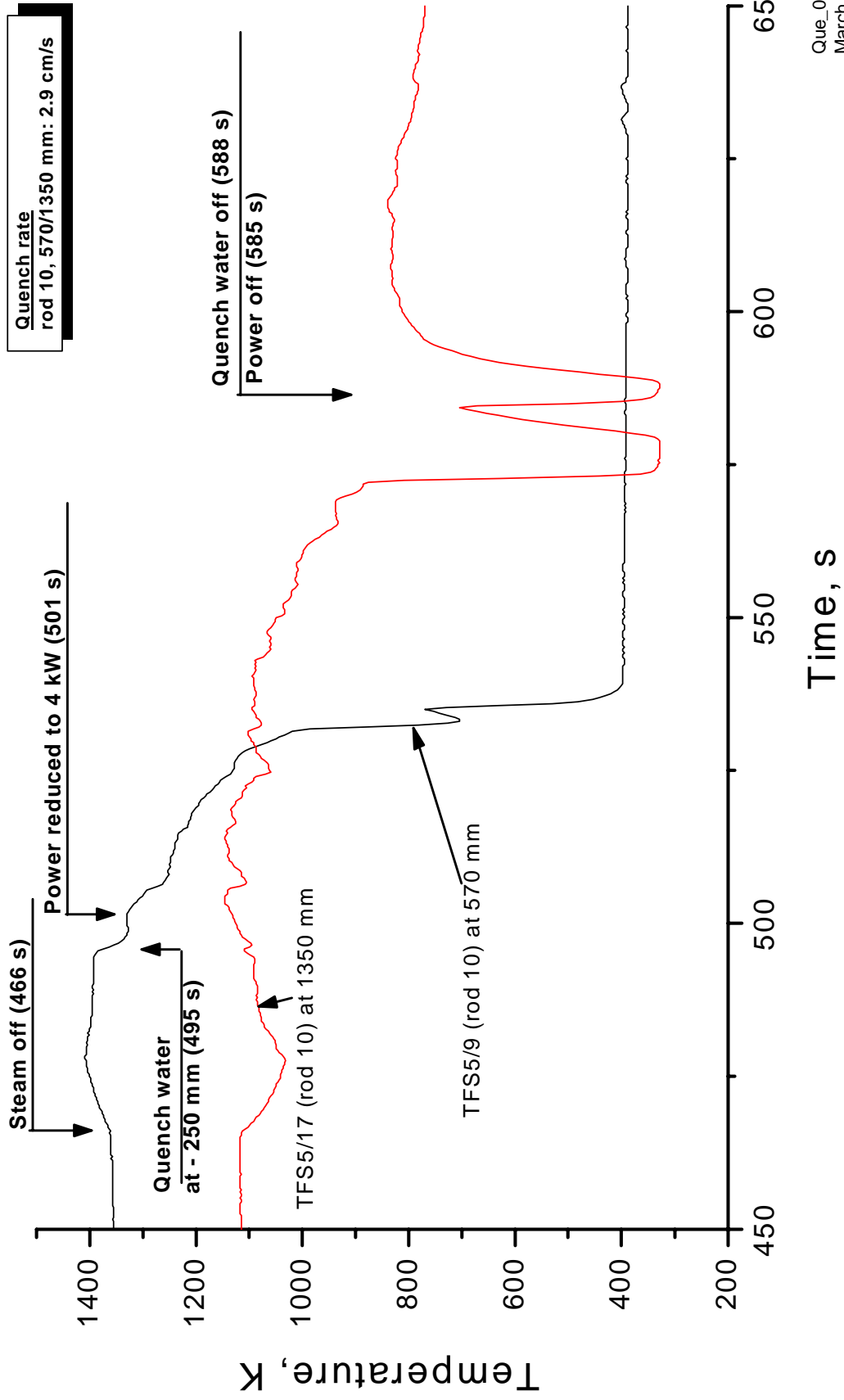


Que_01_TFS
 March 24, 98 - HIT

Fig 25

QUENCH-01 (Febr. 26, 1998)

Quenching Phase

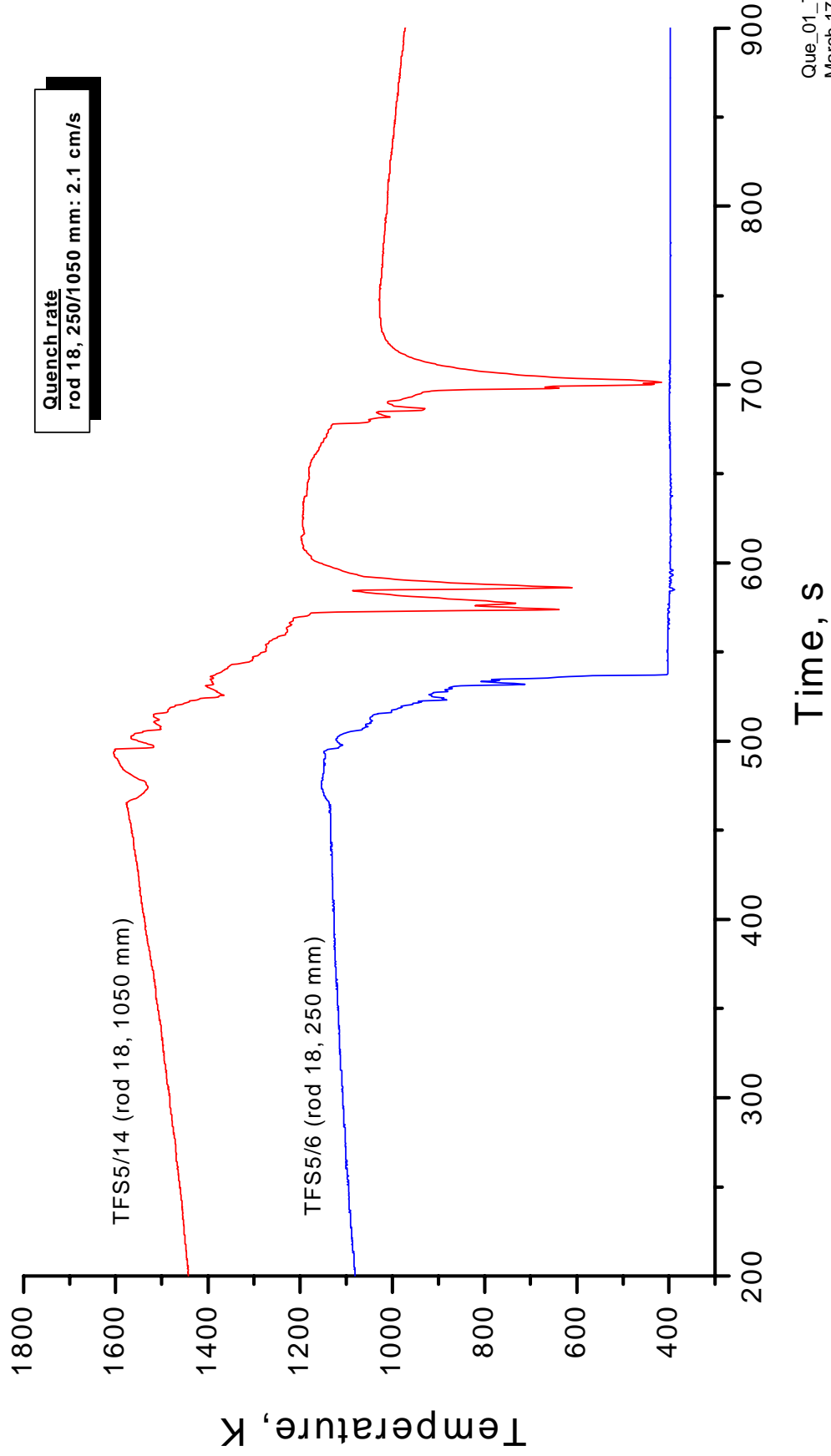


Que_01_TFS
March 18, 98 - HIT

Fig 26

QUENCH-01 (Febr. 26, 1998)

Quenching Phase



Que_01_TFS
March 17, 98 - HIT

Fig 27

QUENCH-01 (Febr. 26, 1998)

Quenching Phase

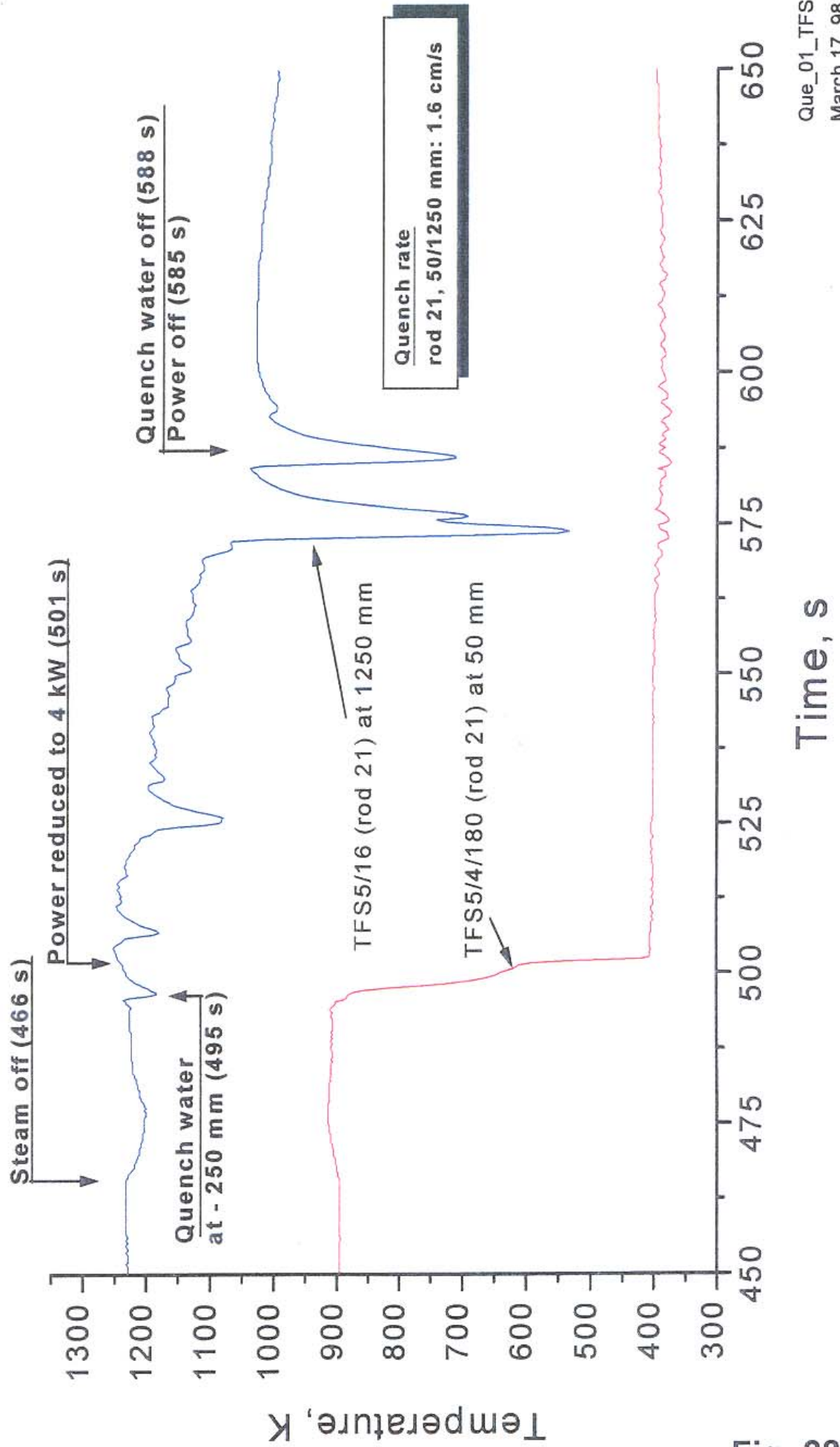
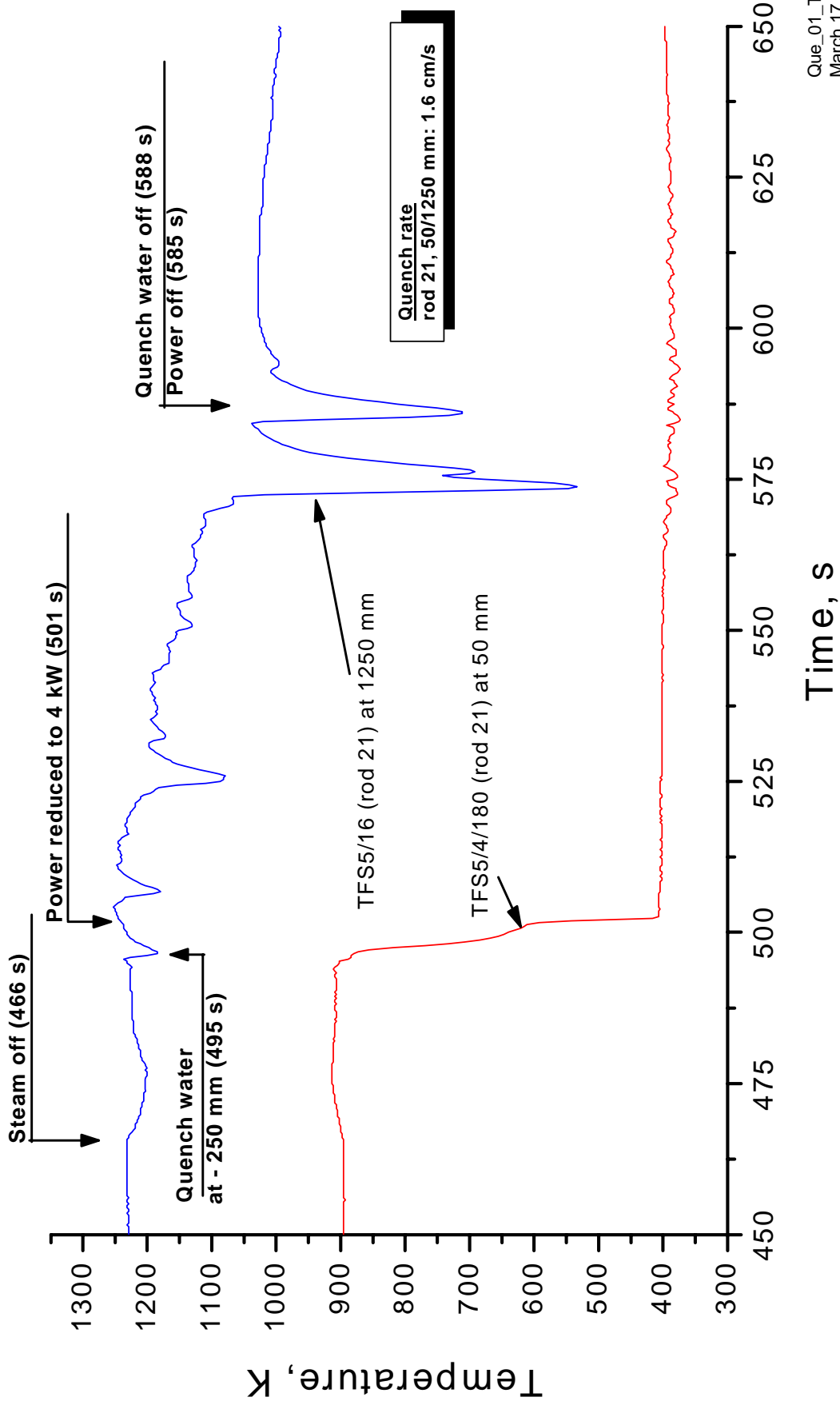


Fig. 28

QUENCH-01 (Febr. 26, 1998) Quenching Phase

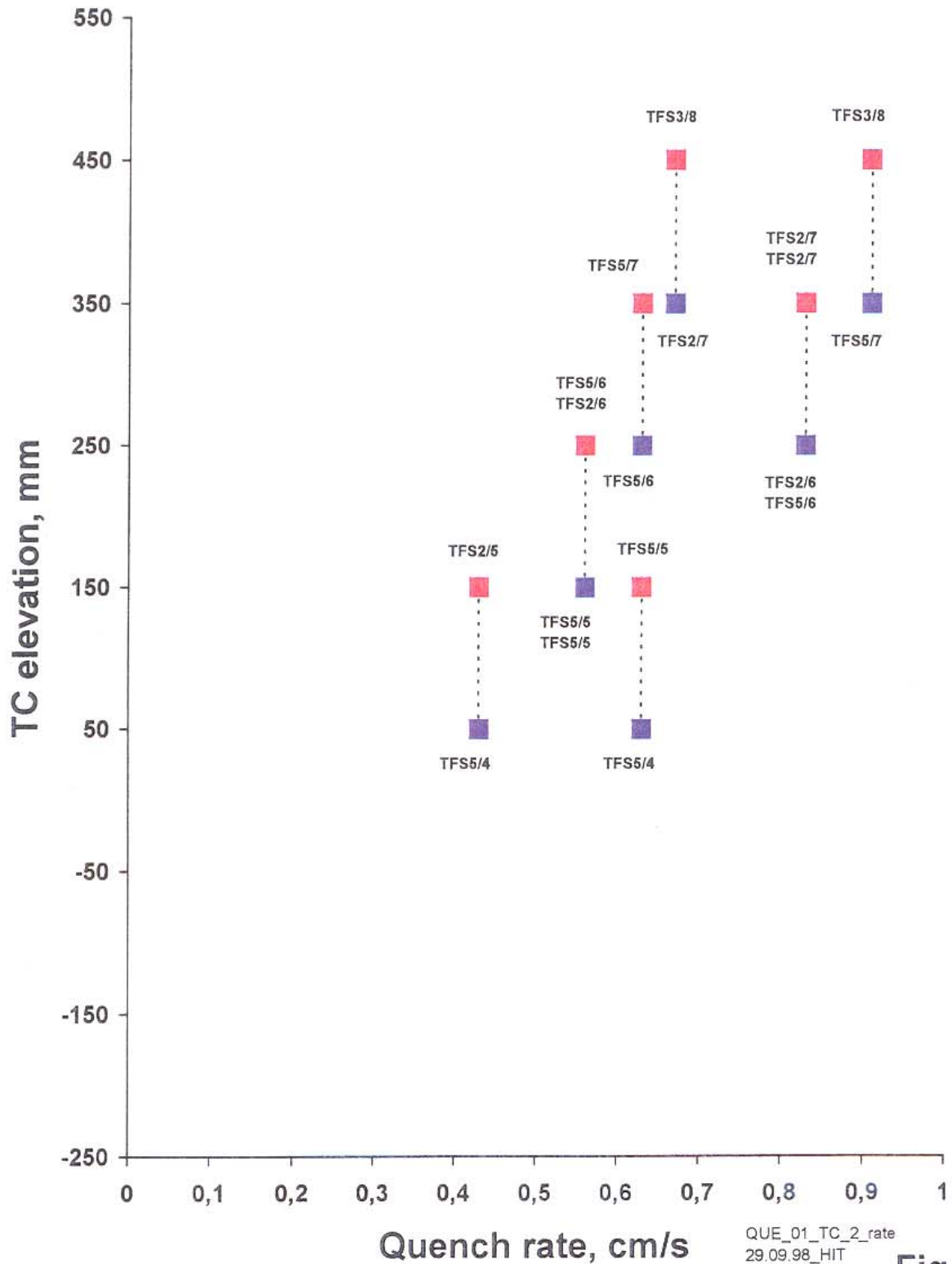


Que_01_TFS
March 17, 98 - HIT

Fig 29

Test QUENCH-01

Quench rate evaluated from temperatures (onset of quenching) of thermocouple pairs fixed at different rods at elevations located closest to each other



QUE_01_TC_2_rate
29.09.98_HIT

Fig. 30

Test QUENCH-01 - Temperature at onset of quenching as a function of elevation

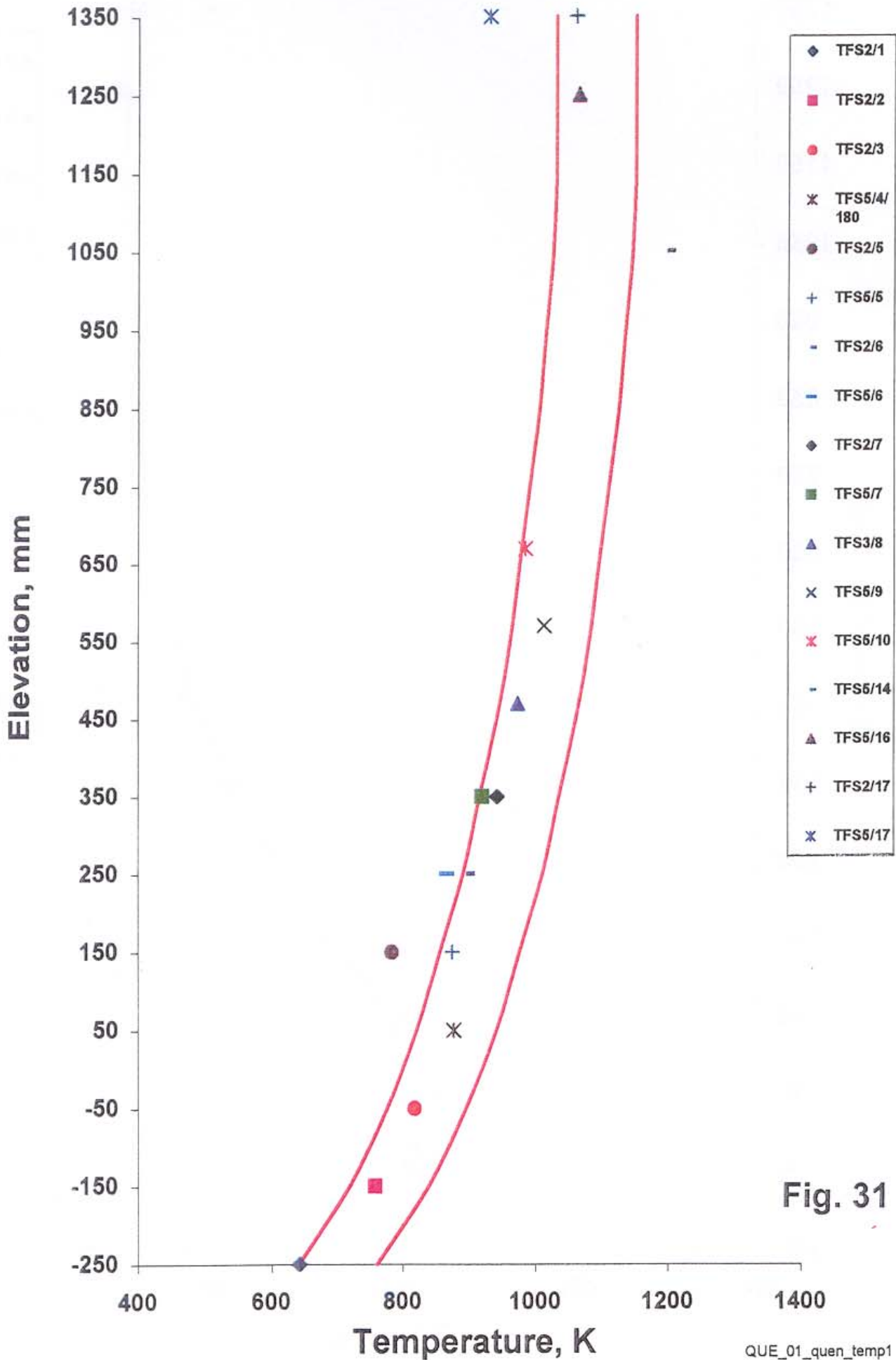


Fig. 31

Test QUENCH-01 - Onset of quenching as a function of elevation

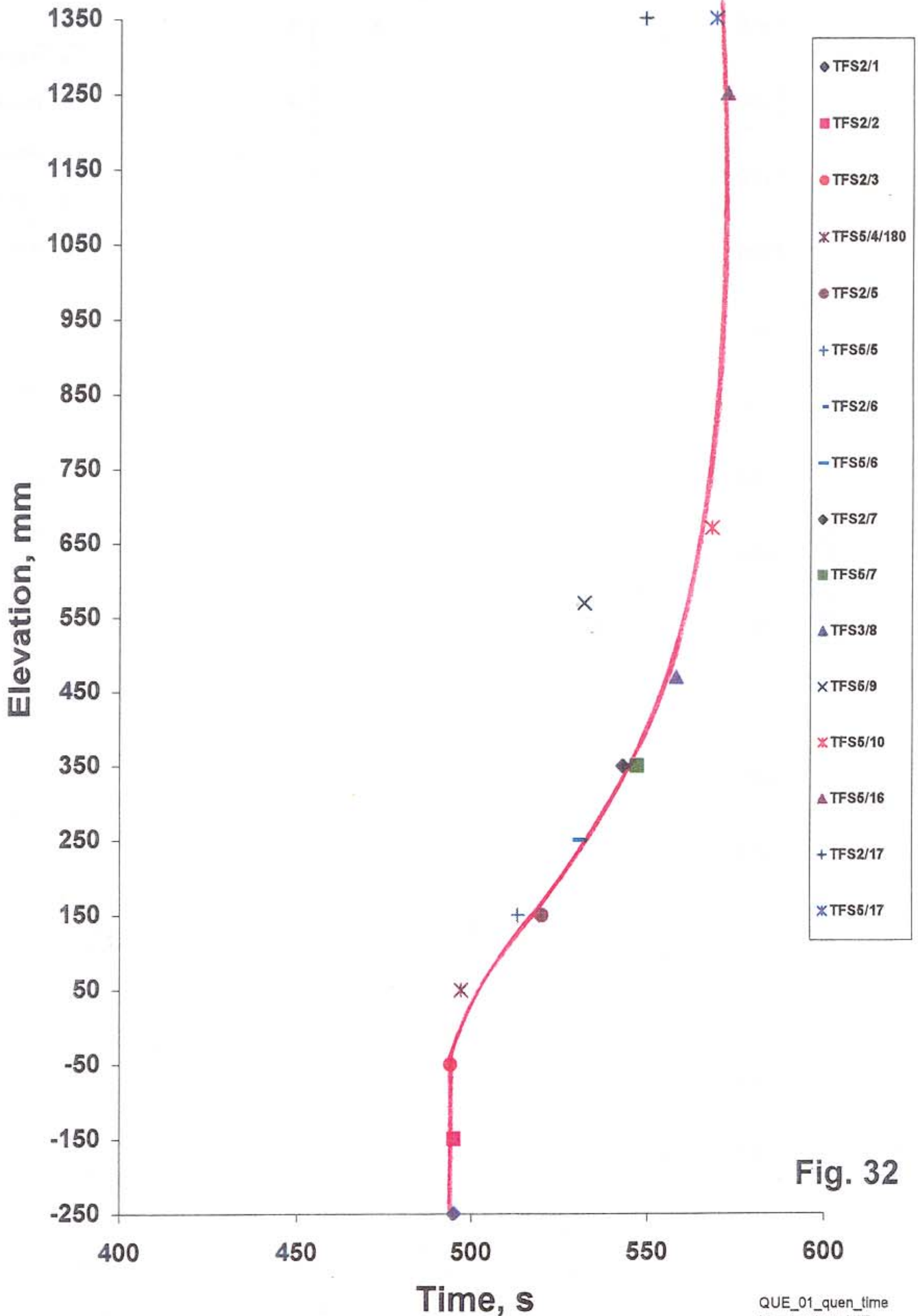


Fig. 32

QUE_01_quen_time
March 24,98_HIT

Test QUENCH-01 - Onset of cooling as a function of elevation

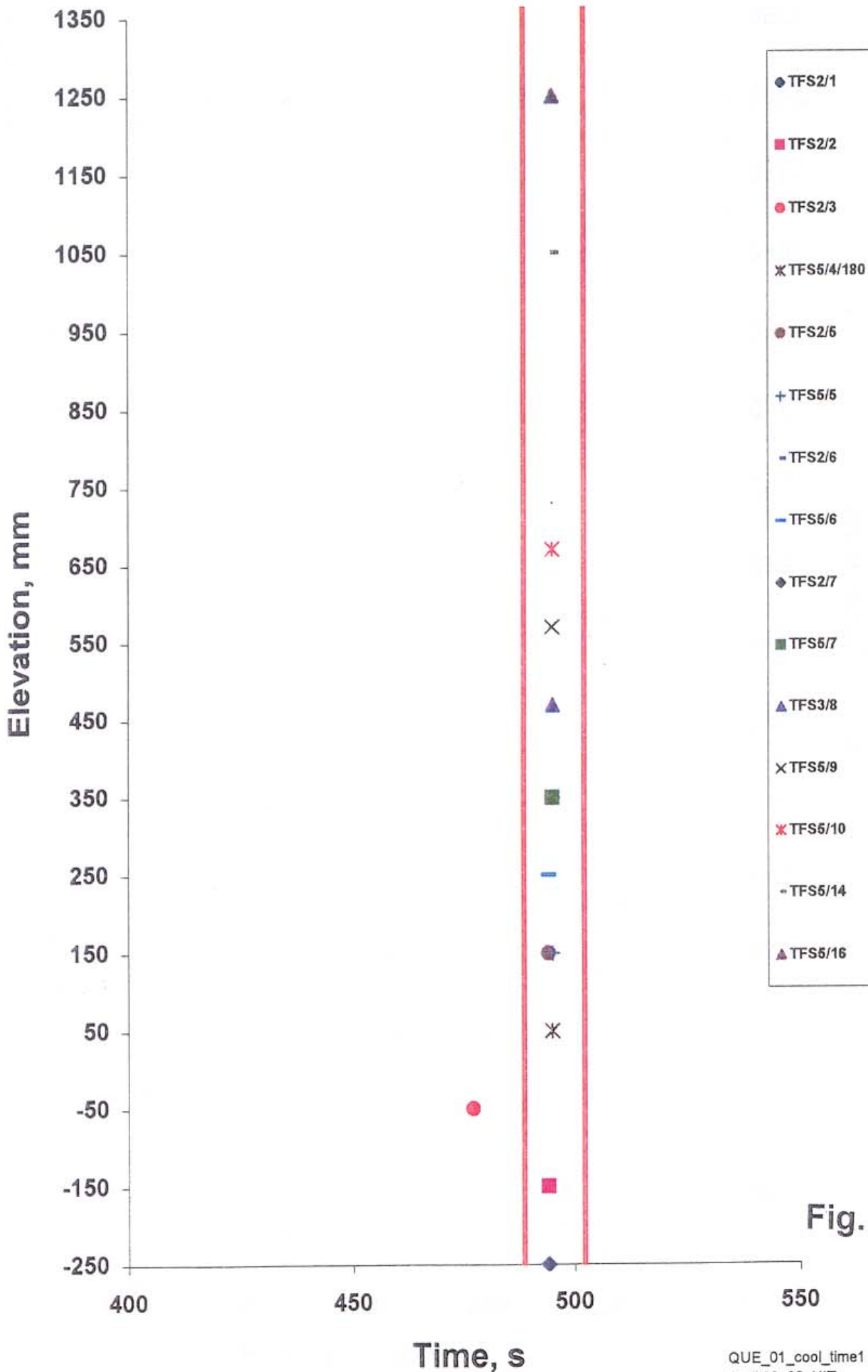


Fig. 33

Test QUENCH-01 - Temperature at onset of cooling as a function of elevation

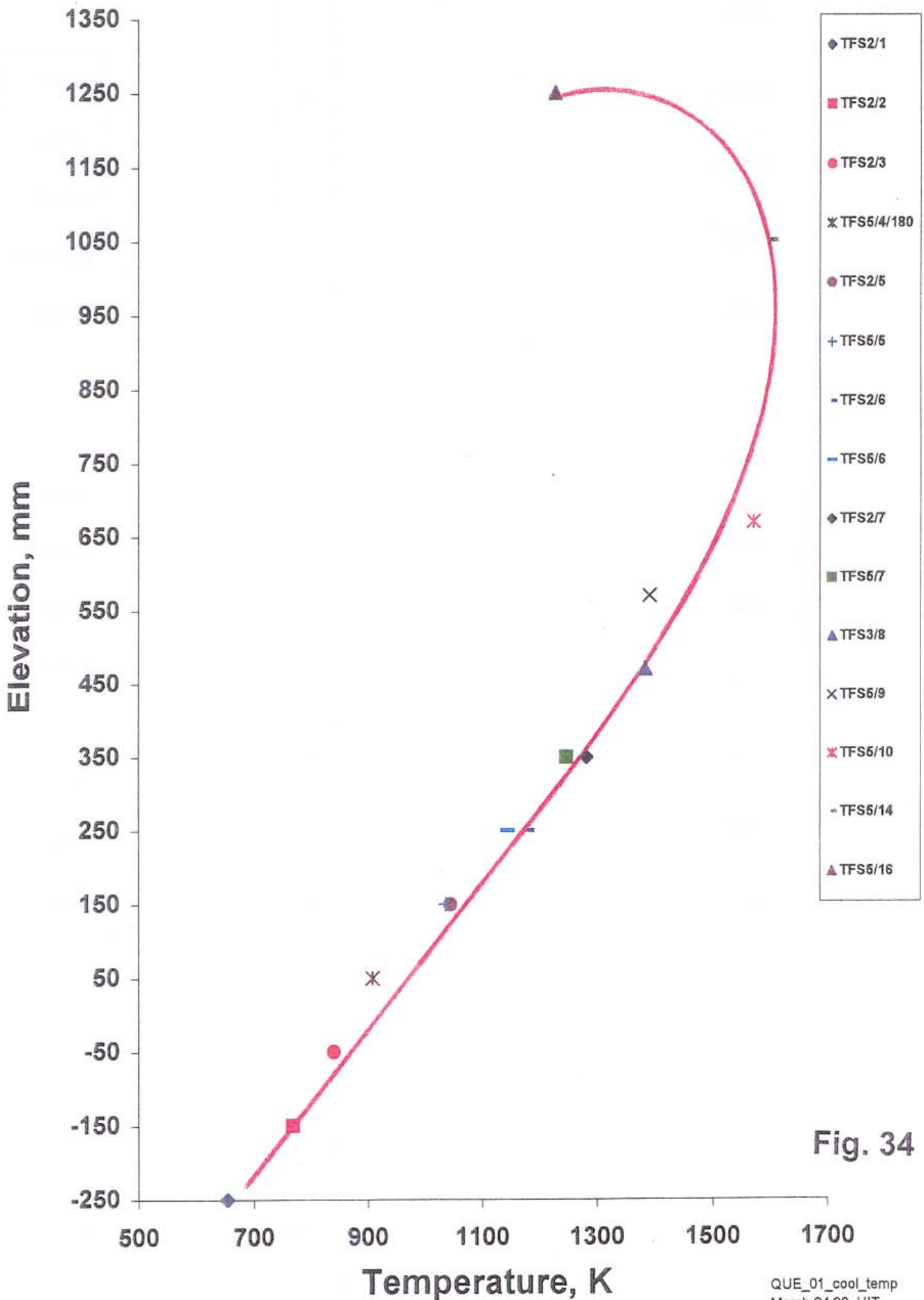
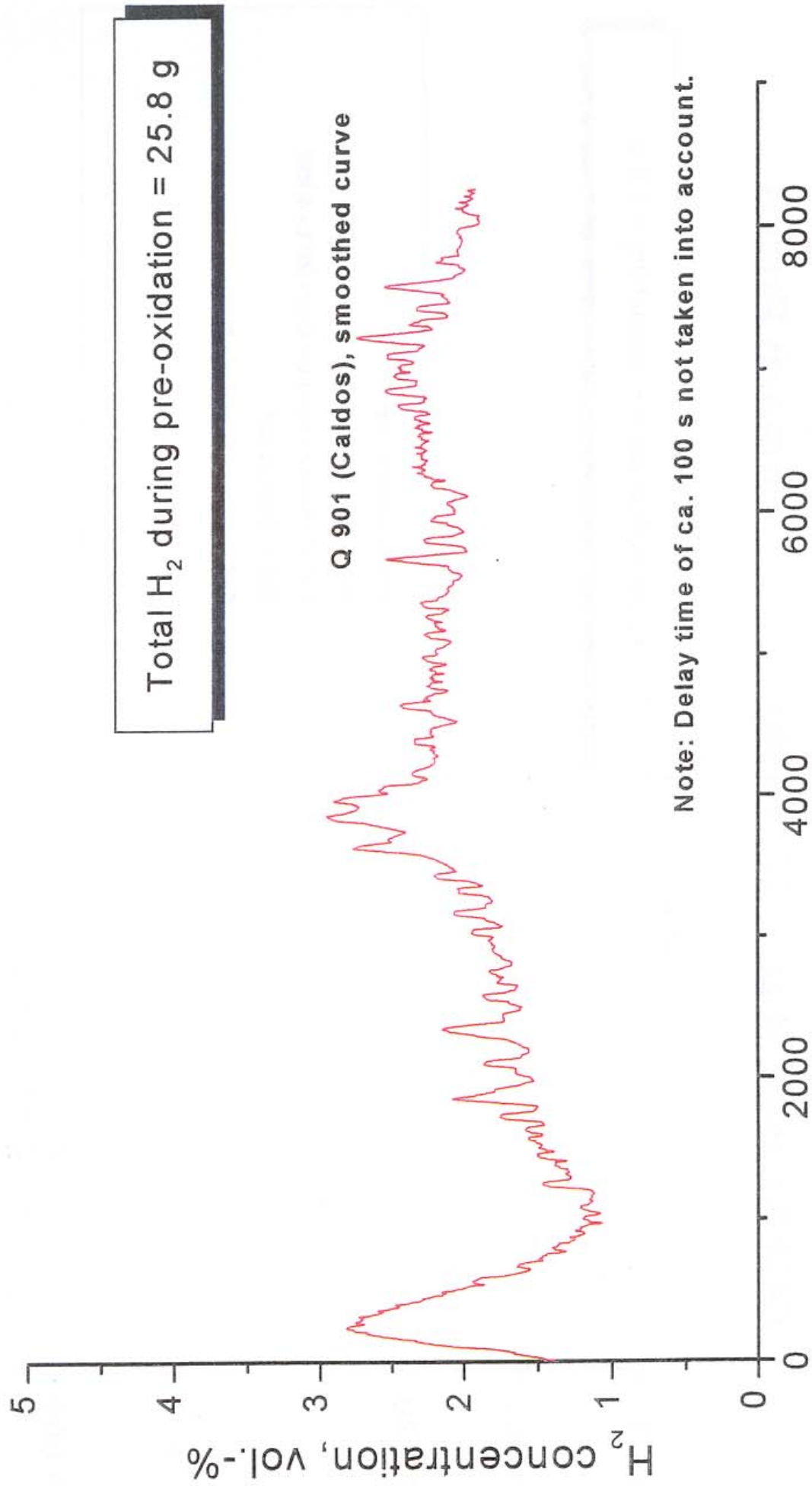


Fig. 34

QUENCH-01 (Febr. 26, 1998)

Pre-Oxidation Phase



QUENCH-01 (Febr. 26, 1998)

Transient + Quench Phase

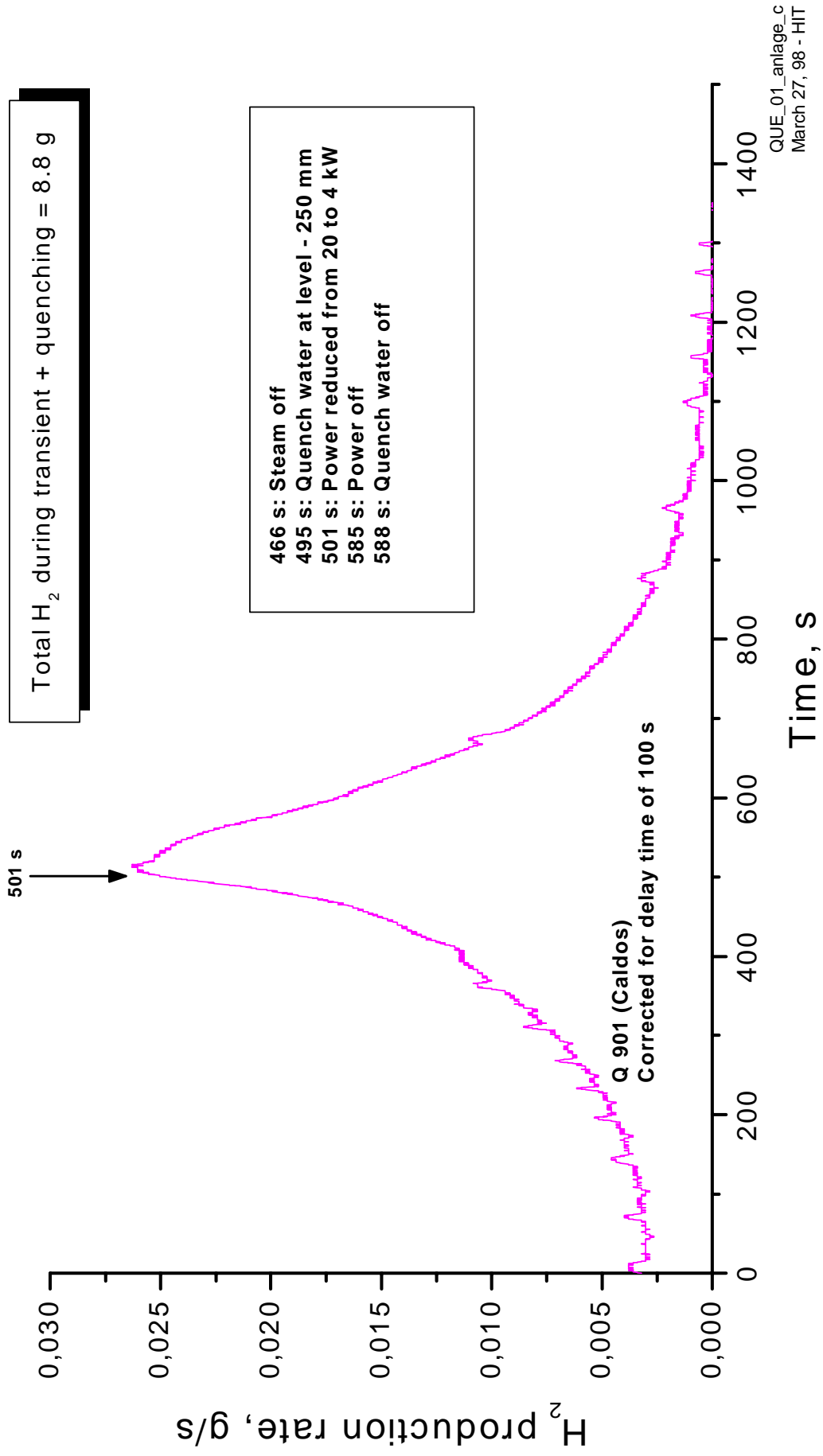
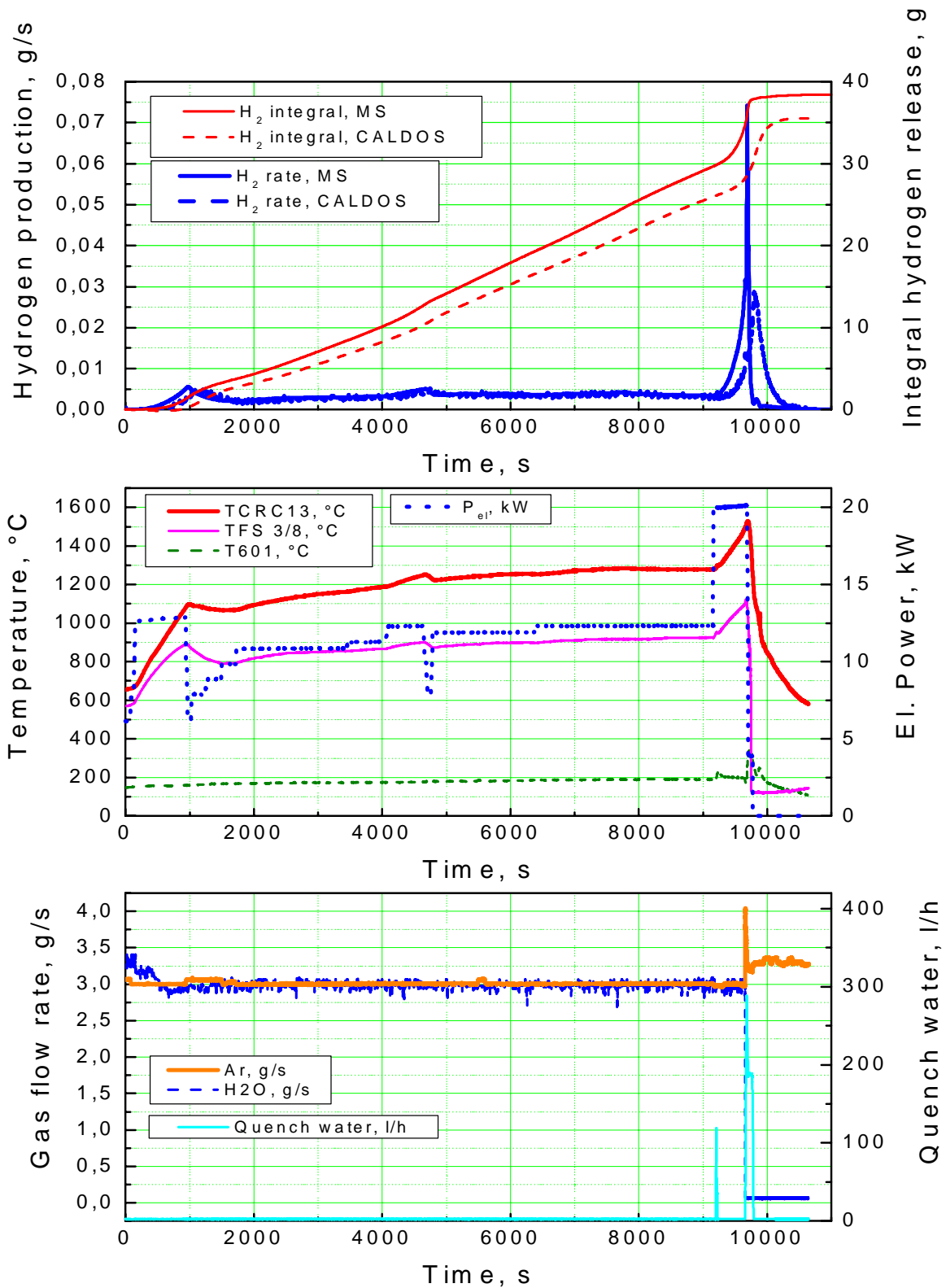


Fig 36

QUENCH-01:

Pre-oxidation, transient, and quench phase

Hydrogen measurement and data of the facility



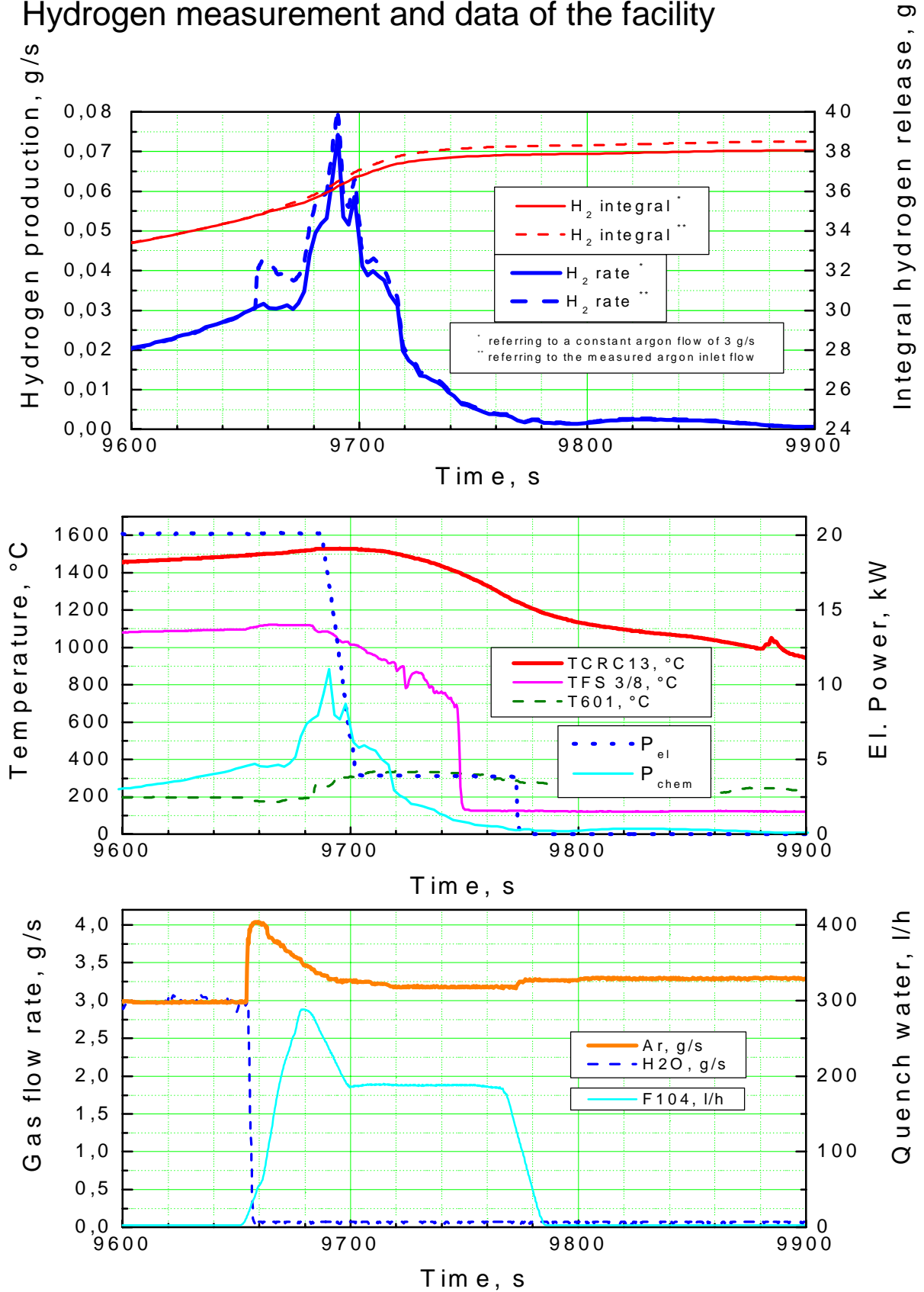
FZK/IMF, Steinbrück, 16.4.98

Fig 37

QUENCH-01:

Quench phase

Hydrogen measurement and data of the facility



FZK/IMF, Steinbrück, 16.4.98

Fig 38

QUENCH-01: Electric and chemical power during the transient and quench phase

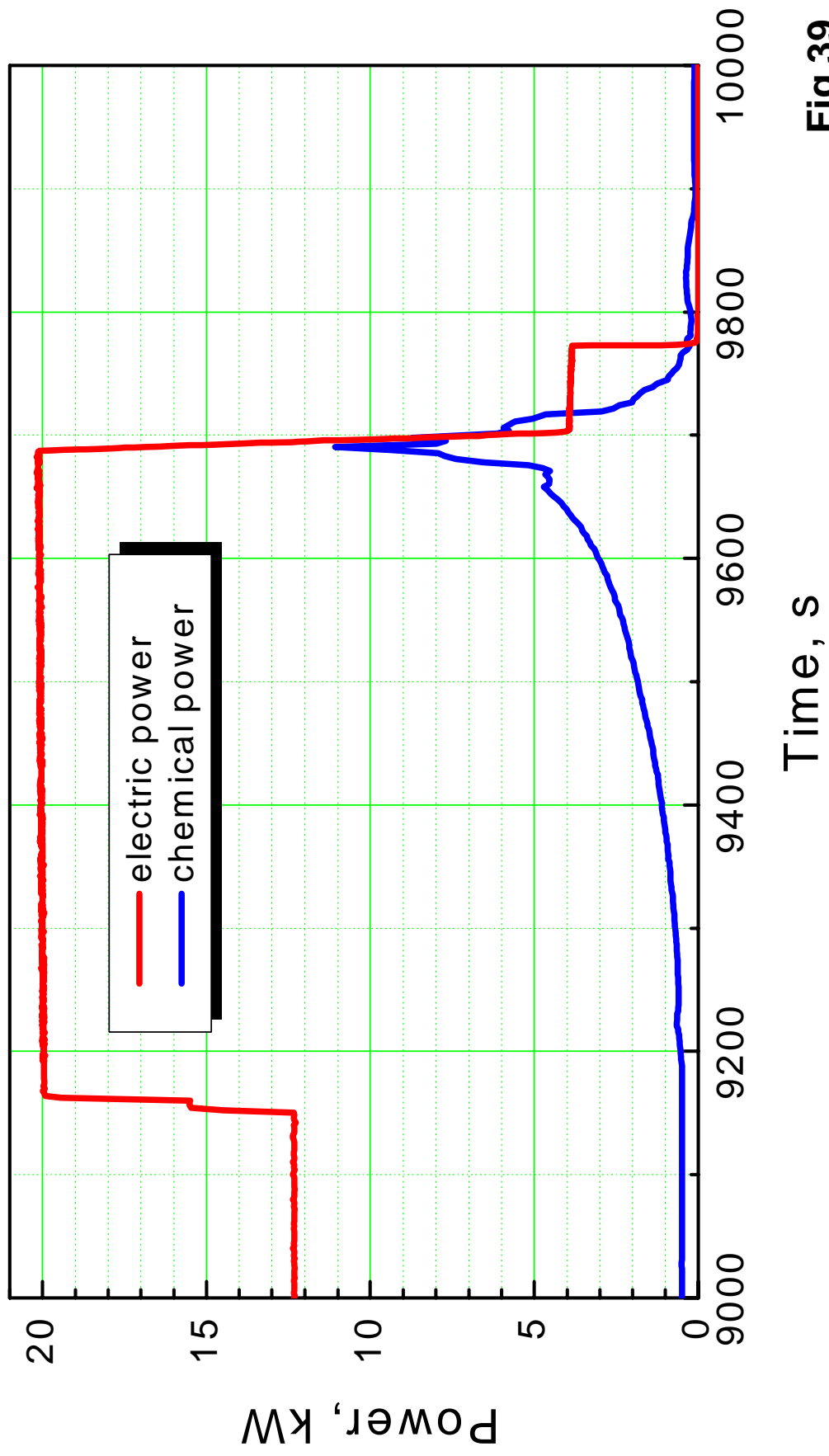


Fig 39

Test QUENCH-01:

Absorbed hydrogen in the remaining Zry-4 metal of cladding, shroud and corner rod and oxide layer

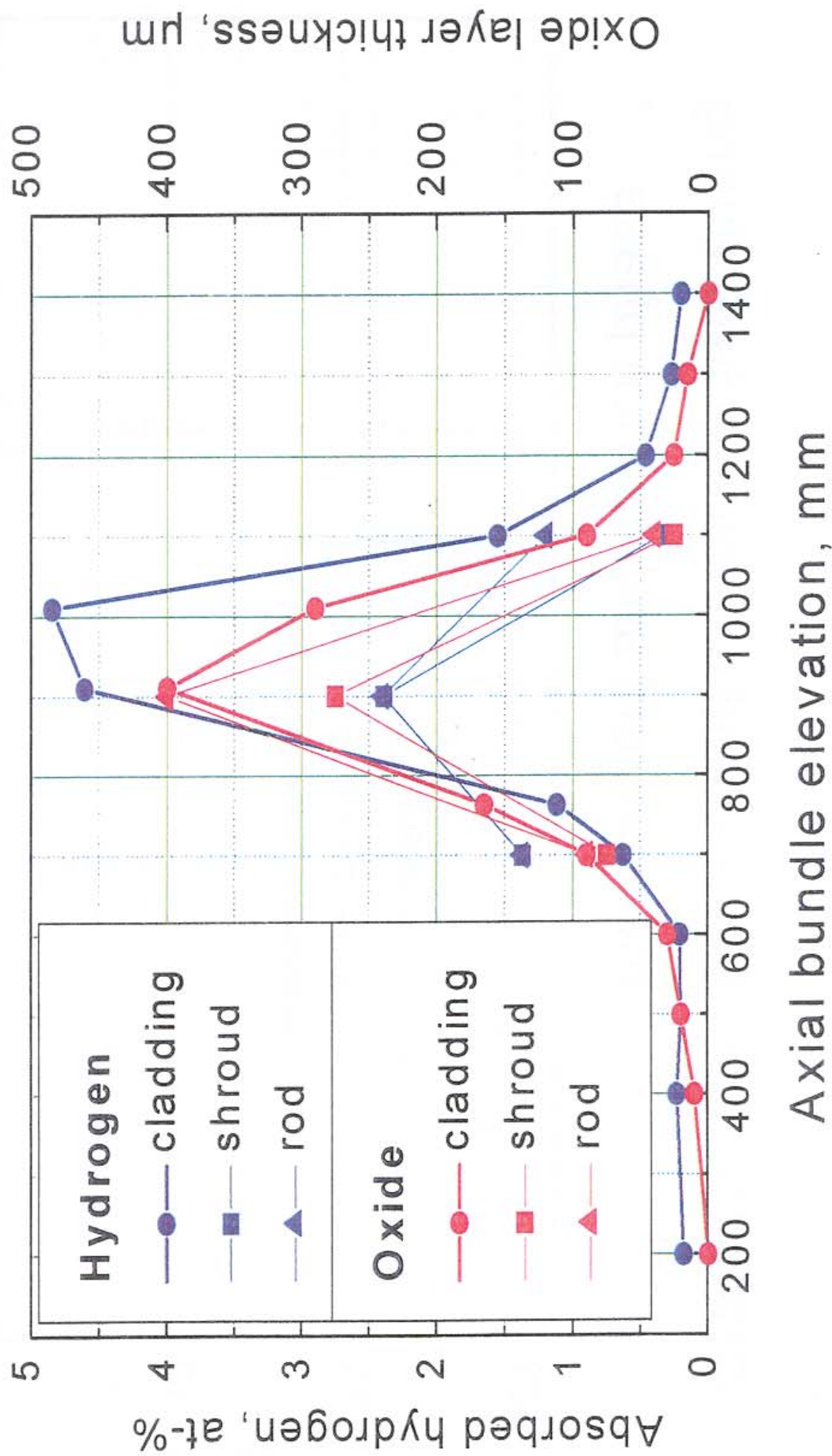


Fig. 40

Cut-out of an Observation Window at the Shroud, Schematic



Test QUENCH-01
Opening between
 0° and 180° (top-viewed)

Fig. 41

QUENCH-01 Test Bundle

Cut-out of Shroud and Rod Removal (Top View)

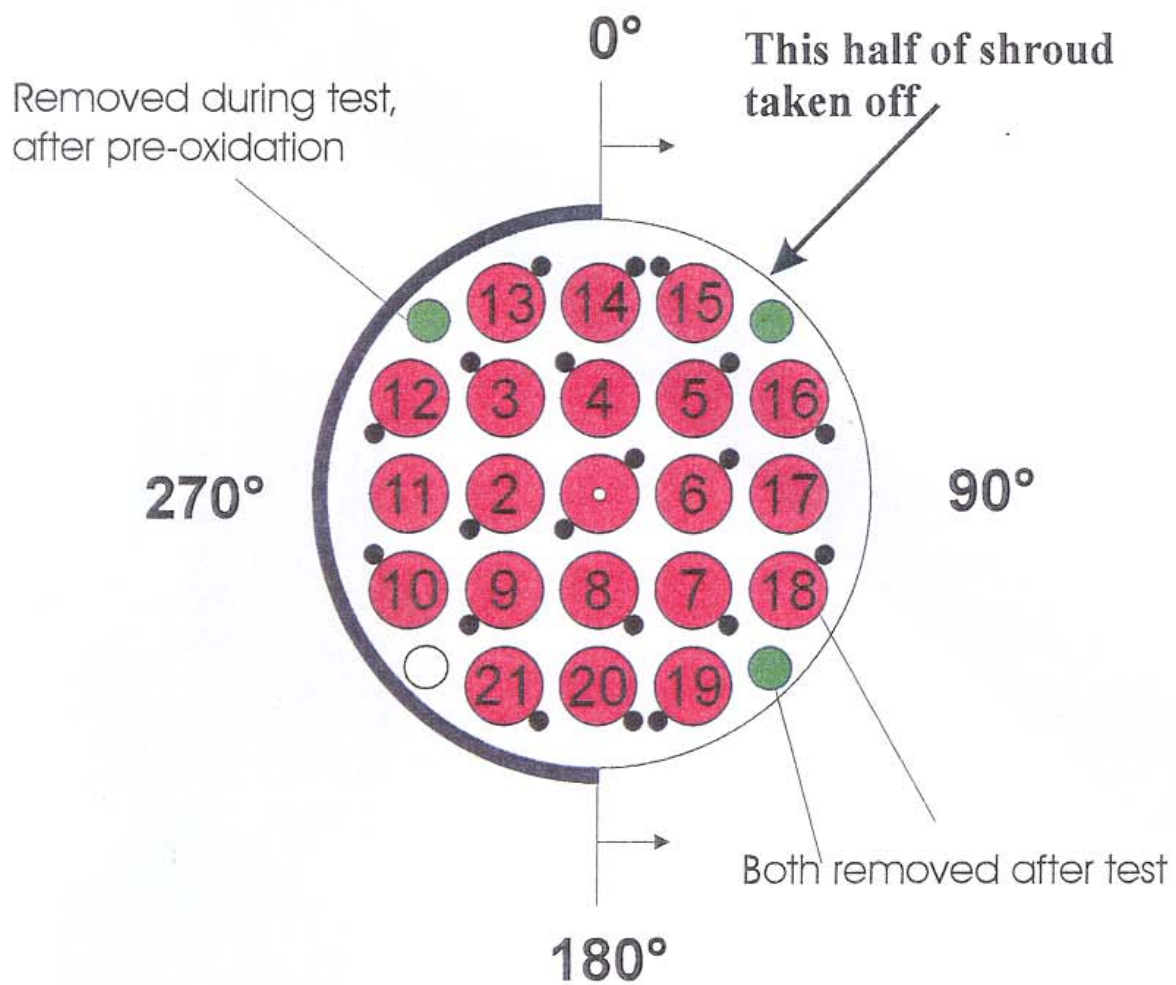
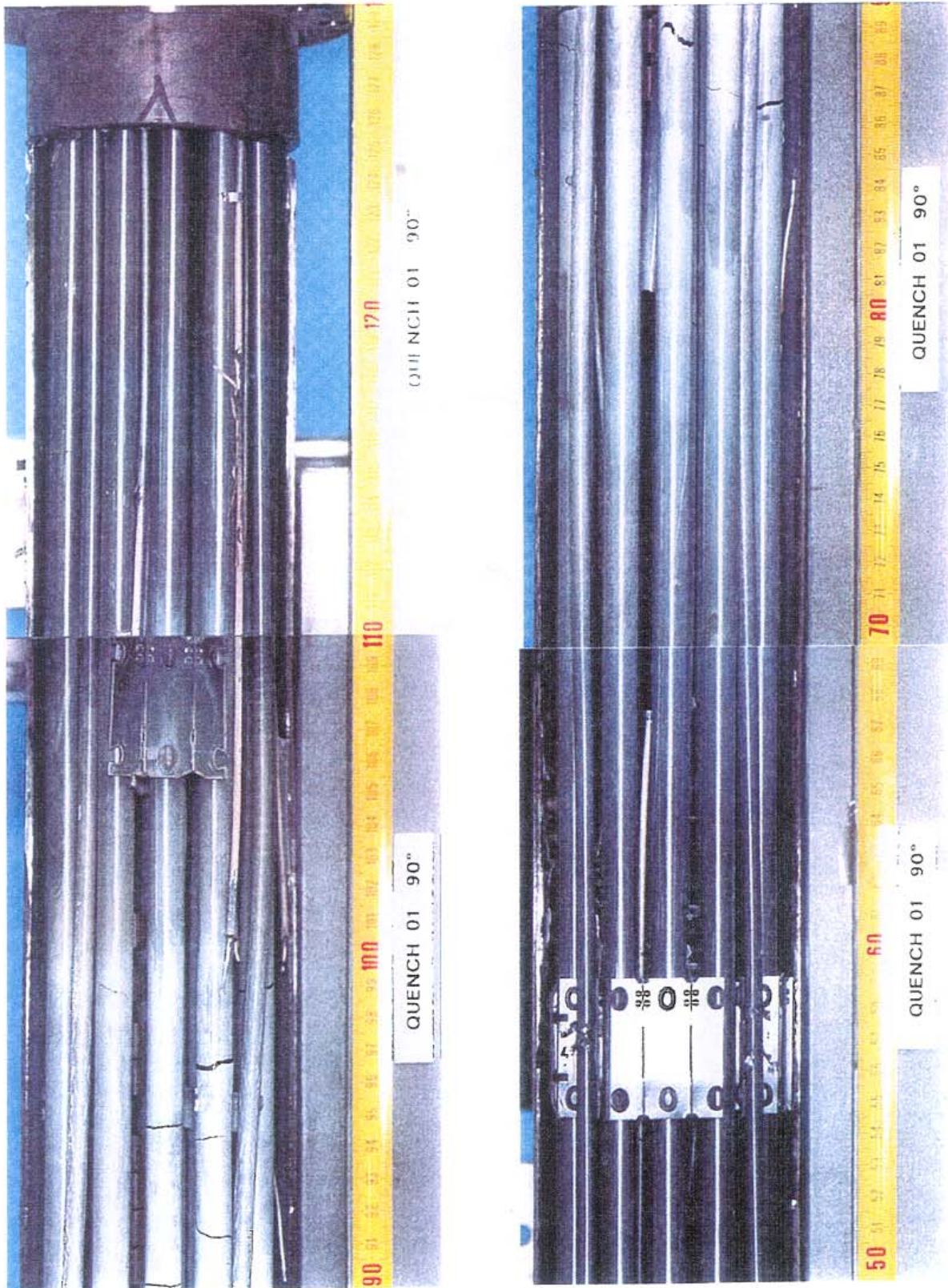


Fig. 42

QUENCH-01 Posttest view of the bundle



QUENCH-01; Post-Test
Cladding Breaches in the Region of 900 mm



Fig. 44

Sectioning of Test Bundle QUENCH-01

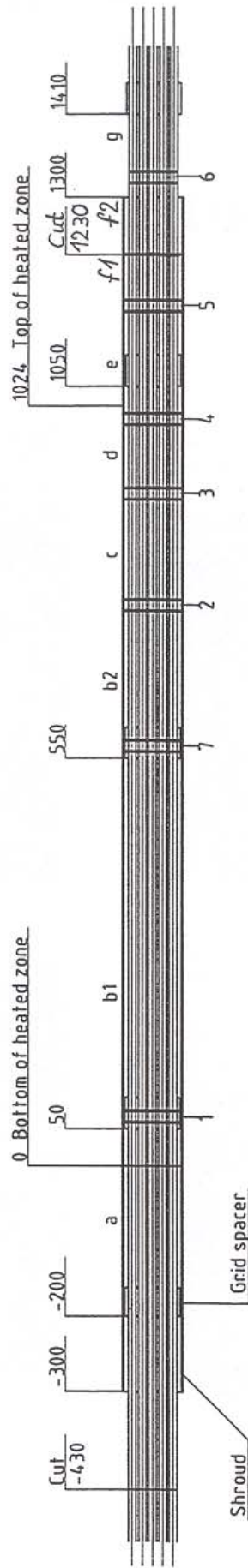
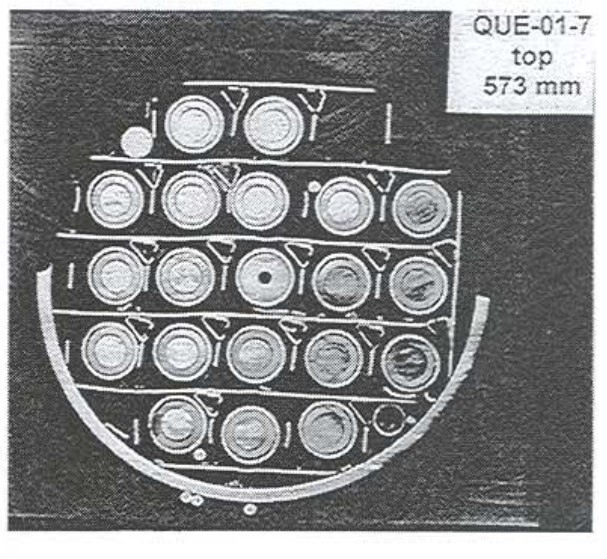
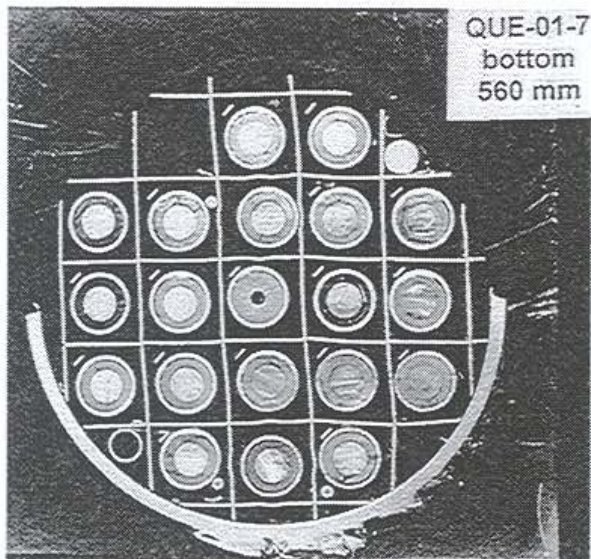
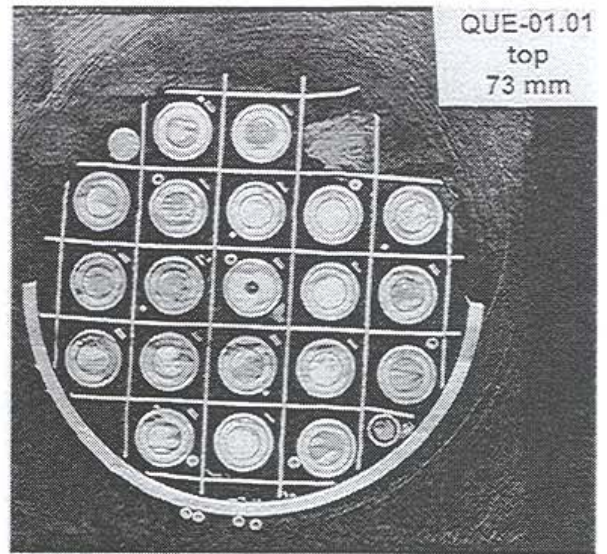
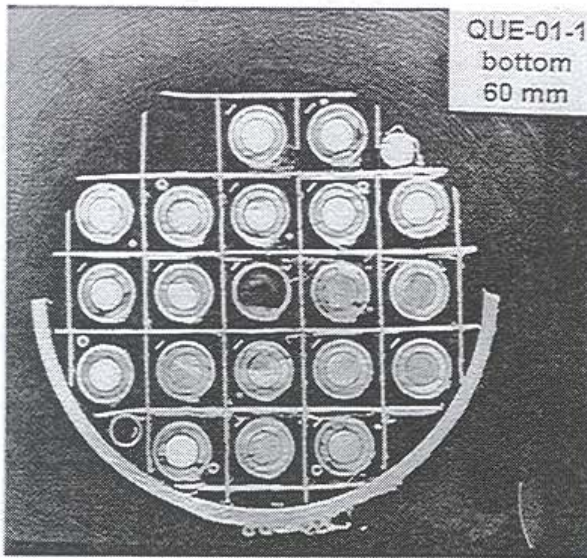


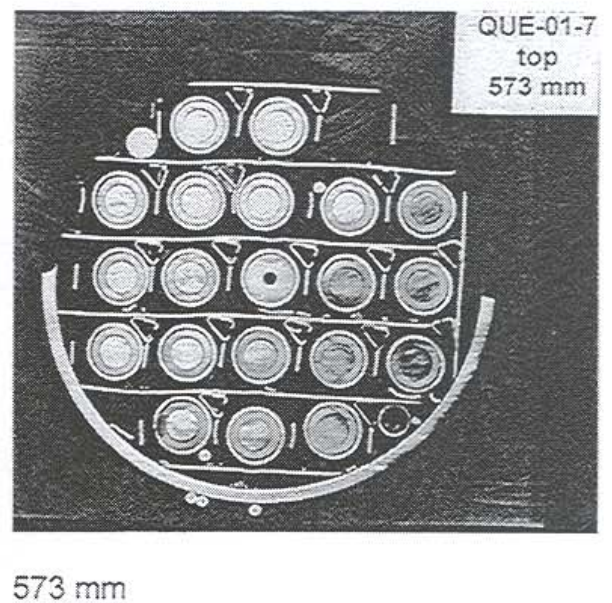
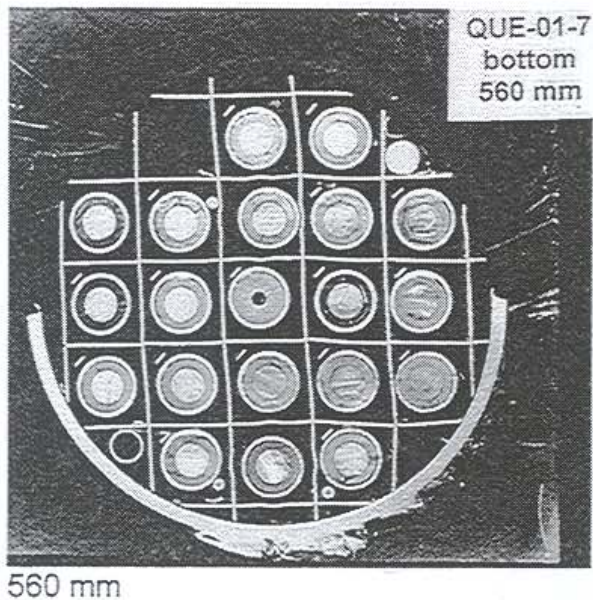
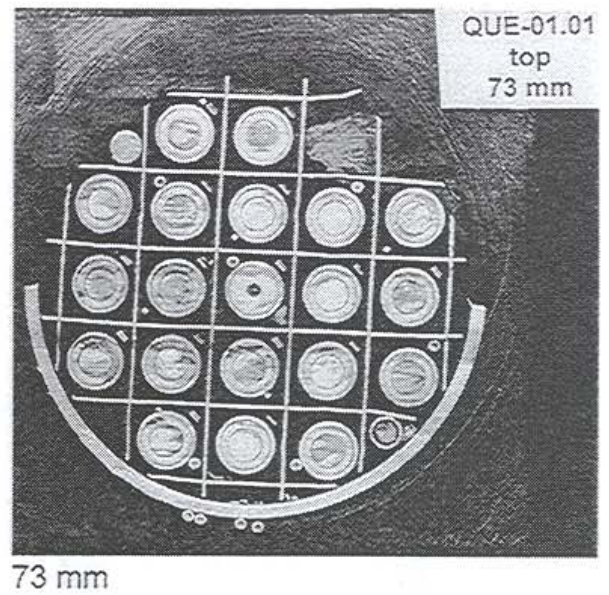
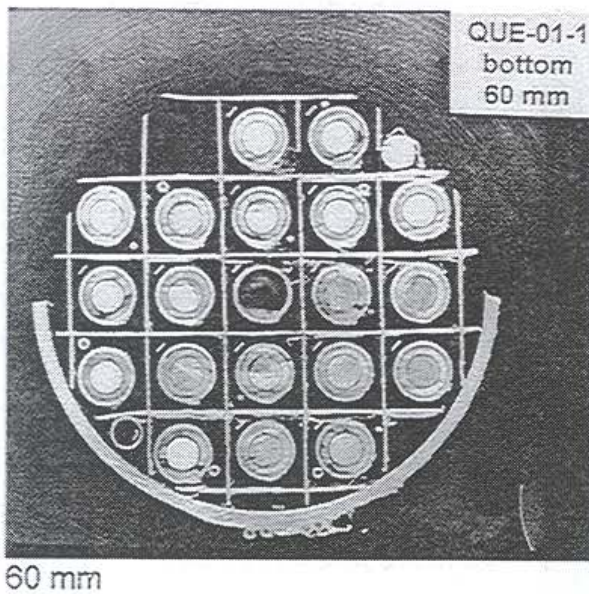
Fig. 45

HIT - 13.05.98

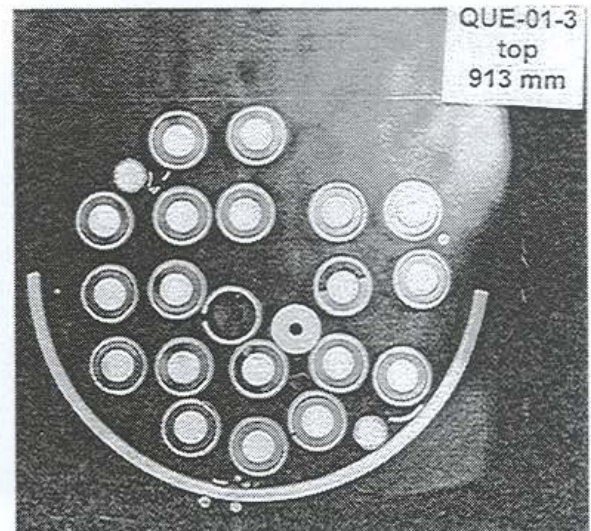
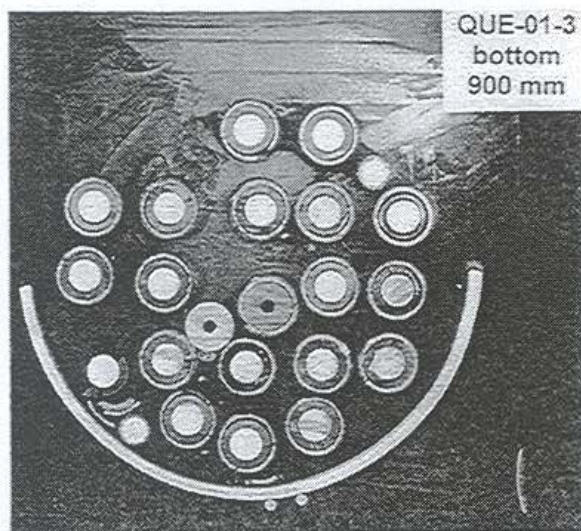
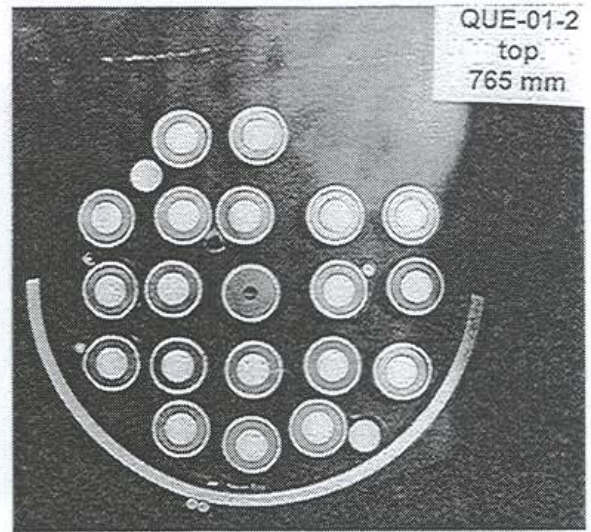
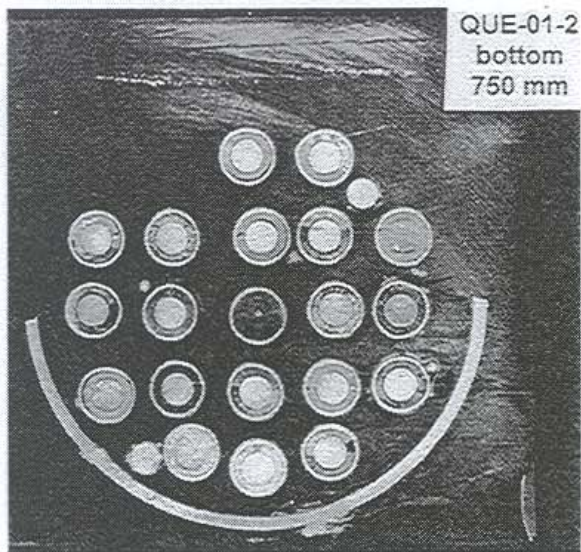
QUENCH-01, Cross Sections



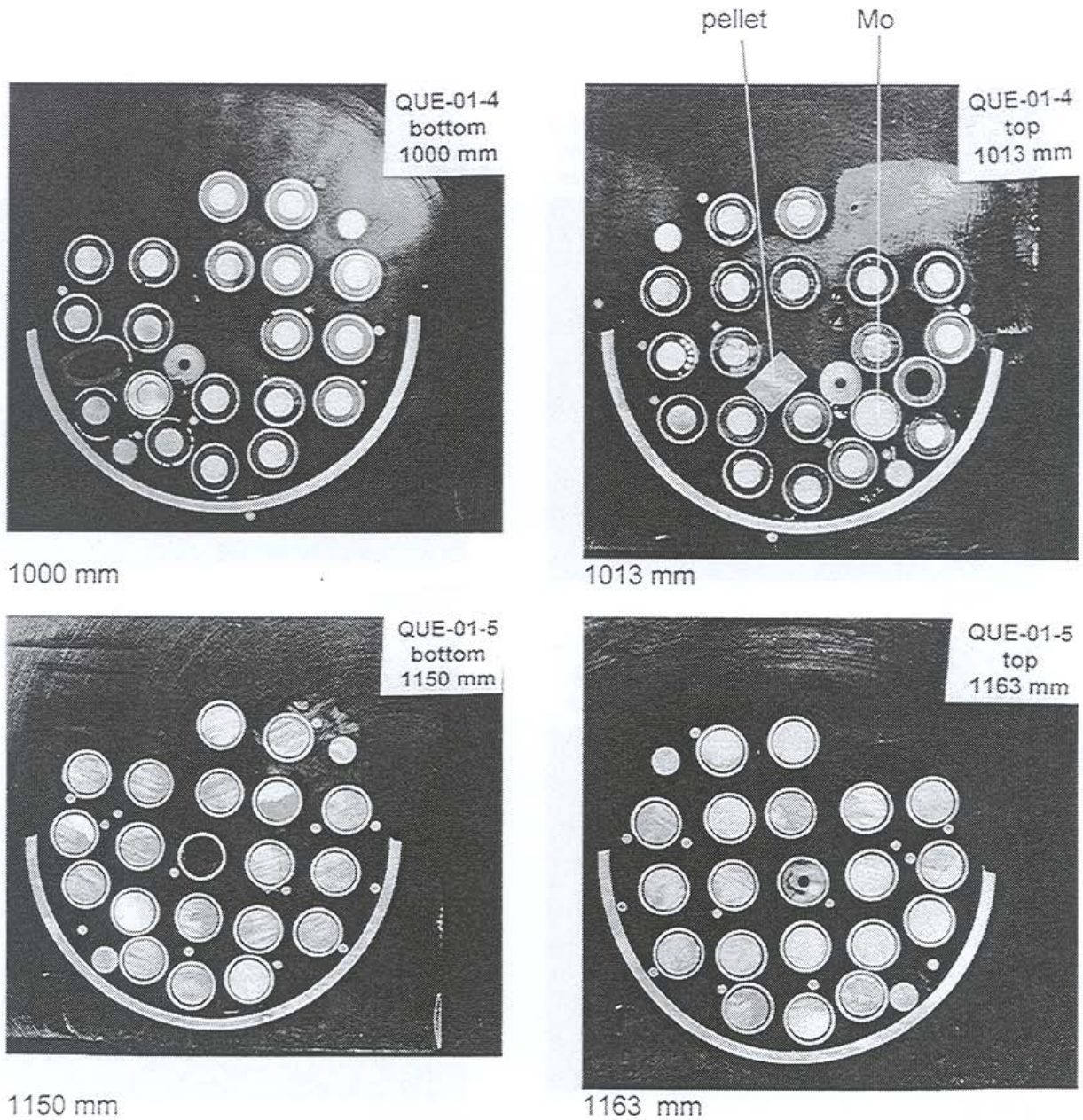
QUENCH-01, Cross Sections



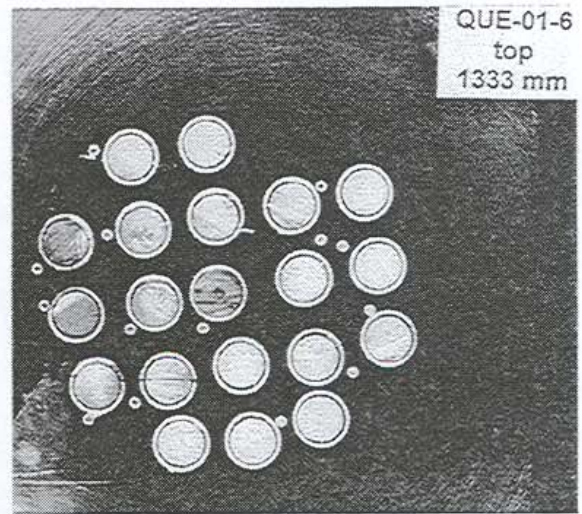
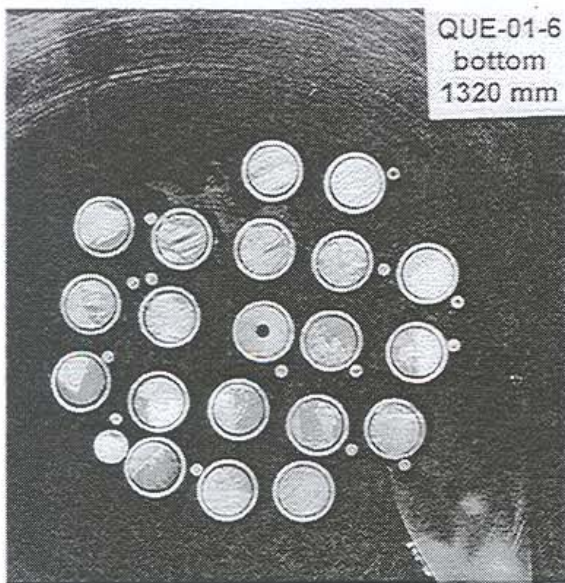
QUENCH-01, Cross Sections



QUENCH-01, Cross Sections



QUENCH-01, Cross Sections



QUENCH-01: Horizontal cross section of the bundle at elevation 913 mm

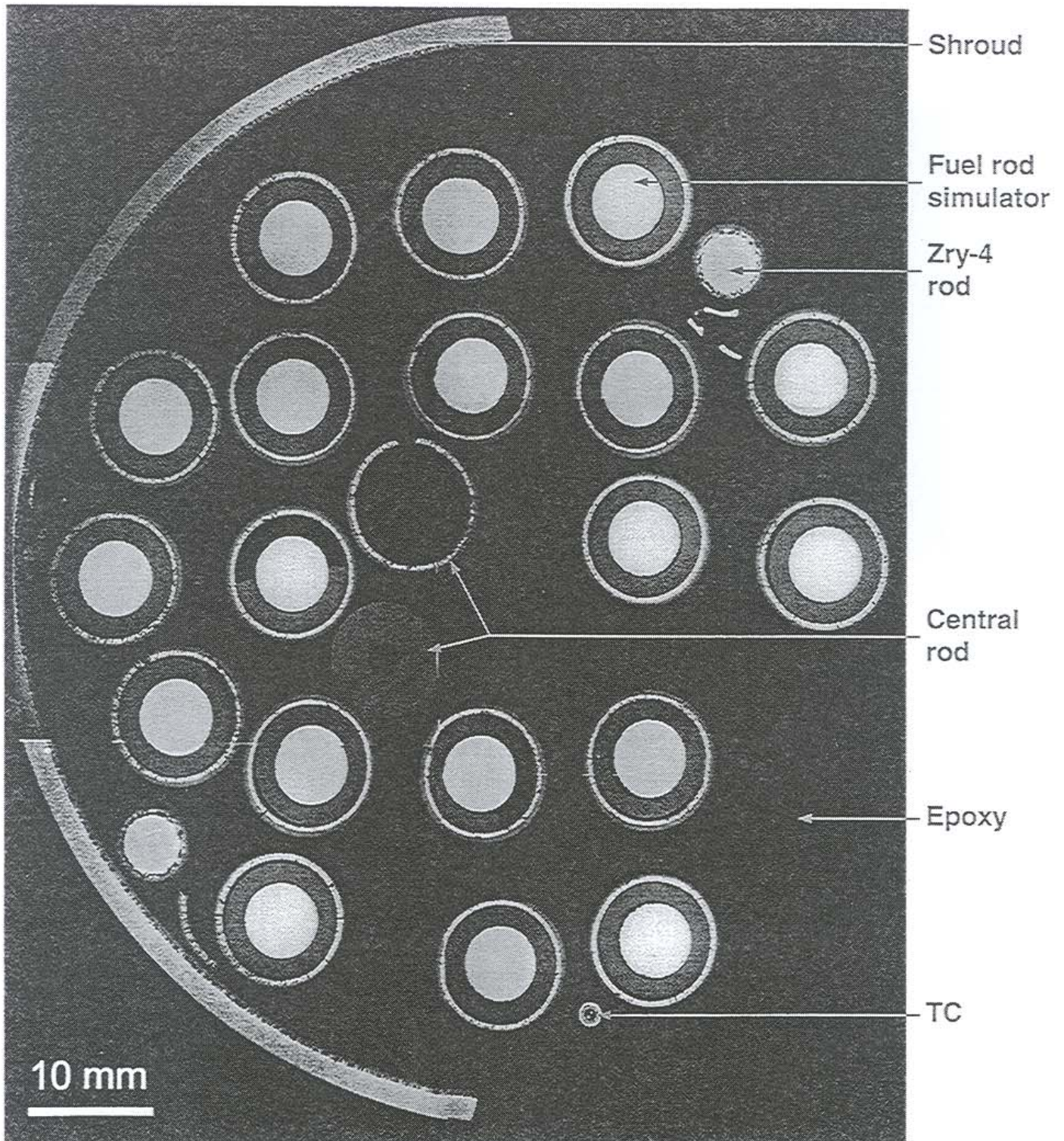


Fig. 47

QUENCH-01:
Horizontal cross section of the bundle
at axial elevation 913 mm

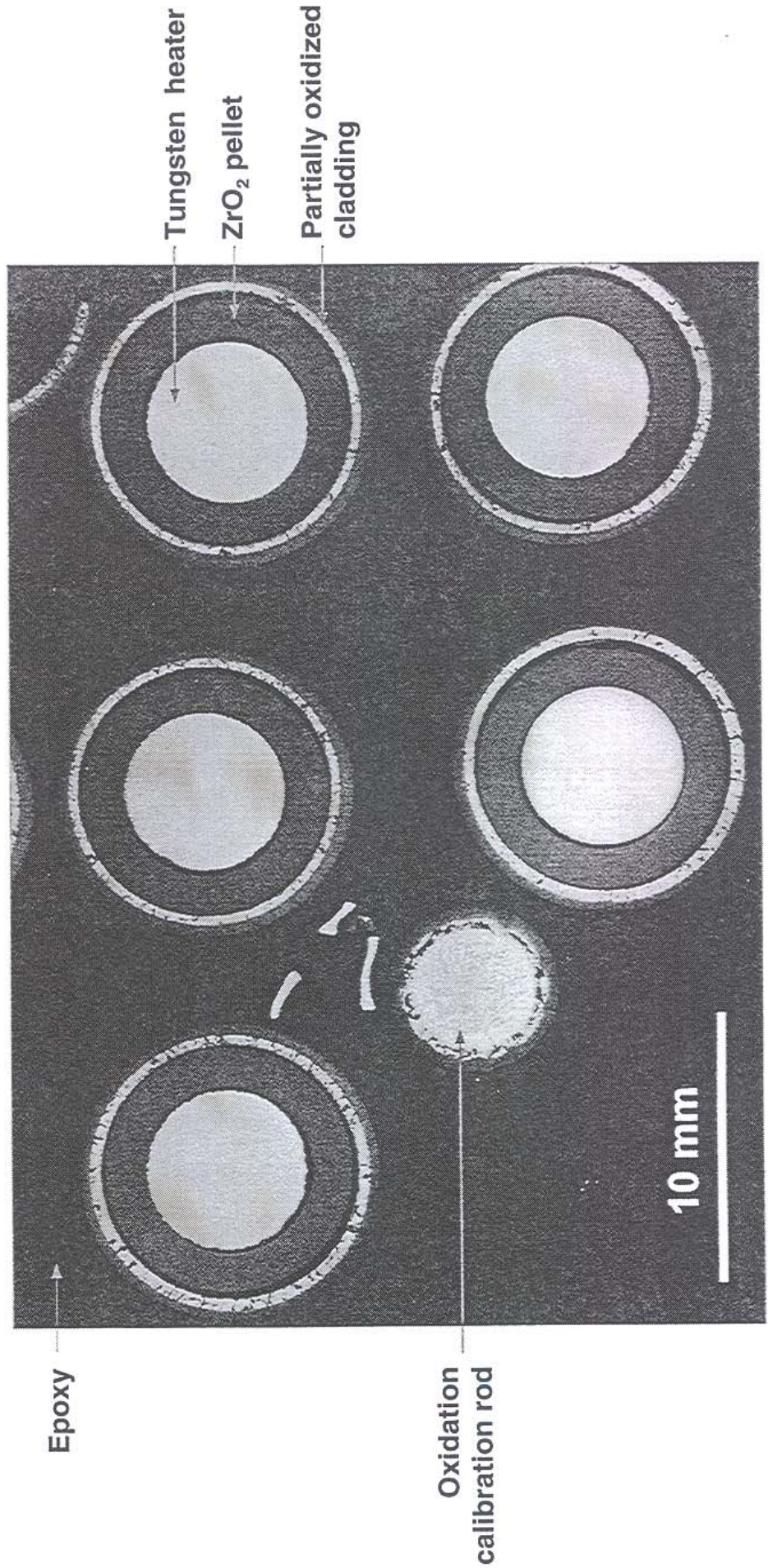


Fig. 48

Macroscopic appearance of one fuel rod simulator at different bundle elevations

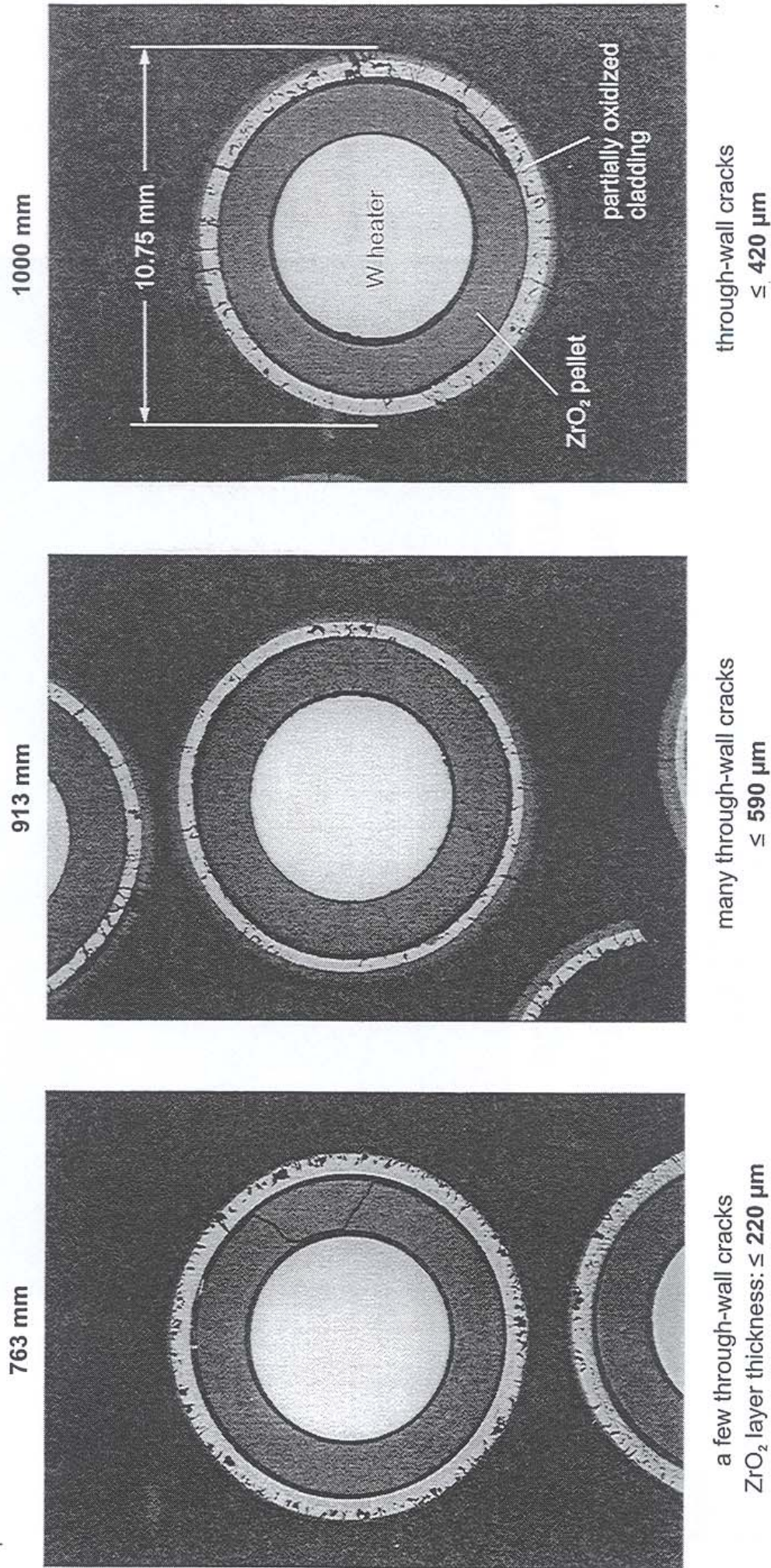
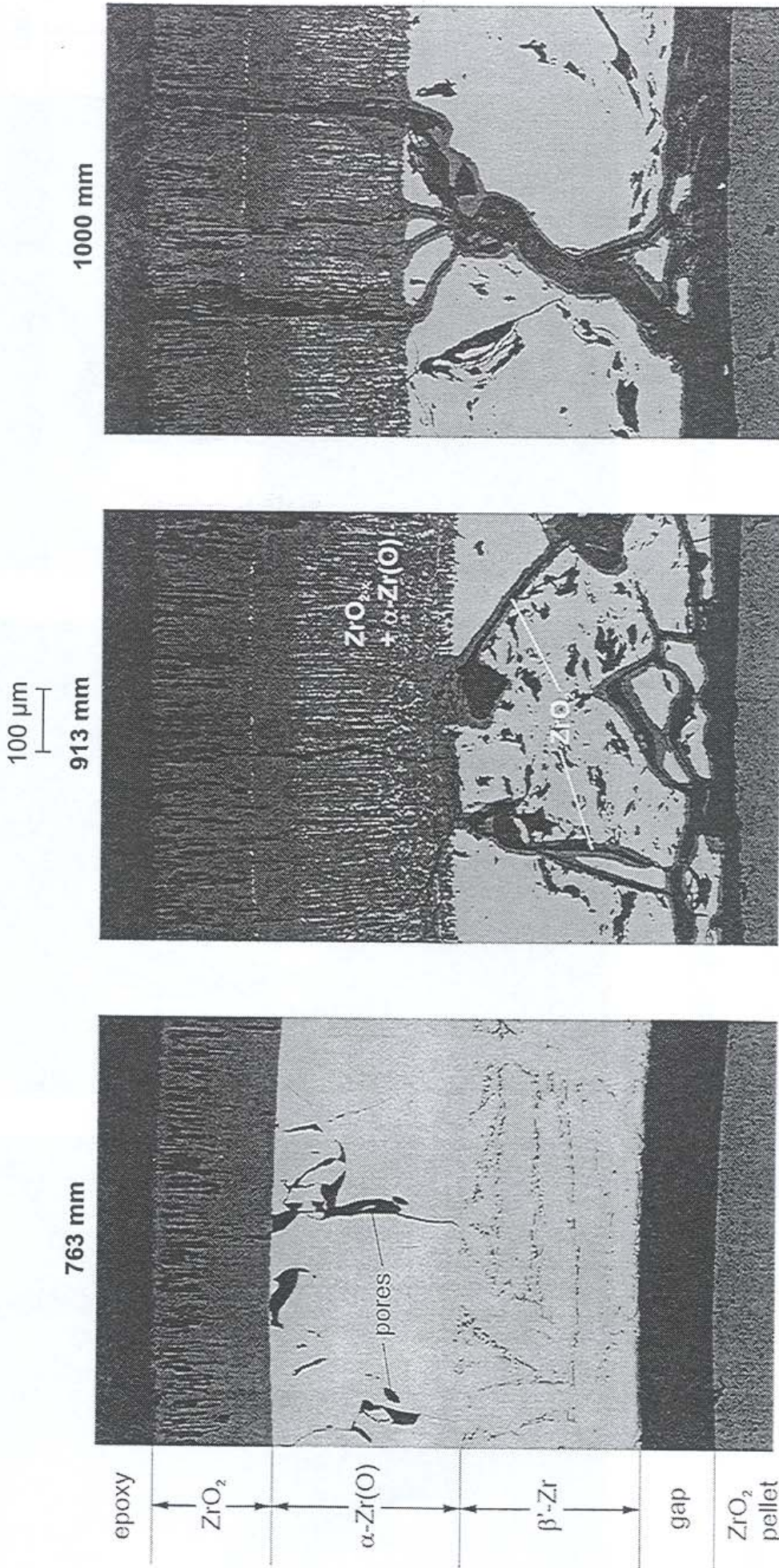


Fig. 49

Test QUENCH-01

Oxidation of Zircaloy cladding at different axial bundle elevation



oxidation of crack surfaces during flooding

no through-wall cracks

Test QUENCH-01

Fig. 50

Oxidation of crack surfaces which formed during flooding

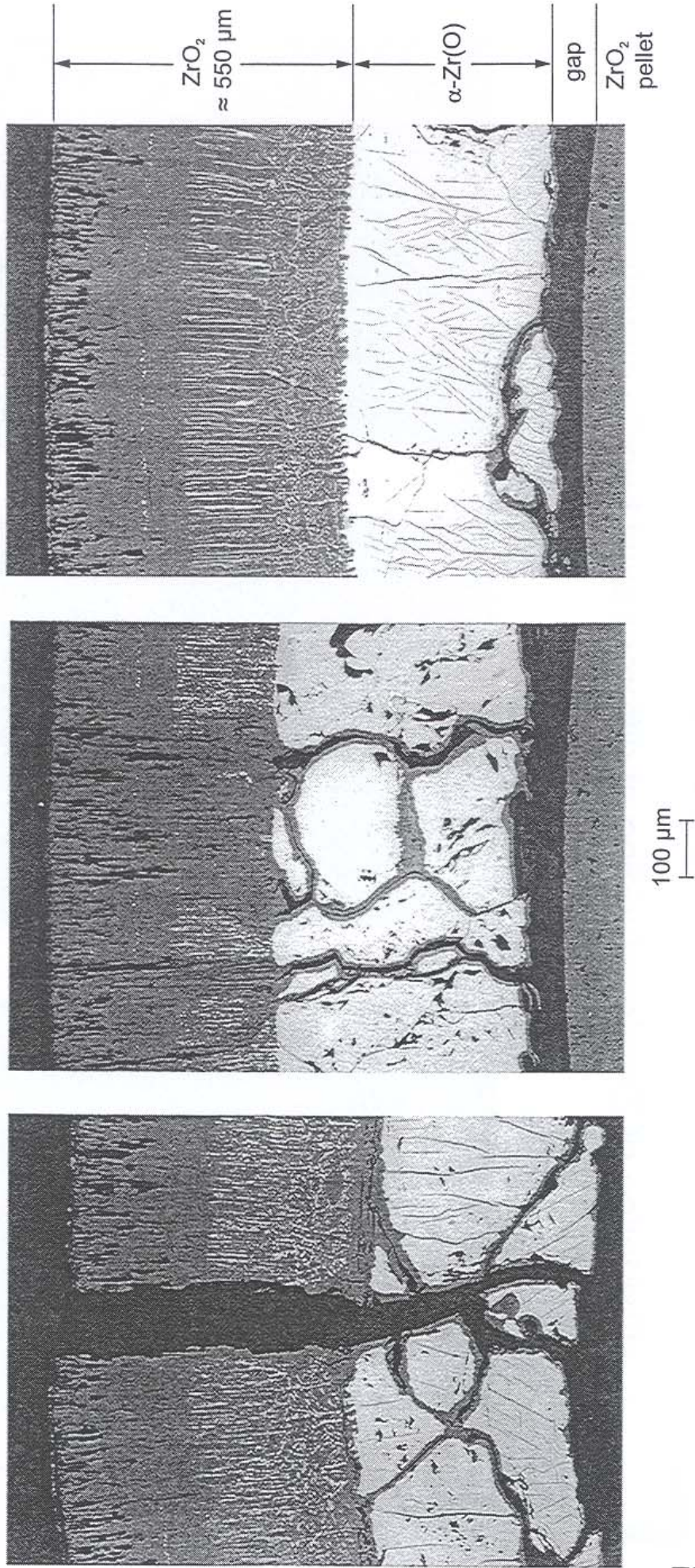
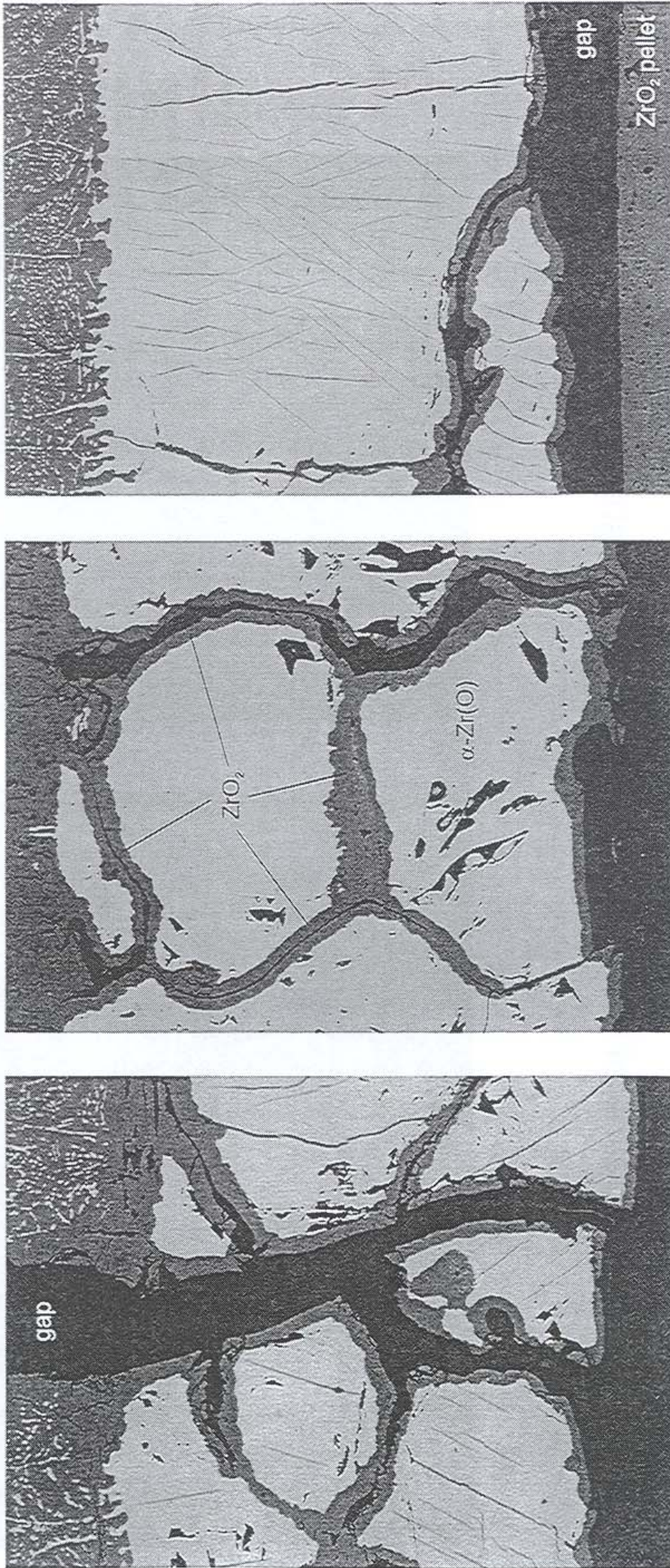


Fig. 51

Test QUENCH-01; bundle elevation 913 mm (QUE-01-3)

Oxidation of crack surfaces which formed during quenching



50 μm

Test QUENCH-01; bundle elevation 913 mm (QUE-01-3)

Fig. 52

Oxidation of the outer and inner Zircaloy shroud surfaces

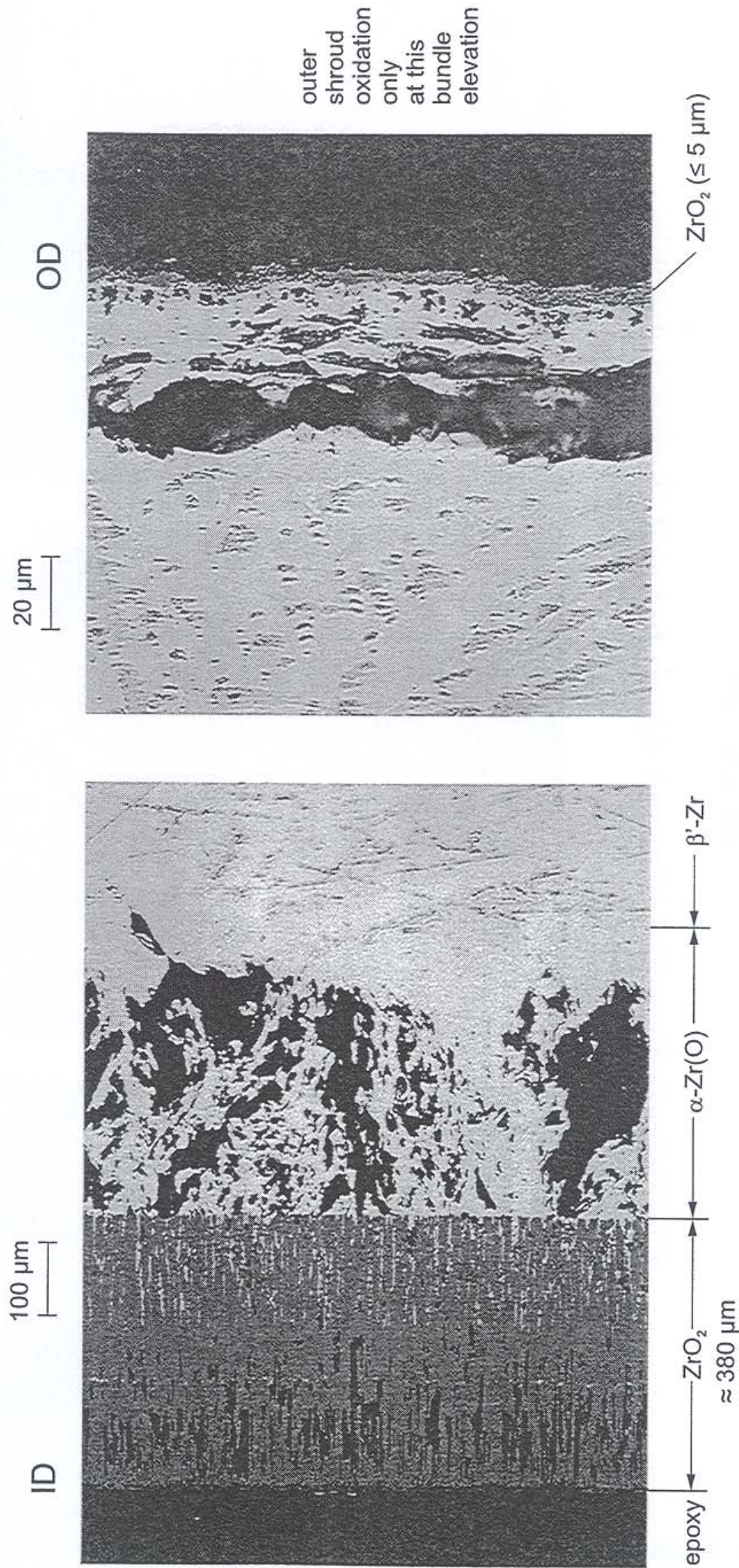
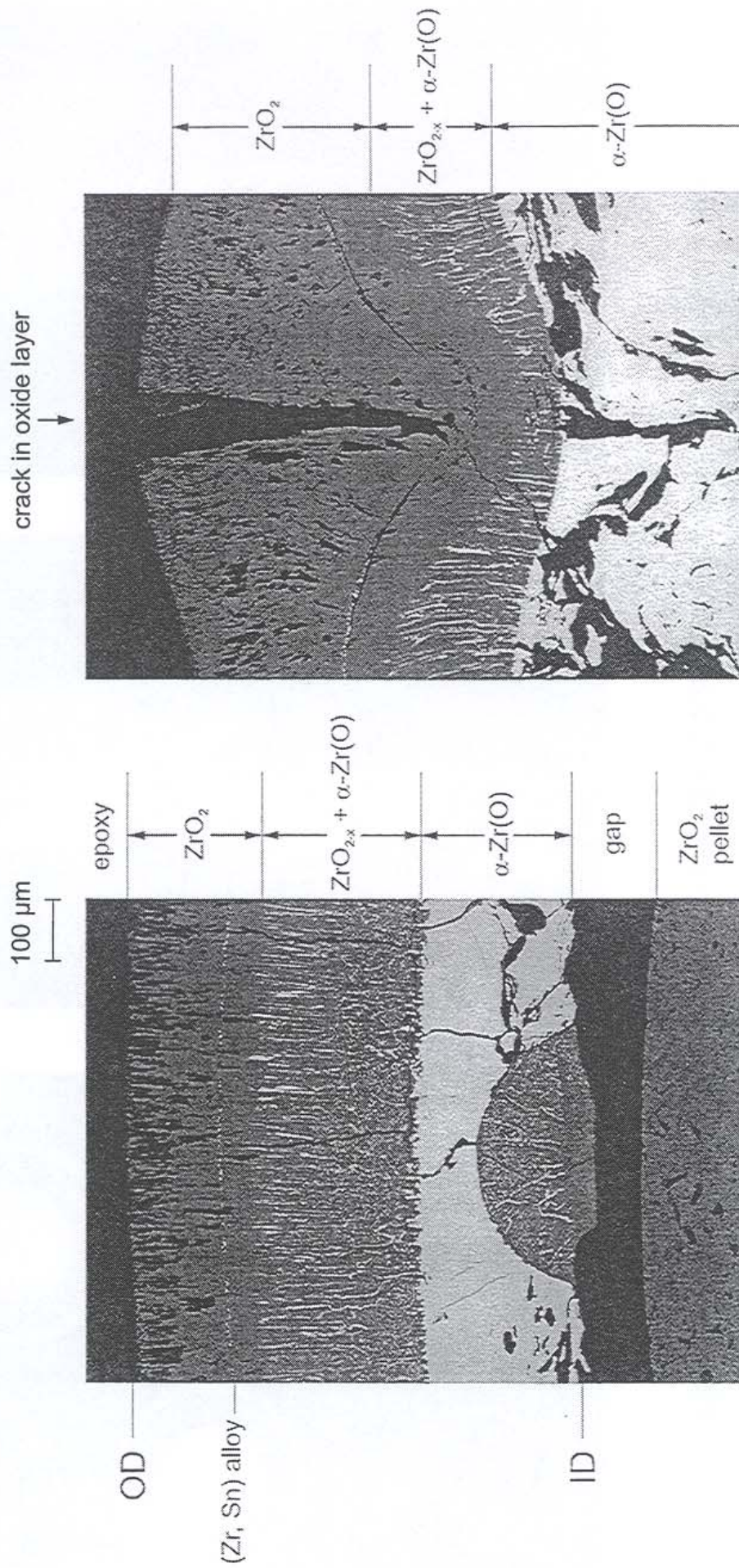


Fig. 53

Test QUENCH-01; bundle elevation 913 mm (QUE-01-3)

Localized, increased oxidation of Zircaloy cladding and rod surfaces



localized cladding ID oxidation

localized increased Zry rod oxidation

Test QUENCH-01; bundle elevation 913 mm (QUE-01-3)

Fig. 54

External and internal Zircaloy cladding tube oxidation of the central rod

200 μm

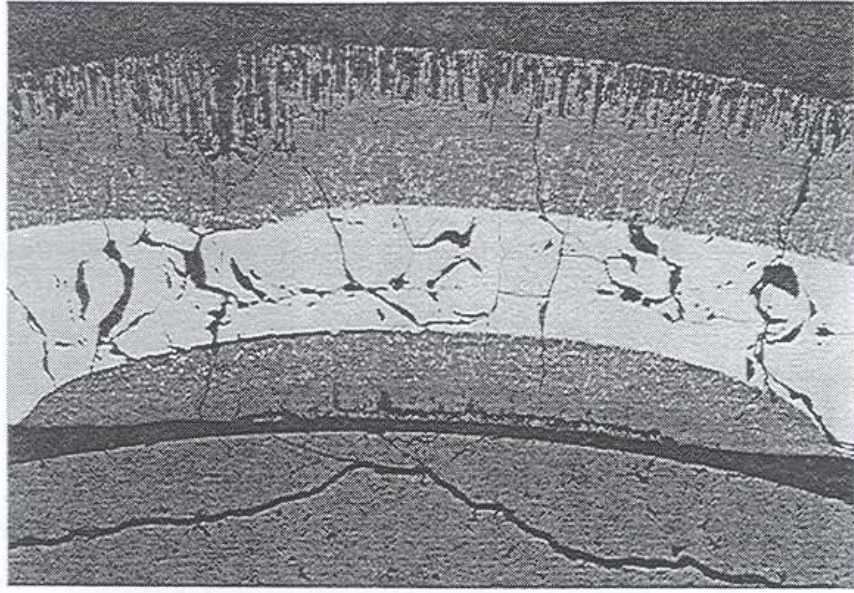
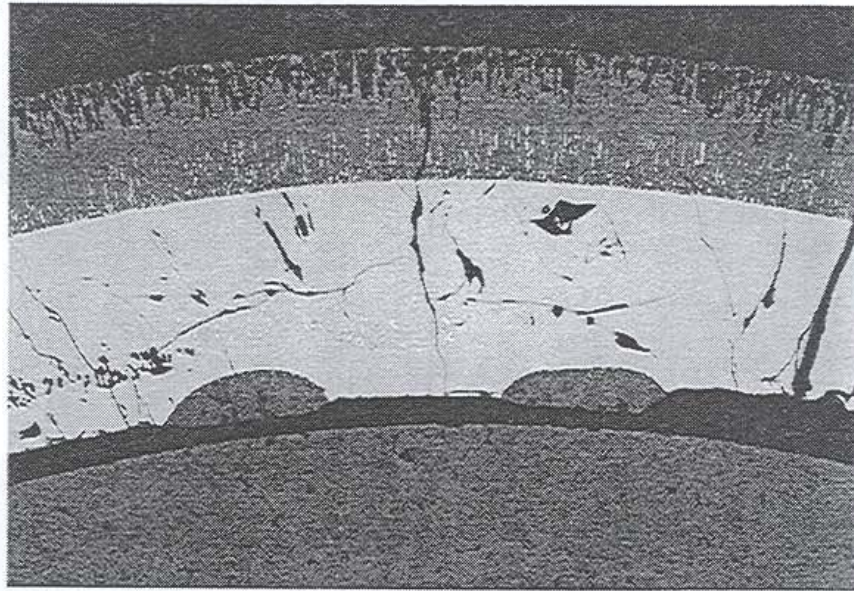
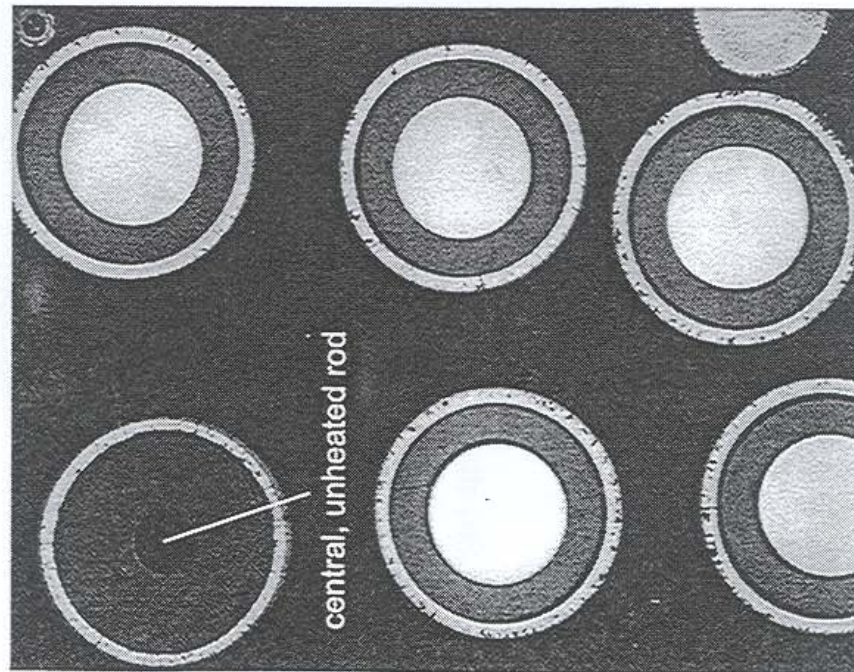


Fig. 55

Test QUENCH-01; bundle elevation 763 mm (QUE-01-2)

Through-wall crack formation in cladding tube of central rod

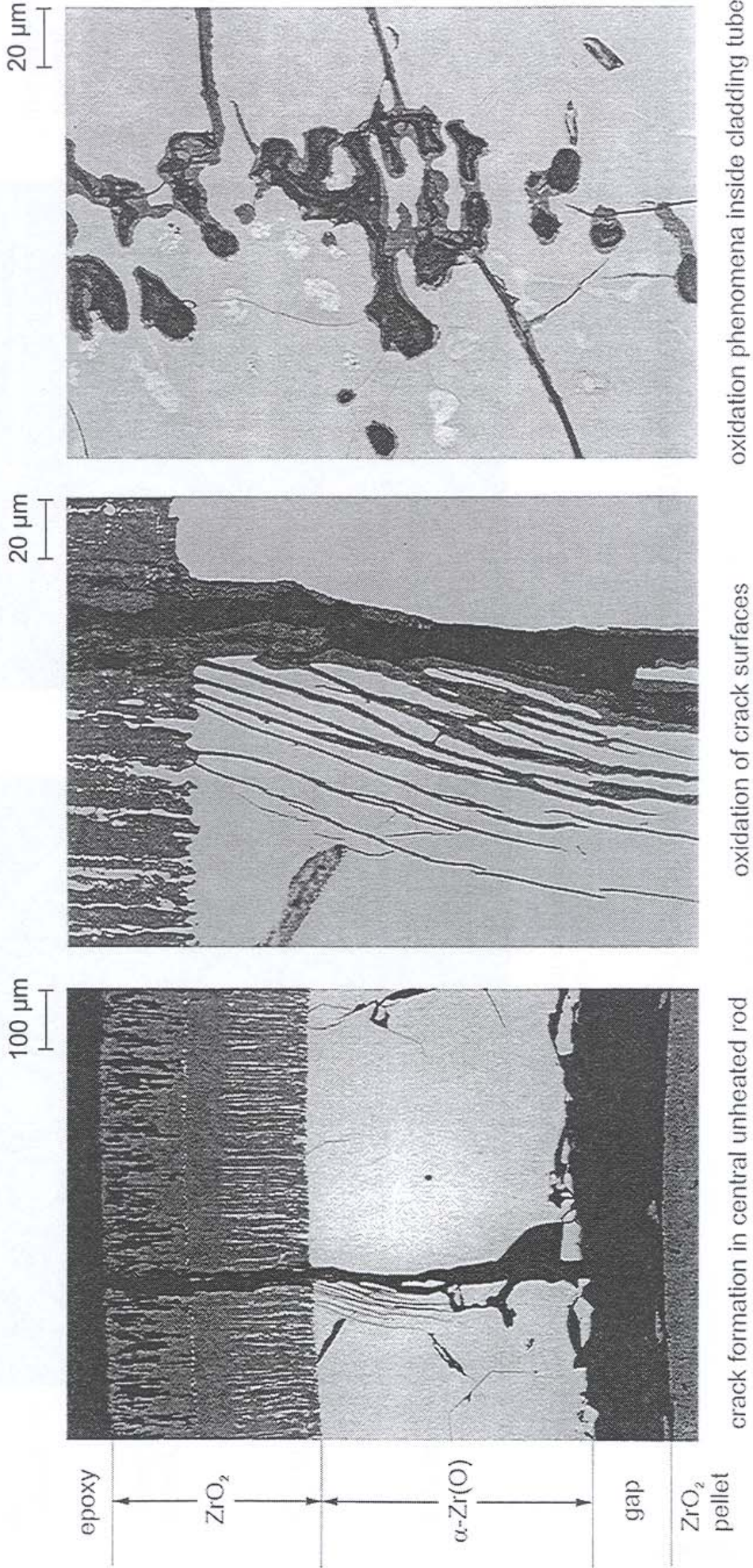
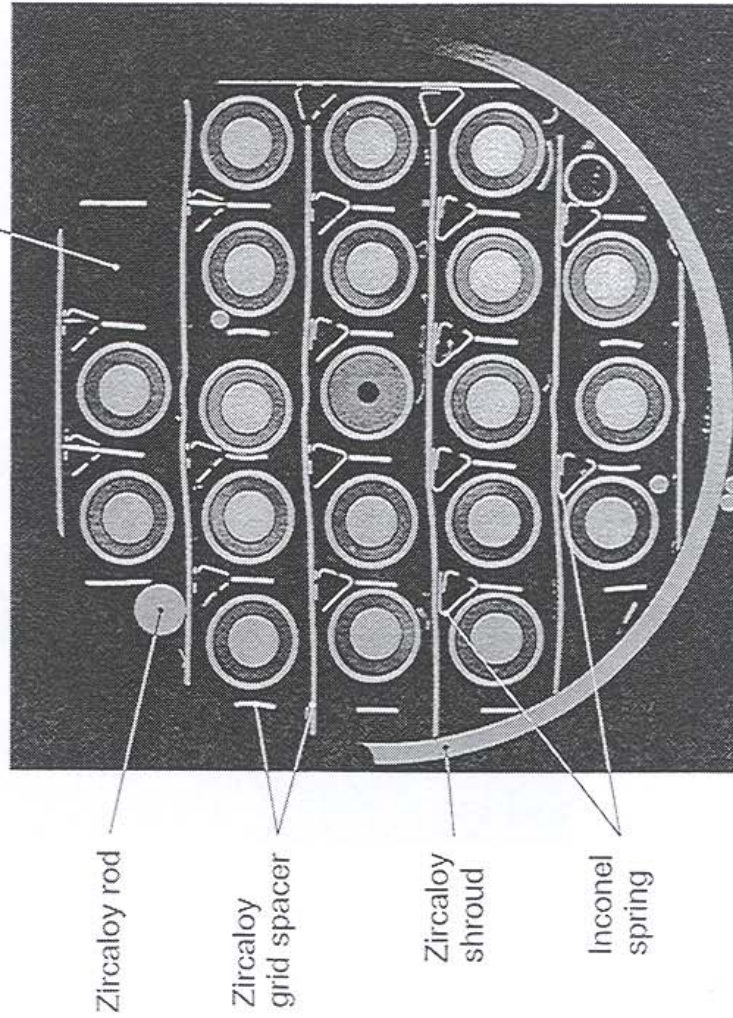


Fig. 56

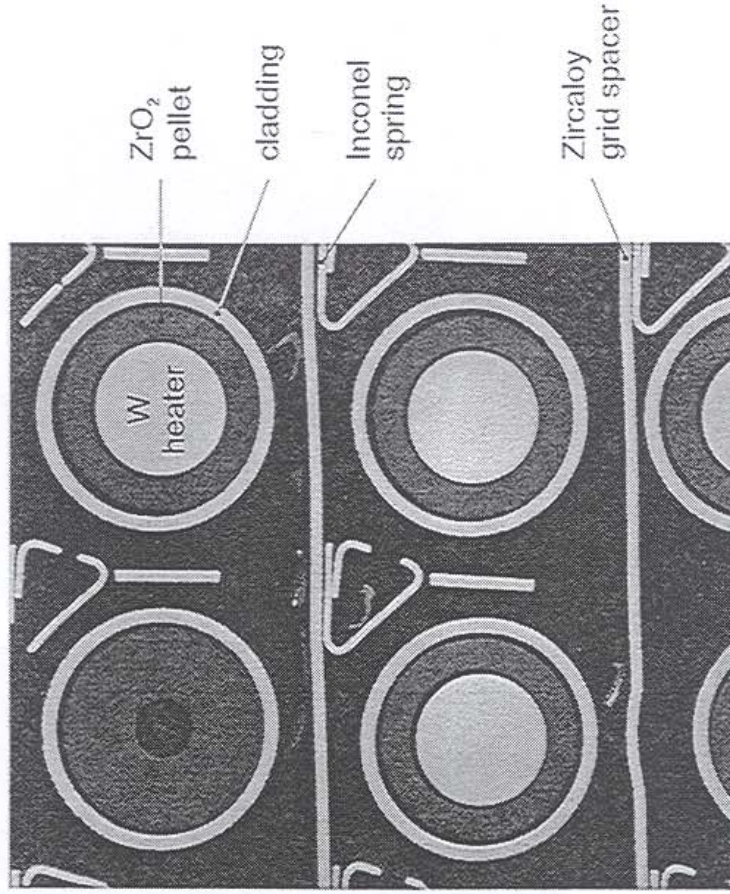
Test QUENCH-01; bundle elevation 763 mm (QUE-01-2)

Physico-chemical behavior of the grid spacer and cladding tubes

rod taken out for
chemical examinations



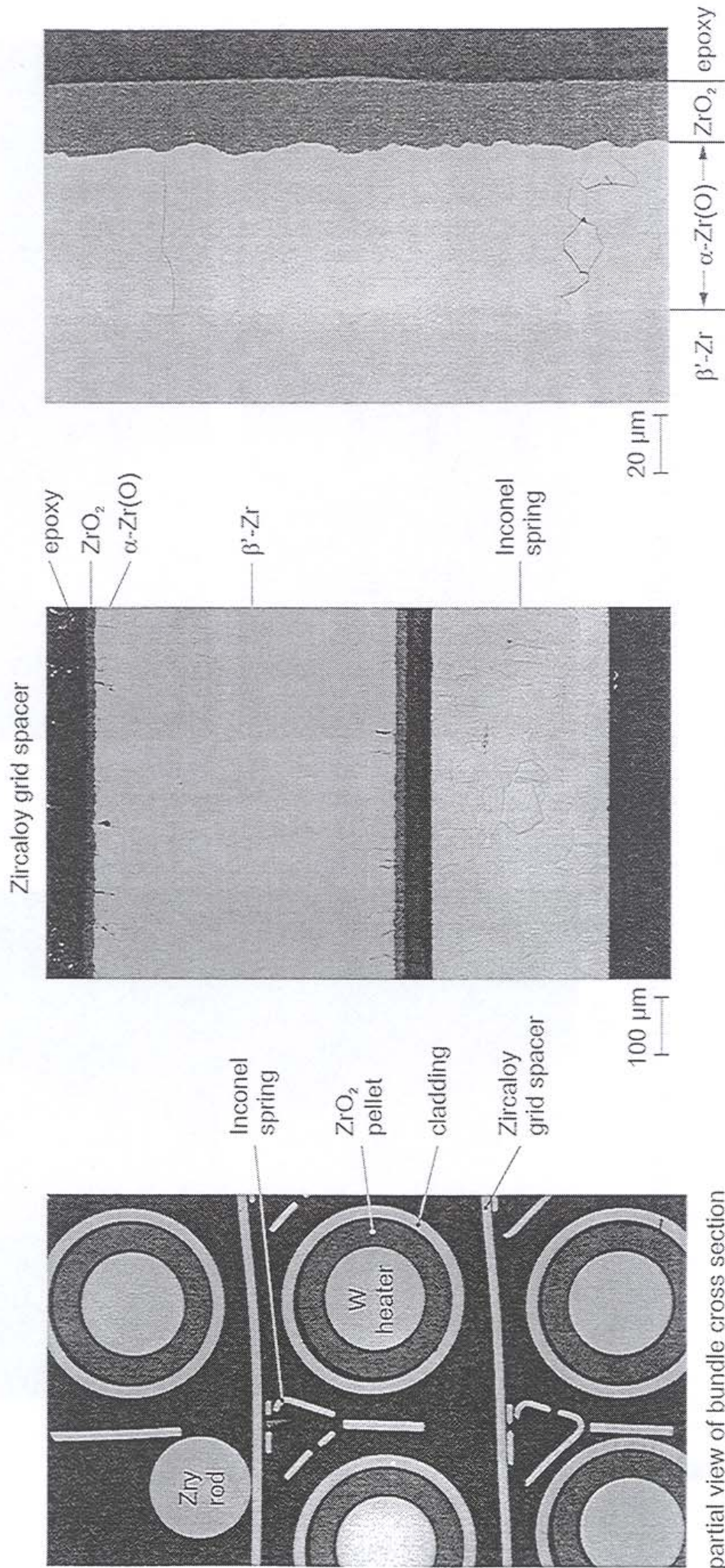
total view of bundle cross section
at the Zircaloy grid spacer elevation



Test QUENCH-01; bundle elevation 573 mm (QUE-01-7)

Fig. 57

Oxidation of Zircaloy cladding tubes and grid spacer

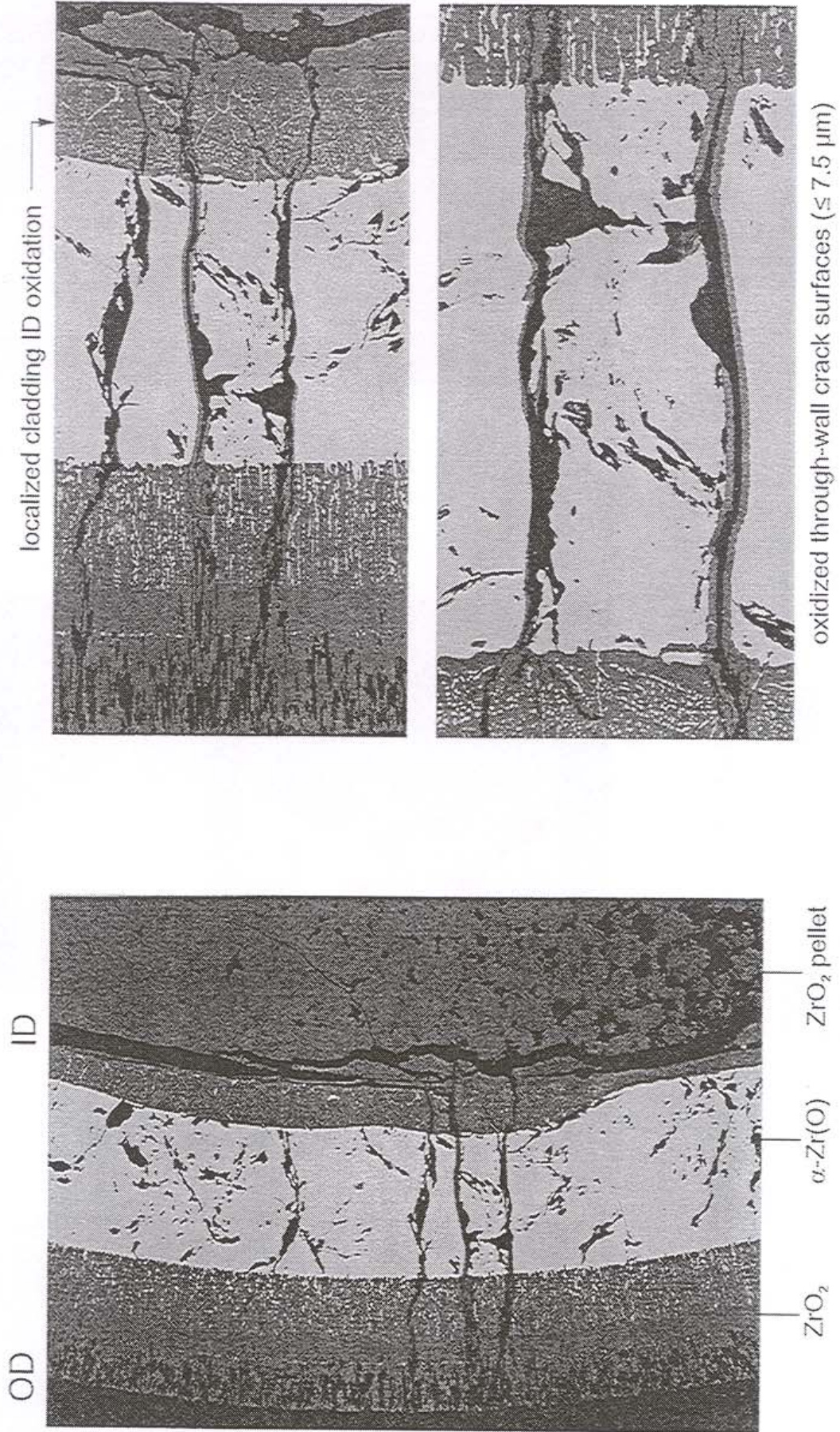


partial view of bundle cross section

Fig. 58

Test QUENCH-01; bundle elevation 573 mm (QUE-01-7)

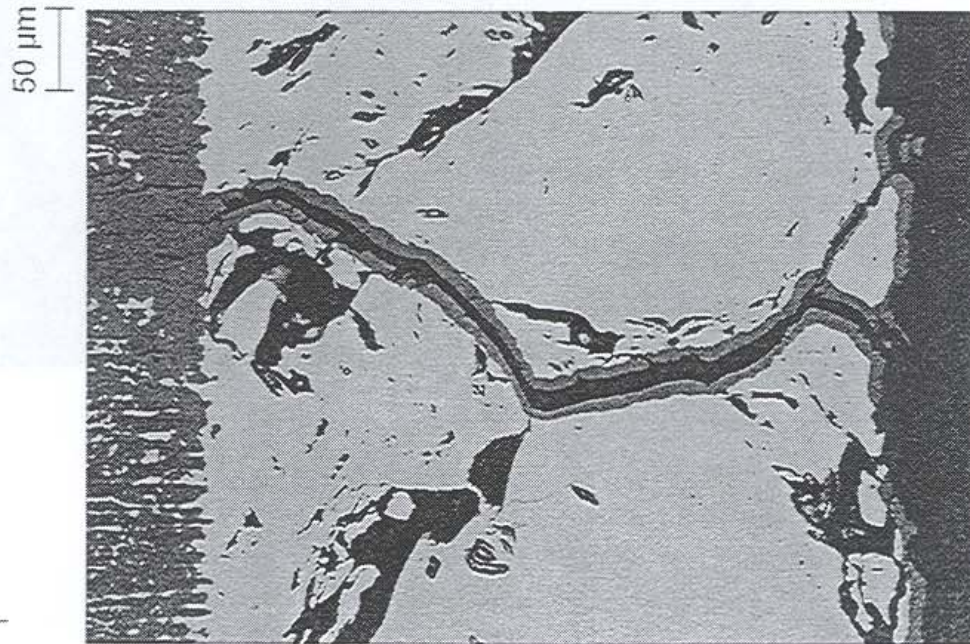
Localized, increased oxidation of the cladding inner surface



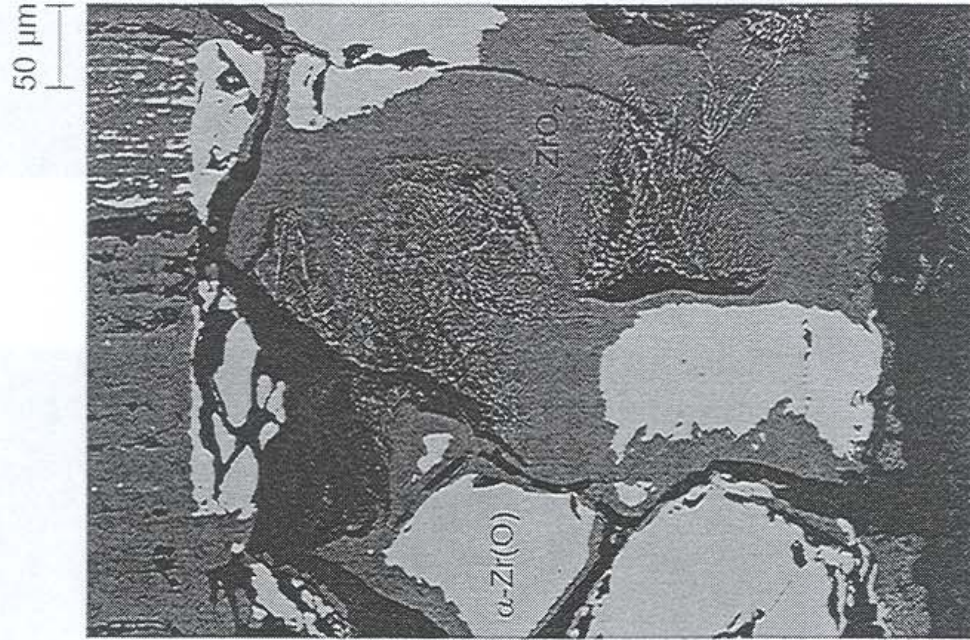
Test QUENCH-01; bundle elevation 1000 mm (QUE-01-4)

Fig. 59

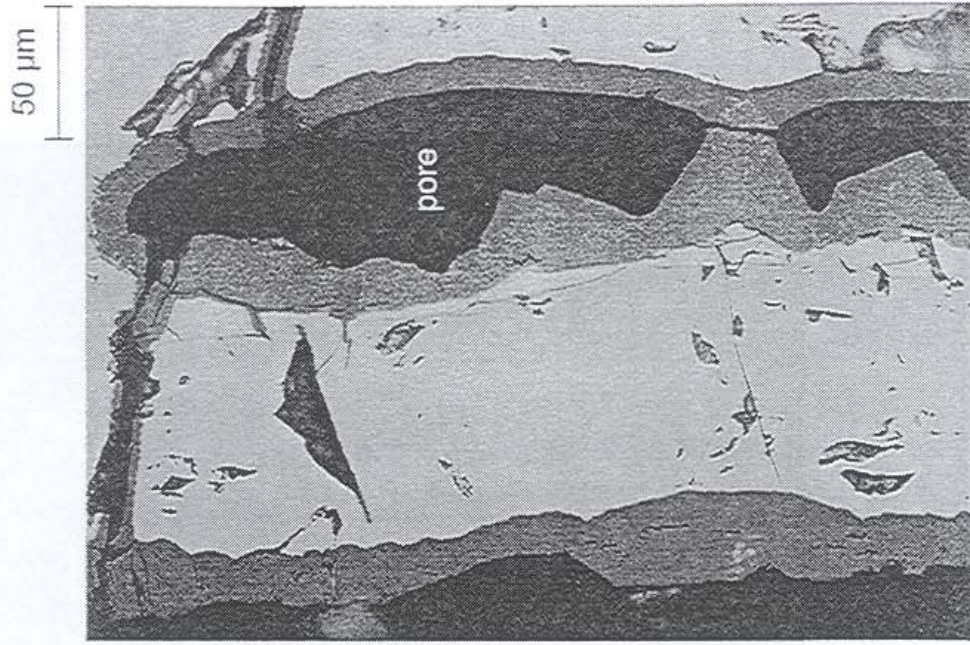
Oxidation of crack surfaces which formed during flooding



homogeneous crack surface oxidation



irregular crack surface oxidation



oxidation of "channels" inside α -Zr(O) phase

Test QUENCH-01; bundle elevation 1000 mm (QUE-01-4)

Oxidation behavior of the wire thermocouples

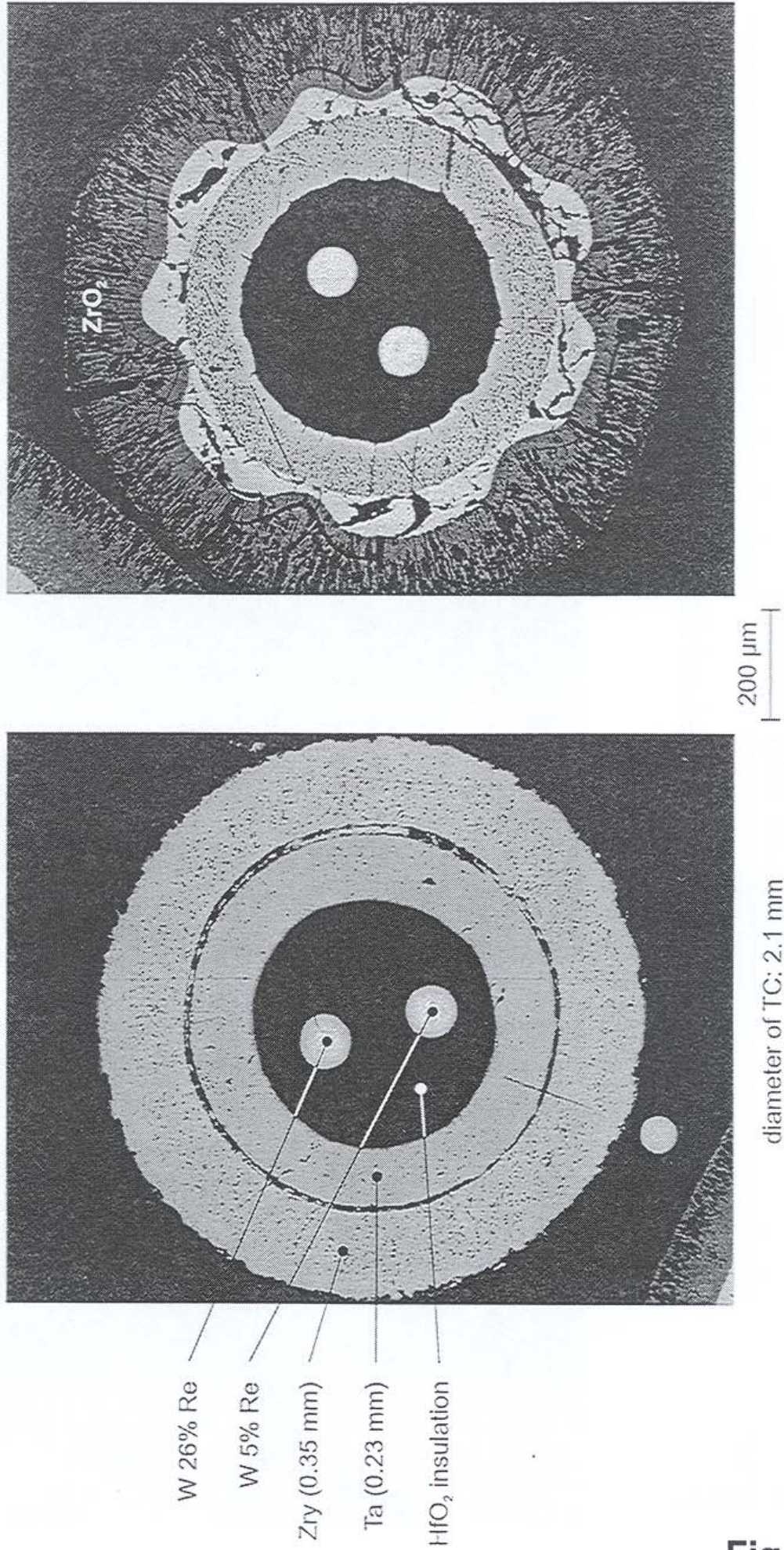
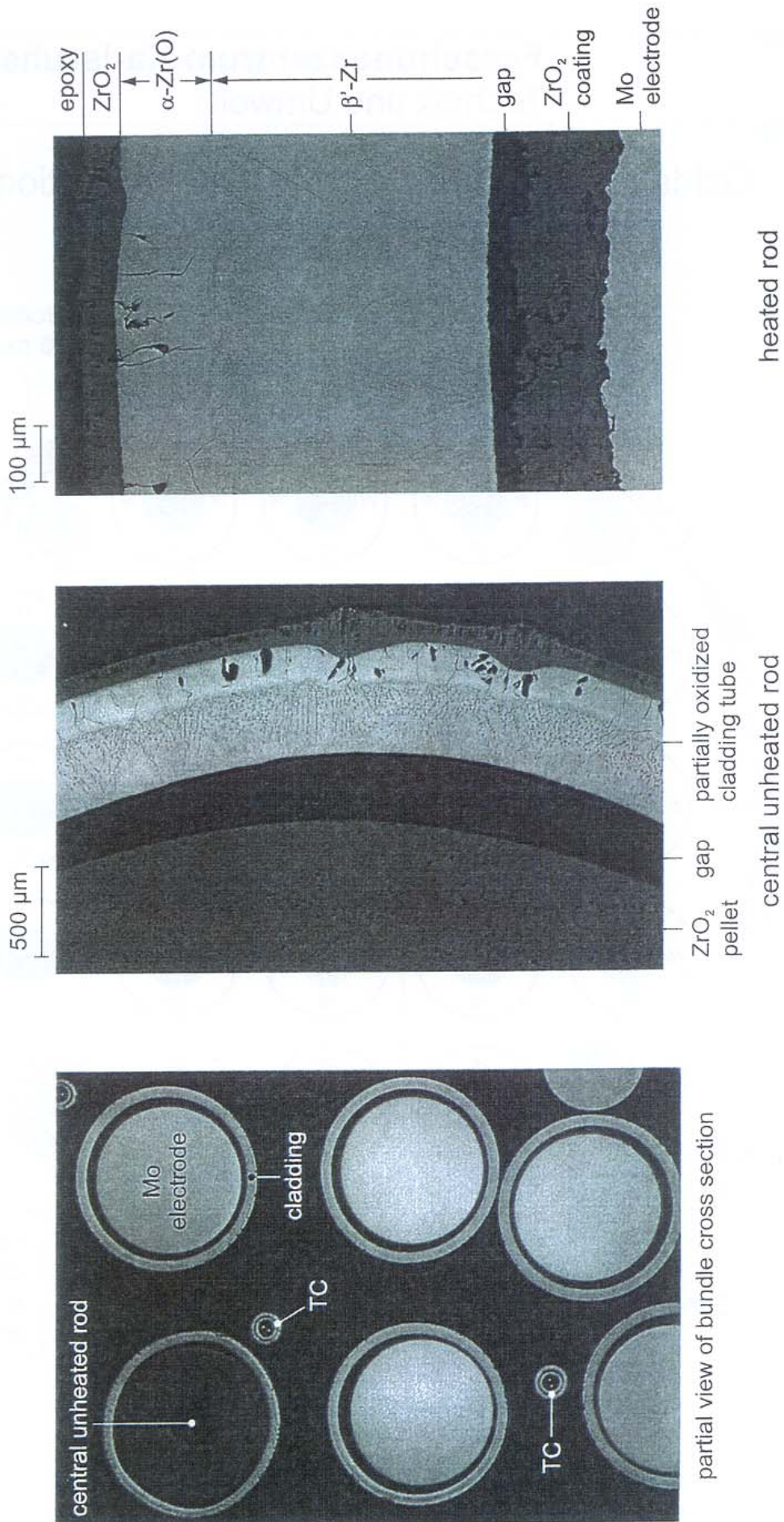


Fig. 61

Test QUEENCH-01; bundle elevation 1000 mm (QUE-01-4)

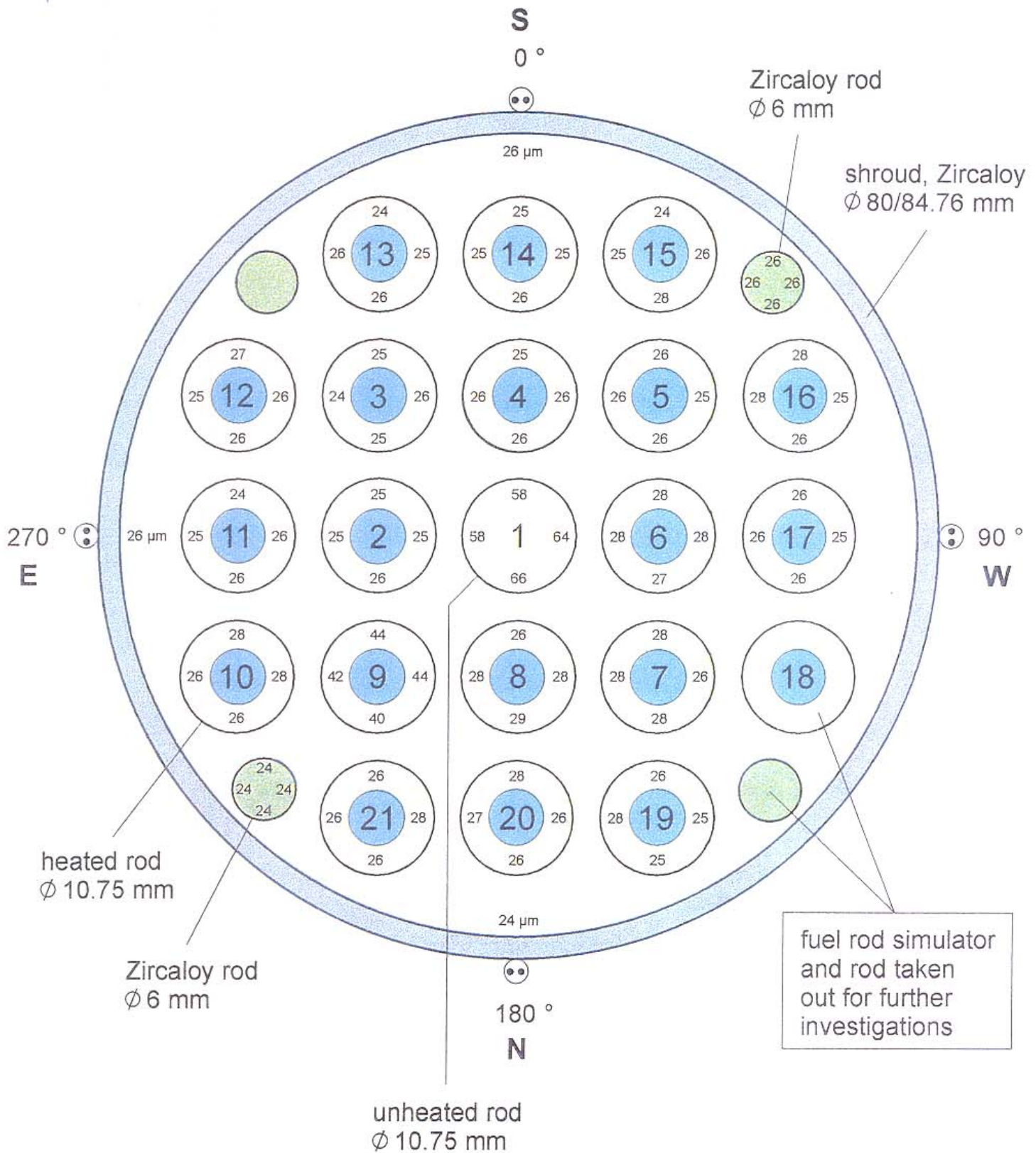
Oxidation of Zircaloy cladding tubes



Test QUENCH-01; bundle elevation 1163 mm (QUE-01-5)

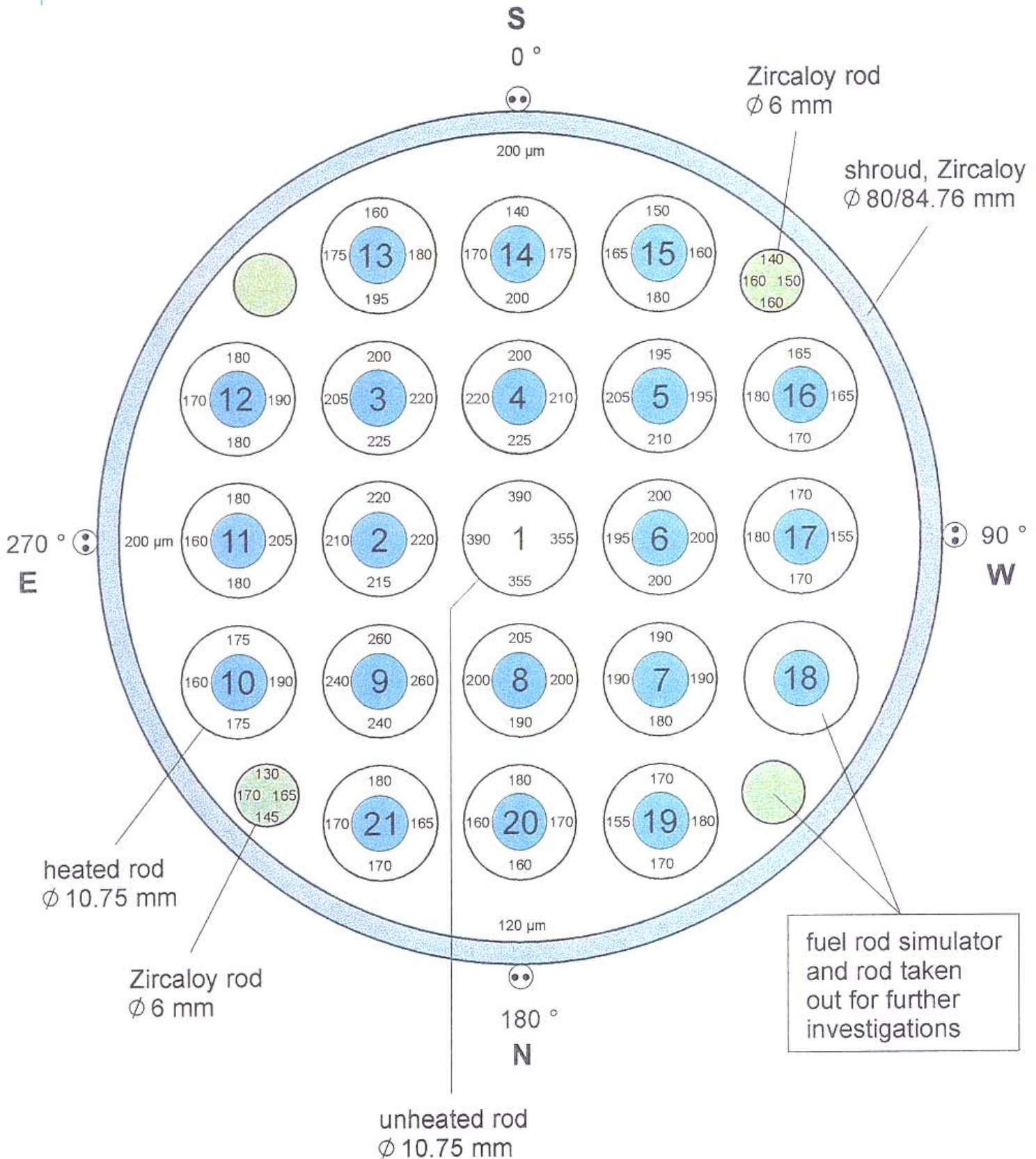
Fig. 62

Oxide layer thicknesses at bundle elevation 573 mm



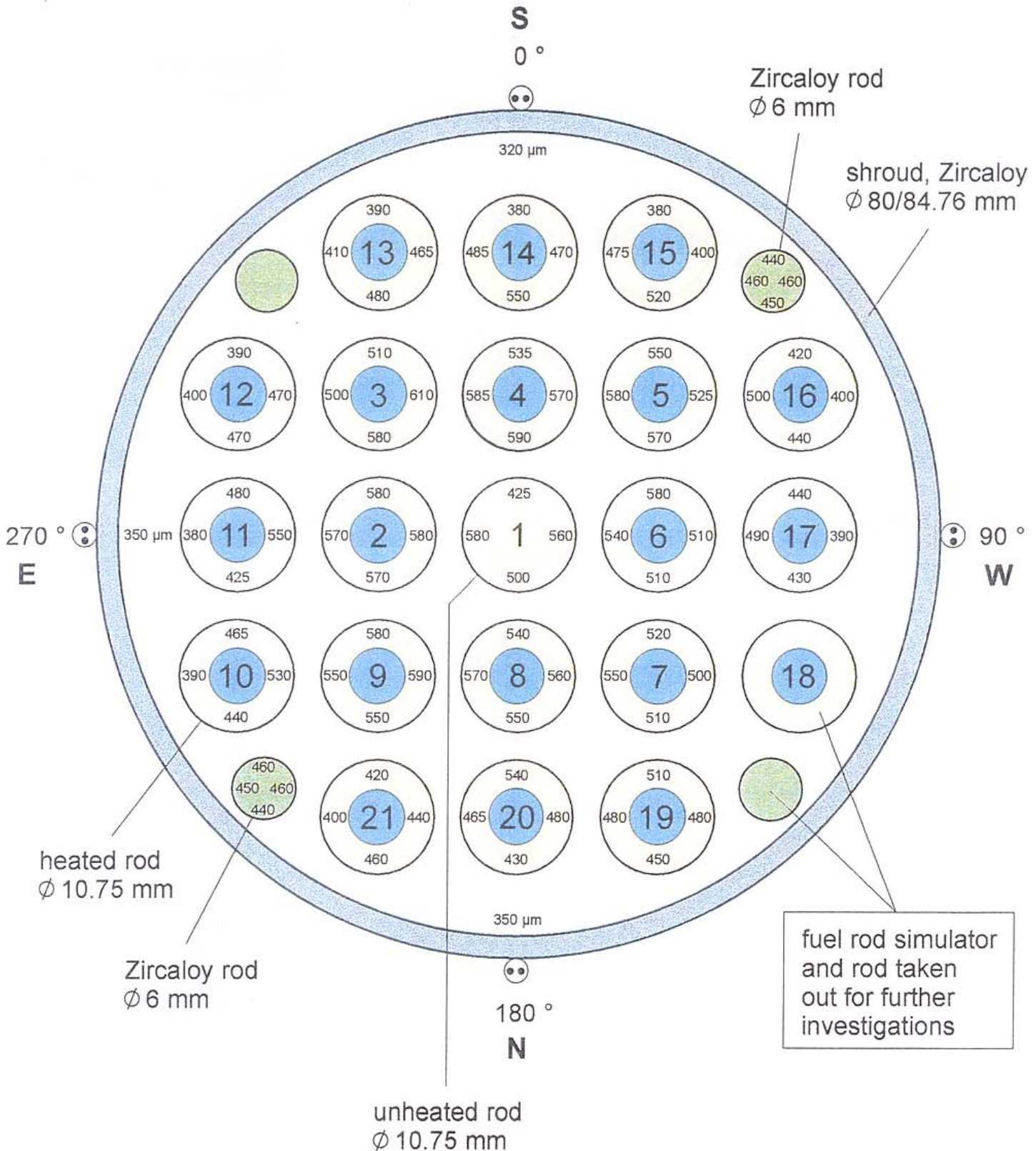
Test QUENCH-01; Cross section QUE-01-7 Fig. 63

Oxide layer thicknesses at bundle elevation 763 mm



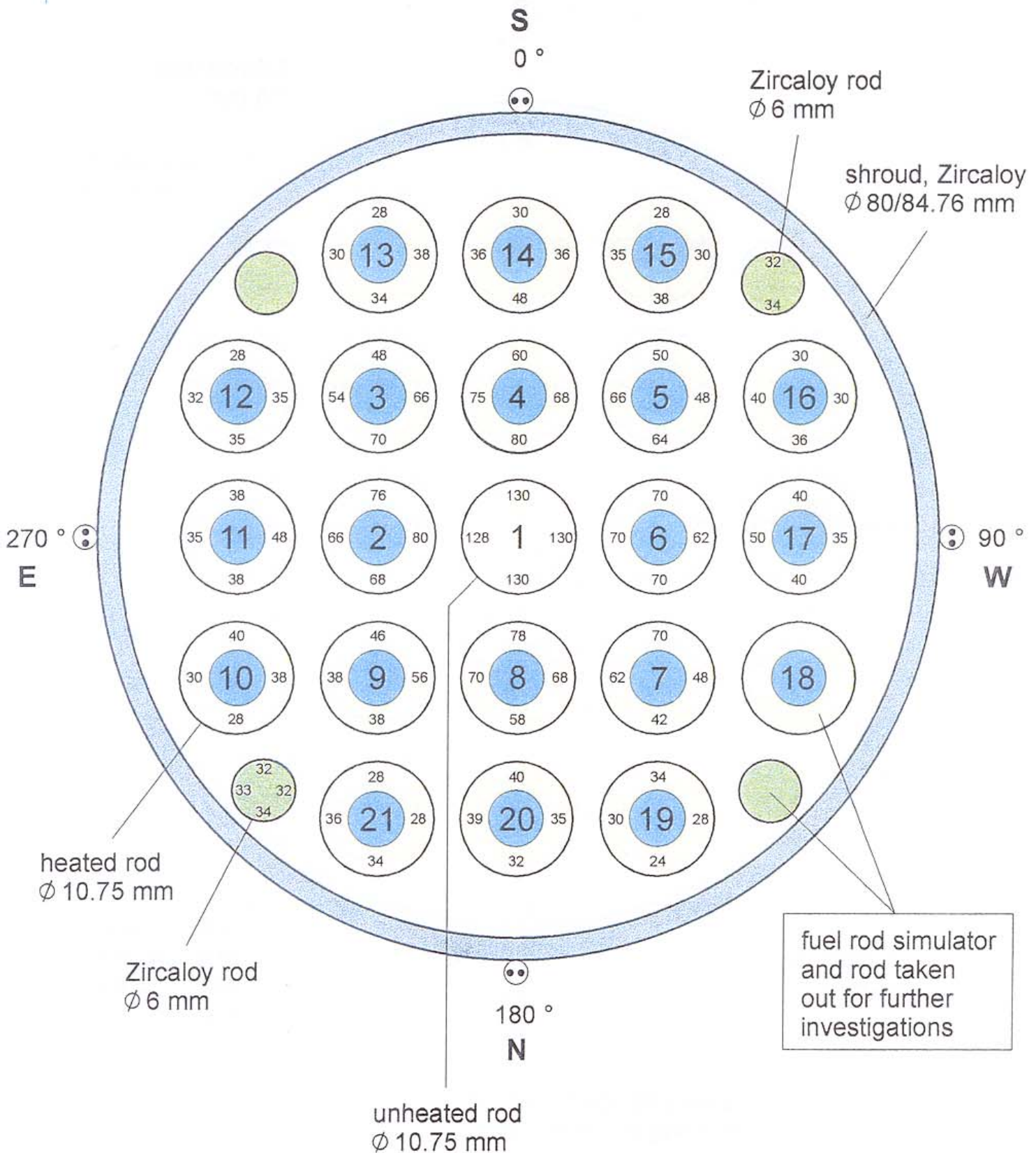
Test QUENCH-01; Cross section QUE-01-2 Fig. 64

Oxide layer thicknesses at bundle elevation 913 mm



Test QUENCH-01; Cross section QUE-01-3 Fig. 65

Oxide layer thicknesses at bundle elevation 1163 mm



Test QUENCH-01; Cross section QUE-01-5 Fig. 67

Oxide layer thicknesses of Zircaloy cladding tubes and calibration rods at different bundle elevations

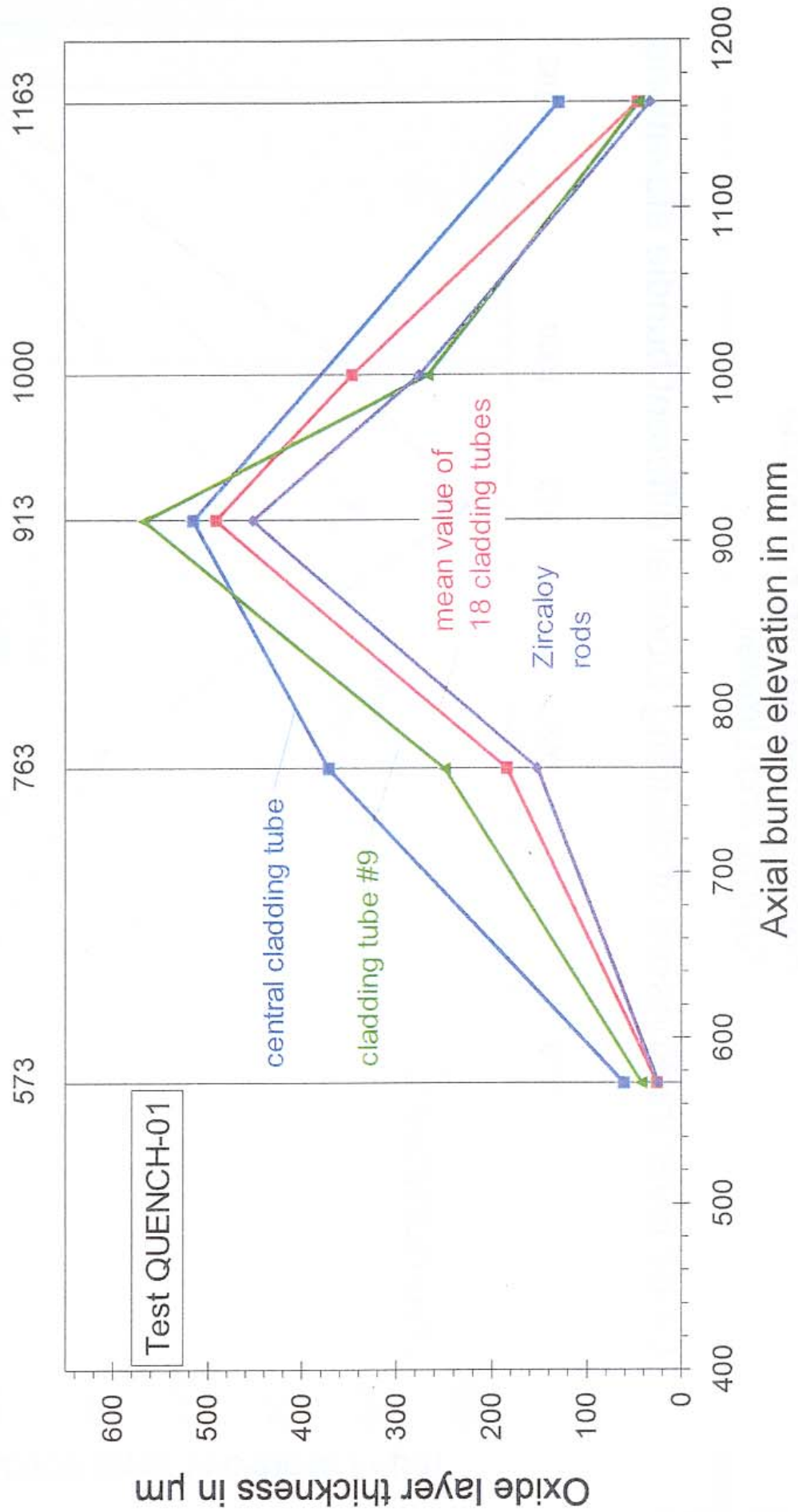


Fig. 68

Oxide layer thicknesses of cladding tubes at different bundle elevations

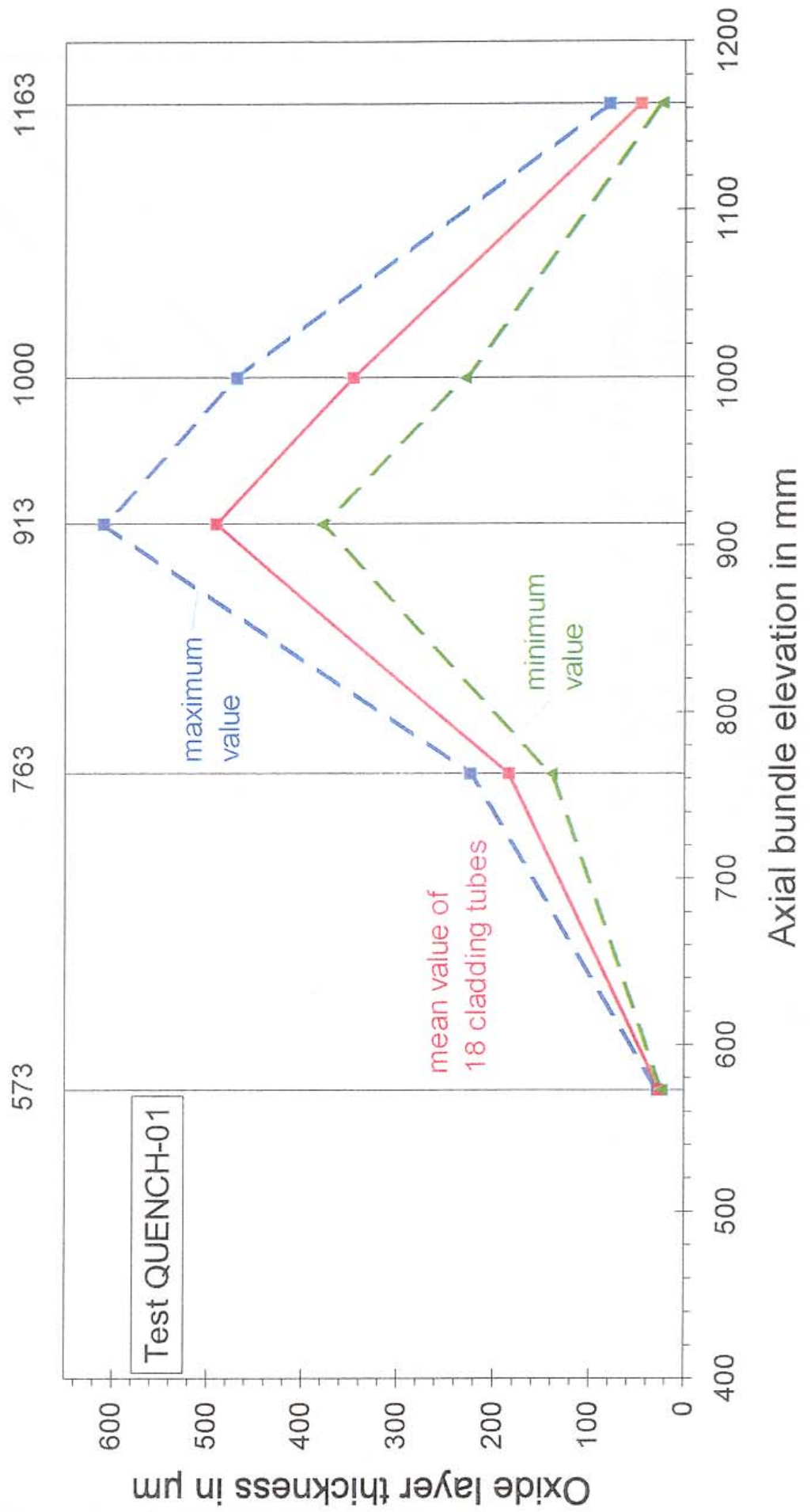
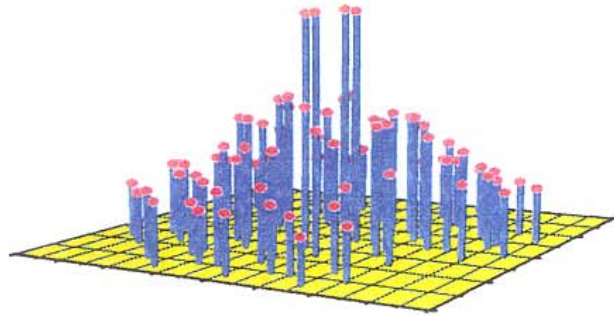
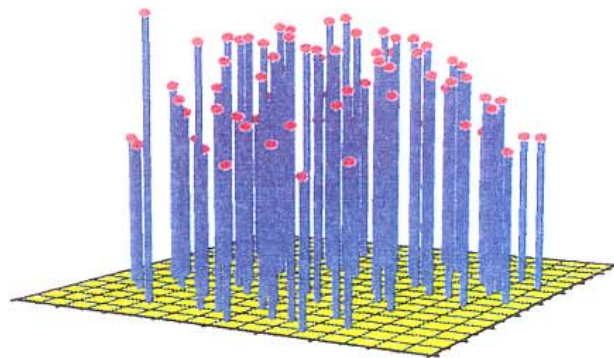


Fig. 69

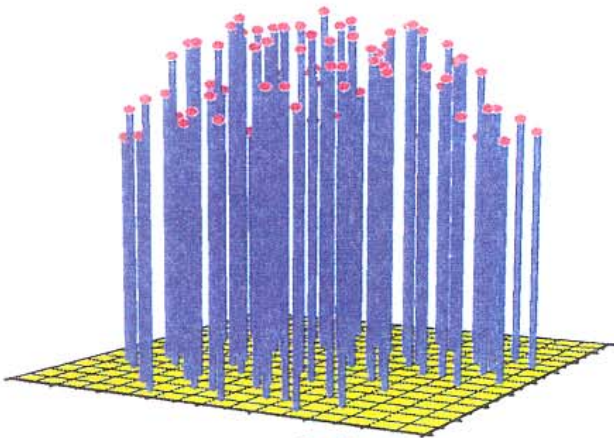
QUENCH-01: Oxide layer thickness distribution at various axial bundle elevations



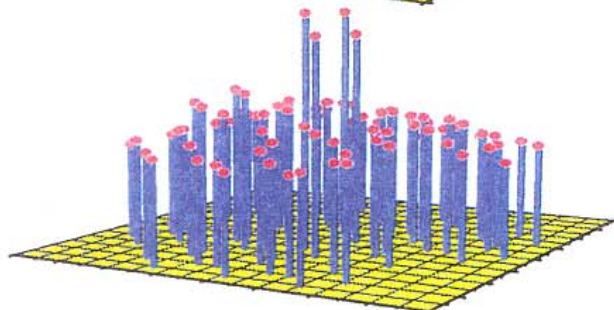
1163 m m



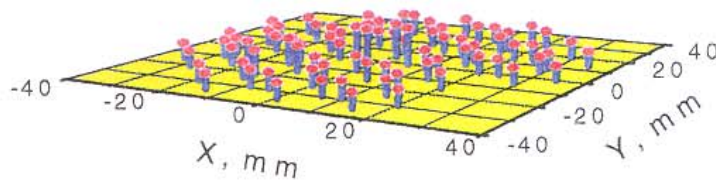
1000 m m



913 m m



763 m m



573 m m

Fig. 70

Oxide layer thicknesses of the Zircaloy rods before and after the quench test

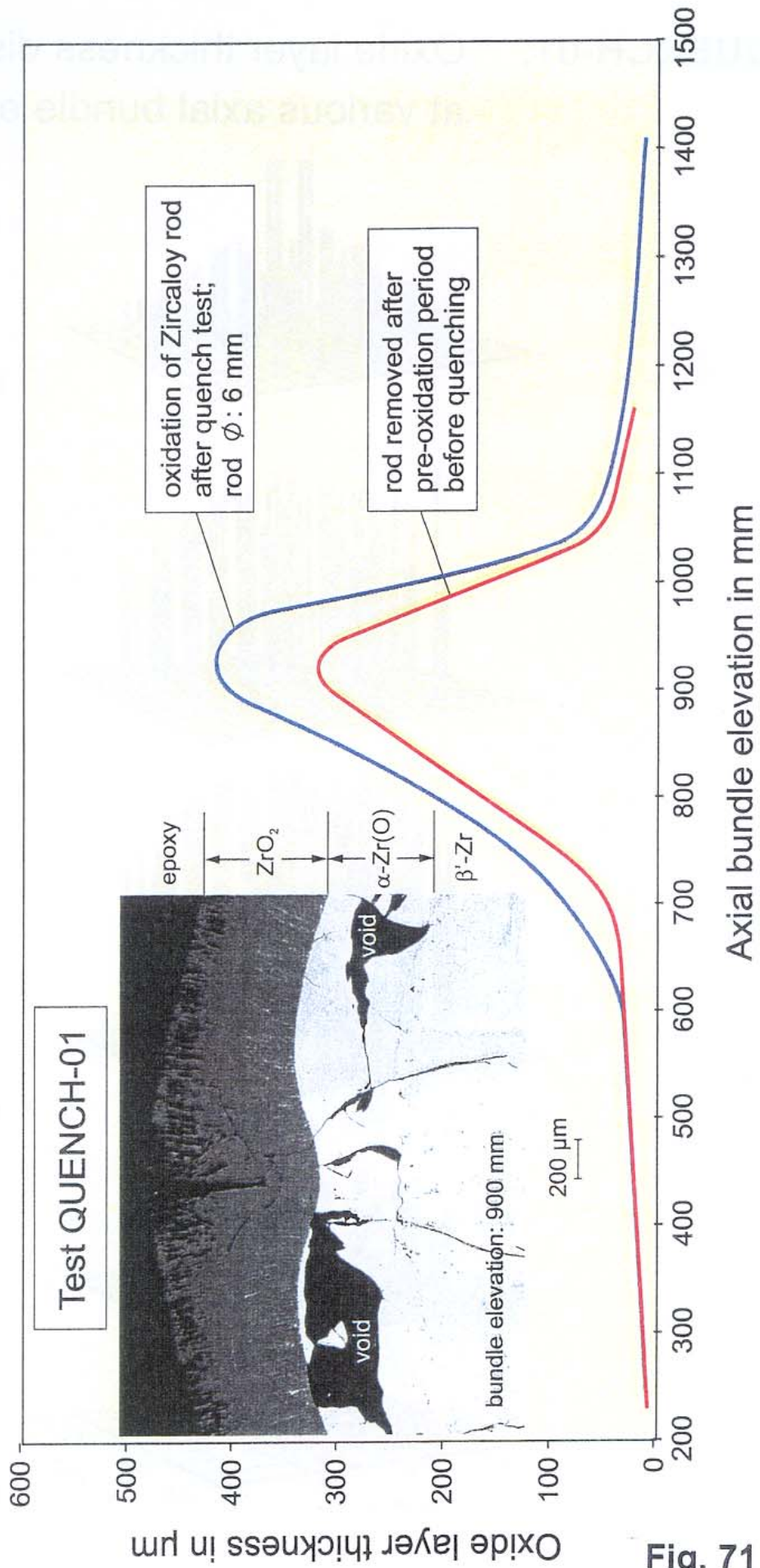


Fig. 71

Oxide layer thicknesses versus bundle elevation
of various components after the quench test

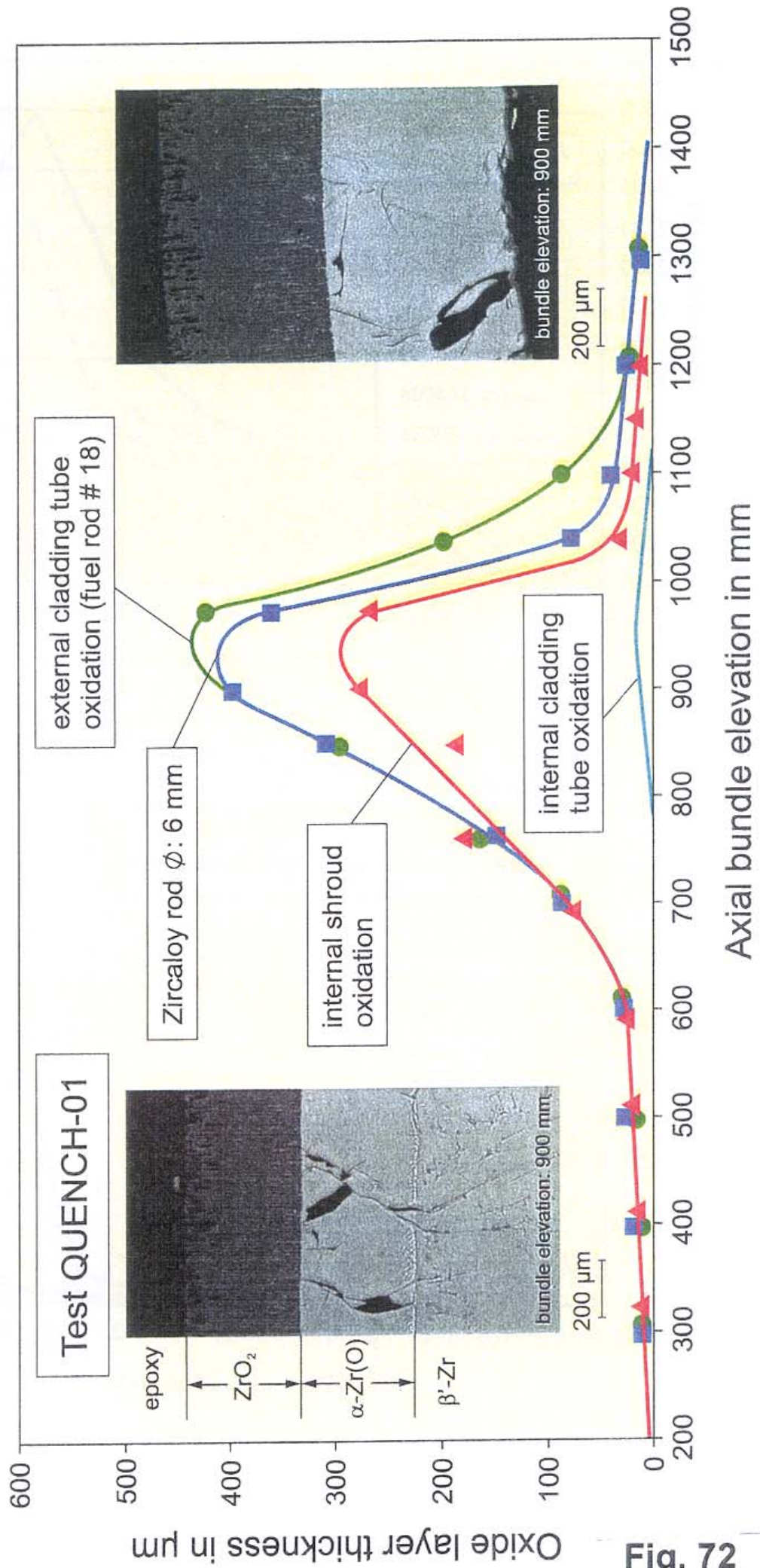


Fig. 72

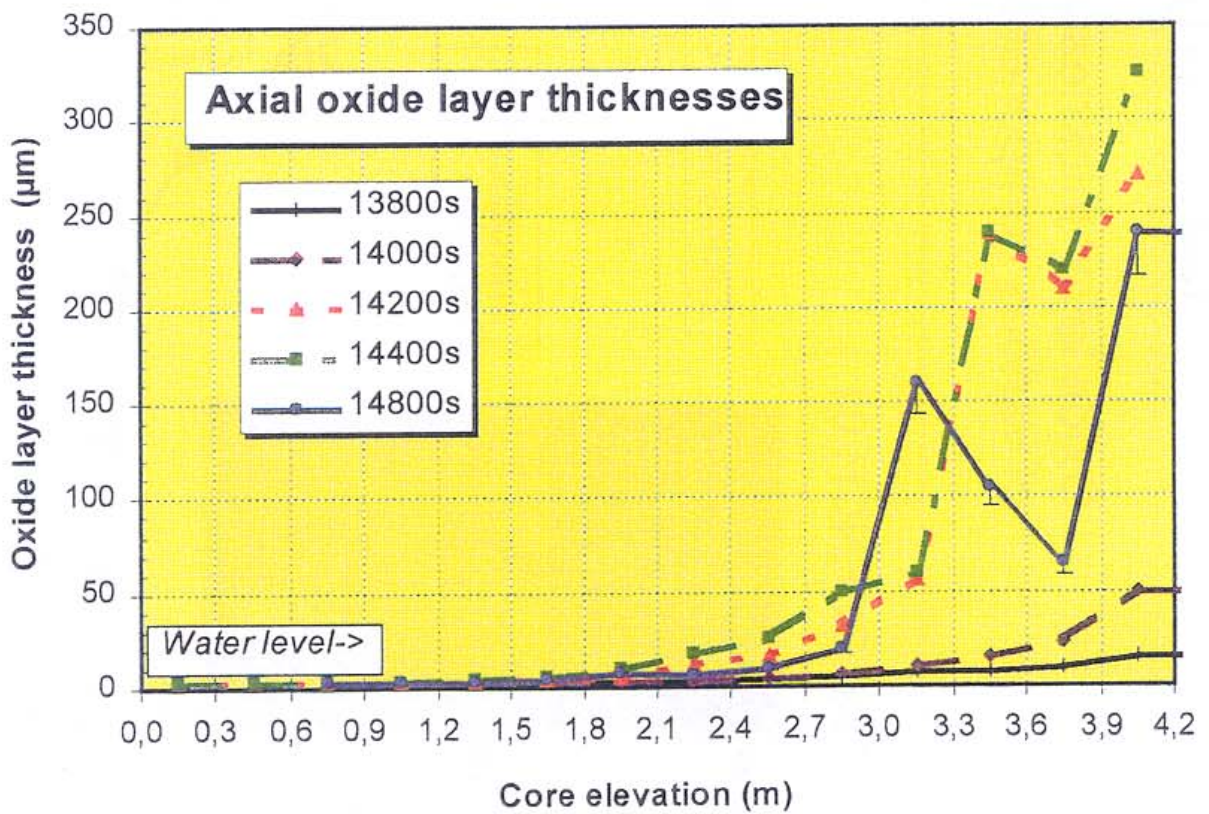
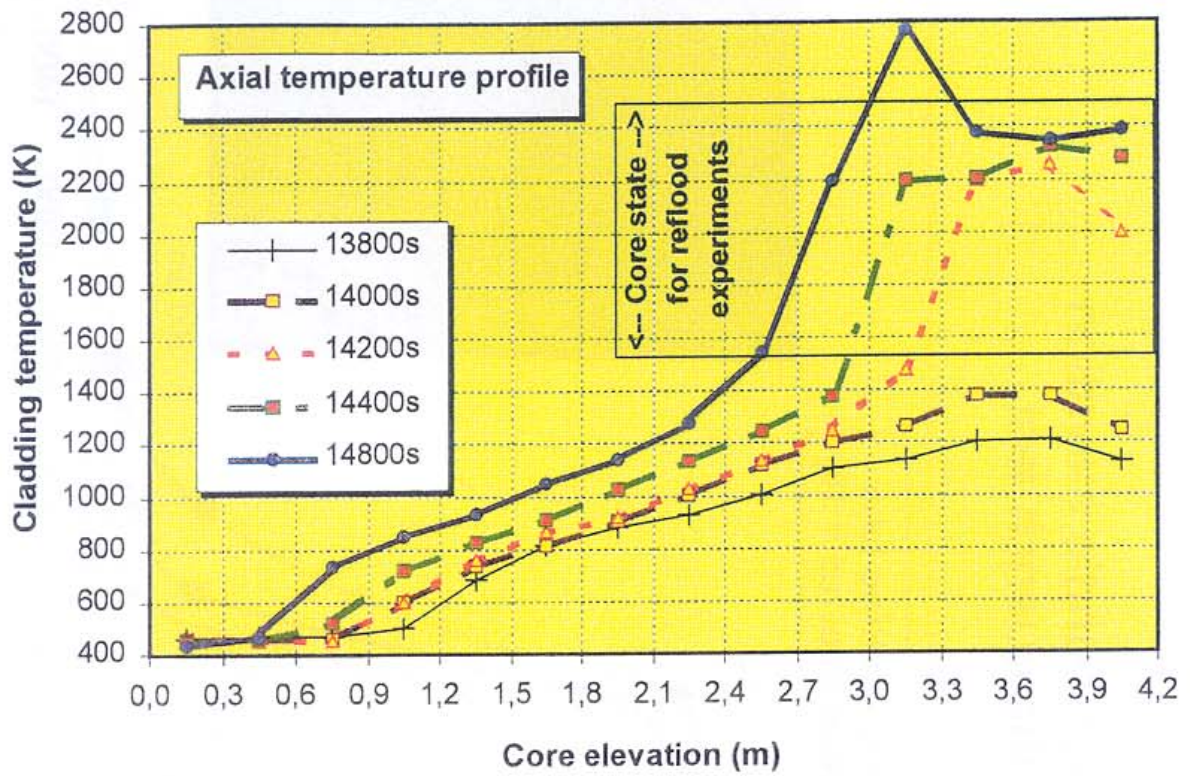


Fig. 73

QUENCH-01 q01r01

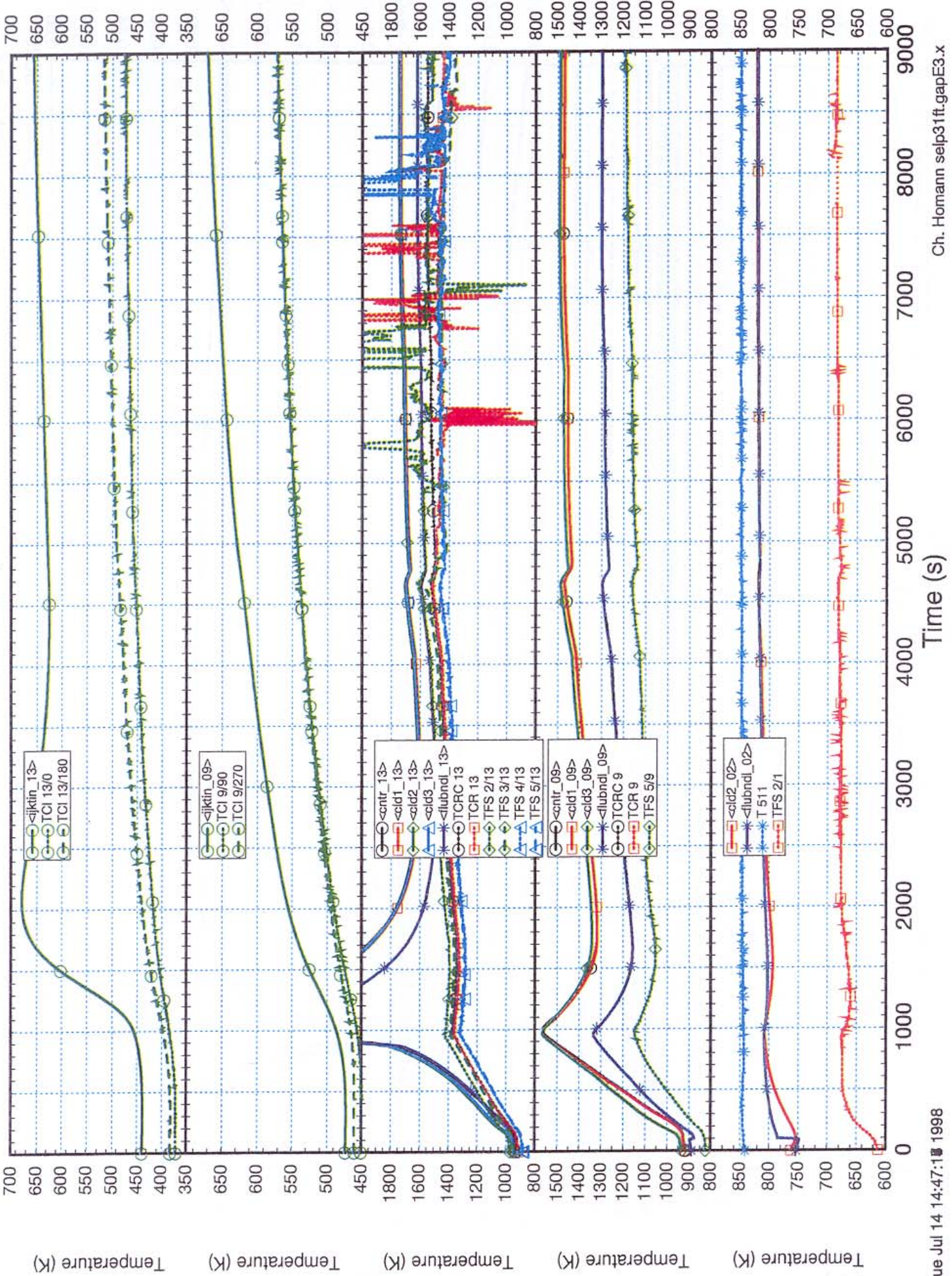


Fig. 76

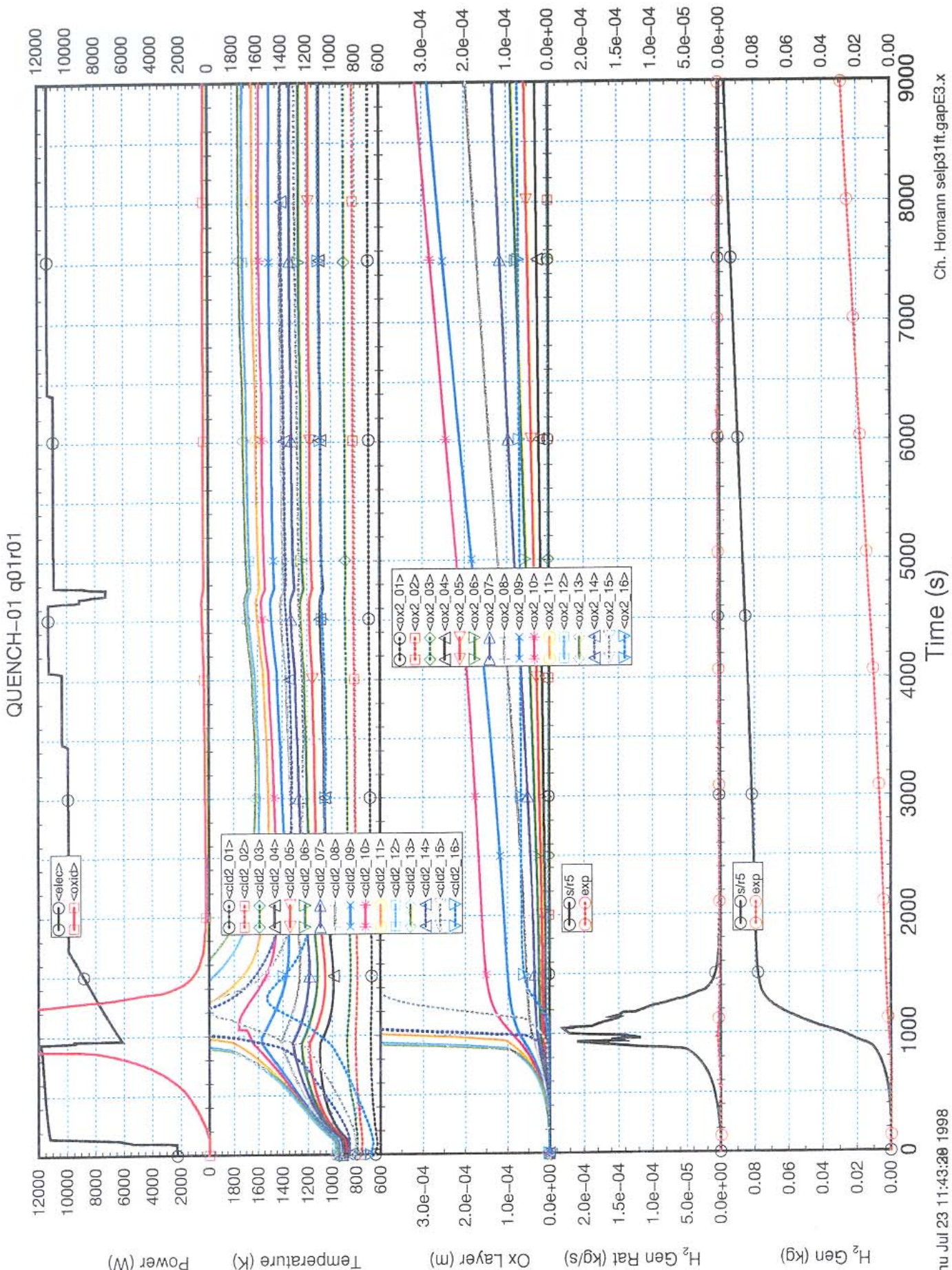


Fig. 77

QUENCH-01 q01r03

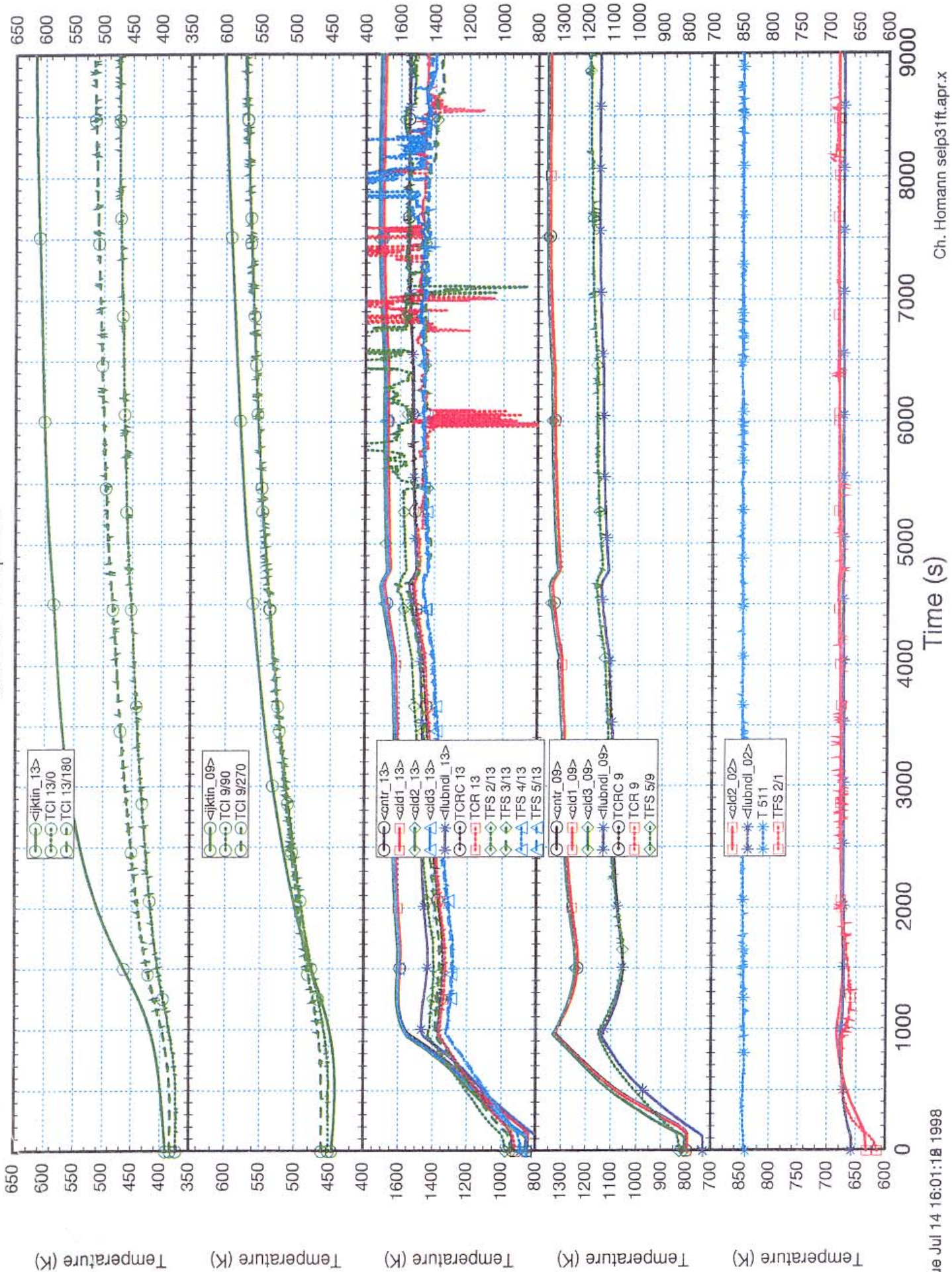


Fig. 78

QUENCH-01 q01r03

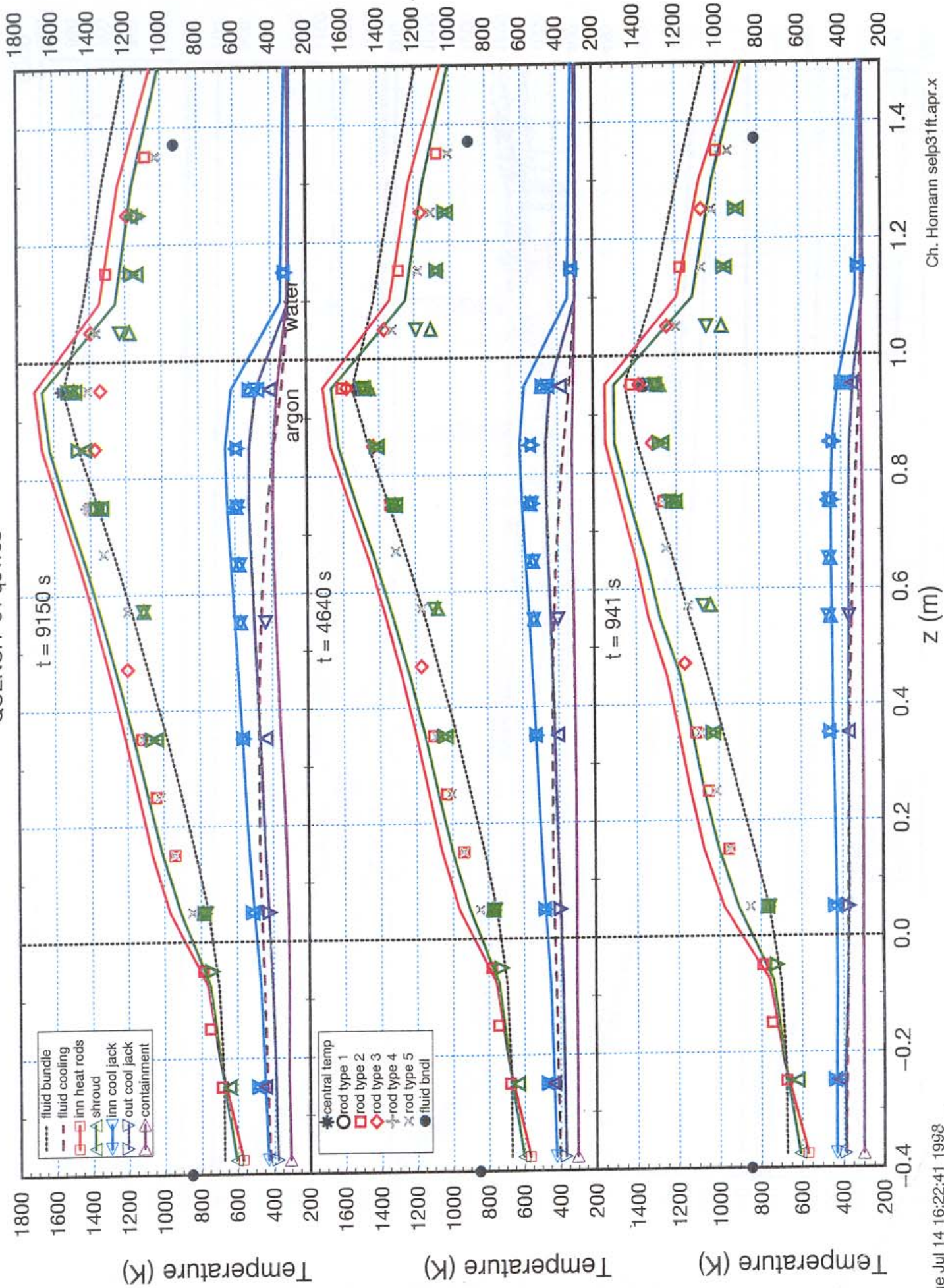


Fig. 79

QUENCH-01 q01r11

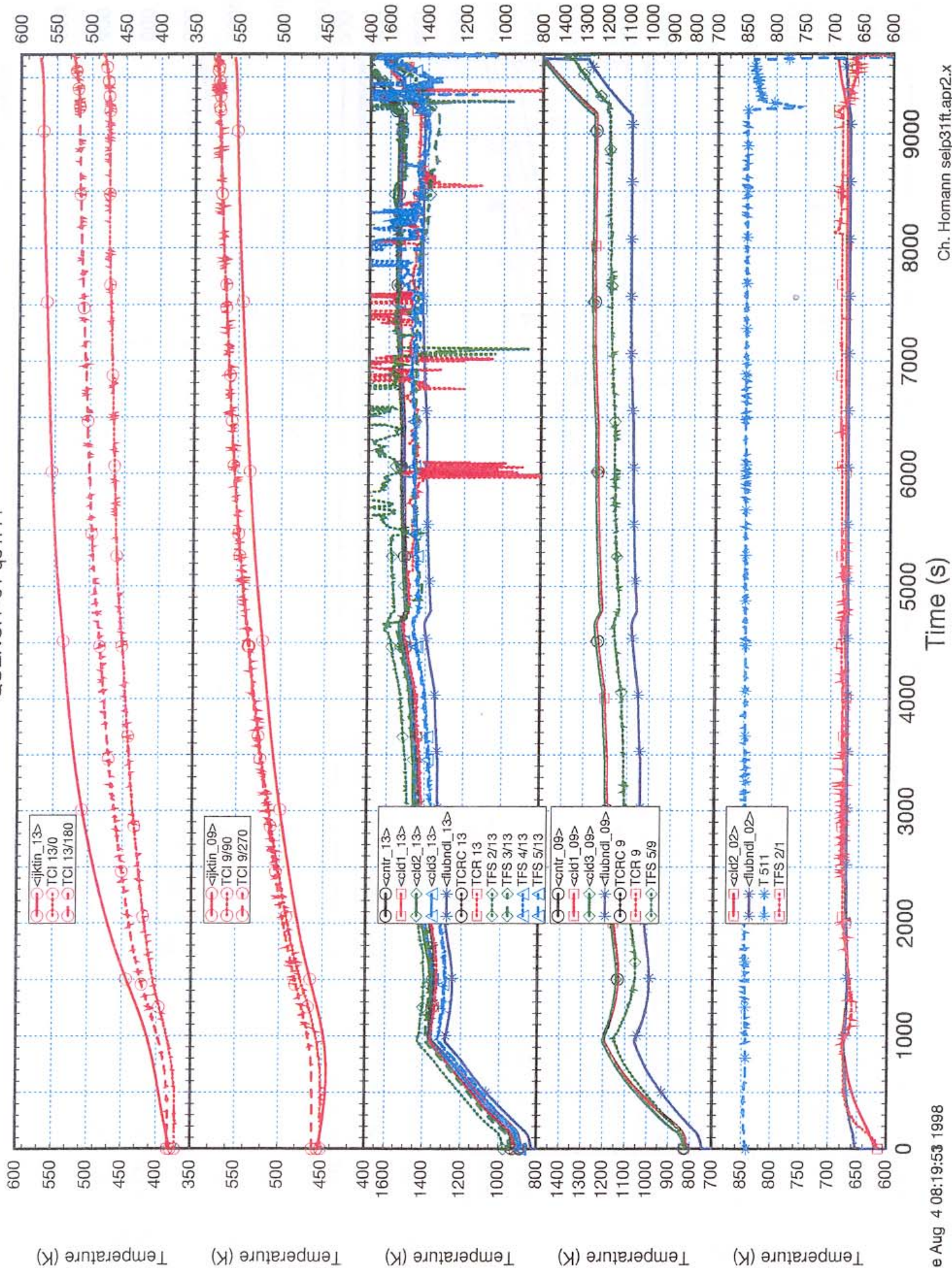


Fig. 80

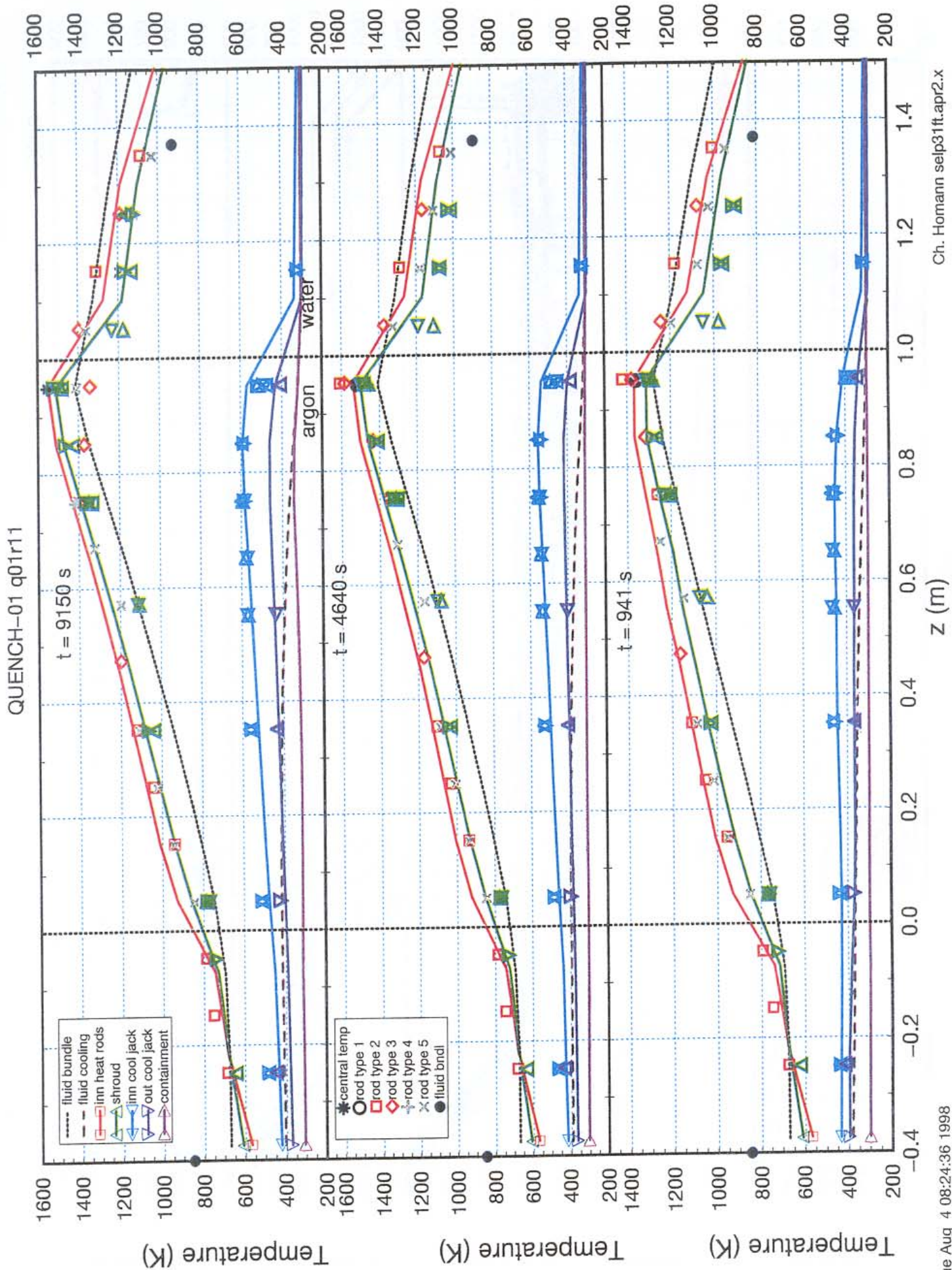


Fig. 81

QUENCH-01 q01r11

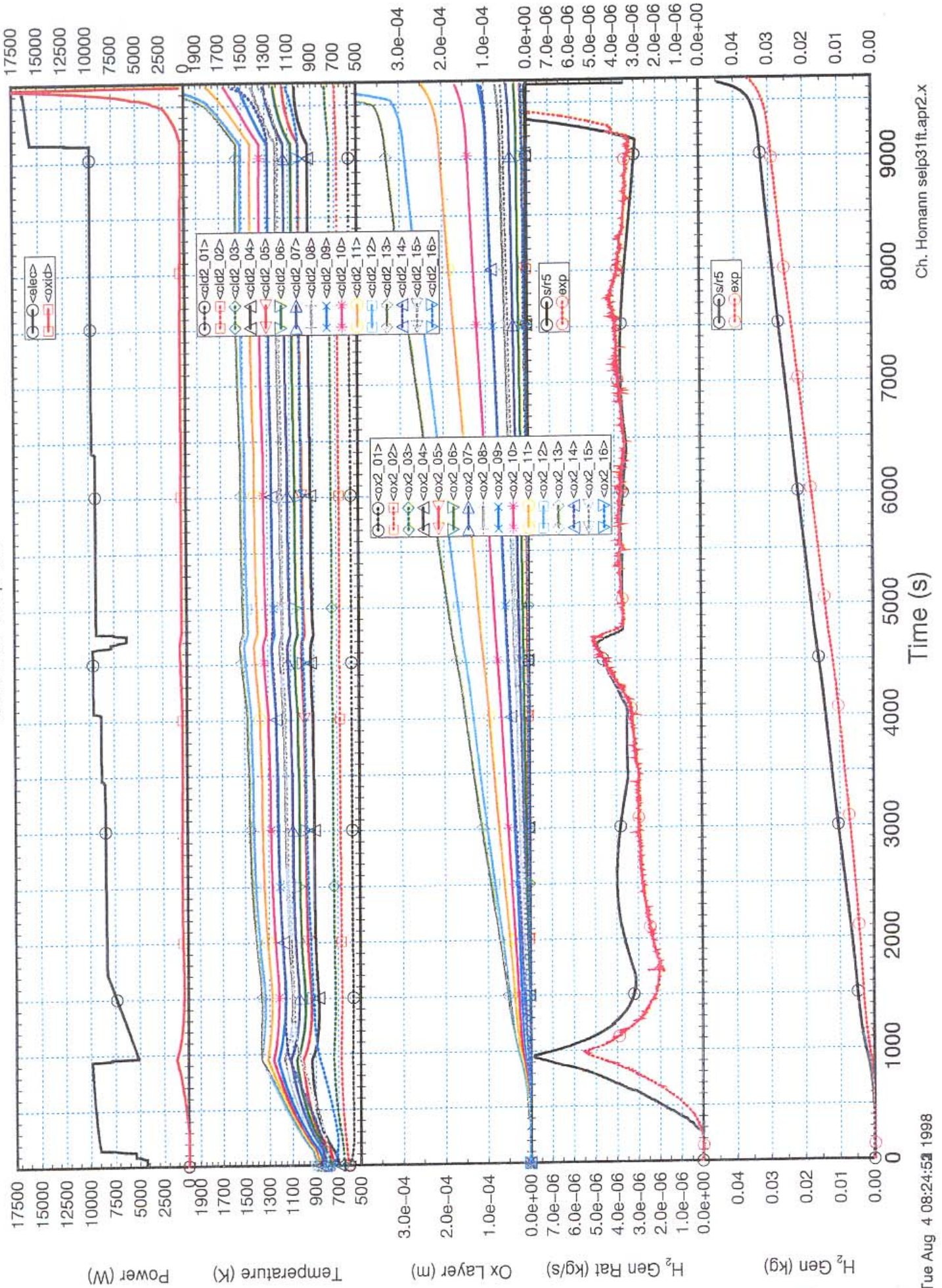


Fig. 82

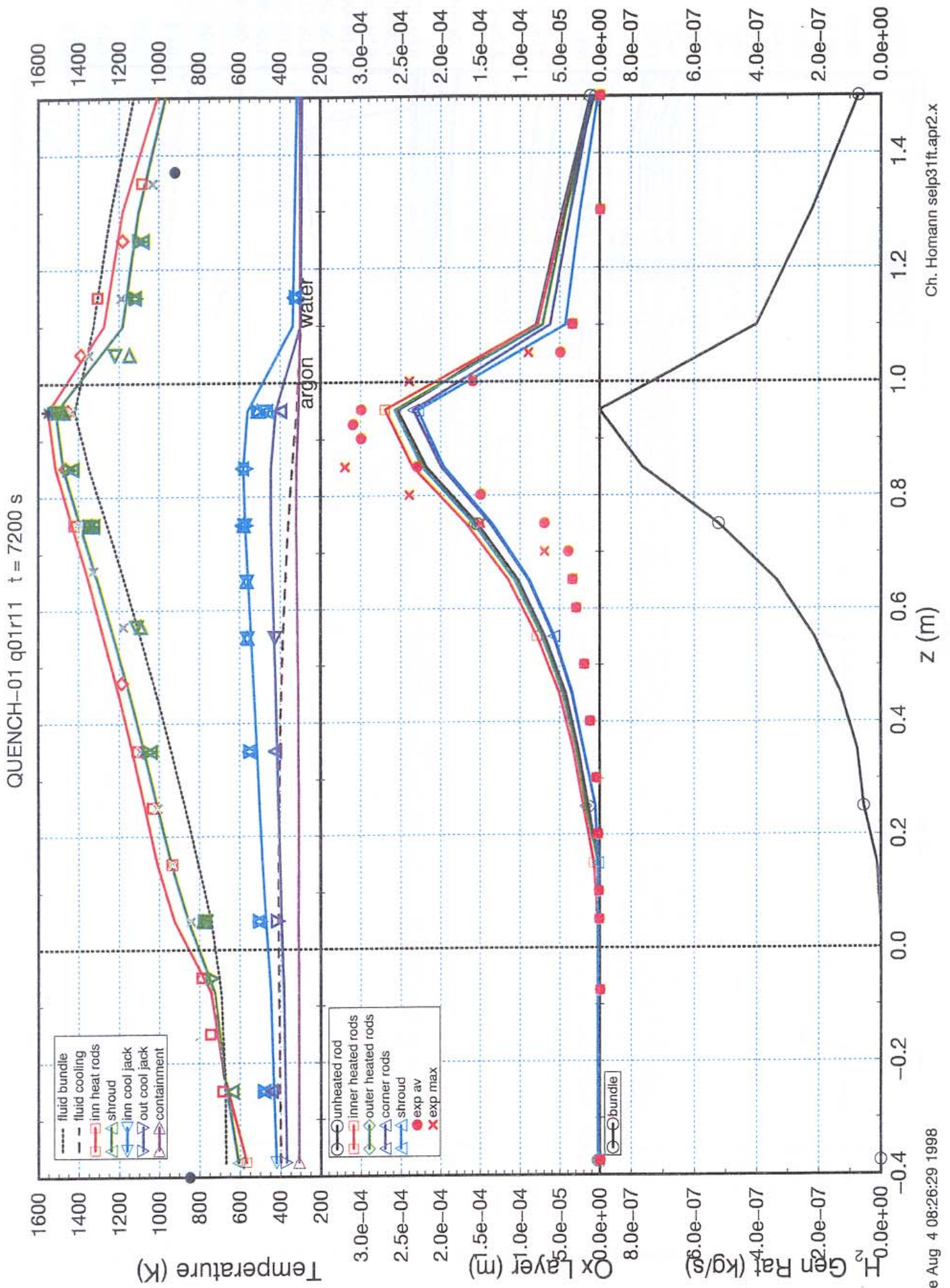


Fig. 83

Appendix

Appendix

Gas Flow Delay Measurements in the QUENCH Facility

The carrier gas has to transport the generated hydrogen to the mass spectrometer and to the Caldos analyzing system. As the hydrogen arrives with delay at both analyzing systems it is necessary to determine the response time. So, two test series in the QUENCH facility were set up:

1. Gas flow delay measurements with a H₂ injection at ambient temperature with two different argon flow rates: 3 und 6 g/s. The H₂ injection rate amounted to 50 and 25 l/min (standard) or 0.0744 g/s and 0.0372 g/s, respectively.
2. Gas flow delay measurements with a He injection at 1000 K with 3 g/s argon + 3 g/s steam and ca. 2 bar pressure in the off-gas line. The helium injection rate amounted to 60 and 30 l/min (standard) or 0.2 g/s and 0.1 g/s, respectively.

During all tests both gases, i. e. hydrogen and helium, were injected into the bundle at the elevation 700 mm, i. e. at an elevation where the major portion of the hydrogen is produced during the QUENCH experiments. The input flow was controlled with help of a MKS flow meter. The test program and the designation of the data files is provided in [Table A-1](#).

The delay measurements at ambient temperature were carried out independently of the QUENCH-01 main test whereas the testing at 1000 K and under the typical gas flow rates (3 g/s argon + 3 g/s steam) was performed prior to the pre-oxidation phase of test QUENCH-01 (see Fig. 14). For the latter tests helium was used instead of hydrogen because hydrogen would have been absorbed by the hot Zircaloy bundle components. Helium is recorded correctly by the mass spectrometer but not by the Caldos system which is calibrated for an argon/hydrogen mixture. The delay time, however, can also be determined with this gas for Caldos.

The response of the two measuring devices to the gas injections was analyzed. [Figure A-2](#) shows typical results of two tests for both measurement devices with high (60 l/min) and low (30 l/min) helium input.

The evaluation of the input and of the Caldos response data is provided in [Table A-2](#) for the delay measurements at ambient temperature and in [Table A-3](#) for the meas-

measurements performed at 1000 K under the typical gas flow rates (3 g/s argon + 3 g/s steam). The results of the reaction times of the Caldos analyzing system are summarized in [Table A-4](#). (The terms used in these tables are explained in [Fig. A-1](#)). As an average delay time for the typical test conditions a time of 100 s can be taken for the correction of the Caldos signal. In comparison, the delay time of the mass spectrometer is very short (4 - 8 s) due to its location near the outlet of the test section.

It must be noted that the evaluation of the data should only be taken with respect to the delay times. The balance, i. e. the comparison of the total gas injected to the total gas measured, is approximately 25 % off². Several areas of possible errors have been checked.

Results of a renewed check of the MKS flow meter that was used for the gas injection measurement (input flow) are provided in [Figs. A-3 and A-4](#) for helium and hydrogen, respectively. For the calibration of the MKS flow meter a highly accurate flow meter (Vol-U-Meter No. 1066-2) was used. The nominal values were set at the MKS system and compared to the actual reading of the Vol-U-Meter. As one can see the difference (error) is less than 1 %.

Another check was made on the argon flow meter F 401. This instrument was compared to the accurate MKS flow meter at a maximum flow rate 72 l/min (standard) which corresponds to 2.14 g/s. (The target flow rate for the F 401 instrument during the QUENCH experiments is 3 g/s.) The result of the check was that the argon flow meter F 401 did not measure correctly: The actual value was 15 % lower than the measured one. Although this percentage does not account completely for the difference between total gas injected and total gas measured, the incorrect measurement of the argon flow meter F 401 is in the right direction to explain the deficiency of the balance. With less argon in the system (test facility) the concentration of the hydrogen in an Ar/H₂ gas mixture is larger than evaluated. Therefore, a correction of 15 % has to be applied to the argon flow measurement.

² This holds for both the mass spectrometer and the Caldos device.

Table A-1: Test program of the gas flow delay measurements and designation of the data files

Measurements at ambient temperature (Febr. 20, 1998)

- 3 g/s argon
 - H₂ injection rate: a) 50 l/min i. N.³ → **LZM_02 [LZM_06]**
 - b) 25 l/min i. N. → **LZM_03 [LZM_07]**

- 6 g/s argon
 - H₂ injection rate: a) 50 l/min i. N. → **LZM_04 a (Test interrupted)**
 - LZM_04 b [LZM_08]**
 - b) 25 l/min i. N. → **LZM_05 [LZM_09]**

- 3 g/s argon
 - H₂ injection rate: 50 l/min i. N., 60 s → **LZM_10**

Measurements at operating conditions (3 g/s argon + 3 g/s steam, ca. 2 bar, 1000 K), Febr. 26,1998

- Helium injection rate: a) 60 l/min i. N. → **LZM_11**
- b) 30 l/min i. N. → **LZM_12**

Note: LZM data files in brackets [] = Repetition of measurements.

³ Referred to standard conditions, i. e. 273 K and 1 bar (0.1 MPa)

Table A-2: Results of the time-lag measurements in the QUENCH facility (Febr. 20, 1998)

H₂ injection at ambient temperature

Test	Argon [g/s]	H ₂ input				Max. H ₂ signal at CALDOS			Delay time ^{***})			
		[l/min]	H ₂ on [h]	1 st signal [h]**)	H ₂ off [h]**)	Duration [s]	Total [g]	[Vol. %]	[g/s]	1 st signal	Time [s]	
LZM_02	2.94	50 [*])	12:08:26	12:08:57	12:18:16	630	46.87	38.4	0.095	62.12	12:10:03	97
LZM_03	3.0	25 [*])	13:00:22	13:00:23	13:11:53	691	25.71	23.4	0.046	32.38	13:02:11	109
LZM_04a	6.04	50	13:40:21	-	-	-	****)	-	-	-	-	-
LZM_04b	6.04	50	13:55:43	13:55:51	14:04:24	521	38.76	23.6	0.094	49.23	13:57:12	89
LZM_05	6.04	25	14:13:29	14:13:30	14:23:30	601	22.36	13.1	0.045	27.24	14:15:08	99
LZM_08	6.04	50	14:31:52	14:32:25	14:41:38	586	43.60	23.8	0.093	54.98	14:33:22	90
LZM_09	6.04	25	14:51:37	14:51:38	15:02:32	655	24.37	13.1	0.045	29.68	14:53:16	99
LZM_06	3.01	50	15:14:15	15:14:47	15:27:25	790	58.78	38.7	0.095	77.39	15:15:55	100
LZM_07	3.01	25	15:40:18	15:40:19	15:52:26	728	27.10	23.5	0.046	34.23	15:42:12	114
LZM_10	3.01	50	16:04:46	16:05:19	16:05:47	61	4.54	12.8	0.022	5.90	16:06:29	103

^{*}) 50 l/min standard = 0.0744 g/s H₂; 25 l/min standard = 0.0372 g/s H₂.

^{**}) H₂ on and H₂ off = time when H₂ injection valve was opened and closed, respectively; 1st signal = time when data acquisition system has received the first value.

^{***}) Time between onset of H₂ input (H₂ on) and onset of response signal (1st signal) at CALDOS system.

^{****}) No equilibrium reached.

Table A-3: Results of the time-lag measurements in the QUENCH facility (Febr. 26, 1998)
Helium injection at 1000 K

Test	Argon [g/s]	Steam [g/s]	[l/min]	He on			He input			Delay time ^{***})	
				[h]	1 st signal	He off [h]**)	Duration [s]	Total [g]	1 st signal	Time [s]	
LZM_11	3.0	3.0	60*)	14:29:36	14:29:37	14:38:40	544	108.8	14:30:56	83	
LZM_12	3.0	3.0	30*)	14:51:49	14:51:51	15:00:28	513	51.3	14:53:19	90	

*) 60 l/min standard = 0.2 g/s He; 30 l/min standard = 0.1 g/s He.

***) He on and He off = time when He injection valve was opened and closed, respectively; 1st signal = time when data acquisition system has received the first value.

****) Time between onset of He input (He on) and onset of response signal (1st signal) at CALDOS system.

Table A-4: Reaction times of the CALDOS system in the QUENCH facility

Test	Argon [g/s]	Steam [g/s]	H ₂ input [l/min]	He input [l/min]	Max. CALDOS signal [Vol.-%]	Delay time*) [s]	Time to max. signal [s]	Time at max. signal [s]	Drop-off time**) [s]	Time differ- ence***) [s]
LZM_02	2.94	-	50	-	38.4	97	452	279	464	238
LZM_03	3.0	-	25	-	23.4	109	585	201	362	204
LZM_04a****)	6.04	-	50	-	-	-	-	-	-	-
LZM_04b	6.04	-	50	-	23.6	89	314	260	215	142
LZM_05	6.04	-	25	-	13.1	99	498	139	184	135
LZM_08	6.04	-	50	-	23.6	90	421	119	313	43
LZM_09	6.04	-	25	-	13.1	99	500	346	143	178
LZM_06	3.01	-	50	-	38.7	100	679	203	543	191
LZM_07	3.01	-	25	-	23.2	114	708	110	366	204
LZM_10****)	3.01	-	50	-	12.6	103	127	60	369	229
LZM_11****)	3.0	3.0	-	60	*****)	83	421	151	624	108
LZM_12****)	3.0	3.0	-	30	*****)	90	398	137	591	106

*) Time between onset of H₂ input (He input) and the first increase of the CALDOS signal.

**) Time from maximum CALDOS signal to initial value (< 0.05 vol.-%).

***) Time between end of gas input and and first decrease of the max. CALDOS signal.

****) No equilibrium reached.

*****) Carrier gas argon + steam injected at 1000 K.

*****) Evaluation only correct with respect to the time signals; the CALDOS system is calibrated with H₂/argon.

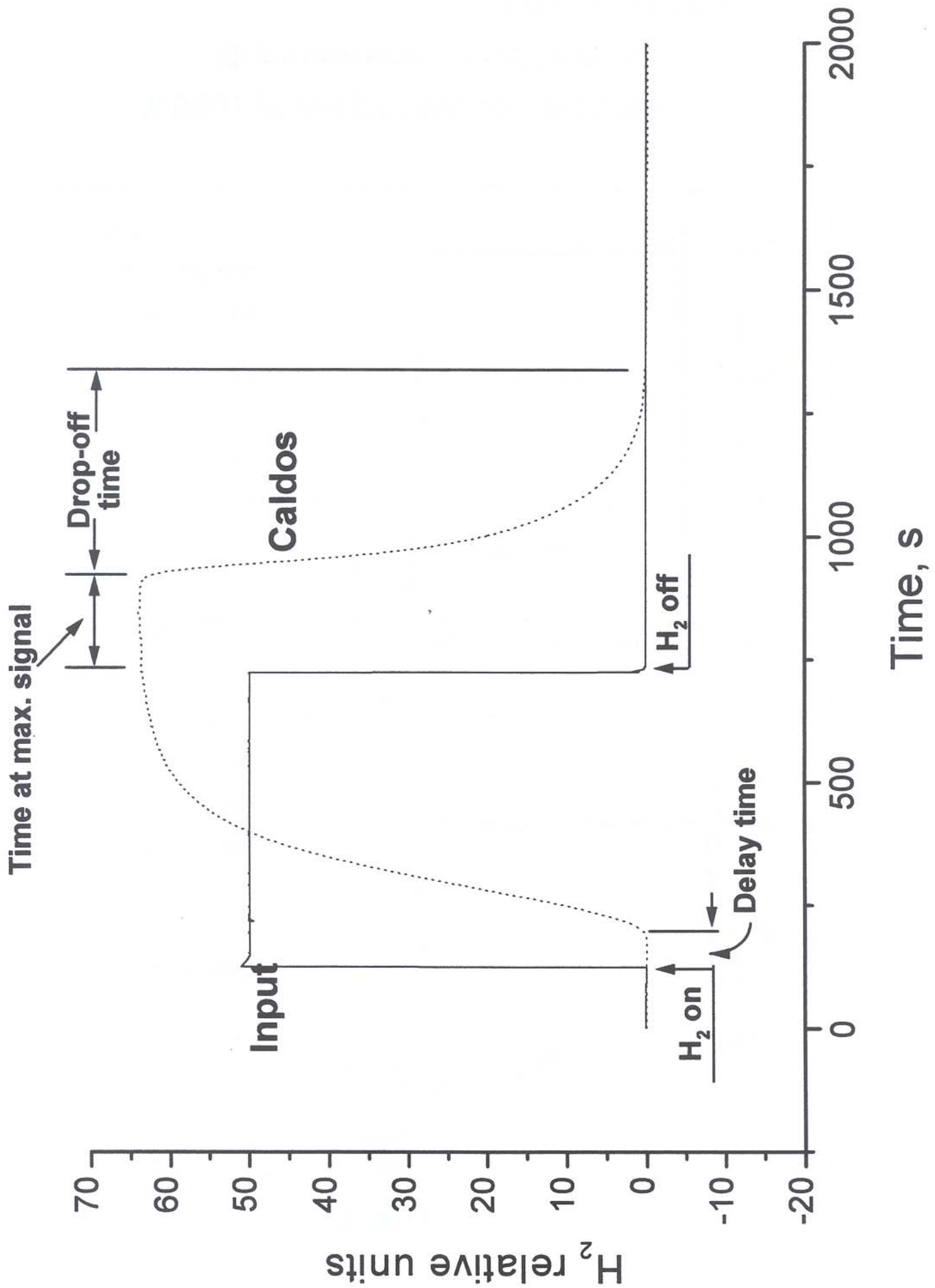


Fig. A-1

QUENCH-01

Gas flow delay time measurements

under steam/argon atmosphere at 1000 K

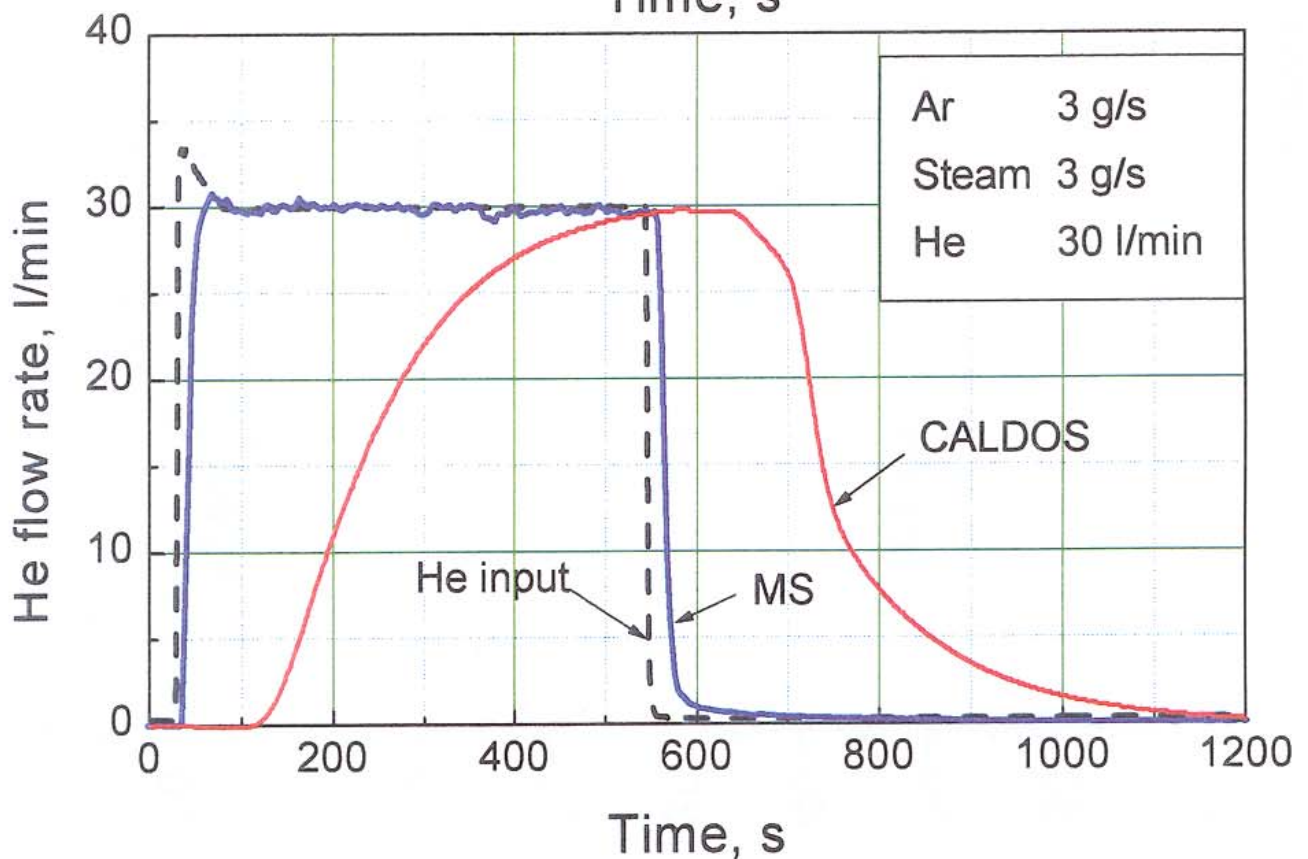
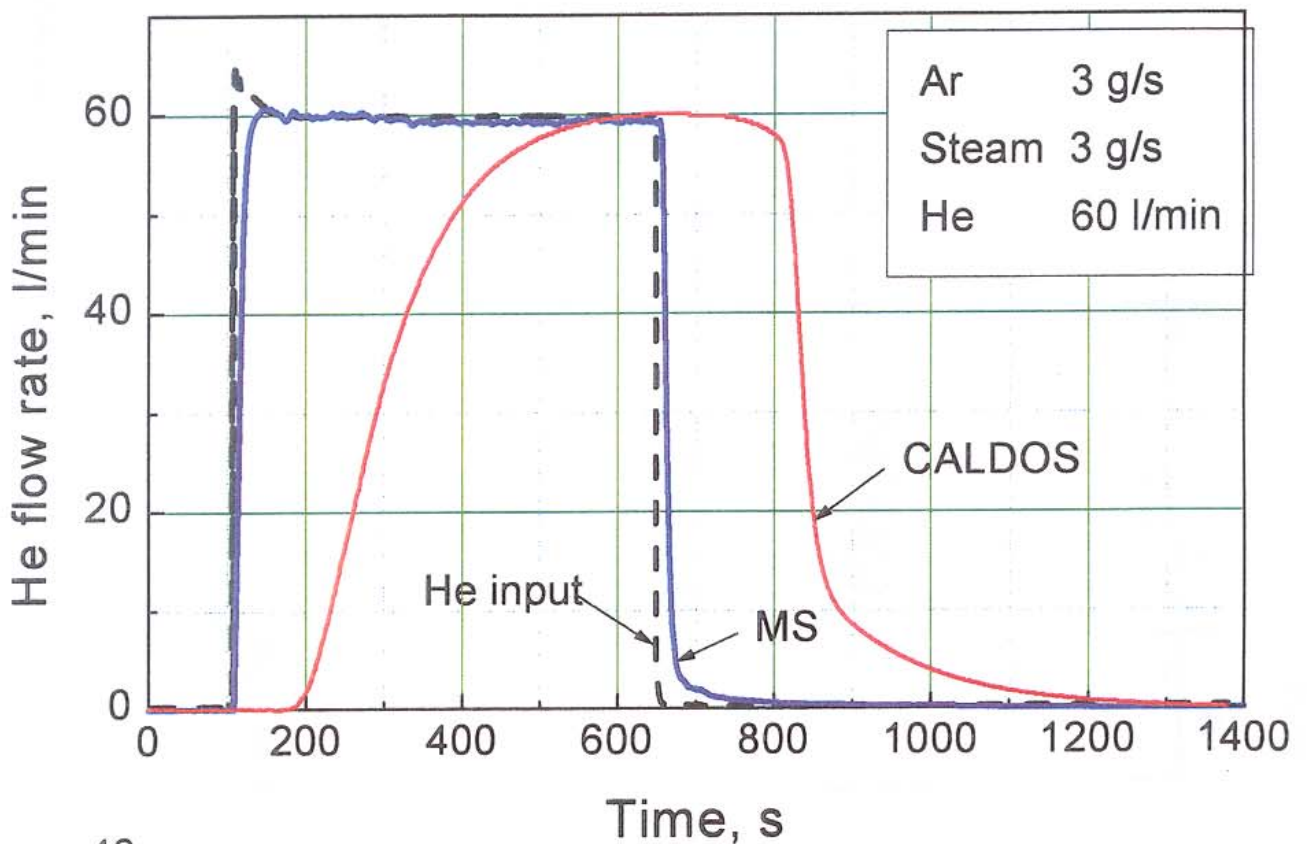
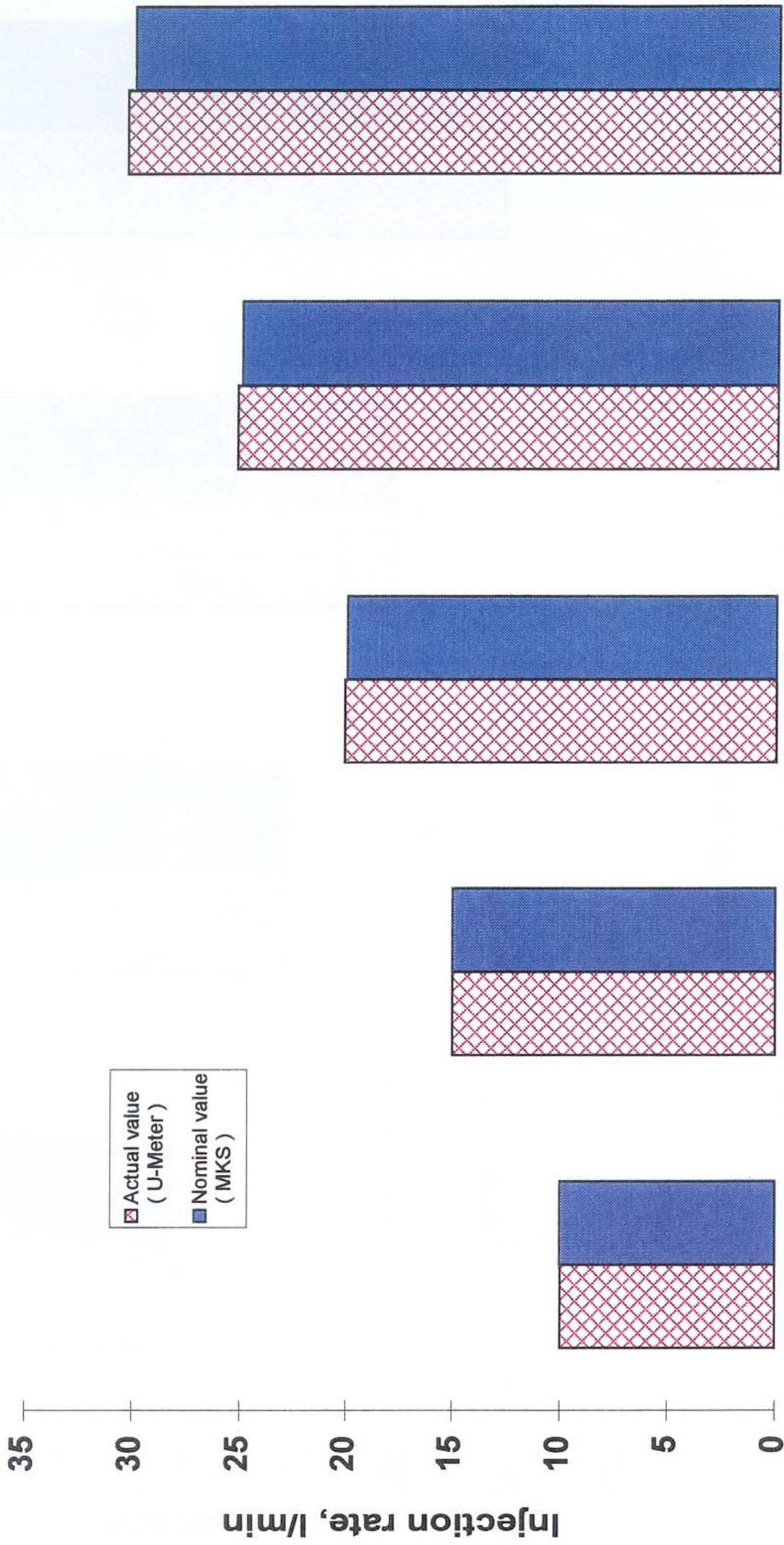


Fig. A-2

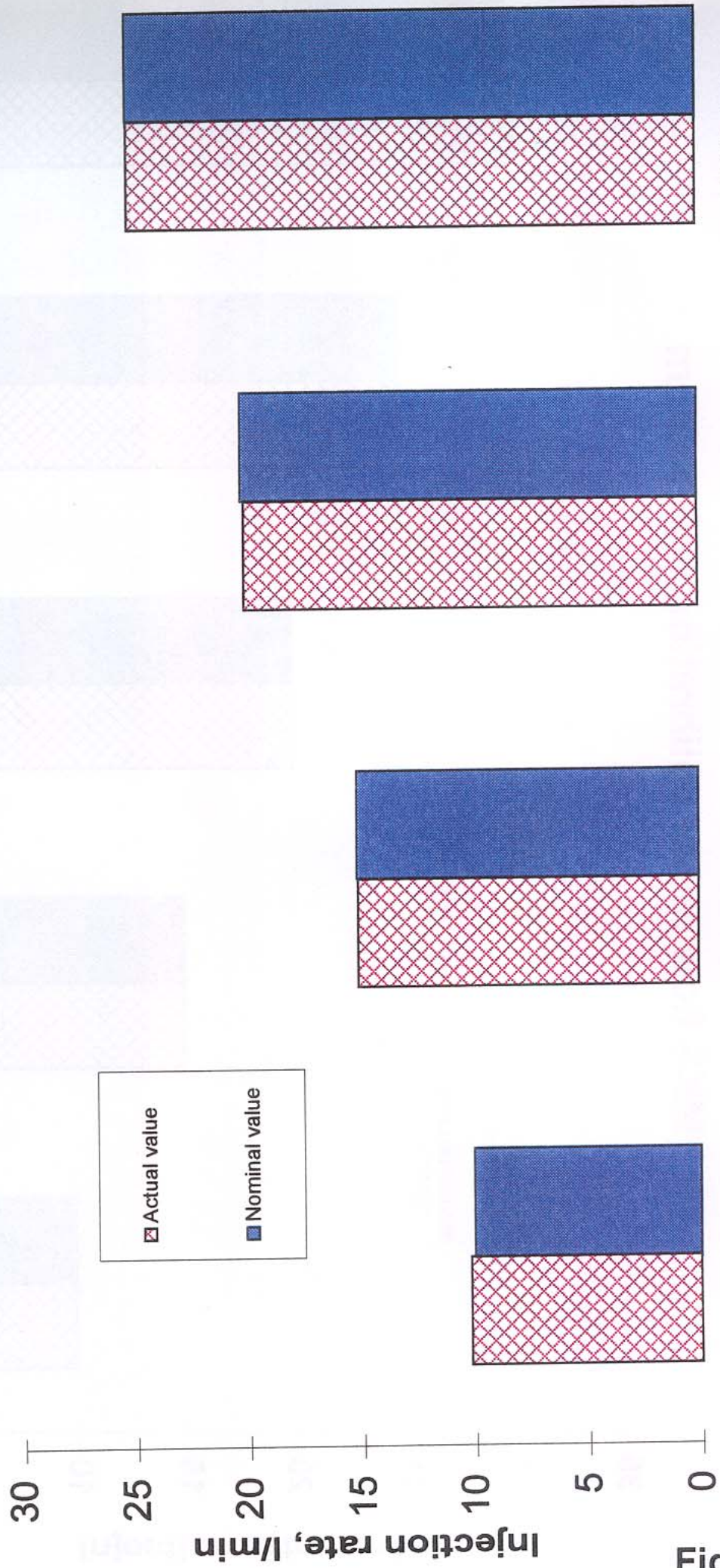
MKS flow meter calibration with helium



Fort He mks.xls
 April 13, 98 - HIT

Fig. A-3

MKS flow meter calibration for H₂ using N₂ (FH2 = 1.01 FN2)



Fort H2 mks.xls
April 14, 98 - HIT

Fig. A-4